

# Design, synthesis and biological evaluation of 6-alkoxypurine derivatives as kinase inhibitors

A dissertation presented

by

Álvaro Lorente Macías

Department of Medicinal and Organic Chemistry

School of Pharmacy

and

Institute of Biopathology and Regenerative Medicine

The Center for Biomedical Research



**UNIVERSIDAD  
DE GRANADA**

International doctoral thesis

Programa de doctorado en Biomedicina (B11.56.1)

Universidad de Granada

Granada, Spain

September 2019

Editor: Universidad de Granada. Tesis Doctorales  
Autor: Álvaro Lorente Macías  
ISBN: 978-84-1306-360-7  
URI: <http://hdl.handle.net/10481/57973>

**Design, synthesis and biological evaluation of 6-alkoxypurine derivatives  
as kinase inhibitors**

by

Álvaro Lorente Macías

**Resumen**

El cáncer es la segunda causa de muerte en el mundo, solo superada por las enfermedades cardiovasculares. A pesar de que se ha avanzado mucho en su prevención, diagnóstico y tratamiento, el número de casos sigue aumentando de forma alarmante año tras año. Es por ello que tanto la industria farmacéutica como centros de investigación de todo el mundo están centrando sus esfuerzos en el estudio de los mecanismos moleculares que están detrás de esta enfermedad, con el objetivo de encontrar nuevas estrategias para su tratamiento.

Producto de ello, las proteínas cinasas han surgido como prometedoras dianas moleculares para tratar la enfermedad. Estas proteínas pertenecen a una familia constituida por más de 500 enzimas que intervienen en multitud de procesos y actúan como reguladores de la actividad celular. Alteraciones en su función y expresión producen una pérdida de control en la homeostasis celular que lleva finalmente a la aparición de procesos cancerosos además de otras enfermedades. De esta manera, la sobreexpresión o hiperactividad de ciertas proteínas cinasas se ha descrito como un factor determinante en el desarrollo de muchos tipos de cánceres como leucemias, cáncer de mama, cáncer de colon, etc.

Todo ello, junto con el surgimiento de las llamadas terapias dirigidas, ha permitido el desarrollo de inhibidores selectivos de estas proteínas, dando lugar al descubrimiento de moléculas como el Imatinib que han supuesto un cambio de paradigma en el pronóstico de enfermedades como las leucemias, en las que hasta ahora su tratamiento estaba limitado a tratamientos de quimioterapia muy agresivos con bajas tasas de supervivencia asociadas.

Sin embargo, a pesar de los éxitos obtenidos con estas nuevas terapias, el desarrollo de inhibidores selectivos de proteínas cinasas es un campo que presenta ciertas

limitaciones, principalmente debido a la gran similitud estructural que presentan las proteínas de esta familia. Este hecho hace que la inhibición selectiva de la o las cinasas diana sea una tarea especialmente complicada.

En esta tesis se describe el desarrollo de pequeñas moléculas derivadas del anillo de 6-alcoxypurina como inhibidores de proteínas cinasas para el tratamiento de distintos tipos de cánceres. La progresión química de las diferentes familias de compuestos sintetizados ha sido guiada mediante cribados fenotípicos y ensayos de proliferación celular en un panel compuesto por 6 líneas de células cancerígenas (Jurkat, K563, HeLa, G361, MDA-MB-231 y HCT-116).

El diseño inicial de estas moléculas se basó en las estructuras de inhibidores selectivos de DAPK1 previamente descritos por nuestro grupo que presentaron potentes actividades pro-apoptóticas en células tumorales. Inicialmente, sobre estos inhibidores se realizaron modificaciones en las posiciones 6, 8 y 9 del anillo de purina con el objetivo de generar moléculas con mejores actividades biológicas. Así, la introducción del grupo fenetilo en posición N9 dio lugar a compuestos inductores de apoptosis en células Jurkat que fueron 2 veces más potentes que los compuestos líderes de partida.

Sin embargo, a pesar de la sustancial mejora en la actividad, los compuestos sintetizados presentaron elevados valores de liofilia, lo que podría dificultar optimizaciones posteriores y su uso en ensayos *in vivo*. Debido a ello, se introdujo un novedoso cambio del grupo *tert*-butilo en posición N9 del compuesto líder por grupos *N,N*-dimetilamino y 1-azacicloalcan-1-ilo, que dieron lugar a compuestos estructuralmente muy parecidos pero con propiedades fisicoquímicas mejoradas.

Con el objetivo de explorar esta nueva estructura purínica, se desarrolló una nueva metodología sintética que incluyó una estrategia de diversificación estructural basada en cicloadiciones alquino-azida catalizadas por cobre, que permite la generación de amplias familias de purinas y derivados sustituidos en posiciones 6, 8 o 9. Así, se sintetizó una familia de 35 compuestos que presentaron dos efectos fenotípicos diferentes: por un lado los compuestos sustituidos en posición C8 por fenilo indujeron apoptosis principalmente en células Jurkat; y por otro lado, se observó que uno de los compuestos sustituido en C8 por H presentó una potente actividad como bloqueador del ciclo celular en la fase G2/M en todas las líneas de células cancerígenas utilizadas.



Buscando optimizar las actividades de ambas clases de compuestos se llevó a cabo la exploración de la posición N9, en la que se introdujeron diferentes grupos 1-azacycloalcan-1-ilo así como los clásicos grupos isopropilo y *tert*-butilo presentes en esta posición en multitud de inhibidores derivados de purinas.

Pese a que ninguno de los derivados mantuvo el efecto de parada en G2/M, los ensayos realizados con los derivados generados de compuestos pro-apoptóticos mostraron un elevado grado de selectividad celular, que varió dependiendo del grupo 1-azacycloalcan-1-ilo presente en la estructura, por células Jurkat o K562. En contraposición, los compuestos que presentaron grupos isopropilo y *tert*-butilo, no mostraron ningún tipo de selectividad.

Como resultado de este trabajo se generaron 64 derivados de 6-alcoxipurina mediante el uso de 4 rutas sintéticas diferentes. Se consiguió una mejora sustancial de la actividad pro-apoptótica del producto de partida y además, por primera vez en análogos purínicos se describen sustituciones de los grupos alquilo en posición N9 por *N,N*-dimetilamina y grupos 1-azacycloalcan-1-ilo, cuyos derivados presentan propiedades fisicoquímicas mejoradas y mayor selectividad celular.



**Design, synthesis and biological evaluation of 6-alkoxypurine derivatives  
as kinase inhibitors**

by

Álvaro Lorente Macías

**Abstract**

Deregulation of protein kinases activity has emerged as a key mechanism by which cancer cells acquire the ability to escape normal physiological constraints on growth and survival. From the vast efforts made by the industry and academia on the development of molecules able to inhibit these proteins, many common structural elements present in kinase inhibitors have emerged, among which the purine ring system play a dominant role.

In this thesis I present the development of different families of 6-alkoxypurine derivatives guided by a phenotypic approach by the use of a panel of 6 cancer cell lines. Thus, it is shown the exploration process of 6-alkoxypurine DAPK1 inhibitors and the design and synthesis of the first 9-*N,N*-dialkylamino or 9-(1-azacycloalkan-1-yl) substituted purines to replace the typical alkyl groups presented at this position in many purine-based kinase inhibitors. This modification together with the implementation of a CuAAC diversification strategy at the C6 position generated a large compound library with molecules that exhibited two types of activities: apoptotic induction and G2/M arrest. Furthermore, these new purine scaffolds showed great improvements in their physicochemical properties compared to previous compound libraries and optimization efforts made over the most active compounds showed that the 9-*N,N*-dialkylamino or 9-(1-azacycloalkan-1-yl) substituted purines lead to more selective activity profiles compared with the classic 9-purinealkylated analogs.



## Table of Contents

Resumen .....	v
Abstract.....	ix
Table of Contents.....	xi
Table of Sections .....	xiii
List of Figures .....	xvii
List of Tables .....	xxi
List of Abbreviations .....	xxiii



## Table of Sections

<b>1. Introduction</b> .....	<b>1</b>
1.1. Cancer .....	3
1.1.1. Epidemiology of cancer: The numbers & impact of cancer .....	3
1.1.2. Cancer treatments .....	5
1.1.3. Comparison between chemotherapy and target treatments.....	13
1.2. Kinases in cancer .....	14
1.2.1. Structure of protein kinases.....	15
1.2.2. Kinase inhibitor binding sites.....	16
1.3. Discovery of kinase inhibitors.....	22
1.3.1. Target-based drug discovery .....	22
1.3.2. Phenotype-based drug discovery .....	28
1.4. Apoptosis and cancer .....	31
1.4.1. Types of programmed cell death .....	31
1.4.2. Mechanisms of apoptosis induction .....	32
1.4.3. Apoptosis checkpoints and cancer.....	34
1.4.4. Protein kinases and apoptosis.....	37
1.5. Purine derivatives as antitumor drugs .....	40
<b>2. Objectives</b> .....	<b>45</b>
<b>3. Materials and Methods</b> .....	<b>48</b>
3.1. Chemistry methods .....	49
3.1.1. Chemicals .....	49
3.1.2. Chromatography .....	49
3.1.3. Nuclear Magnetic Resonance .....	49
3.1.4. Mass Spectrometry .....	50
3.1.5. Physicochemical properties.....	50
3.2. Cells and culture .....	50

3.2.1. Cell Splitting .....	50
3.2.2. Analysis of cell cycle.....	51
3.2.3. Annexin-V staining.....	51
3.2.4. Dose response cell viability assay .....	52
<b>4. Results.....</b>	<b>57</b>
4.1. Design, synthesis and biological evaluation of chemical library 1.....	57
4.1.1. Design of chemical library 1 .....	57
4.1.2. Synthesis of chemical library 1 .....	58
4.1.3. Screening of chemical library 1.....	59
4.1.4. Annexin-V analysis .....	61
4.1.5. Cell proliferation studies.....	62
4.1.6. Physicochemical properties .....	63
4.2. Design, synthesis and biological evaluation of chemical library 2.....	65
4.2.1. Design of library 2.....	65
4.2.2. Synthesis of chemical library 2a.....	66
4.2.3. Design of chemical library 2b .....	67
4.2.4. Synthesis of chemical library 2b .....	68
4.2.5. Screening.....	68
4.2.6. Physicochemical properties.....	69
4.3. Design, synthesis and biological evaluation of chemical library 3.....	71
4.3.1. Design of chemical library 3 .....	71
4.3.2. Synthesis of chemical library 3 .....	73
4.3.3. Screening.....	75
4.3.4. Cell proliferation studies.....	80
4.3.5. Annexin-V analysis .....	82
4.3.6. Physicochemical properties .....	83
4.4. Optimization of compounds 78 and 97 .....	87



4.4.1.	Design of optimized 78- and 97-derived libraries.....	87
4.4.2.	Optimization of lead compound 78 .....	88
4.4.2.1.	Synthesis of the 78-derived optimized library.....	88
4.4.2.2.	Cell cycle analyses .....	89
4.4.3.	Optimization of lead compound 97 .....	91
4.4.3.1.	Synthesis of the 97-derived optimized library.....	91
4.4.3.2.	Cell viability studies.....	92
4.4.4.	Physicochemical properties.....	93
<b>5.</b>	<b>Discussion .....</b>	<b>97</b>
<b>6.</b>	<b>Conclusions.....</b>	<b>111</b>
<b>7.</b>	<b>References.....</b>	<b>115</b>
<b>Appendix</b>	<b>.....</b>	<b>135</b>
A.	General synthesis for the compounds from chemical library 1 .....	137
B.	General synthesis for the compounds from chemical library 2.....	146
Chemical library 2a.	.....	146
Chemical library 2b.	.....	151
C.	General synthesis for the compounds from chemical library 3 .....	155
D.	General synthesis for the compounds from the optimization of compounds 78 and 97 .....	173
E.	Synthesis of 4-(azidomethyl)thiazole ( <b>100</b> ) .....	187



## List of Figures

<b>Figure 1</b>   Estimated number of cancer cases and deaths by type, 2018.....	4
<b>Figure 2</b>   Estimated leading sites of new cancer cases and deaths by gender, 2018.....	4
<b>Figure 3</b>   Chemical structures of representative chemotherapeutic agents used in cancer treatment .....	8
<b>Figure 4</b>   Chemical structures of representative small molecule inhibitors used in cancer treatment .....	10
<b>Figure 5</b>   Structure and subregions of a typical protein kinase domain.....	15
<b>Figure 6</b>   Different types of reversible small-molecule kinase inhibitors.....	17
<b>Figure 7</b>   Chemical structures of different types of representative reversible small-molecule kinase inhibitors .....	19
<b>Figure 8</b>   Representative type V bisubstrate and bivalent inhibitors.....	20
<b>Figure 9</b>   Irreversible and reversible covalent bond formation between acrylamides, cyanoacrylamides and thiols.....	21
<b>Figure 10</b>   Phenotype-based versus target-based drug discovery.....	22
<b>Figure 11</b>   Summary of the chemical optimization of SRI571 (Imatinib) by high-throughput screening .....	25
<b>Figure 12</b>   Discovery of ABT-199 (Venetoclax) by fragment-based drug discovery ..	28
<b>Figure 13</b>   Discovery of eCF309 by phenotype-based drug discovery .....	30
<b>Figure 14</b>   Extrinsic and intrinsic apoptotic signaling pathways.....	33
<b>Figure 15</b>   Mechanisms contributing to evasion of apoptosis and carcinogenesis.....	36
<b>Figure 16</b>   Summary of the major kinase pathways that control cell survival and proliferation.....	38
<b>Figure 17</b>   Purine ring .....	40
<b>Figure 18</b>   Synthesis of the initial 18-purine library.....	41
<b>Figure 19</b>   Chemical optimization of 6a by phenotypic approach.....	43
<b>Figure 20</b>   Proposed modifications of 6d for the development of the chemical library 1.....	57
<b>Figure 21</b>   Synthetic procedure for the preparation of compounds <b>24 – 32</b> and <b>27i – 32i</b> by Route A and B .....	58
<b>Figure 22</b>   Selective effect of compounds <b>6d</b> , <b>27</b> and <b>28</b> .....	60
<b>Figure 23</b>   Membrane phosphatidylserine expression after treatment of Jurkat cells with compounds <b>27</b> and <b>28</b> .....	62

<b>Figure 24</b>   Dose-response curves and calculated IC <sub>50</sub> values for compounds <b>27</b> , <b>28</b> and <b>6d</b> .....	63
<b>Figure 25</b>   Chemical structure of representative ATP-competitive purine-based kinase inhibitors .....	65
<b>Figure 26</b>   Proposed modifications of <b>6d</b> for the development of the chemical library 2.....	66
<b>Figure 27</b>   Synthetic route for the preparation of compounds <b>41 – 44</b> .....	67
<b>Figure 28</b>   Synthetic route for the preparation of compounds <b>51</b> and <b>52</b> .....	68
<b>Figure 29</b>   Chemical structure of representative protein kinase inhibitor containing the 1,4-disubstituted 1,2,3-triazole moiety. ....	72
<b>Figure 30</b>   Proposed modifications to the purine scaffold for the development of the chemical library 3. ....	73
<b>Figure 31</b>   Synthetic route for the preparation of compounds <b>63 – 97</b> . ....	74
<b>Figure 32</b>   Synthetic route for the preparation of 4-(azidomethyl)thiazole 100 from 4-(chloromethyl) thiazole. ....	75
<b>Figure 33</b>   Effect of compounds <b>78</b> and <b>97</b> on the cell cycle of Jurkat, K562, HeLa, G361, MDA-MB-231 and HCT116 cells .....	77
<b>Figure 34</b>   Comparison of the effect of <b>78</b> on the cell cycle of Jurkat and K562 cells at 48, 72 and 96 h .....	79
<b>Figure 35</b>   Comparison of the effect of <b>78</b> on the cell cycle of HeLa and MDA-MB-231 cells at 48, 72 and 96 h .....	80
<b>Figure 36</b>   Dose-response curves and IC <sub>50</sub> values for compounds <b>78</b> , <b>92</b> , <b>93</b> , <b>94</b> , <b>95</b> and <b>97</b> .....	81
<b>Figure 37</b>   Membrane phosphatidylserine expression after treatment of Jurkat cells with compounds <b>78</b> and <b>97</b> .....	83
<b>Figure 38</b>   General structures of the compounds from the sublibraries 3a – 3e.....	84
<b>Figure 39</b>   General cLog D variation among the five subfamilies from the chemical library 3.....	86
<b>Figure 40</b>   Chemical structures of compounds <b>78</b> (G2/M arrest effect) and <b>97</b> (apoptotic activity) .....	87
<b>Figure 41</b>   Proposed compounds to explore the N9 position of <b>78</b> . ....	88
<b>Figure 42</b>   Synthetic route for the preparation of compounds <b>122 – 126</b> .....	89
<b>Figure 43</b>   Representative experiment where is shown the effect of compounds <b>78</b> , <b>122 – 126</b> over Jurkat and HeLa cells .....	90

<b>Figure 44</b>   Proposed compounds to explore the N9 position of <b>97</b> .....	91
<b>Figure 45</b>   Synthetic route for the preparation of compounds 132 – 136 .....	92
<b>Figure 46</b>   Dose-response curves and calculated IC <sub>50</sub> values for compounds <b>97</b> and <b>132 – 136</b> .....	93
<b>Figure 47</b>   Biological hypothesis of the interaction of the <i>tert</i> -butyl and phenethyl groups with the target .....	100
<b>Figure 48</b>   Relationship between the triazole functionalization and the in vitro activity of the molecules .....	103
<b>Figure 49</b>   Chemical structures of representative C8-H-substituted CDK1 inhibitors .....	104
<b>Figure 50</b>   Chemical structures of representative microtubule-destabilizing colchicine analogs. ....	105
<b>Figure 51</b>   Suggested structural changes to explore the biological implication of the methoxy group and the ether moiety. ....	106
<b>Figure 52</b>   Graphical representation of the electrostatic potential map of the groups attached at the purine N9 position in compounds <b>97</b> and <b>132 – 136</b> .....	107
<b>Figure 53</b>   Chemical structures of representative FDA approved small molecule protein kinase inhibitors containing isopropyl, <i>tert</i> -butyl, cyclopropyl or cyclopentyl groups. ....	109



## List of Tables

<b>Table 1</b>   Phenotypic screening of the chemical library 1 by cell cycle analysis .....	59
<b>Table 2</b>   Summary of membrane phosphatidylserine expression after treatment of Jurkat cells with compounds <b>27</b> and <b>28</b> .....	62
<b>Table 3</b>   Molecular weight (MW) and cLog D values of compounds from the chemical library 1.....	64
<b>Table 4</b>   Phenotypic screening of the chemical library 2a and 2b by cell cycle analysis .....	69
<b>Table 5</b>   Molecular weight (MW) and cLog D values of compounds from the chemical library 2a and 2b.....	70
<b>Table 6</b>   Phenotypic screening of the chemical library 3 by cell cycle analysis .....	75
<b>Table 7</b>   Summary of membrane phosphatidylserine expression after treatment of Jurkat cells with compounds <b>78</b> and <b>97</b> .....	83
<b>Table 8</b>   Molecular weight (MW) and cLog D values of compounds from the subfamily 3a.....	84
<b>Table 9</b>   Molecular weight (MW) and cLog D values of compounds from the subfamily 3b, 3c, 3d and 3e .....	85
<b>Table 10</b>   Summary of the effect in the sub-G1 and G2/M region of compounds <b>122 – 126</b> compared with <b>78</b> .....	90
<b>Table 11</b>   Molecular weight (MW) and cLog D values of compounds from the optimization of <b>78</b> and <b>97</b> .....	94





## List of Abbreviations

<b>1</b>	<sup>13</sup> C-NMR	Carbon-13 nuclear magnetic resonance
	<sup>1</sup> H-NMR	Proton nuclear magnetic resonance
<b>A</b>	ABL	Tyrosine-protein kinase ABL1
	ADP	Adenosine diphosphate
	AKT	Protein kinase B (PKB)
	ALK	Anaplastic lymphoma kinase
	ALL	Acute lymphoblastic leukemia
	AMP-PNP	Adenylyl-imidodiphosphate
	APAF1	Apoptotic protease activating factor 1
	ATP	Adenosine triphosphate
	A-loop	Protein kinase activation loop
<b>B</b>	BAD	BCL-2-associated agonist of cell death
	BAK	BCL-2 antagonist killer 1
	BAX	BCL-2 associated x protein
	BCE	Before common era
	BCG	<i>Bacillus Calmette-Guérin</i>
	Bcl-2	B-cell lymphoma-2 protein family
	BCL-2	Anti-apoptotic B-cell lymphoma protein 2
	BCL-W	BCL-2-like protein 2
	BCL-X <sub>L</sub>	B-cell lymphoma-extra large protein
	BCR-ABL	Breakpoint cluster region protein (BCR) - tyrosine-protein kinase ABL1(ABL) fusion protein
	BFL-1/A1	BCL-2-related protein A1
	BH3	Homology domain 3
	BID	BH3-interacting domain death agonist
	BIK	BCL-2-interacting killer
	BIM	BCL-2-interacting mediator of cell death
	BIR	Baculovirus IAP repeat
	BMF	BCL-2 modifying factor
	BRUCE	BIR repeat containing ubiquitin-conjugating enzyme, also known as BIRC6
	BTK	Bruton's tyrosine kinase
	B-RAF	B-Raf proto-oncogene, serine/threonine kinase
<b>C</b>	CAR	Chimeric antigen receptor
	CD4	T- lymphocyte surface cluster of differentiation 4
	CD6	T- lymphocyte surface cluster of differentiation 6
	CD19	B-lymphocyte antigen cluster of differentiation 19
	CDK	Cyclin-dependent kinase family
	CDK1	Cyclin-dependent kinase 1
	cIAP1	Cellular inhibitor of apoptosis 1, also known as BIRC2
	cIAP2	Cellular inhibitor of apoptosis 2, also known as BIRC3
	CLL	Chronic lymphocytic leukemia
	clog D	Calculated distribution coefficient (adjusted to a specific pH)
	CML	Chronic myelogenous leukemia
	CTLA4	T-lymphocyte-associated protein 4

	CuAAC	Copper(I)-catalyzed alkyne-azide [3 + 2] cycloaddition
	c-Kit	Tyrosine-protein kinase KIT
	C-lobe	Protein kinase C-terminal lobe
<b>D</b>	DAPK	Death-associated protein kinase family
	DAPK1	Death-associated protein kinase 1
	DFG	Aspartic acid-Phenylalanine-Glycine
	DISC	Death-inducing signaling complex
	DMF	<i>N,N</i> -Dimethylformamide
	DMEM	Dulbecco's Modified Eagle Medium
	DMSO	Dimethyl sulfoxide
	DNA	Deoxyribonucleic acid
	DR	Death receptor
<b>E</b>	EBRT	External beam radiation therapy
	EGFR	Epidermal growth factor receptor
	ER	Endoplasmic reticulum
	ERK	Extracellular signal-regulated kinase family
	ERK1	Extracellular signal-regulated kinase 1, also known as MAPK3
	ERK2	Extracellular signal-regulated kinase 2, also known as MAPK1
<b>F</b>	FADD	FAS-associated death domain protein
	FAS	Tumor necrosis factor receptor superfamily member 6 (TNFRSF6)
	FDA	The U.S. Food and Drug Administration
	FGFR	Fibroblast growth factor receptor
	FOXO1	Forkhead box protein O1 transcription factor
<b>G</b>	GSK-3	Glycogen synthase kinase 3
<b>H</b>	HEPES	4-(2-hydroxyethyl)-1-piperazineethanesulfonic acid
	HER2	Human epidermal growth factor receptor 2
	HRK	Protein harakiri or death protein 5 (DP5)
	HRMS	High resolution mass spectra
	HTS	High-throughput screening
<b>I</b>	IAPs	Inhibitors of apoptosis proteins
	IC <sub>50</sub>	Half maximal inhibitory concentration
	ILP2	Inhibitor of apoptosis-like protein 2, also known as BIRC8
	IL-2	Interleukin-2
	InsR	Insulin receptor
	IP	Intellectual property
	ITC	Isothermal titration calorimetry
<b>J</b>	JAK	Janus kinase
<b>L</b>	log P	Octanol-water partition coefficient
<b>M</b>	MAPK1	Mitogen activated protein kinase 1
	MAPK3	Mitogen activated protein kinase 3

	MCL-1	Induced myeloid leukemia cell differentiation protein
	MeCN	Acetonitrile
	MEK	Mitogen-activated protein kinase kinase (MEK1 and MEK2)
	MLIAP	Melanoma inhibitor of apoptosis protein, also known as BIRC7
	MOMP	Mitochondrial outer membrane permeabilization
	mRCC	Metastatic renal cell carcinoma
	mTOR	Mammalian target of rapamycin
	mTORC2	Mammalian target of rapamycin complex 2
	MTT	3-(4,5-dimethylthiazol-2-yl)-2,5-diphenyltetrazolium bromide
	MW	Molecular weight
<b>N</b>	NAIP	Neuronal apoptosis inhibitory protein, also known as BIRC1
	NMR	Nuclear magnetic resonance
	NOXA	Phorbol-12-myristate-13-acetate-induced protein 1
	NSCLC	Non-small cell lung cancer
	N-lobe	Protein kinase N-terminal lobe
<b>P</b>	p53	Tumor protein 53
	PARP1	Nuclear protein poly (ADP-ribose) polymerase 1
	PBS	Phosphate buffered saline
	PCD	Programmed cell death
	Pd <sub>2</sub> (dba) <sub>3</sub>	tris(dibenzylideneacetone)dipalladium(0)
	PDB	Protein Data Bank
	PDD	Phenotype-based drug discovery
	PDGFR	Platelet-derived growth factor receptor
	PD-1	Programmed cell death protein 1
	PD-L1	Programmed cell death ligand 1
	PfPK7	<i>Plasmodium falciparum</i> protein kinase 7
	PI	Propidium iodide
	PI3K	Phosphoinositide 3-kinase
	PIP <sub>2</sub>	Phosphatidylinositol-4,5-bisphosphate
	PIP <sub>3</sub>	Phosphatidylinositol-3,4,5-triphosphate
	PKAc	cAMP-dependent protein kinase catalytic unit
	PKB	Protein kinase B
	PKC	Protein kinase C
	ppm	Parts per million
	PUMA	p53 upregulated modulator of apoptosis
	PTEN	Phosphatidylinositol-3,4,5-trisphosphate 3-phosphatase
<b>R</b>	RAS	Small GTPase protein family
	RAF	RAF proto-oncogene serine/threonine-protein kinase family
	RCC	Renal cell carcinoma
	RNA	Ribonucleic acid
	RO3	Rule of three
	RO5	Rule of five
	ROS1	Proto-oncogene tyrosine-protein kinase 1
	rpm	Revolutions per minute
	RPMI	Roswell Park Memorial Institute medium
	RTK	Receptor tyrosine kinase

<b>S</b>	SAR	Structure-activity relationship
	SEM	Standard error of the mean
	SLL	Small lymphocytic lymphoma
	SMAC	Mitochondria-derived activator of caspases
	SMKI	Small-molecule kinase inhibitor
	S <sub>N</sub> Ar	Nucleophilic aromatic substitution
	SPR	Surface plasmon resonance
	Src	Proto-oncogene tyrosine-protein kinase c-Src
STAT	Signal transducers and activators of transcription	
<b>T</b>	TBDD	Target-based drug discovery
	tBID	truncated BID
	THF	Tetrahydrofuran
	TIL	Tumor-infiltrating lymphocyte
	TLC	Thin layer chromatography
	TNF	Tumor necrosis factor
	TNFR1	TNF receptor 1
	TRAILR	TNF-related apoptosis-inducing ligand receptor family
	TRAILR1	TNF-related apoptosis-inducing ligand receptor 1
TRAILR2	TNF-related apoptosis-inducing ligand receptor 2	
TRADD	TNF receptor-associated death domain	
<b>U</b>	USD	United States Dollar
	UV	Ultraviolet
<b>V</b>	VEGF	Vascular endothelial growth factor
	VEGFR	Vascular endothelial growth factor receptor
<b>W</b>	WHO	World Health Organization
<b>X</b>	XIAP	X-linked inhibitor of apoptosis protein
	Xphos	2-dicyclohexylphosphino-2',4',6'-triisopropylbiphenyl

# **1. Introduction**

---



## 1.1. Cancer

Cancer is much older than humankind. Paleopathologic findings indicate that tumors existed in animals in prehistoric times and non-human primates long before men appeared on Earth.<sup>1</sup> Nevertheless, the earliest written record regarding this disease dates back to Ancient Egypt (circa 3000 years BCE), where breast cancer was described on the Edwin Smith Papyrus. The writing says about the disease, “There is no treatment”.<sup>2</sup>

However, the origin of the word “cancer” emerged much later. The Greek physician Hippocrates (460– 370 BCE), who is considered the “Father of Medicine” described non-ulcer forming and ulcer-forming tumors with the terms *carcinosis* (καρκίνος, “crab”) and *carcinoma* (καρκίνωμα) due to the crab-like appearance of some cancers.<sup>3,4</sup>

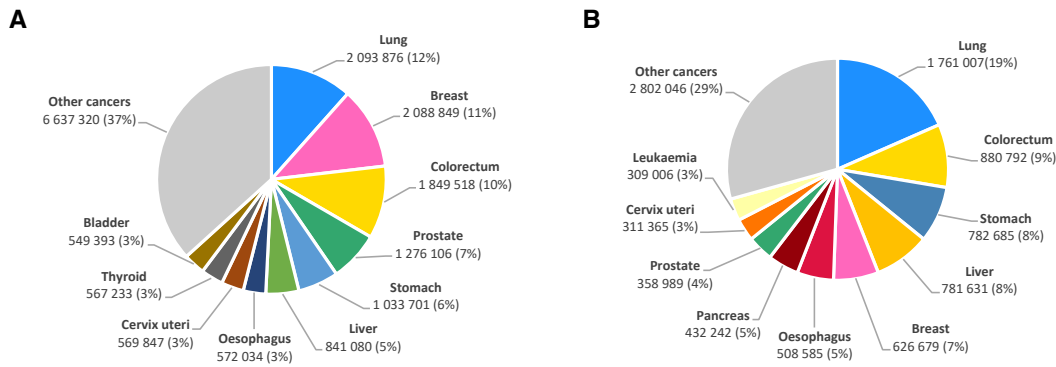
At present, according to the World Health Organization (WHO),<sup>5</sup> cancer is defined as a “generic term for a large group of diseases characterized by the growth of abnormal cells beyond their usual boundaries that can then invade adjoining parts of the body and/or spread to the organs”.

### 1.1.1. Epidemiology of cancer: The numbers & impact of cancer

This condition has become a major health problem worldwide and is currently the second leading cause of death globally only behind cardiovascular diseases. However, cancer costs the world more money than any other disease – about USD 1.16 trillion a year.<sup>6</sup>

According to the International Agency for Research on Cancer, it has been projected that the global cancer burden has risen to 18.1 million new cases and 9.6 million deaths in 2018.<sup>7</sup> And they report that a 20% of men and a 17% of women worldwide will develop cancer during their lifetime, whereas one out of 8 men and one out of 11 women pass away from the disease. In addition, the number of incident cases of cancer are estimated to increase to 29.5 million (a 63 % more) by 2040.

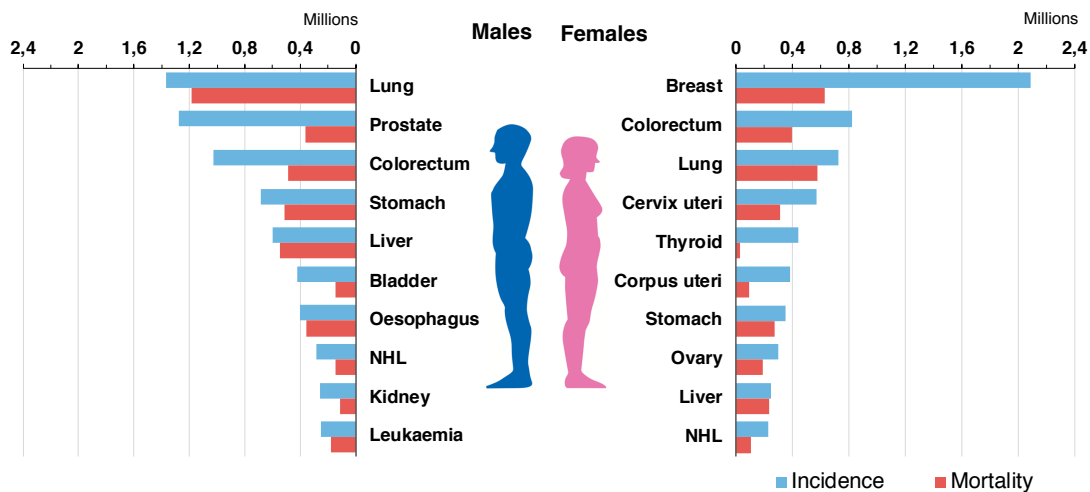
## 1.1. Cancer



**Figure 1 | Estimated number of cancer cases and deaths by type, 2018.** (A) Estimated number of cases in 2018, worldwide, all cancers, both sexes, all ages. (B) Estimated number of deaths in 2018, worldwide, all cancers, both sexes all ages. Adapted from ref. 9.

Although more than 100 types of cancer have been described, only 10 of them cause the 70 % of deaths from this disease, and the first 5 more prevalent – lung, colorectal, stomach, liver and breast cancer, account for more than half of the total number of deaths (Figure 1).<sup>8</sup>

In both sexes combined, the most commonly diagnosed one is lung cancer, which is also the leading cause of cancer death, closely followed by female breast cancer, then by colorectal and prostate cancer for incidence and colorectal, stomach and liver cancer for mortality.



**Figure 2 | Estimated leading sites of new cancer cases and deaths by gender, 2018.** Estimated number of cancer incidence (blue bars) and cancer deaths worldwide (red bars), divided in type of cancer in males and females from all ages. Adapted from ref. 9.



Regarding the differences between genders, lung cancer is the most commonly diagnosed cancer and the leading cause of cancer death in males, followed by prostate and colorectal cancer for incidence, and liver and stomach for mortality.

On the other hand, breast cancer is by far the most frequent cancer among females. This fact is due to the implementation of screening programs that help to early identify the disease. Therefore, the proportion of deaths is significantly lower compared to the rest cancers, although it remains the first cause of cancer death in females. This is followed by colorectal and lung cancer for incidence and conversely for mortality (**Figure 2**).

However, depending on the country, its degree of economic development and their associated social and lifestyle factors, the leading cause of cancer death as well as the most frequently diagnosed cancer vary significantly.<sup>9</sup>

### **1.1.2. Cancer treatments**

Despite the aforementioned data, the progress in the cancer treatments together with earlier diagnosis have led to the achievement of long-term survival in more than half of all patients with cancer. Colorectal and breast cancers are significant examples in which 5-year survival rates have surpassed the double, from 23% and 40% 50 years ago to 57% and 87% at present, respectively.<sup>10</sup>

The existing treatment guidelines for cancer are not fixed and the treatment options vary depending on many factors – the type of cancer, the extent of disease, the risk of recurrence, the patient characteristics such as age and comorbidity, and personal preferences.<sup>11</sup> Moreover, for the majority of cancers a combination of different therapies is the best approach because it increases the chances of a cure or long-term remission, reduces damage to vital organs and tissues and minimize the evolution of drug resistance. Below are summarized the main cancer therapies:

#### **a) Surgery**

This is the oldest form of treatment for cancer. At present, over 80% of cancer cases need surgery.<sup>12</sup> Depending on the type of cancer and how advanced it is, surgery can be used to remove the entire tumor, debulk a tumor or relieving symptoms or side effects caused by a tumor. In addition, it has also an important role in the prevention and early diagnosis of cancer.<sup>13,14</sup>

Surgery represents the first option in the treatment of many tumors – breast, colorectal, thyroid, testis, prostate, melanoma or lung cancer. It works best for solid tumors that are contained in one area, and therefore is not used for leukemia or for cancers that have spread.<sup>15</sup> Although for some cancers surgery can be used alone, it is habitually used together with radiotherapy, chemotherapy, immunotherapy, targeted therapies or a combination of them.

### **b) Radiation therapy**

Nearly 50 out of 100 people have radiotherapy at some point during their cancer treatment.<sup>16</sup> This treatment is based on the use of X-rays, gamma rays and other sources of radiation to destroy cancer cells within the localized tumor microenvironment by damaging their DNA. Radiotherapy can be used alone or in combination with surgery, chemotherapy (chemoradiation) or both.

The therapeutic radiation can be delivered from outside the patient, known as external beam radiation therapy (EBRT); or from inside, by implanting radioactive sources in cavities or tissues (brachytherapy) or through systematic administration of radiopharmaceutical agents.<sup>17</sup> The type of radiation used mainly vary on the tumor location in the body, its proximity to sensitive normal tissues and its size.

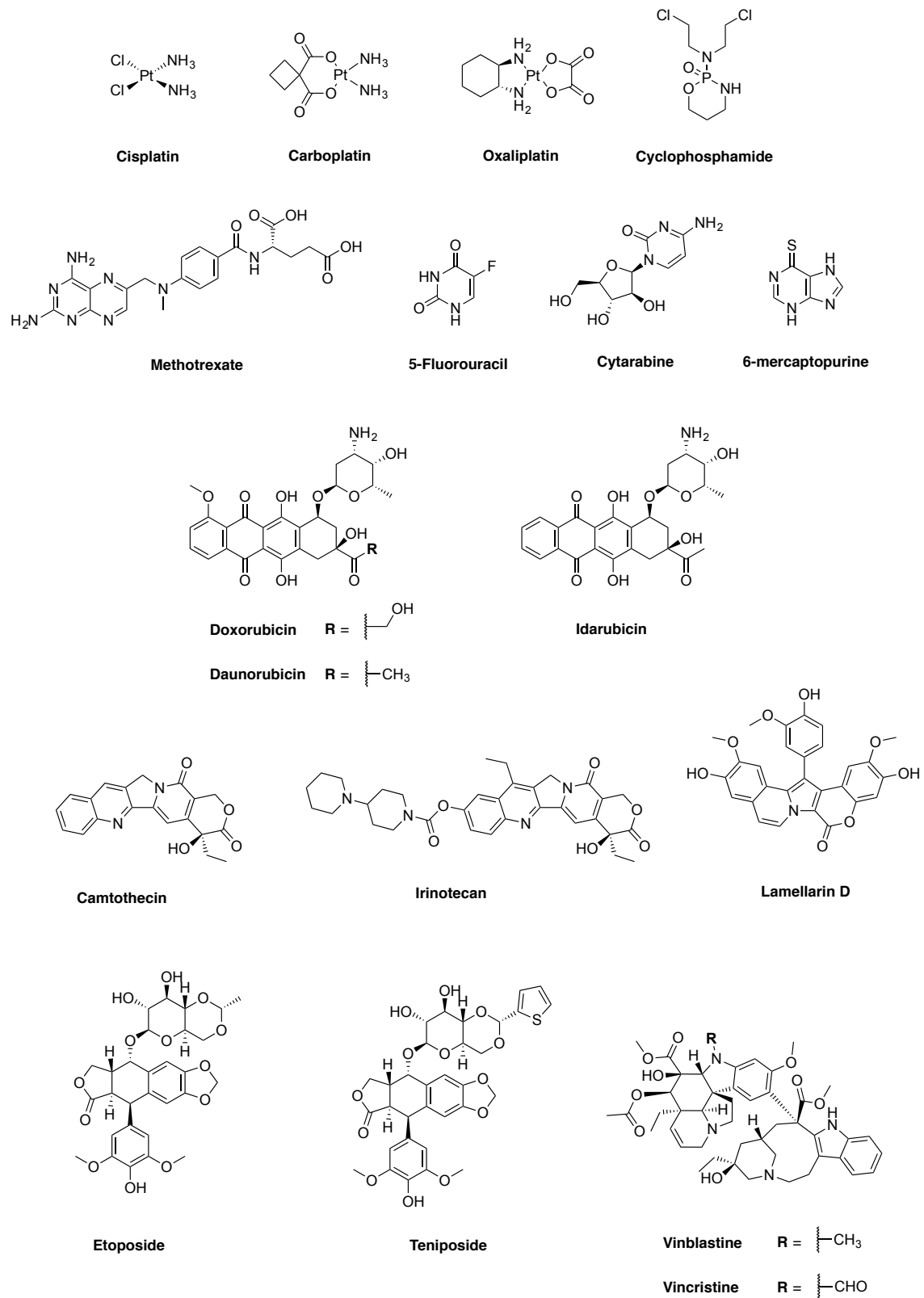
Commonly EBRT is often used for well-localized tumors like glioblastoma, lung cancer, or testicles. Brachytherapy is used to treat cervix, breast, prostate, eye, head and neck cancers.<sup>18</sup> And systemic radiation is usually employed after surgery to treat certain types of thyroid cancer by the use of iodine-131.<sup>19</sup>

### **c) Chemotherapy**

In 2018 the global chemotherapy utilization was 57.7%, which means that 9.8 million people would benefit from this treatment at some point during their illness.<sup>10</sup> Chemotherapy is a completely different approach to surgery and radiotherapy to treat cancer. Instead of physically removing a tumor or part of it, chemotherapy uses pharmacological agents to target rapidly growing and dividing cells, among which are the cancer cells. Chemotherapeutic agents can be classified based on their mechanism of action as:

- **Alkylating agents.** They are the most commonly used chemotherapeutic drugs. These compounds induce damage to both nuclear and mitochondrial DNA by the addition of alkyl groups. As a consequence, the cell undergoes programmed cell death or apoptosis.<sup>20</sup> Examples of alkylating agents include cisplatin, carboplatin, oxaliplatin and cyclophosphamide (Figure 3).
- **Antimetabolites.** These drugs are incorporated into macromolecules, such as DNA or RNA, thus inhibit their natural function or by inhibiting essential biosynthetic processes.<sup>21,22</sup> Commonly used antimetabolites are methotrexate, 5-fluorouracil, mercaptopurine, thioguanine, cytarabine, cladribine, gemcitabine and fludarabine.
- **Anthracyclines.** These drugs are daunosamine and tetrahydronaphthacene-dione-based chemotherapeutic agents.<sup>23</sup> Anthracyclines exert their effects through three different mechanisms of action. The first one is by generating free oxygen radicals that cause damage to DNA strands and the cell membrane, leading to apoptosis. The second is by intercalating into base pairs and effectively blocking DNA and RNA synthesis, thus preventing the replication of cancer cells. And the third mechanism is by causing inhibition of topoisomerase II, which blocks DNA repair mechanisms.<sup>24</sup> Examples of these chemotherapeutic agents include doxorubicin, daunorubicin, epidoxorubicin and idarubicin.
- **Topoisomerase inhibitors.** They are chemotherapeutic compounds that target either Type I or Type II topoisomerase. These enzymes regulate the torsional stress in DNA to enable essential genome functions.<sup>25</sup> The inhibition of these proteins prevent the DNA supercoiling and therefore block DNA transcription.<sup>26</sup> Examples of Type I inhibitors include camptothecin, irinotecan or lamellarin D, while Type II inhibitors include etoposide and teniposide.
- **Plant alkaloids.** These compounds act by blocking cell division, thus slowing tumor growth and progression. These compounds specifically target the M phase of the cell cycle and act by blocking tubulin assembly into microtubules in the mitotic spindle during cell division.<sup>27</sup> Within this group are included vinblastine and vincristine.

## 1.1. Cancer



**Figure 3 | Chemical structures of representative chemotherapeutic agents used in cancer treatment.**  
Source: own construction.

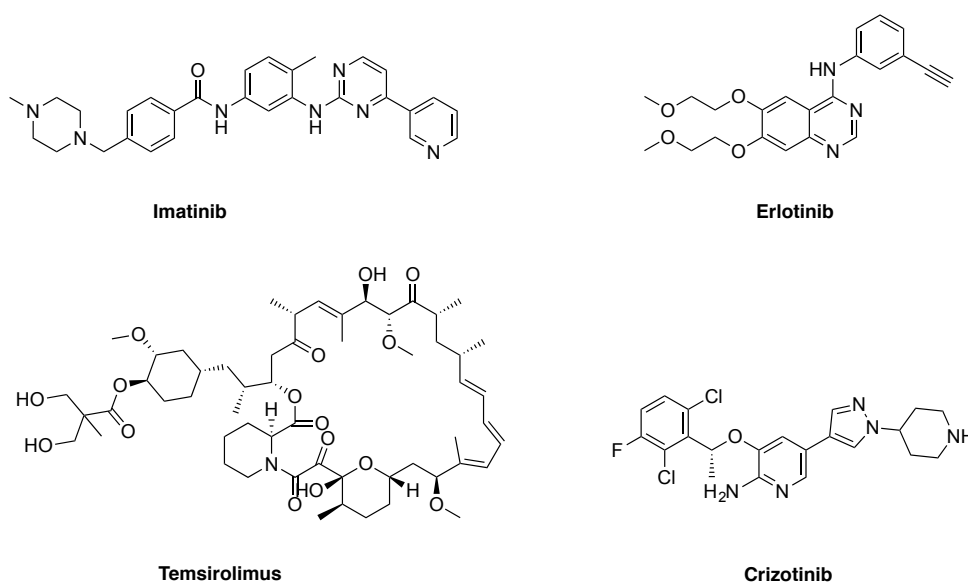
These chemotherapeutic agents can be used as a treatment on its own if the cancer type is very sensitive to it (blood cancer). However, they are often used in conjunction with other treatments as a neoadjuvant therapy to shrink tumors (pre-surgery),<sup>28</sup> as an adjuvant therapy to prevent relapses (following surgery)<sup>29</sup> or as a concomitant therapy with radiotherapy.<sup>30</sup>

#### **d) Targeted therapy**

This therapy emerged from the need of minimizing the significant side effects derived from the lack of specificity of chemotherapy drugs. Targeted therapy is a type of treatment that blocks the growth of cancer cells by interfering with specific biological targets that are essential for carcinogenesis and tumor growth.<sup>31</sup> This type of therapy is also known as “Precision Medicine”, and it is being studied for use alone, or in combination with other cancer treatments such as chemotherapy. Cancer targeted therapy can be divided in two categories:

- **Small molecule inhibitors.** These are organic compounds with a molecular weight below 500 – 900 Da (an arbitrary threshold related to the digestive system’s intracellular absorption ability) designed to interfere with signaling pathways and to act on targets found inside the cell.<sup>32</sup> These inhibitors mainly focus on inhibiting protein kinases and preventing activation of pathways that are dysregulated during cancer.<sup>33</sup>

The most successful small molecule inhibitor so far has been Imatinib (Gleevec<sup>®</sup>, Novartis)<sup>34</sup> (**Figure 4**), an inhibitor of the BCR-ABL fusion kinase, which is now approved for the treatment of chronic myelogenous leukemia (CML).<sup>35</sup> Other examples of small molecule inhibitors currently used in the clinic are erlotinib (Tarveca<sup>®</sup>, Astellas Pharm Global Development Inc.), an epidermal growth factor receptor tyrosine kinase inhibitor used for the treatment of non-small cell lung cancer (NSCLC) and pancreatic cancer; temsirolimus (Torisel<sup>®</sup>, Wyeth Pharmaceuticals), which is a specific mTOR inhibitor used to treat advanced renal cell carcinoma (RCC); or crizotinib (Xalkori<sup>®</sup>, Pfizer Inc.), an anaplastic lymphoma kinase (ALK) and proto-oncogene tyrosine-protein kinase 1 (ROS1) inhibitor used in the treatment of ALK or ROS1-positive NSCLC.<sup>36</sup>



**Figure 4 | Chemical structures of representative small molecule inhibitors used in cancer treatment.**  
Source: own construction.

- **Monoclonal antibodies.** They are designated humanized antibodies, which bind to cancer-associated cellular antigens. Their mechanism of action is through disruption of the interactions between ligand and receptor, either by the antibody blocking the site of interaction or by protein clearance from the system by phagocytic cells or endocytosis.<sup>37,38</sup> Contrary to small molecules inhibitors, monoclonal antibodies used in cancer therapy exclusively target extracellular proteins.

Many monoclonal antibodies have been approved for the treatment of solid tumors. Bevacizumab (Avastin<sup>®</sup>, Genentech Inc.) is one of the most widely used in the clinic. This is a recombinant humanized monoclonal IgG1 antibody that targets vascular endothelial growth factor (VEGF).<sup>39</sup> It is approved for metastatic colorectal cancer, NSCLC, metastatic renal cancer, cervical cancer, ovarian cancer and glioblastoma multiforme. Other examples are trastuzumab (Herceptin<sup>®</sup>, Genentech Inc.) that is raised against HER2 receptor and used for HER2-overexpressing breast or metastatic gastric cancer<sup>40</sup> and cetuximab (Erbix<sup>®</sup>, ImClone Systems and Bristol-Myers Squibb Company) that binds to the epidermal growth factor receptor (EGFR) and used for EGFR-expressing

metastatic colorectal cancer, especially for those patients who fail to respond to current treatments or who develop resistance to them.<sup>41</sup>

### e) Immunotherapy

Tumor escape from the immune system is recognized as one of the key hallmarks of cancer, and therefore it is considered a key point for its treatment.<sup>42</sup> Immunotherapy uses substances to enhance the effector functions of the immune response against cancer cells. Several types of immunotherapy are used to treat cancer. They can be divided into two categories:

- Types of immunotherapy that modulate the response of the immune system that act directly against the cancer:
  - **Checkpoint inhibitors.** Programmed cell death protein 1 (PD-1) and its ligand (PD-L1) and cytotoxic T-lymphocyte-associated protein 4 (CTLA4), are the most clinically relevant immune checkpoints.<sup>43</sup> The interaction of these molecules with their ligands is a fundamental feature in determining the balance intensity of the immune response, as these pathways deliver negative signals to effector cells to properly adjust the effector responses.<sup>44</sup> Therefore, perturbation of these pathways will result in enhanced immune response and prevention of immune exhaustion. Examples of checkpoint inhibitors are Pembrolizumab (Keytruda<sup>®</sup>, Merck & Co. Inc.), an anti-PD-1 monoclonal antibody used for untreated brain metastases in melanoma and NSCLC; Nivolumab (Opdivo<sup>®</sup>, Bristol-Myers Squibb Company),<sup>45</sup> an anti-PD-1 monoclonal antibody used in untreated melanoma brain metastases; or Ipilimumab (Yervoy<sup>®</sup>, Bristol-Myers Squibb Company), an anti-CTLA4 monoclonal antibody employed for the treatment of unresectable or metastatic melanoma.<sup>46</sup>
  - **Adoptive cell transfer.** Types of adoptive cell therapy include chimeric antigen receptor (CAR) T-cell therapy and tumor-infiltrating lymphocyte (TIL) therapy.<sup>47,48</sup> From the first group Axicabtagene ciloleucel (Yescarta<sup>®</sup>, Kite Pharma Inc.), is an anti-CD19 CAR T-cell product

recently approved to treat relapsed or refractory large B-cell lymphoma.<sup>49</sup>

On the other hand, TIL therapy is still in clinical trials.<sup>50</sup>

- Types of immunotherapy that enhance the antitumor response:
  - **Cytokines.** These molecules are important regulators of innate and adaptive immune cells, allowing short and long distance communications between them.<sup>51</sup> Due to this fact, cytokine therapy has been used to enhance the immune system of cancer patients. At present the U.S. Food and Drug Administration (FDA) has approved two cytokines for cancer treatment: interferon alpha (IFN $\alpha$ ) for the treatment of hairy cell leukemia, follicular lymphoma, melanoma or metastatic renal cell carcinoma (mRCC); and interleukin-2 (IL-2) used for the treatment of mRCC and metastatic melanoma. However, many others cytokines are being evaluated in clinical trials.
  - ***Bacillus Calmette-Guérin (BCG).*** This agent is exclusively used for the treatment of non-muscle invasive bladder cancer. The infection of urothelial cells by BCG has a profound effect on stimulation of the immune system.<sup>52</sup> This increases the expression of antigen-presenting molecules, which produce a cytokine release that triggers the immune response and lead an antitumor response mediated by macrophages, natural killer cells, cytotoxic T lymphocytes and neutrophils.<sup>53</sup>

### f) Other treatments

Although the previous therapies are the most widely used, there are many other that are under study. To mention some of them: cryotherapy, hyperthermia (radiofrequency ablation), gene therapy, ultraviolet light treatment, laser treatment, photodynamic therapy, high intensity focused ultrasound, stem cell and bone marrow transplants or hormone therapy, among others.



### **1.1.3. Comparison between chemotherapy and target treatments**

As it has been stated previously, chemotherapeutic drugs target rapidly dividing cells. Consequently, these drugs not only affect cancer cells, but also target certain normal cells with high rates of division, such as those presented in the intestinal epithelium, hair follicles or bone marrow.<sup>54</sup> As a consequence of the lack of specificity of chemotherapy treatments, patients usually experience severe side effects, such as pain, nausea, diarrhea, cardiotoxicity, hair loss, darkened or dry skin and depression of the immune system.<sup>55-57</sup>

Due to this fact, novel approaches are being developed to better treat cancer patients and complement current therapies. Among these, targeted cancer therapy and, particularly, small molecule kinase inhibitors have arisen as the new generation of cancer drugs that are expected to be the alternative to replace systemic chemotherapy in the future.<sup>58</sup> In fact, since the aim of this therapy is to interfere with a specific molecular target that is believed to have a critical role in tumor growth or progression rather than simply interfering with all rapidly growing cells, it is expected to be a more effective and less harmful alternative than classic chemotherapy.

## 1.2. Kinases in cancer

Protein kinases are a large family of over 518 enzymes that catalyze the transfer of the  $\gamma$ -phosphate from ATP (adenosine triphosphate) to substrates that usually contain a serine, threonine or tyrosine residue.<sup>59</sup> Albeit protein kinases account for only about 2.5 % of the human genome,<sup>60</sup> they regulate up to one-third of the proteome.<sup>61,62</sup>

Since virtually every signal transduction process occurs via phosphotransfer cascade, kinases are key nodes in the complex cellular signaling network, regulating a large range of cellular activities, which include growth, proliferation, survival, apoptosis, metabolism, motility, transcription, differentiation, angiogenesis, and response to DNA damage.<sup>63,64</sup>

Due to the high implication of these enzymes in cellular processes, deregulation of kinase function has been linked to multiple types of cancer,<sup>65,66</sup> inflammatory diseases,<sup>67</sup> developmental disorders,<sup>68</sup> infectious diseases,<sup>69</sup> cardiovascular diseases,<sup>70</sup> metabolic disorders<sup>71</sup> and neurodegenerative diseases.<sup>72–74</sup>

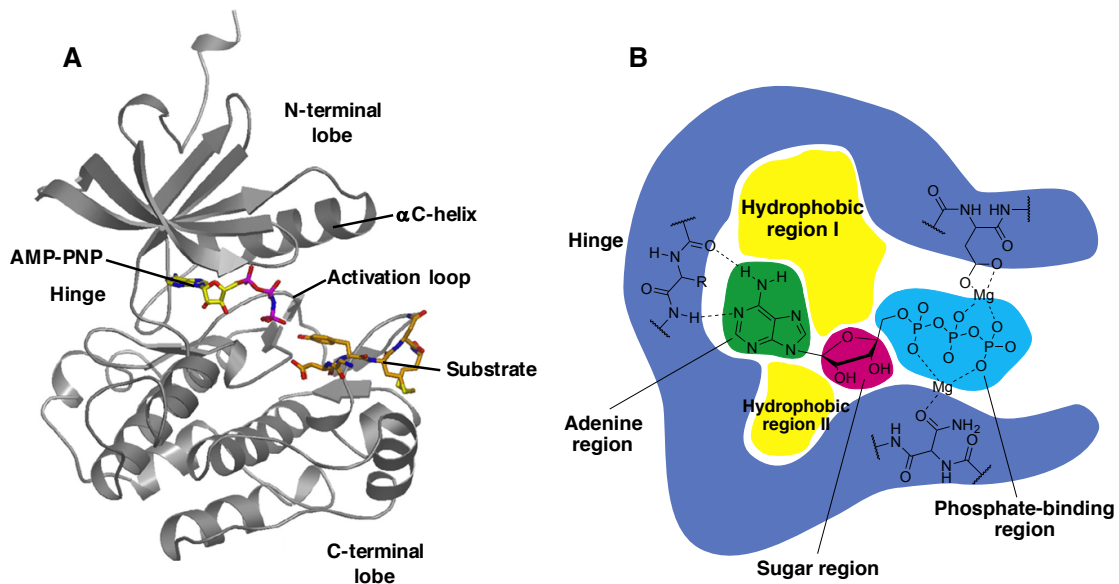
This fact has led to a rapid development of kinase-based therapeutics in the past decades.<sup>75</sup> Hence, since the development in the early 1980s of isoquinolinesulfonamides as the first protein kinase inhibitors,<sup>76</sup> and the first FDA approval of a kinase inhibitor (imatinib, Gleevec<sup>®</sup>, Novartis) in 2001,<sup>77</sup> a total of 50 kinase inhibitor drugs have been approved to date (May 2019),<sup>78</sup> mainly for the treatment of different types of cancers and a few non-cancer indications.

These approved drugs target a small number of kinases, including BCR-ABL, EGFR, ALK, PDGFR, B-RAF, JAK, c-Kit, BTK, CD4, CD6, and FGFR. The majority of these inhibitors are tyrosine kinase inhibitors, such as **cabozantinib** (Cabometyx<sup>®</sup>, Exelixis Inc.), **crizotinib** (Xalkori<sup>®</sup>, Pfizer Inc.), **erlotinib** (Tarceva<sup>®</sup>, Astellas Pharm Global Development Inc.) or **ibrutinib** (Imbruvica<sup>®</sup>, Pharmacyclics LLC). Others are serine/threonine kinase inhibitors, such as **abemaciclib** (Verzenio<sup>®</sup>, Eli Lilly) and **vemurafenib** (Zelboraf<sup>®</sup>, Plexxicon and Roche) and **idelalisib** (Zydelig<sup>®</sup>, Calistoga Pharmaceuticals Inc.), **copanlisib** (Aliqopa<sup>®</sup>, Bayer), **duvelisib** (Copiktra<sup>®</sup>, Verastem Inc.) and the recently approved **alpelisib** (Piqray<sup>®</sup>, Novartis),<sup>79,80</sup> are lipid kinase inhibitors (PI3K inhibitors).<sup>32</sup>

### 1.2.1. Structure of protein kinases

Even though protein kinases diverge in their primary amino acid sequence, their three-dimensional structures are strikingly similar. This is especially notable in the catalytic domain, which is constituted of about 300 highly conserved amino acids.<sup>81</sup>

The catalytic domain consists of two lobes: an N-terminal lobe (N-lobe), containing five-stranded beta sheets ( $\beta$ 1- $\beta$ 5) and one conserved alpha helix ( $\alpha$ C-helix); and a C-terminal lobe (C-lobe) comprising six alpha helices, and where the activation loop is located (A-loop). Both lobes are connected by a flexible hinge region (**Figure 5A**).<sup>82</sup> These structures fold into a bi-lobed catalytic core structure with the ATP-Mg complex situated in a deep cleft located between the lobes.<sup>83,84</sup>



**Figure 5 | Structure and subregions of a typical protein kinase domain.** (A) Structure of a typical protein kinase domain. The protein backbone is shown in cartoon form in gray, and the peptide substrate is shown in orange. The non-hydrolyzable ATP mimetic AMP-PNP is shown in yellow. From PDB structure 1ir3. (B) Schematic representation of ATP binding site divided into subregions. Adapted from ref. 85 (A) and 86 (B).

The A-loop, controls the access of the substrate to the active site. This segment starts with the conserved amino acid sequence Asp-Phe-Gly (DFG), which can adopt a great variety of conformations, although the catalytically competent and commonly phosphorylated (DFG-in conformation), and the “inactive” conformer (DFG-out conformation) are the most druggable. In the active state of the protein, the Asp residue from the DFG-motif points away from the active site, occupying a hydrophobic back

pocket adjacent to the ATP binding site. While when the DFG-motif moves back of the pocket, it partially blocks the substrate and ATP binding region, resulting in an activation loop conformation, resulting in the inactive protein conformation.<sup>87,88</sup>

Another important indicator of kinase activity is the conformation of the  $\alpha$ C-helix. When the  $\alpha$ C-helix adopts an inward conformation ( $\alpha$ C-in conformation) the conserved glutamine residue in the helix forms a salt bridge with a lysine in the  $\beta$ 3 strand. At this point, the lysine side chain establishes hydrogen bonds with oxygen atoms of the  $\alpha$  and  $\beta$  phosphates of the ATP that together with two  $Mg^{2+}$  ions allow the phosphate transfer.<sup>89</sup> A disruption of the salt bridge ( $\alpha$ C-out conformation) blocks the coordination of the phosphate groups, being a strong indicator of kinase inactivity.<sup>90</sup>

In the active conformation (DFG-in and  $\alpha$ C-in), ATP have access to the protein kinase active site. The adenine ring from ATP establishes hydrogen bonds with the hinge, while the triphosphate groups and the ribose ring bind in a hydrophilic pocket extending to the substrate binding site.<sup>91</sup>

In addition to the regions used by the ATP to dock and position correctly for the catalytic process, there have been described other areas in the vicinity of the ATP binding site as the hydrophobic pocket I, hydrophobic pocket II or the previously mentioned back pocket (or allosteric pocket), as well as pockets outside the ATP binding site.<sup>92</sup> These areas are not occupied by the ATP (**Figure 5B**). However, they present structural differences among the different kinases, and consequently are critical structures for the design of inhibitors that can bind selectively to the target kinase.<sup>93,94</sup>

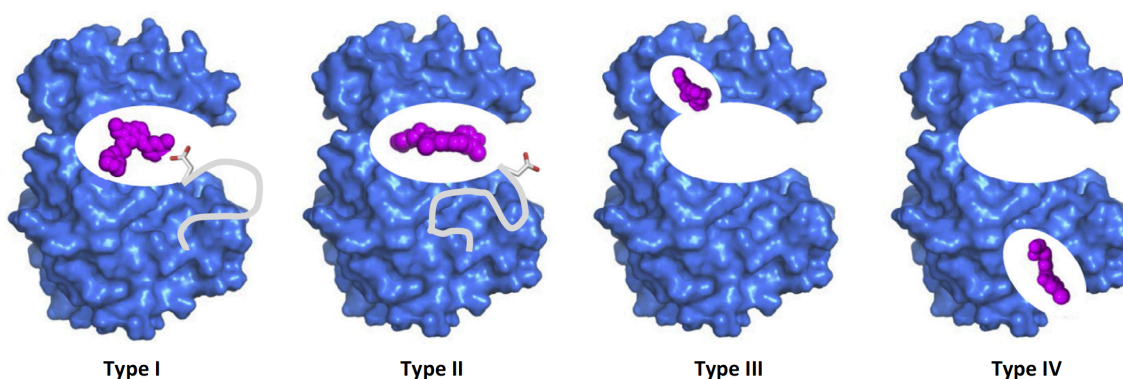
### 1.2.2. Kinase inhibitor binding sites

Based on their binding mode, small-molecule kinase inhibitors (SMKIs) can be classified into different categories:

#### a) Type I inhibitors.

The majority of ATP-competitive inhibitors belong to this group. This type of inhibitor binds to the active kinase conformation, characterized by an open activation loop, the aspartate residue of the DFG motif facing toward the active site (DFG-in), and the  $\alpha$ C-helix adopting an “in” conformation.<sup>95</sup> These inhibitors interact with the kinase

hinge residues through the formation of one to three hydrogen bonds and through hydrophobic interactions with different lipophilic pockets surrounding the adenine ring binding region of ATP.<sup>96</sup>



**Figure 6 | Different types of reversible small-molecule kinase inhibitors.** Type I inhibitors bind to the active conformation of the kinase with the aspartate residue (white backbone) of the DFG motif pointing into the ATP-binding pocket; type II inhibitors bind and stabilize the inactive conformation of the kinase with the flipped aspartate residue facing outward of the binding pocket; type III inhibitors occupy an allosteric pocket that is adjacent the ATP-binding pocket but does not overlap with it; type IV inhibitors bind to an allosteric pocket remote from the ATP-binding pocket. Adapted from ref. 86.

Although the chemical structures are different, type I inhibitors are generally constituted by a heterocyclic ring that locates into the adenine binding site. This core is decorated by different side chains that interact with the adjacent hydrophobic regions I and II.<sup>96</sup> An example of type I kinase inhibitor is **dasatinib** (Sprycel<sup>®</sup>, Bristol-Myers Squibb Company) that binds to the active conformation of BCR-ABL and it is used to treat CML and ALL (acute lymphoblastic leukemia) (**Figure 7**).

#### **b) Type II inhibitors.**

In contrast, although type II kinase inhibitors still have contact with the hinge, these inhibitors bind to the kinase in an inactive protein conformation. This conformation is characterized by a closed activation loop and the aspartate residue of the DFG motif protruding from the ATP binding site (DFG-out).<sup>97</sup> This type of inhibitors lock the protein in the inactive conformation by exploiting an additional hydrophobic pocket (back pocket) adjacent to the ATP binding site that is formed during the transition from the DFG-in to the DFG-out conformation.

In comparison with type I inhibitors, type II are generally less promiscuous. This is because the active protein kinase conformations are highly conserved within the kinase family, while inactive conformations are much more variable.<sup>98</sup> Examples of FDA-approved type II kinase inhibitors are **imatinib**, **nilotinib** (Gleevec<sup>®</sup> and Tasisign<sup>®</sup>, respectively, Novartis) both targeting BCR-ABL or **sorafenib** (Nexavar<sup>®</sup>, Bayer and Onyx Pharmaceuticals Inc.) targeting vascular endothelial growth factor receptor (VEGFR) (**Figure 7**).

### c) Type I ½ inhibitors.

Type I ½ inhibitors bind within the ATP-binding pocket of an inactive kinase conformation with a DFG-in and  $\alpha$ C-helix out conformation, thereby exhibiting binding features of both type I and II inhibitors. An example of this type of inhibitor approved by FDA is **dabrafenib** (Tafinlar<sup>®</sup>, GlaxoSmithKline) (**Figure 7**) targeting B-RAF and used in the treatment of BRAF-V600/K mutants in melanoma.

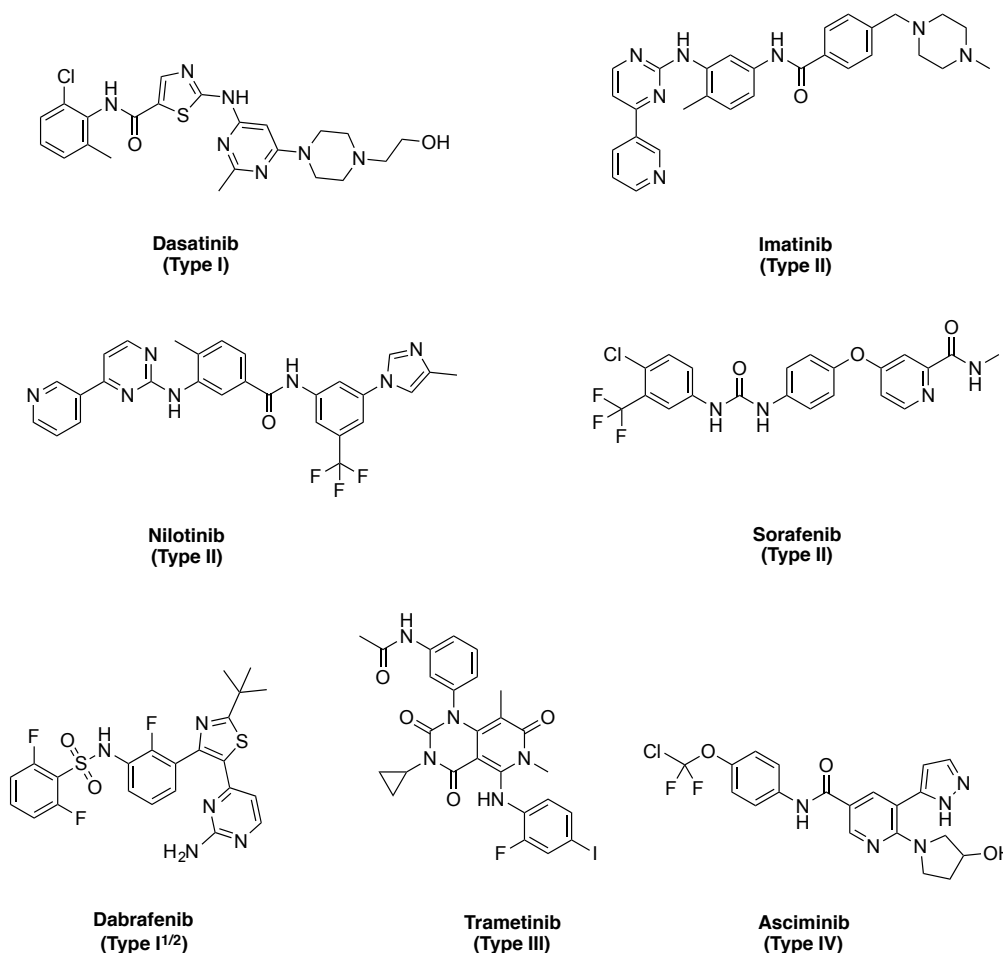
### d) Type III inhibitors.

In the third type of kinase inhibitors is constituted by compounds that bind exclusively in an allosteric pocket adjacent to ATP without making any interaction with the ATP-binding site.<sup>93,99</sup> These inhibitors bind to an inactive conformation of kinases and may or may not be ATP competitive.<sup>59</sup> The MEK inhibitor **trametinib** (Mekinist<sup>®</sup>, GlaxoSmithKline) (**Figure 7**) is the only type III kinase inhibitor approved by the FDA and is also used for the treatment of melanoma bearing mutant BRAF-V600E/K.

### e) Type IV inhibitors.

Type IV inhibitors also bind in an allosteric pocket and do not engage in any interaction with the ATP-binding site. However, conversely to type III inhibitors, the allosteric binding site is distant from the active site, and they act stabilizing an inactive form of the kinase.<sup>100</sup> An example of type IV inhibitor is **asciminib** (Novartis) (**Figure 7**), a BCR-ABL inhibitor currently in clinical trials. No type IV agents have been approved by the FDA yet.

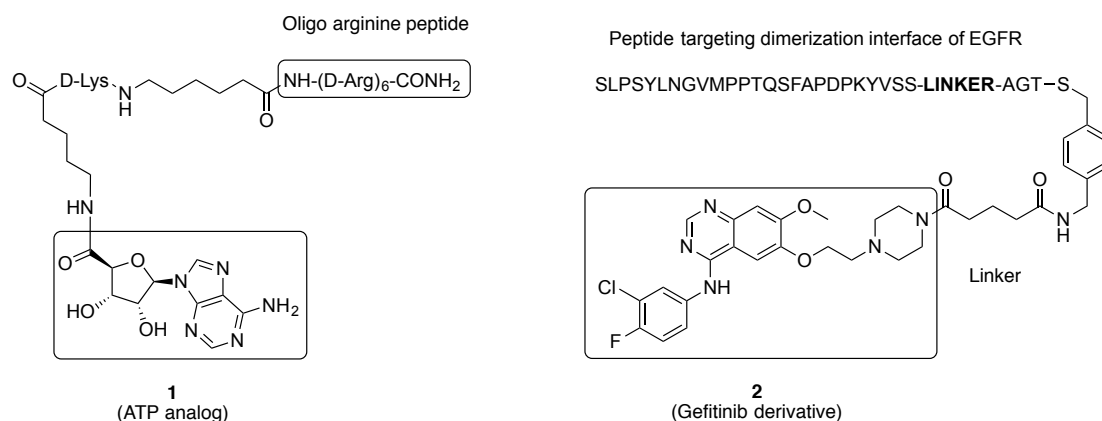
Inhibitors belonging to the two previous categories (type III and IV) interact with binding sites and regulatory structures that are unique to a particular kinase. This is why these inhibitors tend to exhibit the highest degree of target selectivity.



**Figure 7 | Chemical structures of different types of representative reversible small-molecule kinase inhibitors.** Source: own construction.

#### f) Type V inhibitors.

Type V inhibitors are bisubstrate and bivalent inhibitors that span two regions of the protein kinase. Typically, these inhibitors chemically combine elements from type I-IV inhibitors, and are generated by linking an ATP-competitive small molecule to a ligand that targets a region outside of the ATP-binding cleft of a kinase of interest.<sup>101</sup> Consequently, this approach leads to inhibitors with high potency and selectivity of inhibition, although the high molecular weight of these inhibitors may hinder their oral bioavailability and cell penetration.<sup>102</sup> Examples of type V kinase inhibitors are shown in **Figure 8**.



**Figure 8 | Representative type V bisubstrate and bivalent inhibitors.** (A) A bisubstrate analog inhibitor, that links an ATP analog with an oligoarginine substrate site binding peptide targets PKAc kinase. (B) A bivalent inhibitor targeting EGFR. Adapted from ref. 101.

### g) Type VI inhibitors.

The type I-V inhibitors are reversible. In contrast, type VI inhibitors are capable of forming an irreversible, covalent bond to the ATP-binding pocket of the targeted kinase, most frequently by reacting with a nucleophilic cysteine residue.<sup>103</sup>

The design of this type of inhibitors typically begins with already described inhibitors with submicromolar binding affinity to the target of interest.<sup>104</sup> Over these scaffolds and aided by structure-guided approaches, an electrophilic moiety is incorporated into the structure. The obtained molecules initially bind noncovalently to the target, and then, if the electrophilic “warhead” is appropriately located, covalent bond formation takes place by reacting towards a close electron-rich sulfur present in a cysteine residue, permanently disabling enzymatic activity (**Figure 9**).

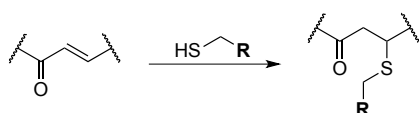
Among the FDA-approved kinase inhibitors belonging to this group are **afatinib** (Gilotrif<sup>®</sup>, Boehringer Inglerheim) (**Figure 9**) targeting EGFR in NSCLC, **ibrutinib** (Imbruvica<sup>®</sup>, Johnson & Johnson) targeting Bruton’s tyrosine kinase (BTK) used to treat B cell cancers, and **osimertinib** (Tagrisso<sup>®</sup>, AstraZeneca) targeting EGFR T970M mutants in NSCLC.

Although a large number of kinases have cysteine residues in and around the ATP-binding site, the possibility of forming irreversible covalent bonds with cysteines of off-target proteins has caused many drug developers to be concerned about the potential for toxicity of covalent inhibitors.<sup>105</sup> Owing to this fact, reversible covalent inhibitors have

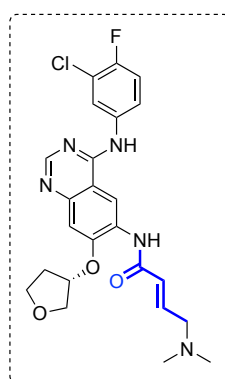
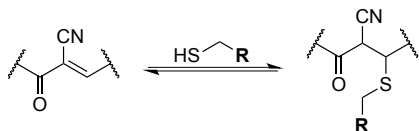


emerged as an alternative to irreversible inhibitors. These type of inhibitors have been developed through the use of electrophiles such as the  $\alpha$ -cyanoacrylamide functionality that undergo reversible Michael addition with cysteine thiols.<sup>106,107</sup> Compound **3** (**Figure 9**) is an example of reversible covalent inhibitors, targeting a noncatalytic cysteine in BTK.<sup>108</sup>

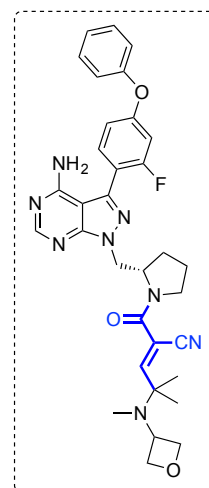
**Irreversible covalent bond formation with cysteine thiols:**



**Reversible covalent bond formation with cysteine thiols:**



**Afatinib**



**3**

**Figure 9 | Irreversible and reversible covalent bond formation between acrylamides, cyanoacrylamides and thiols.** Covalent bond formation of acrylamides and cyanoacrylamides with thiols. Michael adducts of thiols with acrylamides are kinetically stable, whereas cyanoacrylamides form rapidly reversible adducts with thiols. (Afatinib) An irreversible covalent EGFR inhibitor. (3) A cyanoacrylamide-based reversible covalent BTK inhibitor. Adapted from ref. 106.

## 1.3. Discovery of kinase inhibitors

Drug discovery is a very costly and time-consuming process that comprise a series of stages before obtaining a candidate suitable for clinical testing. These stages include the target identification and validation, assay development, screening process, hit compounds identification, lead generation and lead optimization.<sup>109</sup> Among these, the identification of chemical leads represent a key step.<sup>110</sup> Therefore, depending on the approach employed to identify them, kinase inhibitor drug discovery process can be classified into two different categories: target-based drug discovery and phenotype-based drug discovery.

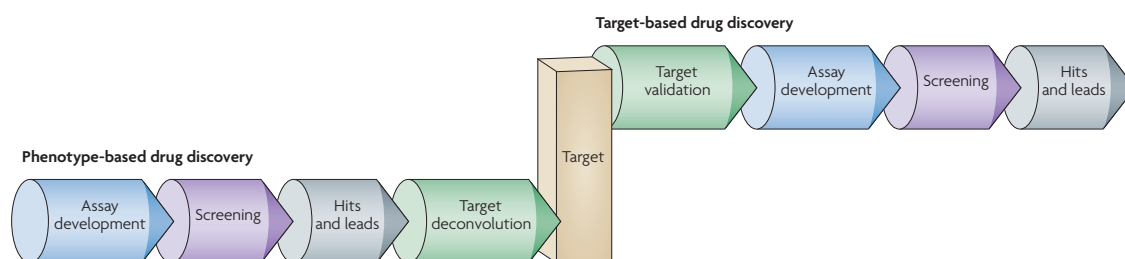


Figure 10 | Phenotype-based versus target-based drug discovery. Taken from ref. 111.

### 1.3.1. Target-based drug discovery

This strategy begins with the selection of a target molecule, a defined protein kinase, that is hypothesized to have an important role in a disease. Then by the use of different screening methodologies and biochemical assays together with the *in silico* protein structure, lead compounds are built. Depending on the approach employed to obtain hit and lead compounds, target-based drug discovery (TBDD) can be classified into two different categories:

#### a) High-throughput screening

The majority of kinase inhibitors developed until date have been discovered by performing high-throughput screening (HTS) of compound collections.<sup>112</sup> HTS is a computer-based serial-testing method that employs robotic systems to identify compounds that are capable of modulating the target of interest. For this purpose this screening method uses miniaturized *in vitro* assays that allow to examine large numbers of synthetic compounds (up to a few million) in very short time.<sup>113,114</sup>

These large set of compounds usually come from archives of inhibitors that were developed by the industry in previous kinase projects or from other medicinal chemistry efforts.<sup>115</sup> The compound sets used for HTS libraries are selected based on their molecular properties, the previous empirical knowledge on suitable scaffolds for kinase inhibitors and by the use of structure-based virtual screening methodologies.<sup>116</sup>

The selected libraries are screened over a single or several targeted protein kinases employing biochemical assays. The results are commonly obtained by optical readout either by detection of ATP depletion (via luciferase), through ADP product formation (via ADP-specific antibody) or by detection of the phosphorylated product.<sup>117</sup> Although full-length proteins are preferred, the use of catalytic domains is widely employed to minimize risks in early project phases.<sup>118</sup> Therefore the majority of inhibitors identified by this methodology bind to the ATP-binding site (type I and II inhibitors).

Typically, from this initial screen many bioactive molecules, which are named positives or primary hits, are identified. Thereafter, successive rounds of screening are conducted over these compounds to validate their activity, potency or to obtain an initial specificity measurement for the target of interest.<sup>119</sup> Particularly, the latter is achieved through the use of kinome-wide screening methodologies that allow to assess their target selectivity and discard promiscuous molecules.<sup>120</sup>

Moreover, hit compounds are also evaluated regarding their structural tractability, compound purity and other physicochemical criteria. Among them, aqueous solubility and octanol-water partition coefficient (log P) play fundamental roles. These two parameters are tightly related as poor aqueous solubility is a typical signature of highly lipophilic compounds (high log P values), and vice versa. To reach a consensus on how to select drug-like compounds with appropriated solubility and permeability values, Lipinski and coworkers from Pfizer Inc. provided a framework for the development of bioavailable drug candidates, which initially was designed for orally available drugs.<sup>121,122</sup> This is commonly referred as the rule of five (RO5) and defines four simple physicochemical parameter ranges:

- No more than 5 hydrogen bond donors.
- No more than 10 hydrogen bond acceptors.
- A molecular weight less than 500 Da.

- log P between -0.4 and 5.

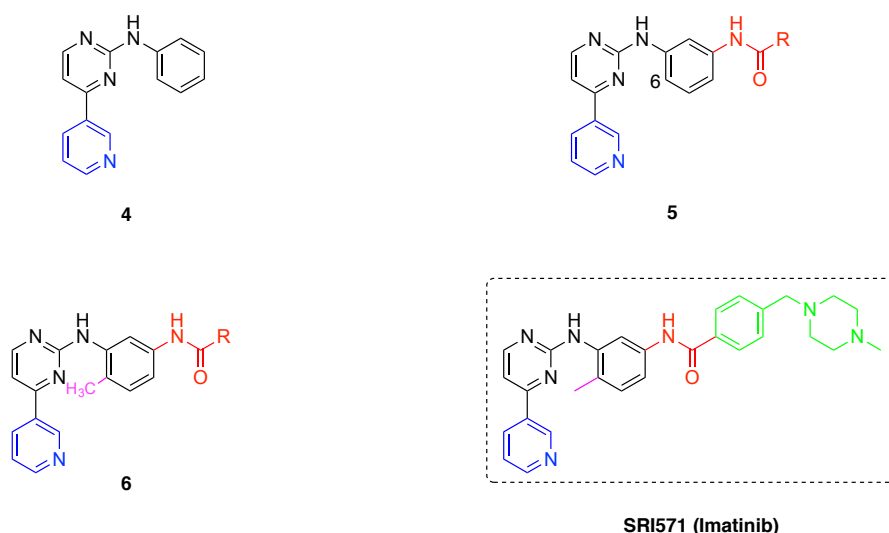
However, these rules were established for drug-size compounds that generally are larger and more lipophilic molecules than their predecessor hits.<sup>123,124</sup> This way, looking to extend the RO5 to hit selection for efficient lead discovery, the rule of three (RO3) was suggested:

- No more than 3 hydrogen bond donors.
- No more than 3 hydrogen bond acceptors.
- A molecular weight less than 300 Da.
- log P lower than 3.
- No more than 3 rotatable bonds.
- A polar surface area = 60 Å.

The implementation of these filters result in the identification of hit compounds, which typically are constituted by molecules derived from the same chemotype or that share similar chemical features. These compounds then enter into the “hit-to-lead” phase, and by the use of different medicinal chemistry strategies, specific analogs or small arrays of these molecules are synthesized in order to study the structure-activity relationship (SAR) behind these chemical series.<sup>125</sup> The hit-to lead process ends with the identification of a series of compounds with appropriate drug-like properties such as pharmacokinetics, bioavailability or specificity.<sup>126</sup> These properties will be later improved in a lead optimization process by further medicinal chemistry efforts. Finally, the compounds that emerge from here go through clinical trials before eventual approval by the corresponding regulatory office.

- **Development of Imatinib**

A successful small molecule protein kinase inhibitor generated via this methodology is the BCR-ABL inhibitor imatinib (Gleevec®, Novartis). This represents a landmark drug that has vastly improved the outcome of patients with chronic myelogenous leukemia (CML) that are Philadelphia chromosome-positive.<sup>127</sup> Indeed, today, someone with CML who is in remission after two years of imatinib treatment has the same life expectancy as someone who does not have cancer.<sup>128</sup>



**Figure 11 | Summary of the chemical optimization of SRI571 (Imatinib) by high-throughput screening.** Adapted from ref. 77.

The development of imatinib started with the identification of the lead compound in a HTS for inhibitors of protein kinase C (PKC). This compound was a phenylaminopyrimidine derivative **4** (Figure 11), and was selected not only for its activity but due to its promising “lead-like” properties and high potential for diversity.<sup>129</sup> From here, the medicinal chemistry efforts made on this scaffold led to a series of structural modifications that finally concluded in the discovery of imatinib.

Initially, derivatives bearing a 3'-pyridyl group at the 4'-position of the pyrimidine provided a strong PKC inhibition that was translated into an enhanced *in vitro* activity. Furthermore, inhibitory activity against tyrosine kinases, such as BCR-ABL kinase, was observed when an amide group was attached to the phenyl ring during the optimization of this compound series **5** (Figure 11). At this point, a fundamental observation from the SAR analysis revealed that the substitution of position 6 of the diaminophenyl ring completely removed the PKC inhibitory activity by blocking rotation about the C-N bond. However, despite the loss of activity against PKC, the simple methyl substituted analog **6** retained or even enhanced the activity against tyrosine kinases.<sup>77</sup>

Subsequently, a highly polar side chain (an N-methylpiperazine) was introduced in order to improve the low solubility in water and poor oral bioavailability of the first series of selective inhibitors. In addition to this, to avoid the mutagenic potential of aniline moieties a spacer was added between the phenyl ring and the N<sup>1</sup> atom from the N-

methylpiperazine.<sup>130,131</sup> From this series, the best compound was SRI571 (Imatinib) and was selected for clinical development (**Figure 11**).

#### **b) Fragment-based drug discovery (FBDD)**

Over the past few years, fragment-based drug discovery (FBDD) has become an established alternative technique of classical HTS for lead generation.<sup>110</sup> This is because FBDD offers potential solutions to some challenges derived from the use of HTS as the need of large compound libraries, inappropriate values for molecular properties or lack of intellectual property space around classical kinase inhibitors (specially type I and II).<sup>85</sup>

FBDD involves the identification of moieties (typically with molecular weight less than 150 Da) that bind to different portions of the target kinase and are then expanded or linked together to generate drug leads.<sup>132</sup>

In contrast to HTS that attempts to evaluate as many compounds as technologically possible, FBDD screening requires a smaller number of compounds (typically several thousand), usually tested at high concentration, in the hope of finding low-affinity but high ligand/ligand-lipophilicity efficiency fragments that can be readily optimized into potent lead molecules.<sup>133</sup>

Typically, unfocused fragment libraries are built to include a great diversity of chemical structures and functional groups that are well precedented in drugs.<sup>134</sup> However, pharmaceutical companies have recently constructed kinase-focused fragment libraries in order to increase hit discovery rates.<sup>135</sup>

The identification of hit (fragments) is done either by measuring the kinase activity using biochemical methodologies, by the use of biophysical methods to detect fragment binding such as nuclear magnetic resonance (NMR) spectroscopy, X-ray crystallography, isothermal titration calorimetry (ITC), surface plasmon resonance (SPR), mass spectrometry or by computational methods.<sup>136</sup> Once the hits are selected, they are optimized using medicinal chemistry, often with additional structural input such as docking, to generate lead compounds that subsequent undergo lead optimization process.

The first kinase inhibitor developed by the FBDD approach and approved by the FDA was vemurafenib (Zelboraf<sup>®</sup>, Roche).<sup>137</sup> A B-RAF kinase inhibitor indicated for the

treatment of advanced melanoma with BRAF V600E mutation that in fact was the first fragment-based drug ever approved.<sup>138</sup>

- **Development of Venetoclax**

Another successful example of the use of FBDD to develop kinase inhibitors relates to the Bcl-2 protein family. These proteins play fundamental roles in apoptosis or, programmed cell death. Antiapoptotic members such as BCL-X<sub>L</sub> and BCL-2 have been found overexpressed in many cancers, contributing to tumorigenesis, progression and in the case of BCL-2, also increasing sensitivity to anticancer drugs and enhancing *in vivo* survival.<sup>139,140</sup> However, the protein-protein interactions of the Bcl-2 protein family have made finding potent and selective small-molecule inhibitors of these proteins a big challenge.

Researchers from Abbott screened a 10,000-member fragment library by NMR approach leading to the identification of three fragment hits (**Figure 12**) that bind at two nearby sites on BCL-X<sub>L</sub>. Subsequently, these molecules were linked leading to compound **7**. Then a NMR-based model of this compound with BCL-X<sub>L</sub> indicated that a linker optimization could lead to a better interaction of the compound with a deep protein pocket. Consequently, the linker was remodeled to replace the carboxylic acid with an acylsulfonamide, leading to a second set of compounds that ultimately led to compound **8**.<sup>141</sup> As a result of considerable lead optimization efforts conducted to remove binding to human serum albumin and increase the affinity of **8** for other BCL family members, the early candidate **ABT-737** was generated.<sup>142</sup> Additional medicinal chemistry yielded **ABT-263**, an orally bioavailable compound with improved pharmacodynamics that binds with high affinity to both BCL-2 and BCL-X<sub>L</sub>.<sup>143</sup>

Finally, the cocrystal structures of BCL-2 with **ABT-263** and other close analogs were used to guide the rational design of **ABT-199**, a first-in-class BCL-2 selective inhibitor.<sup>144</sup> **ABT-199** or **venetoclax** (Venclexta<sup>®</sup>, Abbvie Inc. and Genentech Inc.) was approved by the FDA in 2016 for the treatment of chronic lymphocytic leukemia (CLL) or small lymphocytic lymphoma (SLL), with or without 17p deletion.

It is important to note that the final molecule ABT-199 has an unusually high molecular weight (868 Da) and a high calculated log P (>>5) for a drug candidate, which are properties that compounds derived from HTS would never have. This demonstrates

### 1.3. Discovery of kinase inhibitors

the potential that fragment-based approaches have to discover and explore new potential pharmacologically active molecules.

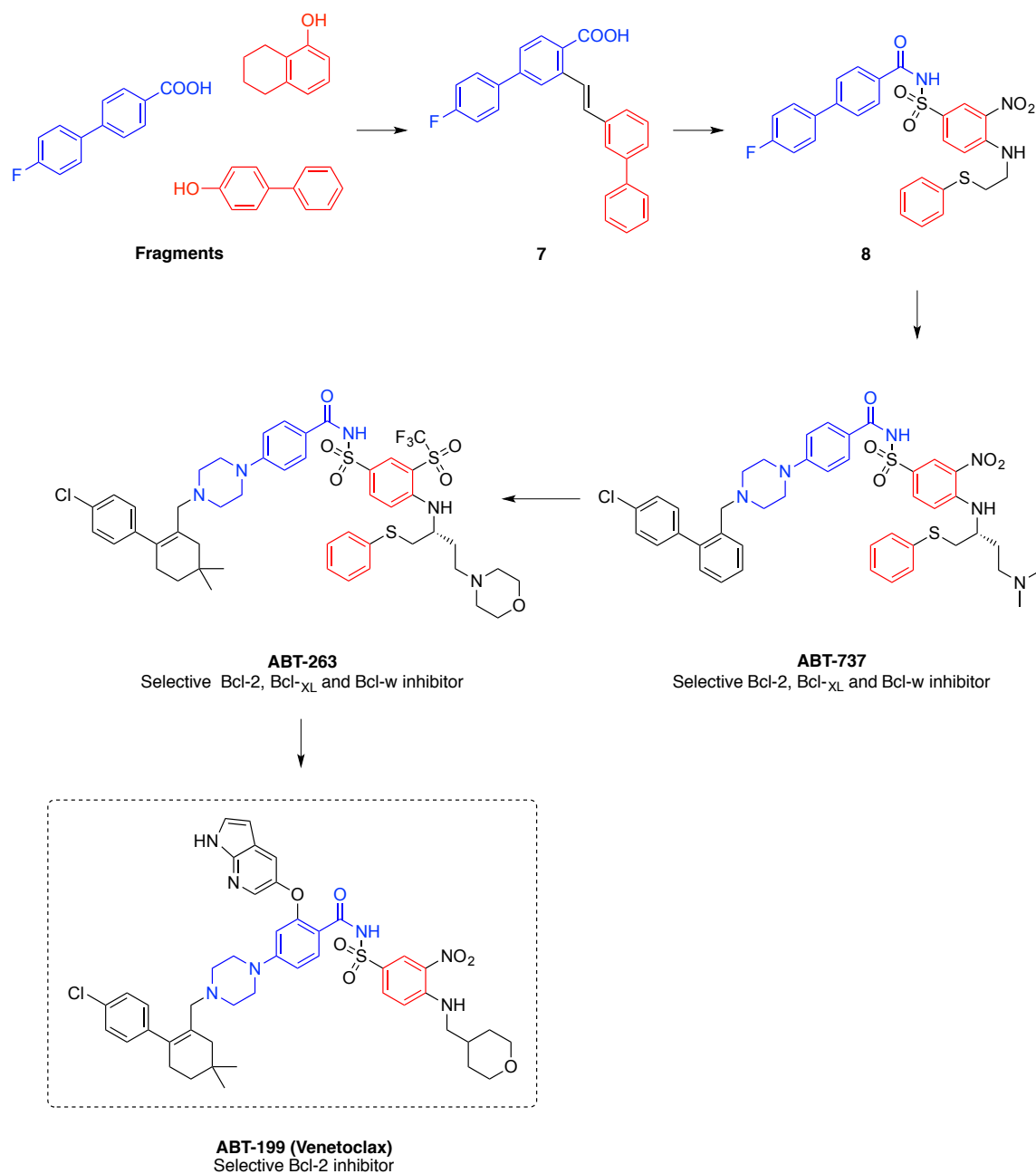


Figure 12 | Discovery of ABT-199 (Venetoclax) by fragment-based drug discovery. Adapted from ref. 110.

### 1.3.2. Phenotype-based drug discovery

Despite TBBDD approaches have been extensively used in the pharmaceutical industry since the 1980s, in the last few years there has been a revival in interest in phenotypic drug discovery (PDD) approaches, which rely on the observed effects that



compounds produce in cells, tissues or organisms, rather than on a purified target protein.<sup>145,146</sup>

The renaissance of PDD has been due to the fact that for the past decade there has been a steady decline in the number of new molecules that enter clinical development and reach the market.<sup>147</sup> Several studies connect this with the extended use of TBDD strategies and the complexity of target validation processes. Although TBDD has been established a superior method for the discovery of “me-too” drugs, the majority of the “firs-in-class” small molecule drugs have been discovered by the use of phenotypic screenings.<sup>148–151</sup>

In PDD, molecules are screened for their ability to modulate an observed phenotype in cell-based assays of model organisms with the aim of select hit or lead compounds.<sup>152</sup> Typical phenotypic cellular endpoints are cell viability, cell death, cell morphology, cell cycle phase, proliferation or migration.<sup>153</sup> From here, hits are identified and are taken through hit to lead drug design, and then on to lead optimization through the application of iterative SAR determinations and phenotypic screening campaigns.

When the lead compounds have been characterized and shown to give consistent phenotype modulation in multiple follow-up assays, target deconvolution to define compounds’ mechanism of action occurs.<sup>111,152</sup> Typically, this is achieved by the use of chemical proteomics strategies, expression cloning-based methods or genetic-based screens, among others.<sup>154</sup> However, although it is highly desirable, target identification is not required for regulatory approval (according to FDA guidance<sup>155</sup>) and it is estimated that between a 7% to an 18% of the FDA-approved drugs lack a defined molecular target.<sup>156</sup>

- **Development of eCF309**

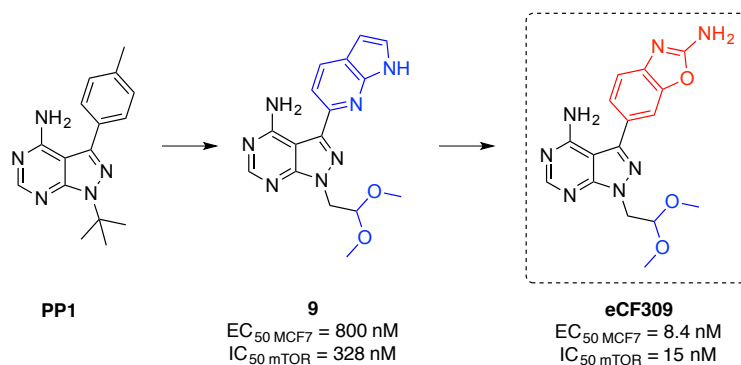
An example of the application of this phenotypic strategy was the discovery of eCF309, a highly selective mTOR inhibitor.

The development of this molecule began with **PP1**, a promiscuous tyrosine kinase inhibitor with poor physicochemical properties.<sup>157</sup> Initially, the *tert*-butyl group at the N1 position of PP1 was substituted with flexible water-solubilizing moieties in order to improve the drug-likeness (**Figure 13**). Additional medicinal chemistry at the C3 position

### 1.3. Discovery of kinase inhibitors

---

led to a compound set that was screened over MCF7 (breast cancer) cells. Compound **9** exhibited the most antiproliferative activity and its kinome profile performed to identify the molecular target showed that **9** inhibited mTOR in the submicromolar range ( $IC_{50} = 328$  nM).<sup>158</sup> Further potency and mTOR selectivity optimization was made by replacement of the pyrrolopyridine substituent at C3 by different heteroaromatic moieties. As a result emerged **eCF309**, which exhibited a potent and selective inhibition of mTOR signaling both *in vitro* ( $IC_{50} = 15$  nM) and in cells ( $EC_{50} = 8.4$  nM).<sup>159</sup>



**Figure 13 | Discovery of eCF309 by phenotype-based drug discovery.** Source: own construction.

## 1.4. Apoptosis and cancer

Among the different strategies used in phenotype drug discovery to identify molecules with potential antitumor activity, cell death induction by interfering with the programmed cell death machinery is the most broadly employed.

### 1.4.1. Types of programmed cell death

Programmed cell death (PCD) is a normal physiological form of cell death that is mediated by an intracellular program with the aim to eliminate any pathological cell in order to reinstate tissue homeostasis. Deregulation of this process is associated with the development of a wide variety of diseases, including cancer, neurodegeneration and developmental and immunological disorders.<sup>160</sup> Among the described PCD types, apoptosis, necroptosis and autophagy are the main ones.

#### a) Apoptosis

This is the primary form of programmed cell death that occurs in the body. The apoptotic process is characterized by a series of specific and well-regulated biochemical and morphological cellular changes that ultimately lead to cell death with minimal damage to surrounding tissues. The cellular changes include cytoplasmatic shrinkage, chromatin condensation (pyknosis), nuclear fragmentation (karyorrhexis), plasma membrane blebbing and loss of adhesion to neighbor cells or to the extracellular matrix, culminating with the formation of small vesicles (apoptotic bodies) that are degraded within lysosomes of the surrounding phagocytic cells.<sup>161</sup> Biochemical modifications include chromosomal DNA fragmentation and protein cleavage, protein cross-linking and phosphatidylserine externalization.<sup>162</sup>

#### b) Autophagy

It is a highly conserved catabolic process performed by the cell to allow the degradation of internal components, such as organelles, soluble proteins, macromolecular complexes, aggregated proteins and foreign bodies.<sup>163,164</sup> This process is initiated by the formation of double-membraned cup-shaped structures (phagophores). After elongation, sequestration of cytoplasmic material and fusion of the membranes, these structures lead to the formation of a double-membrane vesicles called autophagosomes, which

## 1.4. Apoptosis and cancer

---

subsequently fuse with lysosomes and form autolysosomes, where the cytoplasmic material is degraded.<sup>165,166</sup>

### c) Necroptosis

This is a regulated form of necrotic cell death. Therefore, necroptosis is generally characterized by a necrotic morphotype, which include cell swelling, organelle dysfunction, membrane disruption and cell lysis, with the consequently release of the intracellular content and the activation of pro-inflammatory responses.<sup>167</sup>

### d) Others forms of programmed cell death

Although the aforementioned forms represent the major types of programmed cell death, many other regulated cell death processes have been identified. These include **anoikis**, a form of apoptosis triggered by inappropriate cell/extracellular matrix interactions;<sup>168</sup> **ferroptosis**, a form of regulated necrosis marked by iron-dependent lipid peroxidation;<sup>169</sup> **pyroptosis**, also known as caspase-1-dependent programmed cell death;<sup>170</sup> or **parthanatos**, a form of regulated necrosis induced by the overactivation of the nuclear protein poly (ADP-ribose) polymerase 1 (PARP1)<sup>167</sup>.

## 1.4.2. Mechanisms of apoptosis induction

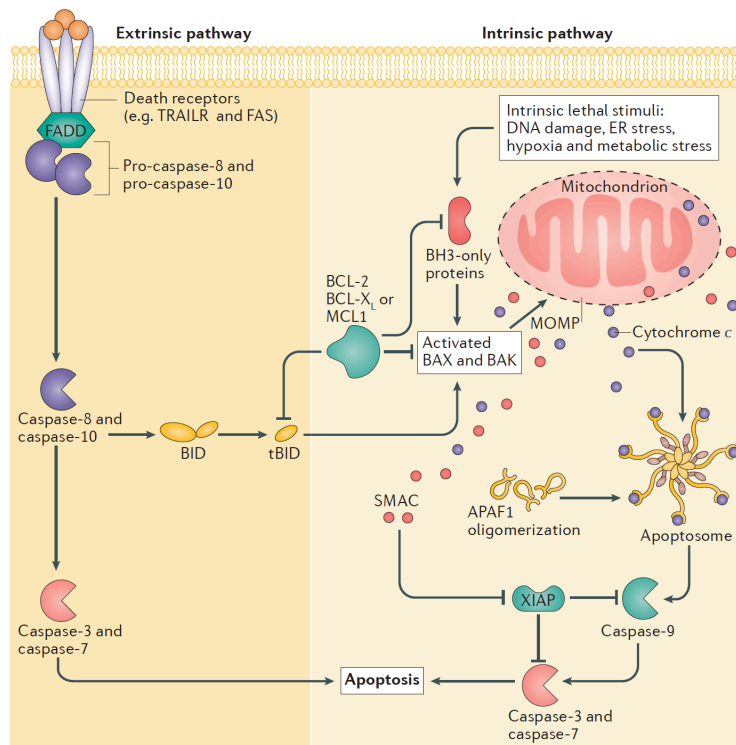
Many cells that die in humans do so by apoptosis. This mechanism naturally occurs to maintain the tissue homeostasis during development and aging but also as a defense mechanism to eliminate damaged cells.<sup>171</sup>

Caspases are the principal executors of this type of PCD. They are a family of cysteine-aspartic proteases that selectively cleavage cellular components leading to the morphological and biochemical hallmarks of apoptosis.<sup>172</sup> Depending on the pathway through caspases are activated, apoptosis can be triggered by two pathways: the extrinsic or death receptor pathway and the intrinsic or mitochondrial pathway (**Figure 14**).

### a) Extrinsic pathway

As its name implies, the extrinsic pathway requires extracellular stimulation to induce apoptosis. This occurs through the binding of cell death signals (also called death ligands) to death receptors (DRs), such as TNF-related apoptosis-inducing ligand receptor

1 (TRAILR1), TRAILR2, FAS or TNF receptor 1 (TNFR1), all of them cytoplasmic transmembrane receptors. After ligand binding, adaptor proteins such as FAS-associated death domain protein (FADD) or TNF receptor-associated death domain (TRADD) are recruited to the receptor. Then procaspases-8 and -10 bind to the adaptor protein, forming the death-inducing signaling complex (DISC). This complex activates both procaspases leading to the caspase-8 and -10 that are able to activate executioner caspase-3 and -7, which begin the protein and cytoskeleton cleavage leading to apoptosis.<sup>173,174</sup>



**Figure 14 | Extrinsic and intrinsic apoptotic signaling pathways.** Taken from ref. 174.

### b) Intrinsic pathway

This pathway is triggered by a wide variety of intracellular stress stimuli such as DNA damage, growth factor deprivation, hypoxia, endoplasmic reticulum (ER) stress, high concentrations of  $\text{Ca}^{2+}$ , irradiation and oxidative stress. These cell-stress signals promote mitochondrial outer membrane permeabilization (MOMP) through the accumulation of Bcl-2 homology domain 3 (BH3)-only proteins that leads to the activation of BAX and BAK proteins.

As a consequence of the MOMP, mitochondrial intermembrane space proteins such as cytochrome *c* and second mitochondria-derived activator of caspases (SMAC) are

released into the cytosol. The cytochrome *c* binds apoptotic protease activating factor 1 (APAF1), leading to the formation of the apoptosome. Within this complex, procaspase-9 is transformed into the active caspase-9, which cleave and activate the effector caspase-3 and -7, leading to cell death. SMAC facilitate caspase activity by inhibiting an endogenous inhibitor of caspase function, the X-linked inhibitor of apoptosis protein (XIAP).<sup>175</sup>

In addition, as a mechanism to ensure apoptosis, both extrinsic and intrinsic pathways are connected through the caspase-8 cleavage of BID (BH3 interacting-death domain agonist), which generates its active and truncated form tBID that eventually triggers MOMP.

### 1.4.3. Apoptosis checkpoints and cancer.

Resisting cell death is one of the hallmarks of cancer.<sup>42</sup> There are many strategies by which tumor cells acquire the capability to limit or circumvent the programmed cell death machinery.<sup>176</sup> They can be mainly divided into: imbalance between pro-apoptotic and anti-apoptotic proteins; impaired death receptor signaling; and reduced caspase activity (Figure 15).<sup>177</sup>

#### a) Imbalance between pro-apoptotic and anti-apoptotic proteins.

- **Bcl-2 protein family.** Proteins of the B-cell lymphoma-2 (Bcl-2) family regulate the intrinsic apoptotic pathway by controlling MOMP. This control is driven through direct protein-protein binding interactions between the different proteins of the family.<sup>178</sup> Bcl-2 family can be divided into three groups of proteins based on their primary function: anti-apoptotic proteins (BCL-2, BCL-X<sub>L</sub>, BCL-W, MCL-1, BFL-1/A1), pro-apoptotic BH3-only proteins (BID, BAD, BIK, BIM, BMF, HRK, NOXA, PUMA, etc.) and executioner pro-apoptotic proteins (BAX, BAK).

In the absence of apoptotic signals, the anti-apoptotic Bcl-2 family members block the apoptosis process by inhibiting both BH3-only and executioner proteins. In contrast, the presence of apoptotic stimuli upregulate BH3-only proteins and/or downregulate anti-apoptotic Bcl-2 proteins. This creates a

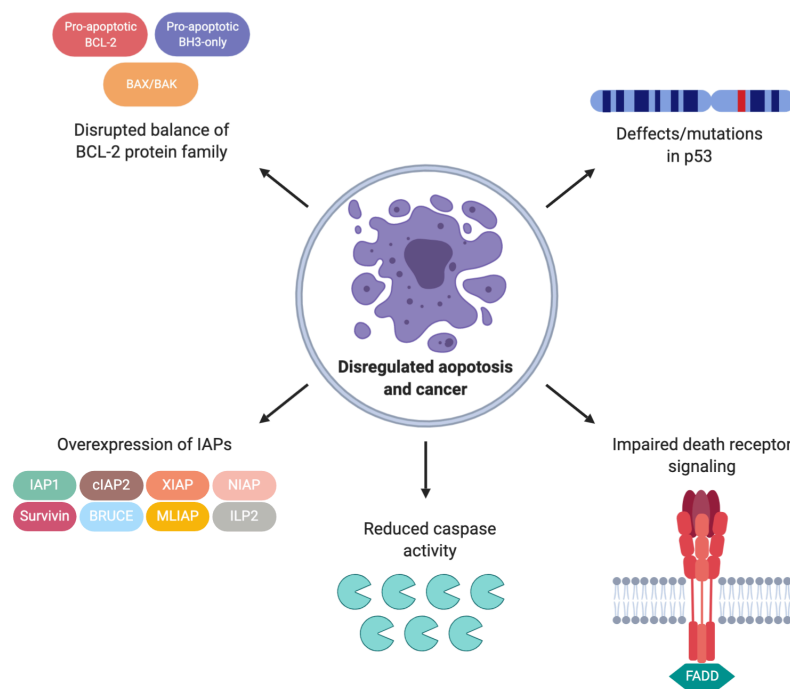
protein imbalance that leads to the activation of executioner proteins (BAX, BAK), which finally undergo MOMP and trigger apoptosis.<sup>179</sup>

Either an increase in the expression of anti-apoptotic Bcl-2 protein members, a decrease of pro-apoptotic Bcl-2 proteins, or a downregulation of apoptotic executioner proteins have been observed in many cancer types such as NSCLC, breast cancer, CML and melanoma.<sup>180</sup> Additionally, oncogenic mutations in these cancers result in somatically activated downstream kinase signaling pathways (RTK/RAS, JAK/STAT, PI3K/AKT/mTOR) that also control Bcl-2 family protein expression and ultimately suppress apoptosis.<sup>179,181</sup>

- **p53.** Tumor protein 53 (p53) is the major tumor suppressor and it has been reported to be mutated in more than 50% of human cancers. Under normal cellular conditions the levels of p53 are very low. However, cellular stress, particularly DNA damage and oncogene activation, induces p53 accumulation and activation. This triggers the intrinsic apoptotic pathway by upregulation of pro-apoptotic proteins (BIM, PUMA, NOXA) that eventually induce MOMP by BAX/BAK activation.<sup>182</sup> Apart from apoptosis, p53 is known to control senescence, cell cycle, metabolic adaptation and DNA repair by regulating more than 500 genes.<sup>183</sup>
- **Inhibitors of apoptosis proteins (IAPs).** The IAP protein family is constituted by a group of proteins characterized by the presence of the baculovirus IAP repeat (BIR) domain.<sup>184</sup> In the human body this family is formed by 8 members: IAP1, cIAP2, XIAP, NAIP, Survivin, BRUCE, MLIAP and ILP2. Among other cellular process, IAPs are involved in controlling both the extrinsic and intrinsic apoptosis pathways by inhibiting the caspase activity. The caspase inhibition by IAPs is mediated through the interaction of their conserved BIR domains with the caspase active sites, leading to inactive caspases and promoting their degradation. Abnormal expression of IAPs is frequently found in many cancers including NSCLC, pancreatic cancer, melanoma and lymphoma, and also contribute to disease progression and chemoresistance.<sup>185,186</sup>

**b) Impaired death receptor signaling**

The binding of death ligands to their death receptors is the initial step that triggers the extrinsic pathway of apoptosis. Alterations in the death receptor signaling pathway either by downregulation of death receptors, receptor dysfunction and mutations on adaptor proteins or DISC components promote cell survival by resistance to extracellular apoptotic signals. These alterations have been identified in several types of tumors including breast, bladder and lung cancers.<sup>187,188</sup>



**Figure 15 | Mechanisms contributing to evasion of apoptosis and carcinogenesis.** Adapted from ref. 177.

**c) Reduced caspase activity**

Caspases are the final effectors of apoptosis. Therefore, it is not surprising that altered caspase function has been found in many types of cancer.<sup>177</sup> The caspase dysfunction is commonly due to mutations of these proteins or downregulation of the caspase activity by the inactivation of upstream signal mediators through previously mentioned mechanisms.<sup>189</sup>



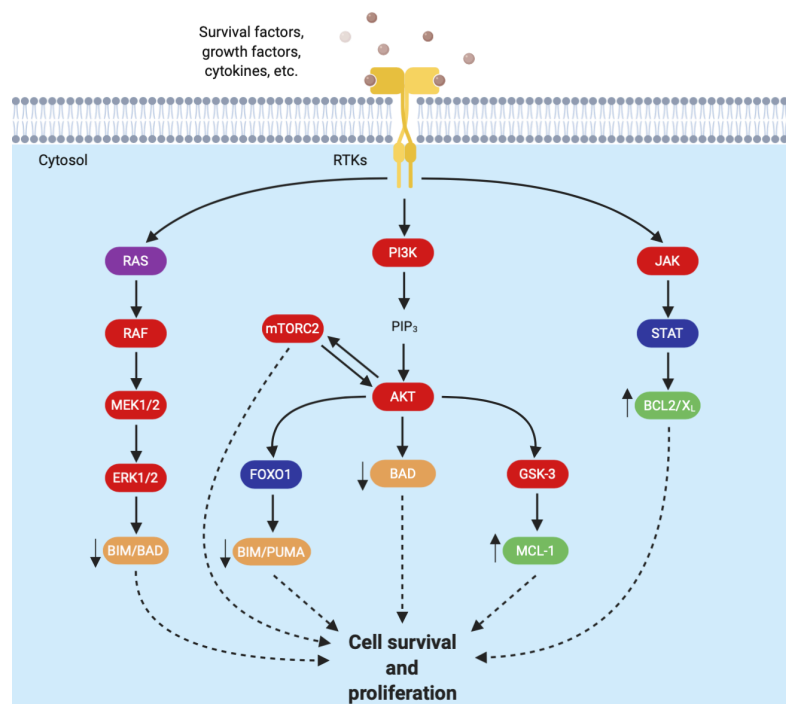
### 1.4.4. Protein kinases and apoptosis

Apoptosis is regulated by an intricate interplay between pro-apoptotic and anti-apoptotic proteins. Protein kinases are involved in the regulation of either proliferation and cell death pathways by the activation or inhibition of key members of the cellular signaling machinery.

The most studied kinase-regulated cell proliferation pathways are RAS/RAF/ERK, PI3K/AKT and JAK/STAT.<sup>190</sup> These routes are initiated with the activation of transmembrane receptor tyrosine kinases (RTKs), such as EGFR, HER2, FGFR and insulin receptor (InsR), in response to survival and proliferation stimuli (growth factors, hormones and cytokines). This initiates signaling cascades that finally influence the transcription and post-transcriptional modification of certain downstream targets to commit cell survival. (**Figure 16**)

- a) **RAS/RAF/ERK pathway.** Receptor activation induces RAS phosphorylation and activation, which then activates RAF. Once active, RAF phosphorylates and activates MEK, a dual specificity tyrosine/threonine kinase that in turn activates by phosphorylation ERK1 and ERK2. Both kinases activate cell survival and proliferation by downregulation of pro-apoptotic BH3-only proteins (BIM, BAD) expression.<sup>191,192</sup>
- b) **PI3K/AKT/mTOR pathway.** RTKs stimulation trigger activation of PI3K, which phosphorylates the lipid phosphatidylinositol-4,5-bisphosphate (PIP<sub>2</sub>) producing phosphatidylinositol-3,4,5-triphosphate (PIP<sub>3</sub>). AKT (also called Protein Kinase B, PKB) binds to PIP<sub>3</sub>, is phosphorylated and activated.<sup>193</sup> The catalytically active AKT promotes cell survival and proliferation through the interaction with several key mediators, including FOXO1 transcription factor, and mTORC2.<sup>194,195</sup>

## 1.4. Apoptosis and cancer



**Figure 16 | Summary of the major kinase pathways that control cell survival and proliferation.** Purple: GTPase, red: protein kinase, orange: pro-apoptotic Bcl-2 protein, green: anti-apoptotic Bcl-2 protein, blue: transcription factor. Source: own construction.

In addition to this, the mediators of these pathways are also regulated by other kinases and proteins forming an intricate regulation network. Among these secondary regulatory proteins are the protein kinase C (PKC), which activates RAF;<sup>191</sup> PTEN, an inhibitor of the PI3K pathway; the Src family kinases;<sup>196</sup> or the death-associated protein kinase family (DAPK), which regulates ERK and microtubule assembly.<sup>197,198</sup>

Deregulation of these pathways is a common feature of cancer cells to evade apoptosis and has been reported in many types of cancer. Typically, these alterations include mutations on *ras* genes, which have been identified to be present in 30% of all human cancers; the generation of constitutively active tyrosine kinase BCR-ABL, which is present in CML; the aberrant activation of STATs;<sup>199</sup> or activating mutations of PI3K.<sup>200</sup>

For this reason, reversion of apoptosis evasion is a highly desired effect in cancer therapy. Thus the majority of chemotherapeutic and targeted drugs exert their action by inducing apoptotic cell death. Chemotherapeutic drugs typically activate the intrinsic apoptotic pathway by different mechanisms. Carboplatin induces a cytosolic release of Ca<sup>2+</sup>, mitochondrial depolarization and oxidative stress that ultimately activate caspases

leading to apoptosis.<sup>201</sup> Doxorubicin acts in a similar manner, because it induces oxidative stress while at the same time decreases anti-apoptotic BCL-2 protein expression.<sup>202</sup> On the other hand, targeted drugs directly bind to a specific, typically upregulated or altered (BCR-ABL, ALK, B-RAF, JAK, BTK, etc.), pro-survival protein and inhibiting it, promoting apoptotic cell death or improving the treatment effectiveness.

## 1.5. Purine derivatives as antitumor drugs

The purine ring system is the most abundant nitrogen-based heterocycle in nature.<sup>203,204</sup> This scaffold is a component of guanine and adenine, and therefore appears in nucleic acids and cofactors. Moreover, this scaffold is presented in many ligands and substrates from key regulatory elements such as protein kinases, polymerases and G proteins.<sup>205,206</sup> Due to the ability of purines to establish polar interactions through their nitrogen atoms or interact with hydrophobic pockets, several compound libraries based on this ring have been generated in the search for inhibitors of biological processes.<sup>207</sup>

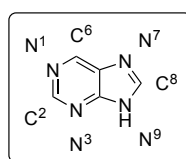


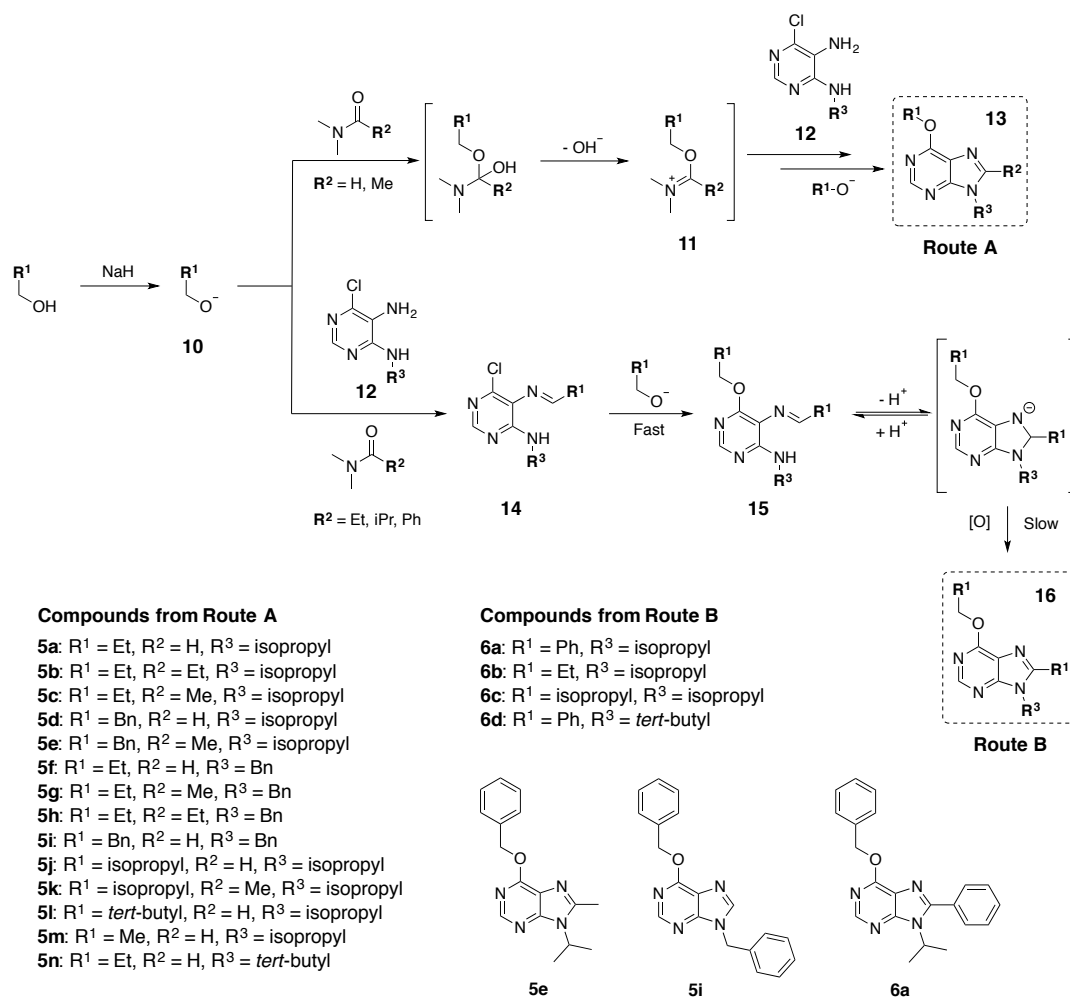
Figure 17 | Purine ring.

Typically, purine analogs have been designed by substitution of the positions 2, 6, 8 or 9 with different aliphatic or aromatic groups. Our group developed a new synthetic strategy to prepare purine derivatives substituted at positions C6, C8 and N9, using different 6-chloro-4,5-diaminopyrimidines, alcohols and *N,N*-dimethylamides under strong basic conditions.<sup>208,209</sup>

Additionally, we reported that two different synthetic pathways can take place, depending on the size of *N,N*-dimethylamide's side chain ( $R^2$  group):

- When amides with small  $R^2$  groups such as *N,N*-dimethylformamide or *N,N*-dimethylacetamide are employed, the purine derivatives generated contain H or methyl at C8, respectively (13). This reaction occurs by in situ generation of alkoxyminium species (11), which are created by reaction between the amides and alkoxydes, Route A (Figure 18).
- On the contrary, when steric hindered amides such as *N,N*-dimethylpropionamide, *N,N*-dimethylisopropionamide or *N,N*-dimethylbenzamide are used, Route A is impeded. Consequently, purine analogs are generated by a metal-free oxidative coupling of primary alkoxydes and diaminopyrimidines with Schiff

base formation (**14**) and subsequent annulation (**16**), **Route B (Figure 18)**. In this case, the substituent in the C8 position comes from the primary alcohol employed.



**Figure 18 | Synthesis of the initial 18-purine library.** Synthetic routes for the preparation of compounds 5a – 5n (Route A) and 6a – 6d (Route B). Chemical structures of most active compounds of this series 5e, 5i, 6a. Adapted from ref. 209 and 210.

Moreover, in both routes take place the displacement of the chlorine atom at C6 by alkoxides, providing the corresponding ether substituent at this position (**13**, **15**). All this, together with the selection of the R<sup>3</sup> moiety of the starting pyrimidine, confer this synthetic methodology the capability to generate a structural diversity of purine analogs in order to produce novel compounds with pharmacological interest.

Motivated by the potential biological properties of these scaffolds, a library of 18 purines was synthesized using a range of different pyrimidines, *N,N*-dimethylamides and alcohols.<sup>210</sup>

Following a phenotypic approach, the compounds were screened against two haematopoietic tumor cell lines: Jurkat (acute T cell leukemia) and K562 (chronic myelogenous leukemia), and cell proliferation was determined by the colorimetric MTT assay after 48 h. From this initial set, compounds **5e**, **5i**, and **6a**, which all interestingly contained the benzyloxy group at the C6 position, inhibited the cell proliferation by 50 % or more at 50  $\mu\text{M}$  and were selected as hit compounds for further phenotypic characterization.

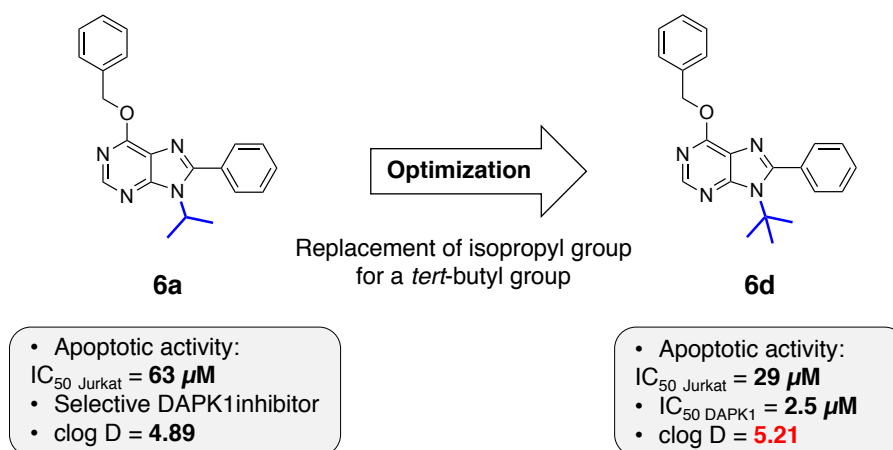
Half-maximal inhibitory concentration ( $\text{IC}_{50}$ ) values were then calculated for the three hits in Jurkat and K562 cells, highlighting the derivative **6a** as the most potent compound, with  $\text{IC}_{50}$  values of 63  $\mu\text{M}$  and 154  $\mu\text{M}$ , respectively.

In order to study the biological mechanism behind this antiproliferative effect, cell cycle analyses were performed with **6a** in both cell lines. The resulted accumulation of cells within the sub-G1 region was consistent with apoptotic populations. This, together with Annexin-V staining assays and caspase activation analysis confirmed that the observed cell death was induced by apoptosis. Additionally, **6a** was tested over primary lymphocytes, where exhibited significantly less activity than in tumor cells.

To identify the target/s that could be responsible of the apoptotic effect induced by **6a**, this compound was tested against a panel of 96 kinases known to be involved in apoptosis processes. Surprisingly, only one kinase showed a significant reduction in its activity (51 % at 10  $\mu\text{M}$ ), the Death Associated Protein Kinase 1 (DAPK1). This protein is a serine/threonine kinase with a tumor suppressive function that also mediate a wide range of cellular processes, including apoptosis, and has been shown to be very difficult to be selectively targeted.<sup>211,212</sup>

The selective inhibition of **6a** for DAPK1 prompted us to optimize this molecule in order to enhance its activity. For this purpose, the isopropyl group at N9 position of the purine ring, which typically binds to lipophilic pockets of kinases, was substituted by a *tert*-butyl group in order to improve the binding affinity with DAPK1. Hence, compound **6d** (**Figure 19**) was synthesized using the same synthetic methodology, and cell cycle analysis,  $\text{IC}_{50}$  determinations (29  $\mu\text{M}$  in Jurkat and 120  $\mu\text{M}$  in K562), Annexin-V and caspase activation assays showed that this new compound possessed improved biological properties than **6a** at the same time that maintained the apoptotic effect. Moreover, an

enzymatic assay of **6d** with DAPK1 revealed an inhibitory activity at the low micromolar level ( $IC_{50}$  of 2.5  $\mu\text{M}$ ) and Western Blot analysis showed that this compound exerts its activity preventing the autophosphorylation of DAPK1 of Ser308 from the regulatory domain.<sup>213</sup>



**Figure 19 | Chemical optimization of 6a by phenotypic approach.** The replacement of the isopropyl group attached at N9 for a *tert*-butyl group to give rise to 6d. Source: own construction.

This way, our group reported the first DAPK1 selective inhibitors. Additionally, these purine scaffolds are atypical kinase inhibitors as they do not contain the classical amino group at the C6 position, which is a structural characteristic of purine kinase inhibitors to interact with the hinge region by hydrogen bonds.<sup>82</sup> Conversely, these 6-benzyloxy purines contain an ether moiety that acts as an hydrogen bond acceptor instead of a donor.<sup>214,215</sup>

Despite this rare structural feature and selectivity, the marked lipophilicity of **6a** and **6d** (cLog D of 4.89 and 5.17, respectively) (**Figure 19**) that seems to be associated with their activity, confers these structures poor physicochemical properties. Therefore, future strategies should be guided to enhance the water solubility of these scaffolds at the same time that certain lipophilic character is maintaining.





## **2. Objectives**

---



The purine core represents a key scaffold for the development of small molecules kinase inhibitors that interfere with the biological machinery of cancer cells. By a novel synthetic methodology, our group developed new purine-based molecules substituted at position C6, C8, C9 and characterized by the presence of an ether group at C6 position. Guided by a phenotypic approach, these unusual structures showed selective pro-apoptotic activities over Jurkat cells. Target deconvolution efforts indicated that they selectively inhibit DAPK1, a protein kinase barely targeted and critically involved in the development of many types of cancer.

The appealing biological activities of these molecules together with the growing interest in targeted therapies for the treatment of cancer took us to initiate a comprehensive study of these scaffolds and generate structural alternatives to solve the lipophilicity issues of these compounds.

Therefore, the main objective of this thesis is the study, by a phenotypic approach, of the 6-alkoxypurine scaffold as a template for the generation of bioactive molecules highly active against cancer cells. To achieve this overall objective, we designed the following

Specific aims:

1. To improve the pro-apoptotic activity of previous compounds (**6a**, **6d**) over Jurkat cells through the introduction of different moieties at positions C2, C6, C8 or N9, using the in-house developed two-step synthetic methodology.
2. To enhance the physicochemical properties of the active 6-alkoxypurine derivatives containing lipophilic groups through the introduction of *N,N*-dialkylamino or 1-azacycloalkane-1-yl moieties at position N9.
3. To develop a synthetic methodology that allows a comprehensive exploration of the 6-alkoxypurine scaffold by the introduction of different substituents at positions C6, C8 and N9, including a structural expansion of the 6-alkoxypurine core at C6 by the implementation of copper(I)-catalyzed alkyne-azide [3 + 2] cycloadditions.
4. Purification and unequivocal characterization of the synthesized compounds by <sup>1</sup>H-NMR, <sup>13</sup>C-NMR and HRMS.

## 2. Objectives

---

5. Biological evaluation of the synthesized compounds by a phenotypic screening approach guided by cell cycle analysis and proliferation measurements over a panel of cancer cell lines, focusing on pro-apoptotic effects.



## **3. Materials and Methods**

## 3.1. Chemistry methods

Reactions involving air sensitive reagents and anhydrous solvents were performed in glassware that had been dried in an oven (110 °C). These reactions were carried out with the exclusion of air using an argon atmosphere. Microwave reactions were performed in a Biotage Initiator microwave synthesizer.

### 3.1.1. Chemicals

Chemicals that were commercially available were obtained from one of the following sources: Thermo Fischer Scientific, Fluorochem, Sigma-Aldrich, VWR International Ltd and Enamine. All reagents were used as received, unless otherwise stated.

### 3.1.2. Chromatography

Reactions were monitored by thin layer chromatography (TLC). TLC was run on Merck TLC Silica gel 60 F<sub>254</sub> plates, with detection being achieved through using a 254 nm UV source and/or by staining with a ninhydrin or KMNO<sub>4</sub> solution dip. Purification was achieved through flash column chromatography using silica gel (40-63 µm, VWR International Ltd or 220-240 mesh, Sigma-Aldrich) as the stationary phase and commercially available solvents (hexane, ethyl acetate, dichloromethane, methanol) as eluent.

### 3.1.3. Nuclear Magnetic Resonance

All NMR spectra were recorded at ambient temperature on a Varian Innova Unity (300 MHz), BRUKER Nanobay Avance III HD (400 MHz) or BRUKER Avance NEO (400 or 500 MHz) spectrometer at the University of Granada's Centro de Instrumentación Científica, or on a 500 MHz Bruker Avance III spectrometer at the School of Chemistry, The University of Edinburgh. Samples were dissolved in deuterated solvents (chloroform-d, DMSO-d<sub>6</sub>) commercially available from Sigma-Aldrich or VWR international Ltd.

<sup>1</sup>H NMR spectra: chemical shifts are reported in parts per million (ppm) relative to tetramethylsilane. The data is reported as follows: chemical shift, integration, multiplicity

(where s = singlet, bs = broad singlet, d = doublet, t = triplet, q = quartet, m = multiplet or by a combination of these terms), and coupling constant (in Hz) and interpretation.

<sup>13</sup>C NMR spectra: chemical shifts are reported in ppm relative to the solvent carbon peak. The data is presented as follows: chemical shift and assignment; and were confirmed by DEPT-135 or DEPTQ-135 (2D-HSQC and 2D-HMBC analysis were used when required). The spectra were interpreted using MestReNova 12.0.4-22023.

#### 3.1.4. Mass Spectrometry

High resolution mass spectra (HRMS) were obtained using a Waters LCT Premier XE Spectrometer at Centro de Instrumentación Científica, School of Pharmacy, The University of Granada.

#### 3.1.5. Physicochemical properties

Chemicalize was used for prediction of calculated log D (cLog D) and pKa values, <http://chemicalize.com/>, developed by ChemAxon Ltd.<sup>216</sup>

### 3.2. Cells and culture

Jurkat (acute T cell leukemia) and K562 (chronic myelogenous leukemia) cell lines were grown in T75 Flasks in RPMI 1640 medium (BioWhittaker, Verviers, Belgium) with 10 % fetal bovine serum (Gibco, Auckland, New Zealand), 1 % L-glutamine (Gibco) and incubated at 37 °C under 5% CO<sub>2</sub>.

HeLa (cervical cancer), G361 (malignant melanoma), MDA-MB-231 (breast cancer) and HCT116 (colon cancer) cell lines were grown in T75 Flasks in Dulbecco's Modified Eagle Medium (DMEM) with 10 % fetal bovine serum (Gibco, Auckland, New Zealand) and 1 % L-Glutamine (Gibco) and incubated at 37 °C under 5% CO<sub>2</sub>.

#### 3.2.1. Cell Subculture

Cell cultures were split at 60 % - 80 % confluence. **Suspension cells** were centrifuged (1500 rpm, 5 min). Cell pellets were resuspended in supplemented RPMI growth media, seeded at dilution factor 1:10 (T75 – 15 mL) and incubated until 60 % - 80 % confluence was achieved. **Adhered cells** were washed with PBS (T75 – 10 mL) and



trypsinized (Trypsin: T75 – 1 mL, 5 min, 37 °C). Trypsin was inactivated with supplemented DMEM growth media (9 mL) and centrifuged (1500 rpm, 5 min). Cell pellets were resuspended in supplemented DMEM growth media, seeded at dilution factor 1:10, unless otherwise stated, in same media (T75 – 15 mL) and incubated until 60 % - 80 % confluence was achieved.

### **3.2.2. Analysis of cell cycle**

For the analysis of cell cycle, 250000 cells/well in 24-well plates (Jurkat, K562), or 200000 cells/well (G361), 150000 cells/well (MDA-MB-231, HCT116) or 50000 cells/well (HeLa) in 6-well plates were cultured in 500 µL (24-well) or 1.5 ml (6-well) of the appropriate media and incubated with the chosen compounds at 30 µM for 48 h. Untreated cells were incubated with the maximum DMSO concentration used.

Cell cycles were analyzed by staining of cells with propidium iodide (PI) staining. Thus, after treatment with the corresponding compounds, the cells were collected and washed with 2 ml phosphate-buffered saline (PBS) at 4 °C and fixed with 100 µL of PBS and 900 µL of 70% ethanol, on ice for 5 minutes. After washing with PBS, cells were resuspended in 250 µL of PBS and another 250 µL of a DNA extraction buffer (0.2M Na<sub>2</sub>HPO<sub>4</sub>, 0.1M C<sub>6</sub>H<sub>8</sub>O<sub>7</sub>, pH 7.8) and incubated at 37 °C for 10 minutes. The supernatant was removed and 200 µL of the staining solution [8 µL propidium iodide (1mg / mL) and 2 µL RNase 100 (µg / mL)] were added and the samples incubated for 10 min at 37 °C in the dark.

Fluorescence was measured in the FL2 detector of the FACScalibur cytometer (Becton Dickinson & Co., NJ, USA) and the analysis of the sub-G1 population (apoptotic cells) was done using the Cell Quest software (BD, Biosciences). Necrotic cells were excluded by Side Scatter gating.

### **3.2.3. Annexin-V staining**

This is an effective method to identify apoptotic cells.<sup>217</sup> This technique relies on the double propidium iodide/annexin V staining. The measurement of Annexin-V-FLUOS (Roche, Mannheim, Germany), is a sensitive test of the PS exposed on the outer membrane leaflet of early apoptotic cells. In the case of necrotic cells, which also expose PS as a result of the loss of membrane integrity, propidium iodide is used to bind to DNA

and thus distinguish necrotic cells from apoptotic cells stained exclusively with Annexin-V-FLUOS .

For the analysis of phosphatidylserine exposure, 250000 cells/well were cultured in 24-well plates in 500  $\mu$ l of the appropriate growth medium and incubated with the chosen compounds at the indicated doses for 48 h. Etoposide was used as positive control and untreated cells were used as controls of live cells.

After treatment, cells were collected and washed with annexin V binding buffer (10 mM HEPES pH 7.4, 140 mM NaCl, 2.5 mM  $\text{CaCl}_2$ ) and re-suspended in 100  $\mu$ l of this buffer. Then, 2.5  $\mu$ l of Annexin-V-FLUOS solution (Roche, Mannheim, Germany) was added to each sample, followed by incubation for 20 min in the dark at room temperature. After a final wash, the pellet was resuspended in annexin V binding buffer containing 10  $\mu$ l of PI at 10  $\mu$ g/ml. Stained samples were immediately analyzed by flow cytometry using a FACSCalibur flow cytometer and analyzed with the Cell Quest software.

#### 3.2.4. Dose response cell viability assay

All final compounds were diluted with DMSO to a final concentration of 100 mM and stored at -20 °C until used.

- **Hematopoietic cells (Suspension cells).** Compounds, including DMSO, were prepared as intermediate solutions at 2x in supplemented RPMI medium. The compounds were then added in serial dilution in 96-well flat-bottomed plates to give a final volume of 50  $\mu$ L/well. Then 50  $\mu$ L of a previously prepared supplemented RPMI medium at 1000 cells/well (Jurkat, K562) were added to each well and the plates incubated for 5 days in an incubator at 37 °C and 5 %  $\text{CO}_2$ . Final compound concentration range among 200  $\mu$ M and 0.05  $\mu$ M. Untreated cells were incubated with the maximum DMSO concentration used (0.2 % v/v). After 5 days, PrestoBlue™ cell viability reagent (10  $\mu$ l) was added to each well and the plates incubated for 90 - 120 min. Fluorescence emission was detected using a Synergy™ HTX Multi-Mode Microplate Reader (excitation 530/20 nm, emission 590/35 nm).

- **Non-hematopoietic (Adherent cells).** Cells were seeded in 96-well flat-bottomed plates at 500 cells/well (G361 and HCT116 cells), 1000 cells/well (HeLa cells) and 2000 cells/well (MDA-MB-231 cells) in 50  $\mu\text{L}$  of supplemented medium and incubated for 24 h in an incubator at 37 °C and 5 %  $\text{CO}_2$ . After 24 h, the media was aspirated from each well and replaced with 100  $\mu\text{L}$  of fresh medium. Compounds, including DMSO, were prepared as intermediate solutions at 2x in supplemented DMEM medium. Then compounds were added in serial dilution to give a final volume of 100  $\mu\text{L}$ /well. Final compound concentration range among 200  $\mu\text{M}$  and 0.05  $\mu\text{M}$ . Untreated cells were incubated with the maximum DMSO concentration used (0.2 % v/v). After 5 days, PrestoBlue™ cell viability reagent (10  $\mu\text{l}$ ) was added to each well and the plates incubated for 90 - 120 min. Fluorescence emission was detected using an Envision® fluorescence plate reader (excitation 530/20 nm, emission 590/35 nm).

All conditions were normalized to the untreated cells (100 %) and curves were fitted using a four parameter logistic fit with minimum value constrained to zero using GraphPad Prism software, to calculate half maximal inhibitory concentration ( $\text{IC}_{50}$ ) values.  $\text{IC}_{50}$  values are expressed as mean of three independent experiments.



## **4. Results**

---

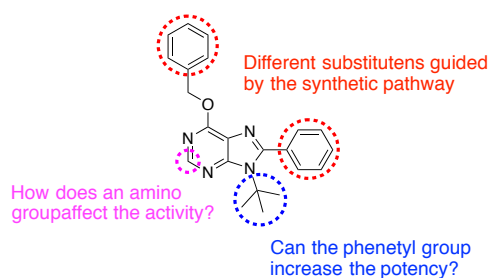


## 4.1. Design, synthesis and biological evaluation of chemical library 1

### 4.1.1. Design of chemical library 1

The starting point for the design of this library was the compound **6d** which as stated before is derived from **6a**, a compound that showed high selectivity for DAPK1 over the rest of kinases involved in apoptosis. This initial chemotype contains the purine ring as the main scaffold and it is substituted at positions 6, 8 and 9 with a benzyloxy, phenyl and *tert*-butyl groups, respectively. This molecule, along with its previous set of compounds, was in-house synthesized by the one-pot synthetic route developed by the group.<sup>210</sup>

Compound **6d** was designed to optimize **6a** by the simple replacement of the isopropyl group at N9 by a *tert*-butyl group. Despite the excellent kinase selectivity exhibited by **6a** and **6d**, they presented unfavorable physicochemical properties, since the three variable positions are occupied by hydrophobic groups. This issue has to be considered especially when the final purpose of these compounds is to be used in the aqueous milieu of live cells.



**Figure 20 | Proposed modifications of 6d for the development of chemical library 1.**

Considering all the above, an array of compounds was designed to investigate how new modifications in the purine scaffold affect the activity of the lead compound and whether any of these modifications enhance their physicochemical properties (**Figure 20**). On the basis of this, two modifications were proposed:

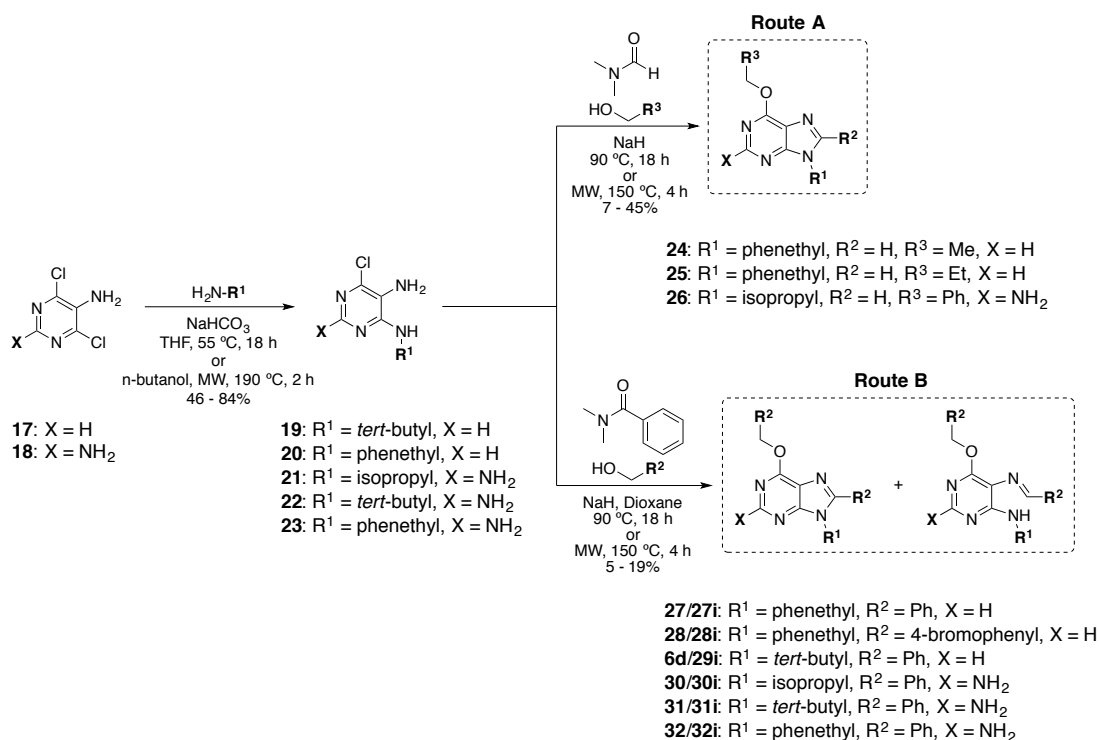
- The first one was directed to the N9-moiety by introducing the phenethyl group as a new lipophilic and sterically hindered substituent.

## 4.1. Design, synthesis and biological evaluation of chemical library 1

- The second proposed modification was the introduction of an amino group at the C2 position of the purine ring. This allows to examine an additional region of the scaffold at the same time that a hydrophilic group is attached to it.
- In addition to the proposed modifications at N9 and C2, the one-pot synthetic procedure allows the introduction of different substituents at the positions C6 and C8 of the purine ring depending on the alcohol and amide employed.

### 4.1.2. Synthesis of chemical library 1

The proposed compound series was prepared via the one-pot synthesis of 6,8,9-substituted purines previously explained.<sup>209</sup> Thus, a 14-member library of **6d** analogs was synthesized and the reaction scheme represented in **Figure 21**.



**Figure 21** | Synthetic procedure for the preparation of compounds **24 – 32** and **27i – 32i** by **Route A** and **B**.

Amination of the commercially available dichloropyrimidines **17** and **18** with alkyl amines in THF or n-butanol gave 4-alkylamino-5,6-chloropyrimidines (**19 – 23**) in good to excellent yields (46 – 84%). These chloropyrimidines were treated with the appropriate alkoxide (generated *in situ* by the corresponding alcohol and sodium hydride), a large excess of the suitable *N,N*-dimethylamine and heated at 90 °C overnight to



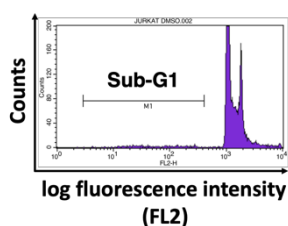
simultaneously underwent a displacement at the C6 position and cyclization reactions to provide the final compounds **24** – **32** in low to moderate yields (5 – 45%) (**Figure 21**)<sup>218</sup>. Typically, when 4,6-dichloropyrimidine-2,5-diamine (**18**) was used as the main core, microwave irradiation was employed to accelerate reaction rates because of its deactivated character.

In addition to the designed compound library, in the cases where *N,N*-dimethylbenzamide was used together with bulky alcohols (benzyl alcohol or 4-bromobenzyl alcohol), the intermediate imines **27i** – **32i** were also isolated in low to moderate yields (5 – 19%).<sup>209</sup>

### 4.1.3. Screening of chemical library 1

Cell cycle analysis was chosen as the primary screening output due to the capability of this method to identify active compounds and discriminate whether the new analogs maintain or not the pro-apoptotic effect of the lead molecule **6d**.

**Table 1 | Phenotypic screening of the chemical library 1 by cell cycle analysis.** Cells were incubated during 48 h with the indicated compounds at 30  $\mu$ M. Then cells were stained with propidium iodide and analyzed by flow cytometry. The data represent percentage of cell population within the sub-G1 region, after subtracting values from negative controls (DMSO) in each cell line. Compound **32** was not tested. Compound **6d** was used as positive control.

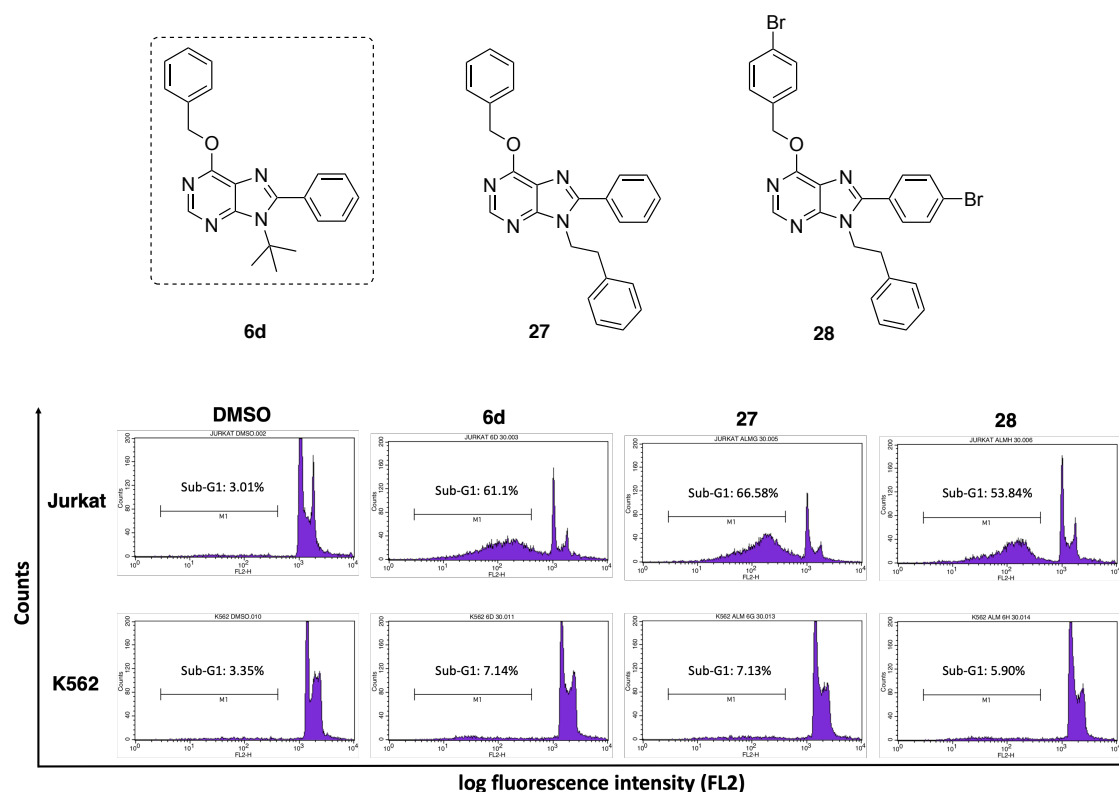


Compd./Cell	Jurkat	K562	HeLa	G361	MDA	HCT
<b>6d</b>	66	6	9	2	4	7
<b>24</b>	3	1	-10	-2	0	0
<b>25</b>	2	0	-10	-2	0	5
<b>26</b>	1	2	7	-1	3	14
<b>27</b>	64	4	-10	12	23	9
<b>28</b>	51	3	-4	0	4	4
<b>30</b>	15	4	6	2	3	9
<b>31</b>	1	1	4	-1	0	7
<b>27i</b>	4	0	-1	0	6	13
<b>28i</b>	18	1	1	3	7	18
<b>29i</b>	3	1	3	1	3	15
<b>30i</b>	2	2	2	0	4	12
<b>31i</b>	2	2	7	41	4	12
<b>32i</b>	25	2	-11	-1	-1	0

#### 4.1. Design, synthesis and biological evaluation of chemical library 1

Thus, the final 14-member library was tested against a panel of six human cancer cell lines (hematopoietic: Jurkat, K562; non-hematopoietic: HeLa, G361, MDA-MB-231 and HCT116) which were treated with each compound for 48 h at a single dose (30  $\mu$ M). Cells treated with **6d** (30  $\mu$ M) or DMSO were used as a positive and negative control, respectively, and the cell cycle profiles were determined by flow cytometry after staining of nuclear DNA with propidium iodide (PI). The percentage of cells within the sub-G1 region (apoptotic cells) was measured and values are shown in **Table 1**.

Compounds **27** and **28** led to a strong accumulation of cells within the sub-G1 region in Jurkat cells. Both compounds showed activities above 50% and did not affect any other cell line, maintaining the cell selectivity and phenotypic effect of the lead compound. It is also important to note that **27** and **28** are the closest analogs of **6d** (**Figure 22**). They all share the same basic structure at **R**<sup>2</sup> and **R**<sup>3</sup> and only differ from **6d** at **R**<sup>1</sup>, where the *tert*-butyl fragment was replaced for a larger substituent, the phenethyl group.



**Figure 22 | Selective effect of compounds **6d**, **27** and **28**.** (A) Chemical structure of **6d** and the most active compounds of the chemical library 1, **27** and **28**. (B) Representative experiment of the selective effect of compounds **6d**, **27** and **28** on the cell cycle of Jurkat cells. Cells were treated for 48 h with **6d**, **27** and **28** at 30  $\mu$ M or their equivalent amounts of DMSO used as vehicle. Cells gated on the sub-G1 region after staining with propidium iodide are indicated. K562 cells were selected as a representative unaffected cell line.

Furthermore, the derivatives with an amino group in the position C2 of the purine ring (**30**, **31**, **32**) completely lost their activity compared to their respective non-aminated analogs (**6a**, **6d** and **27**).

Additionally, the isolated imines obtained as intermediate products in the final reaction were also tested. These non-cycled analogs did not show any significant activity in Jurkat cells and neither in the rest of cell lines with the exception of **31i**, which accumulated 41% of G361 cells in the sub-G1 fraction. These results showed the importance of maintaining the purine scaffold in order to retain the activity of these analogs.

#### 4.1.4. Annexin-V analysis

To further analyze the cell death mechanism of the most active compounds arisen from the previous screening, Annexin-V was used. Annexin-V is a calcium-dependent phospholipid-binding protein with a high affinity for phosphatidylserine, which is a distinct feature of early stages of apoptosis.<sup>219,220</sup>

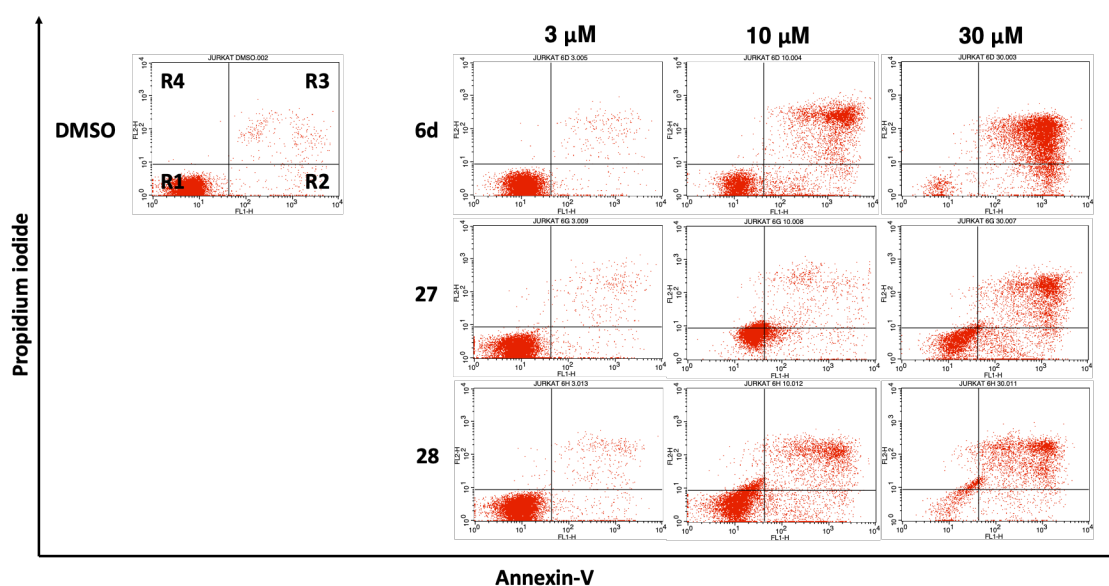
Jurkat cells were treated with compounds **27** and **28** for 48 h at 30  $\mu$ M, 10  $\mu$ M and 3  $\mu$ M. Cells treated with DMSO (30  $\mu$ M) or **6d** were used as a negative and positive control respectively. Flow cytometry analysis of double stained cells with PI and Annexin-V were plotted in two-dimensional dot plots in which Annexin-V is represented versus PI. These plots can be divided in four regions corresponding to:

- **R1**: viable cells (Annexin-V<sup>-</sup>/PI<sup>-</sup>).
- **R2**: early apoptotic cells (Annexin-V<sup>+</sup>/PI<sup>-</sup>).
- **R3**: late apoptotic cells (Annexin-V<sup>+</sup>/PI<sup>+</sup>).
- **R4**: necrotic cells (Annexin-V<sup>-</sup>/PI<sup>+</sup>).

As expected, untreated Jurkat cells presented a negligible apoptotic cell population. However, when the cells were treated with **6g** and **6h** at the indicated doses, transition behavior from early to late apoptotic stages was observed, confirming that these compounds induce cell death by apoptosis in a dose-dependent manner (**Table 2** and **Figure 23**).

**Table 2 | Summary of membrane phosphatidylserine expression after treatment of Jurkat cells with compounds 27 and 28.** The tables collect the percentage of cells within each region **R1** (viable cells), **R2** (early apoptotic cells), **R3** (late apoptotic cells) and **R4** (necrotic cells).

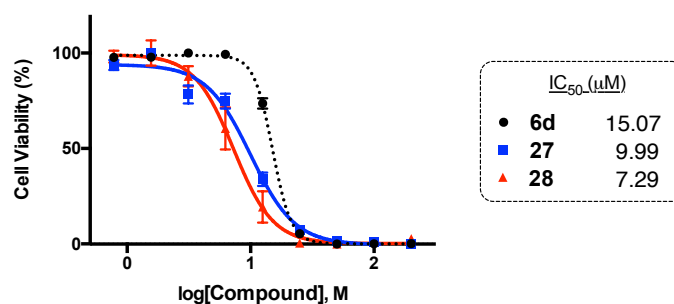
	<b>6d</b>			<b>27</b>			<b>28</b>			<b>DMSO</b>
	3 $\mu$ M	10 $\mu$ M	30 $\mu$ M	3 $\mu$ M	10 $\mu$ M	30 $\mu$ M	3 $\mu$ M	10 $\mu$ M	30 $\mu$ M	30 $\mu$ M
<b>R1</b>	92	39	5	94	29	31	91	56	12	94
<b>R2</b>	5	18	16	2	55	25	5	14	10	3
<b>R3</b>	2	43	80	3	15	44	4	27	77	3
<b>R4</b>	0	0	0	0	1	0	0	3	1	0



**Figure 23 | Membrane phosphatidylserine expression after treatment of Jurkat cells with compounds 27 and 28.** Jurkat cells were treated for 48 h with the indicated doses and the percentages of apoptotic cells were measured by flow cytometry after double staining with propidium iodide and Annexin-V-FLUOS. Untreated cells (DMSO) and cells treated with **6d** were included as negative and positive controls.

#### 4.1.5. Cell proliferation studies

Based on the data from the screening of **library 1**, compounds **27** and **28** were selected to be tested for cell viability against Jurkat cells, using **6d** as a positive control. The cells were incubated with the compounds for 5 days after which cell proliferation was measured using PrestoBlue™ reagent and analyzed by spectrofluorometry. IC<sub>50</sub> values were calculated using 9-point half-log dose-response assays (0.78  $\mu$ M – 200  $\mu$ M) and the results plotted in **Figure 24**.



**Figure 24 | Dose-response curves and calculated IC<sub>50</sub> values for compounds 27, 28 and 6d.** IC<sub>50</sub> values were determined by PrestoBlue™ cell viability assay after incubation of Jurkat cells with compounds 27, 28 and 6d as positive control, for 5 days (dose range: 0.78 – 200 μM) error bars: ± SEM from n = 3.

The most potent compound of this series was **28**, which exhibited an IC<sub>50</sub> of 7.29 μM against Jurkat cells and a 2-fold potency increase over **6d**. Its non-brominated analogue (**27**) was also more potent than the lead compound and displayed an IC<sub>50</sub> value of 9.99 μM.

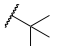
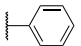
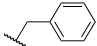
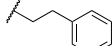
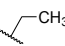
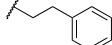
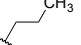
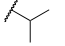
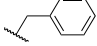
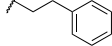
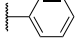
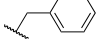
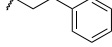
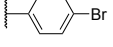
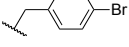
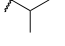
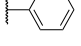
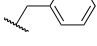
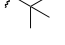
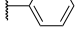
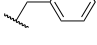
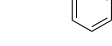
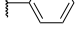
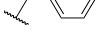
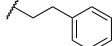
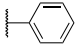
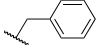
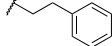
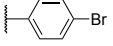
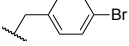
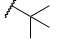
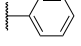
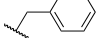
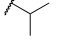
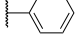
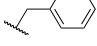
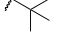
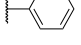
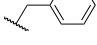

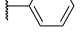
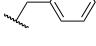
#### 4.1.6. Physicochemical properties

Once the potency of these compounds in cells were established, the physicochemical properties were analyzed to complement their biological behavior. Lipophilicity, which is the most important prerequisite for a drug to cross the cell membranes and, therefore, to interact with its biological target, was calculated. Calculated distribution coefficient (cLog D) was chosen rather than calculated octanol-water partition coefficient (cLog P) since it also considers the pH dependence of the molecules in aqueous solution, being reliable not only for neutral compounds but also for ionizable compounds.<sup>221</sup> Therefore, these values were calculated using Chemicalize by ChemAxon Ltd.<sup>216</sup> at the pH of 7.4 to represent the molecules when they are in a physiological environment.

The overall cLog D values of this library was quite high (**Table 3**), only **24**, **25** and **26** showed acceptable lipophilicity values although none of them was active. The most active compounds (**27** and **28**) displayed cLog D values higher than the reference compound **6d** (cLog D of 5.17). Hence, compound **28**, which showed the best activity values of this series exhibited the highest lipophilicity value (7.66) within the cycled analogs, followed by **27** (6.13), which was the second most potent compound.

#### 4.1. Design, synthesis and biological evaluation of chemical library 1

**Table 3 | Molecular weight (MW) and cLog D values of compounds from the chemical library 1.** Values in red violate RO5.

Compound	R <sup>1</sup>	R <sup>2</sup>	R <sup>3</sup>	X	MW	cLog D
<b>6d</b>				H	358.45	<b>5.17</b>
<b>24</b>		H		H	268.32	2.73
<b>25</b>		H		H	282.35	3.26
<b>26</b>		H		NH <sub>2</sub>	283.34	2.71
<b>27</b>				H	406.49	<b>6.13</b>
<b>28</b>				H	<b>564.28</b>	<b>7.66</b>
<b>30</b>				NH <sub>2</sub>	359.43	4.74
<b>31</b>				NH <sub>2</sub>	373.46	<b>5.02</b>
<b>32</b>				NH <sub>2</sub>	421.50	<b>5.98</b>
<b>Imines</b>						
<b>27i</b>				H	408.51	<b>6.16</b>
<b>28i</b>				H	<b>566.30</b>	<b>7.70</b>
<b>29i</b>				H	360.46	<b>5.21</b>
<b>30i</b>				NH <sub>2</sub>	361.45	4.69
<b>31i</b>				NH <sub>2</sub>	375.48	4.97
<b>32i</b>				NH <sub>2</sub>	423.52	<b>5.92</b>

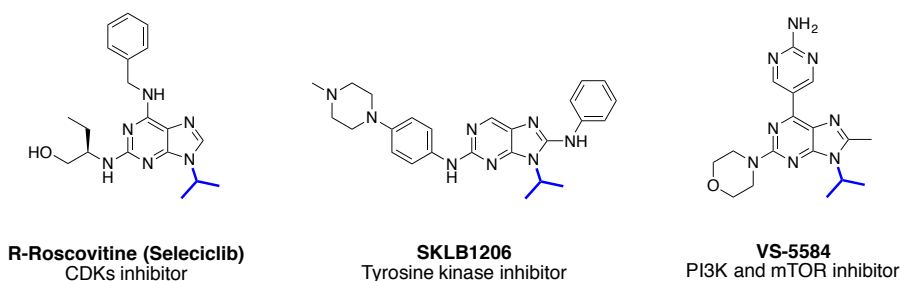
These two compounds together with **6d** presented cLog D values above 5. In addition, **28** was the only active compound of this series with a molecular weight over 500 Da. This correlates with the compound crystal formation observed when these compounds were placed in cell culture medium to be tested in the prior experiments. These poor physicochemical properties result in less amount of compound available to enter the cell and interact with the target, which consequently means less activity and higher IC<sub>50</sub> values.

## 4.2. Design, synthesis and biological evaluation of chemical library 2

### 4.2.1. Design of library 2

Over the years, a large number of purine analogs have been synthesized to better aid in the search for potent and specific inhibitors. This has been successfully carried out by the pharmaceutical industry and academia by the introduction of different substituents at the positions 2, 6, 8 or 9 of the purine ring.<sup>207,222–225</sup>

However, the majority of the analogs have been obtained by exploration of the positions 2, 6 and 8, whereas the 9 position, which for several kinases is known to tolerate a narrow range of substituents, has been typically occupied by the isopropyl group.<sup>226,227</sup> This moiety enables the imidazole ring of the purine to enter the pocket formed by hydrophobic region I.<sup>228</sup> As a consequence, this group is presented in many ATP-competitive purine-based kinase inhibitors. Some examples of this are **Roscovitine** (experimental drug)<sup>229</sup>, **SKLB1206**<sup>230</sup> or **VS5584**<sup>231</sup> (both in clinical trials) (**Figure 25**).



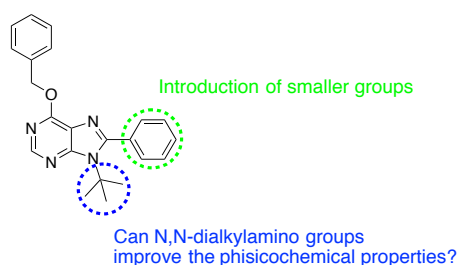
**Figure 25 | Chemical structure of representative ATP-competitive purine-based kinase inhibitors.**

Furthermore, the isopropyl group is commonly interchangeable in kinase inhibitor optimization processes for a *tert*-butyl group to improve binding affinity,<sup>232,233</sup> since both play their roles by occupying a lipophilic domain in the target. However, just a few studies have tried to optimize the substituent in N9.<sup>234</sup> As a consequence, the intellectual property (IP) space around these scaffolds has become increasingly congested.

Taking all the above into account, a novel purine core was proposed to both enhance the physicochemical properties of the compound **6d** and at the same time create a new template upon which new purine families could be generated.

This approach was achieved by the novel introduction of either *N,N*-dialkylamino or 1-azacycloalkan-1-yl residues at the N9 position of the purine ring, decreasing the global lipophilicity of the molecule without altering the lipophilic character of the substituent.

This structural design thus introduced at N9 a substituent through a nitrogen-nitrogen bond which, to best to our knowledge, has not been presented yet in any kinase inhibitors (**Figure 26**). Additionally, the new nitrogen atom attached to the N9 position confers the analogs the ability to establish new interactions with the target via hydrogen bonds, which could help to enhance drug selectivity towards certain targets. In addition to this, the position C8 was also selected to be explored by the replacement of the phenyl group by less lipophilic and sterically hindered groups.



**Figure 26 | Proposed modifications of 6d for the development of chemical library 2.**

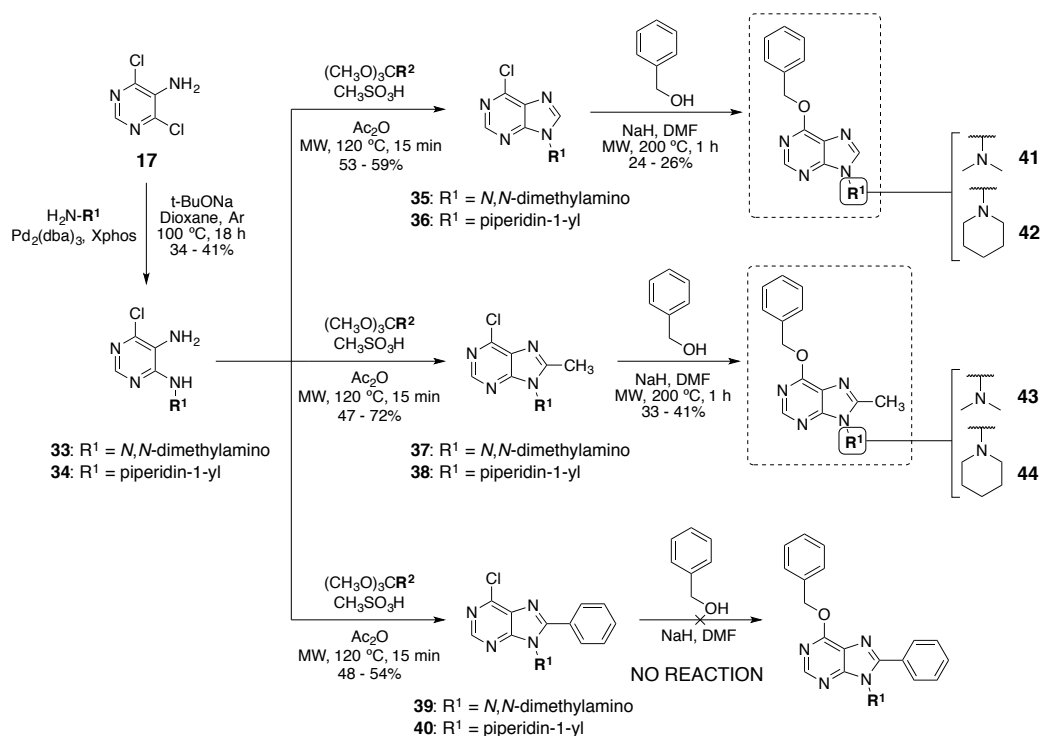
### 4.2.2. Synthesis of chemical library 2a

For the preparation of the designed purines, the appropriate hydrazines were introduced via Buchwald-Hartwig amination<sup>235,236</sup> to the commercially available 4,6-dichloropyrimidin-5-amine **17** with *N,N*-dimethylhydrazine and 1-aminopiperidine in the presence of tris(dibenzylideneacetone)dipalladium(0) ( $\text{Pd}_2(\text{dba})_3$ ) as the palladium source, 2-dicyclohexylphosphino-2',4',6'-triisopropylbiphenyl (Xphos) as ligand and sodium *tert*-butoxide (*t*-BuONa) in dioxane as strong base<sup>237</sup> to give the 4-hydrazinylpyrimidines **33** and **34** in moderate to good yields (34 – 41%).

Cyclization of the pyrimidine ring was performed by reaction of **33** and **34** with the corresponding trimethyl orthoacetate in acetic anhydride and a catalytic amount of methanesulfonic acid,<sup>238–240</sup> giving rise to the compounds **35** – **40** in good yields (47 – 72%). The chlorine atom at the C6 position of the purine derivatives **35** – **40** was then substituted via a nucleophilic aromatic substitution ( $\text{S}_{\text{N}}\text{Ar}$ ) with benzyl alkoxide



(generated in situ by the benzyl alcohol and sodium hydride) in DMF to give compounds **41 – 44** in moderate yields (24 – 41%)<sup>241</sup> (**Figure 27**).



**Figure 27** | Synthetic route for the preparation of compounds **41 – 44**.

However, no reaction happened when, following cyclization reaction, the purine scaffold was substituted at the C8 position with a phenyl group. In these cases, the corresponding 6-chloropurines (**39 – 40**) were recovered instead of the O-alkylated products.

### 4.2.3. Design of chemical library 2b

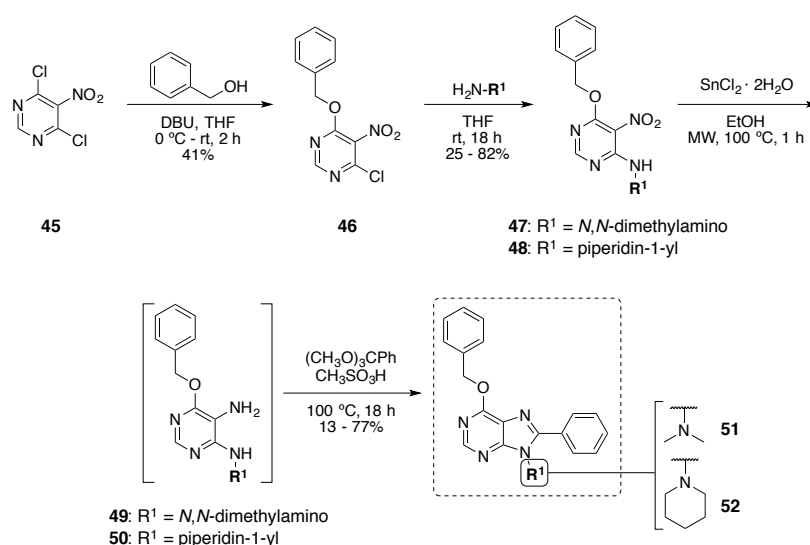
The introduction of either *N,N*-dialkyl or 1-azacycloalkane-1-yl groups at N9 was achieved by a Buchwald-Hartwig amination and that these intermediates underwent the formation of the desired 8-H-substituted and 8-methyl-substituted products. However, the 8-phenyl-substituted analogs could not be obtained by this method as mentioned above.

Consequently, a new synthetic route was designed to achieve the synthesis of these two compounds (**Figure 28**). This was made starting with the 4,5-dichloro-5-nitropyrimidine **45** instead of the aminopyrimidine **17** and by the formation of disubstituted

intermediates **47** and **48** that after the nitro reduction easily undergo to a cyclization reaction that provide the phenyl substituent at the C8 position.

#### 4.2.4. Synthesis of chemical library 2b

Commercially available 4,6-dichloro-5-nitropyrimidine **45** was treated with an equimolar amount of benzyl alcohol in tetrahydrofuran (THF) to give **46** in moderate yield (41%). The chlorine atom at the C4 position of **46** was then substituted via a second  $S_NAr$  with the appropriate *N,N*-dialkylhydrazine in THF to provide the disubstituted purines **47** and **48** in moderate to excellent yields (25 – 82%).



**Figure 28** | Synthetic route for the preparation of compounds **51** and **52**.

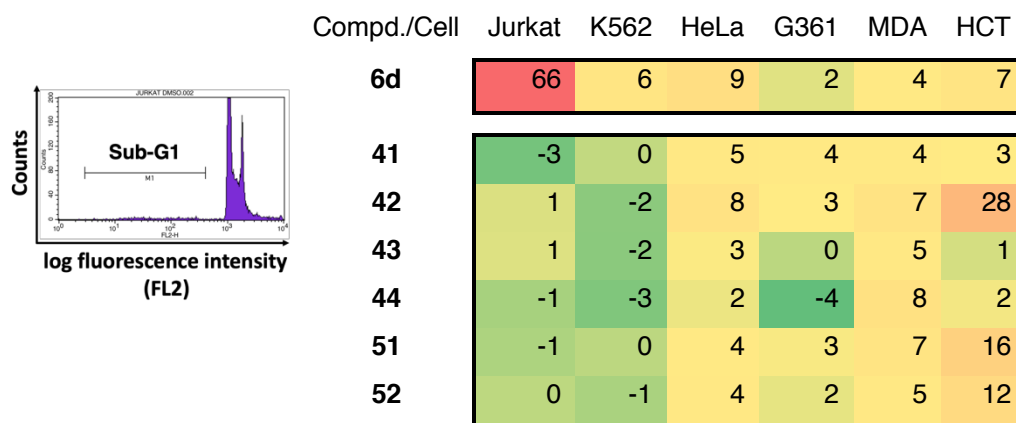
The aminopyrimidines **49** and **50** were generated by a microwave-assisted reduction of the nitro group of **47** and **48** with stannous chloride in ethanol and were used without purification for the next reaction.<sup>242</sup> Lastly, **49** and **50** underwent a cyclization reaction by treatment with trimethyl orthobenzoate and a catalytic amount of methanesulfonic acid providing the purine analogs **51** and **52** in moderate to good yields (13 – 77%).<sup>243</sup>

#### 4.2.5. Screening

Once the 6-member library was completed, it was tested against the same panel of human cancer cell lines previously used with library 1, employing the analysis of the cell cycle to identify alterations induced by the compounds. Thus, the cells were incubated in

the presence of the compounds for two days, in a single dose concentration (30  $\mu$ M), and compared to **6d**.

**Table 4 | Phenotypic screening of the chemical library 2a and 2b by cell cycle analysis.** Cells were incubated during 48 h with the indicated compounds at 30  $\mu$ M. Then cells were stained with propidium iodide and analyzed by flow cytometry. The data represent percentage of cell population within the sub-G1 region, after subtracting values from negative controls (DMSO) in each cell line. Compound **6d** was used as positive control.



As shown in **Table 4**, none of the compounds from the library led to an increase in the sub-G1 cell population in Jurkat cells and neither in the rest of the cell lines, with the exception of HCT116 cells. It is important to emphasize from these results that compound **51** which only differs from **6d** on the *N,N*-dimethylamine moiety at position 9 of the purine ring (instead of the *tert*-butyl group), has utterly lost its activity in Jurkat cells and showed a moderate activity in the HCT116 line. This discriminatory effect is even more potent in **42** which led to an increase of 28% in the sub-G1 population although in this case the similarity with **6d** is lower because the phenyl group at C8 position is not presented on the structure.

#### 4.2.6. Physicochemical properties

The cLog D data obtained for this set of compounds using Chemicalize by ChemAxon Ltd showed values that range between 1 and 4 (**Table 5**), which confers the new analogs a much more appropriate biocompatible physicochemical profile compared with the compounds **6a** (cLog D of 4.89) and specially with **6d** (5.17).

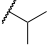
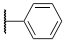
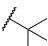
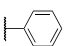
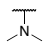
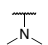
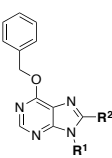
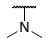
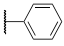
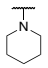
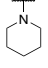
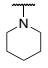
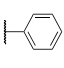
Derivatives with the *N,N*-dimethylamino group showed lower cLog D than those that contain the piperidine ring, since the latter is a more lipophilic moiety. On the other hand,

## 4.2. Design, synthesis and biological evaluation of chemical library 2

analogues that are not substituted at C8 and those that have attached the methyl group shares very close cLog D values.

Lastly, the comparison of cLog D values of compounds **6a** (4.89) and **51** (3.09), which replace the tertiary carbon of the isopropyl group with a nitrogen, showed a remarkable change.

**Table 5 | Molecular weight (MW) and cLog D values of compounds from the chemical library 2a and 2b. Values in red violate RO5.**

Scaffold	Compound	R <sup>1</sup>	R <sup>2</sup>	MW	cLog D
	<b>6a</b>			344.42	4.89
	<b>6d</b>			358.45	5.17
	<b>41</b>		H	269.31	1.06
	<b>43</b>		CH <sub>3</sub>	283.34	1.19
	<b>51</b>			345.41	3.09
	<b>42</b>		H	309.37	1.92
	<b>44</b>		CH <sub>3</sub>	323.40	2.04
	<b>52</b>			385.47	3.98

## 4.3. Design, synthesis and biological evaluation of chemical library 3

### 4.3.1. Design of chemical library 3

On the previous section, a new synthetic route was developed to synthesize novel purine derivatives substituted at the N9 position with either *N,N*-dialkylamines or 1-azacycloalkane-1-yl. These compounds exhibited an improvement in their physicochemical properties compared to the compounds that did not contain the nitrogen atom attached at this position (N9). Apart from the introduction of these moieties, this route also allowed the exploration of C8 by the selection of different orthoesters.

However, the C6 position, which can be modified with this route too is still pending to be explored by our group. For some kinase inhibitors, their interactions with the target protein through this region are known to be responsible for the increased affinity and selectivity of the inhibitors compared with ATP. Therefore, a variety of groups have been explored by others groups<sup>224,226</sup> being substituents that contain lipophilic groups and interact with hydrophobic domains of the target protein the most broadly used in that position.<sup>225</sup>

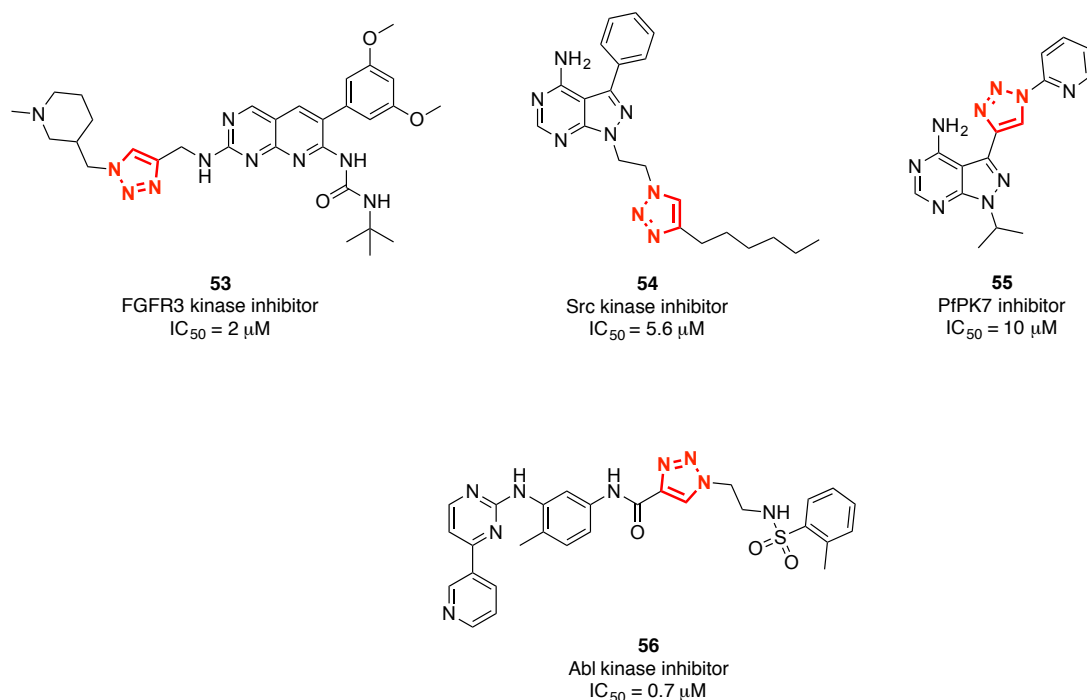
To explore this region of the ring and at the same time maintain the *N,N*-dialkylamines or 1-azacycloalkane-1-yl groups at N9 and alter the C8 position, a copper(I)-catalyzed alkyne-azide [3 + 2] cycloaddition (CuAAC) reaction was smartly implemented into the synthetic route used in the previous section.

The CuAAC process has emerged as the premier example of click chemistry.<sup>244</sup> It is considered a powerful tool to perform selective modifications on structural complex molecules to generate privileged medicinal scaffolds,<sup>245</sup> due to its high degree of dependability, complete specificity, and the compatibility of the reactants.<sup>246–248</sup> This reaction provides 1,4-disubstituted 1,2,3-triazoles, which are well-known to be quite resistant to metabolic degradation and capable of participating in dipole-dipole interactions as well as hydrogen bonding, thus providing additional advantages including cell permeability improvement and target binding.<sup>249</sup> Moreover, this moiety presents a high bioisosteric potential, and it has been used as bioisoster of amide bonds, acyl-

### 4.3. Design, synthesis and biological evaluation of chemical library 3

phosphates and nitrogen-containing five-member ring surrogates in bioactive molecules.<sup>250</sup>

Therefore, this group has successfully been included in molecules with anticancer, antiparasitic, antibacterial or antiviral activities.<sup>251</sup> Many of them have been reported as inhibitors of protein kinases such as FGFR3 tyrosine kinase (**53**)<sup>252</sup>, Src kinase (**54**)<sup>253</sup>, PfPK7 (**55**)<sup>254</sup> and BCR-ABL tyrosine kinase (**56**)<sup>255</sup> (**Figure 29**).



**Figure 29** | Chemical structure of representative protein kinase inhibitor containing the 1,4-disubstituted 1,2,3-triazole moiety.

In order to implement such chemical strategy into the synthetic route employed to prepare compounds from library 2b, the benzyl alcohol attached at C6 was replaced by the propargyl alcohol, providing an alkyne group upon which to perform click chemistry to easily produce a wide variety of analogs.

Target compounds were generated by combining seven different azides (three aromatic azides and two alkyl azides), and five propargyloxy derivatives (three purine analogs plus the nitro and the amino pyrimidine intermediates) and purine rings where at N9 there is the *N,N*-dimethylamino group (**Figure 30**). As a result, a library of 35 purine analogs was designed. Depending on the C8 position, the compounds were classified in five different sub-libraries: **3a**, **3b**, **3c**, **3d**, **3e**. The first two sublibraries corresponding

with the pyrimidine intermediates needed to obtain the purine final libraries which are based on 4,6-disubstituted-5-nitropyrimidines and 4,6-disubstituted-5-aminopyrimidines.

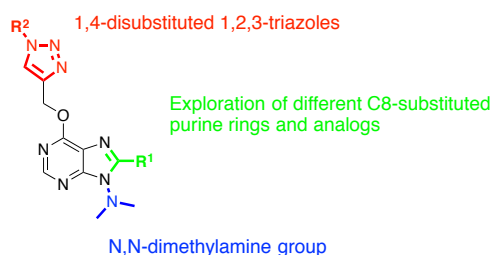


Figure 30 | Proposed modifications to the purine scaffold for the development of chemical library 3.

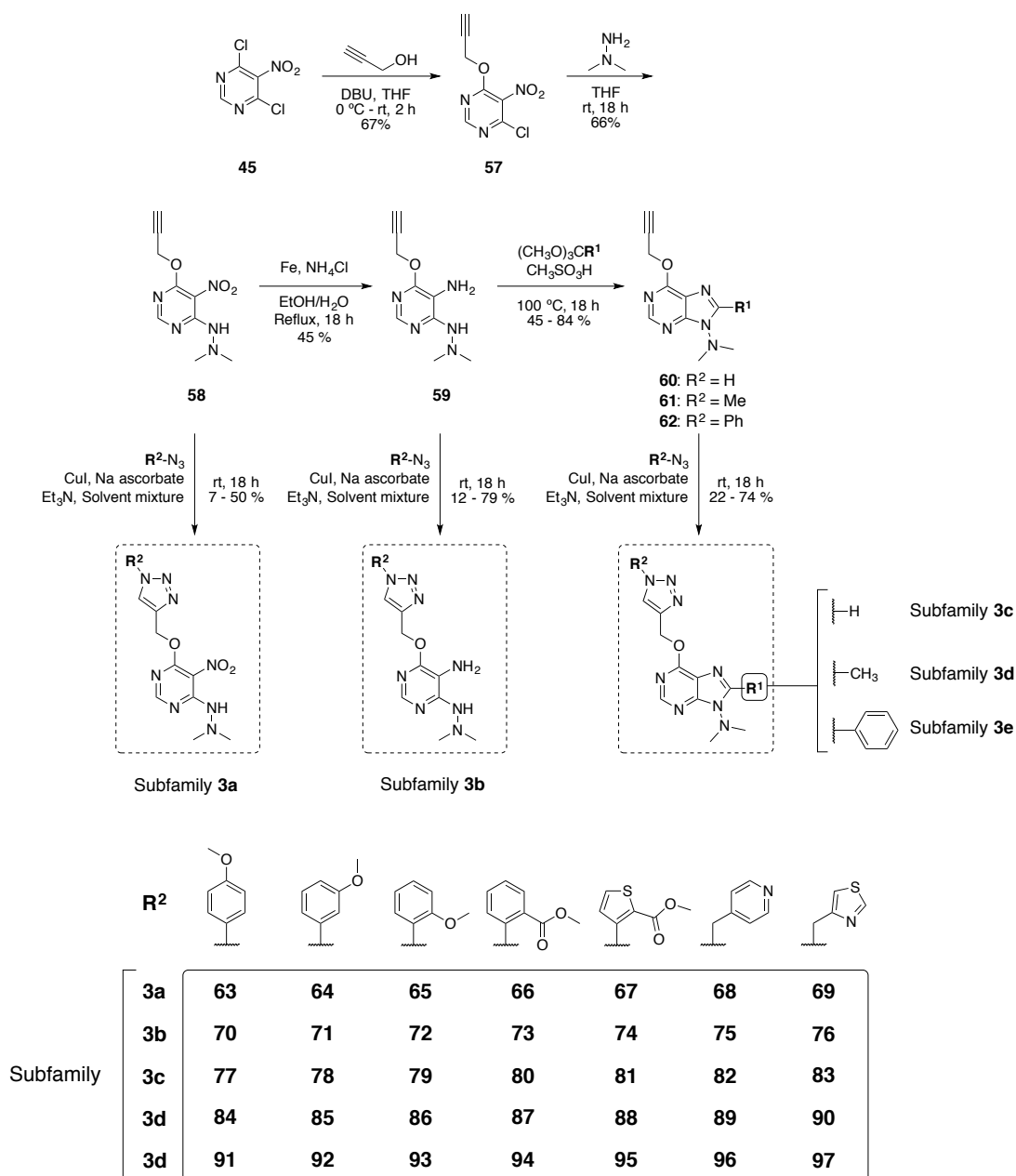
### 4.3.2. Synthesis of chemical library 3

To synthesize the proposed library, commercially available 4,6-dichloro-5-nitropyrimidine was substituted at the C4 position via a  $S_NAr$  with propargyl alcohol in THF to introduce a propargyl group, providing the alkyne **57** in good yield (67%).

This compound subsequently underwent a second displacement with *N,N*-dimethylhydrazine in THF at room temperature to give rise to the disubstituted pyrimidine **58** in similar yield (66%). To continue building the purine scaffold, the nitro group of **58** was reduced with iron and ammonium chloride ( $NH_4Cl$ ) in a refluxing mixture of water and ethanol to provide the aminopurine **59** in moderate yield (45%).<sup>256,257</sup> This reduction methodology was used instead of the one employed in the previous library, where tin(II) chloride and ethanol were used, due to the higher efficiency and easier reaction work-up.

Compound **59** was then treated with the appropriate orthoester and a catalytic amount of methanesulfonic acid to give the 6-propargyloxypurines **60**, **61** and **62** in good yields (45 – 85%). To provide final pyrimidine or purine-based compounds, CuAAC reactions were carried out with the alkynes **58**, **59**, **60**, **61** and **62** and the seven different organic azides, using copper iodide ( $CuI$ ),<sup>258</sup> sodium ascorbate, triethylamine and a solvent mixture of dioxane/ $H_2O$  or MeCN/ $H_2O$  depending on the solubility of the alkyne to give final compounds **63** – **97** most in good to excellent yield (29 – 74%) apart from **65** – **67**, **70**, **72**, **73**, **84** (7 – 24%) (Figure 31).

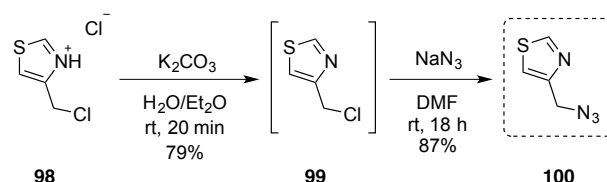
### 4.3. Design, synthesis and biological evaluation of chemical library 3



**Figure 31 | Synthetic route for the preparation of compounds 63 – 97.**

All the organic azides employed in the last reaction step were commercially available except the 4-(azidomethyl)thiazole (**100**), which was synthesized in excellent yield from 4-(chloromethyl)thiazole hydrochloride (**98**) by its conversion to the free base (**99**) under basic conditions followed by a nucleophilic substitution of the chlorine atom with sodium azide (**Figure 32**).



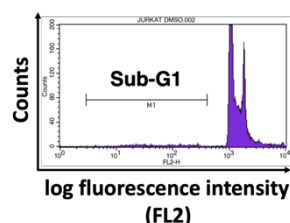


**Figure 32** | Synthetic route for the preparation of 4-(azidomethyl)thiazole 100 from 4-(chloromethyl)thiazole.

### 4.3.3. Screening

Following the same phenotypic screening strategy used with the previous libraries, analysis of the cell cycle was used as the primary output of the screening. Thus, this 35-member library was tested against the same panel of six human cancer cell lines at a single dose (30  $\mu\text{M}$ ) for 48 h, using **6d** (30  $\mu\text{M}$ ) and DMSO as positive and negative control, respectively. The results obtained from the preliminary screening are plotted in **Table 6**.

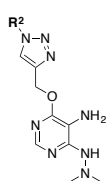
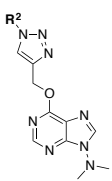
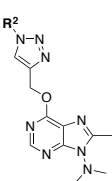
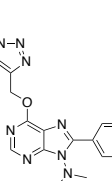
**Table 6** | Phenotypic screening of the chemical library 3 by cell cycle analysis. Cells were incubated during 48 h with the indicated compounds at 30  $\mu\text{M}$ . Then were stained with propidium iodide and analyzed by flow cytometry. The data represent percentage of cell population within the sub-G1 region, after subtracting values from negative controls (DMSO) in each cell line. Compound **6d** was used as positive control. Data from gray area were not calculated.



		Comp.	Jurkat	K562	HeLa	G361	MDA	HCT
		<b>6d</b>	66	6	9	2	4	7
Subfamily	Scaffold							
<b>3a</b>		<b>63</b>	7	1	14	24	4	
		<b>64</b>	16	4	9	18	8	
		<b>65</b>	7	0	3	14	1	
		<b>66</b>	0	0	2	13	1	
		<b>67</b>	1	-1	1	9	2	
		<b>68</b>	1	0	-1	-2	4	7
<b>69</b>	-1	0	0	-1	1	5		

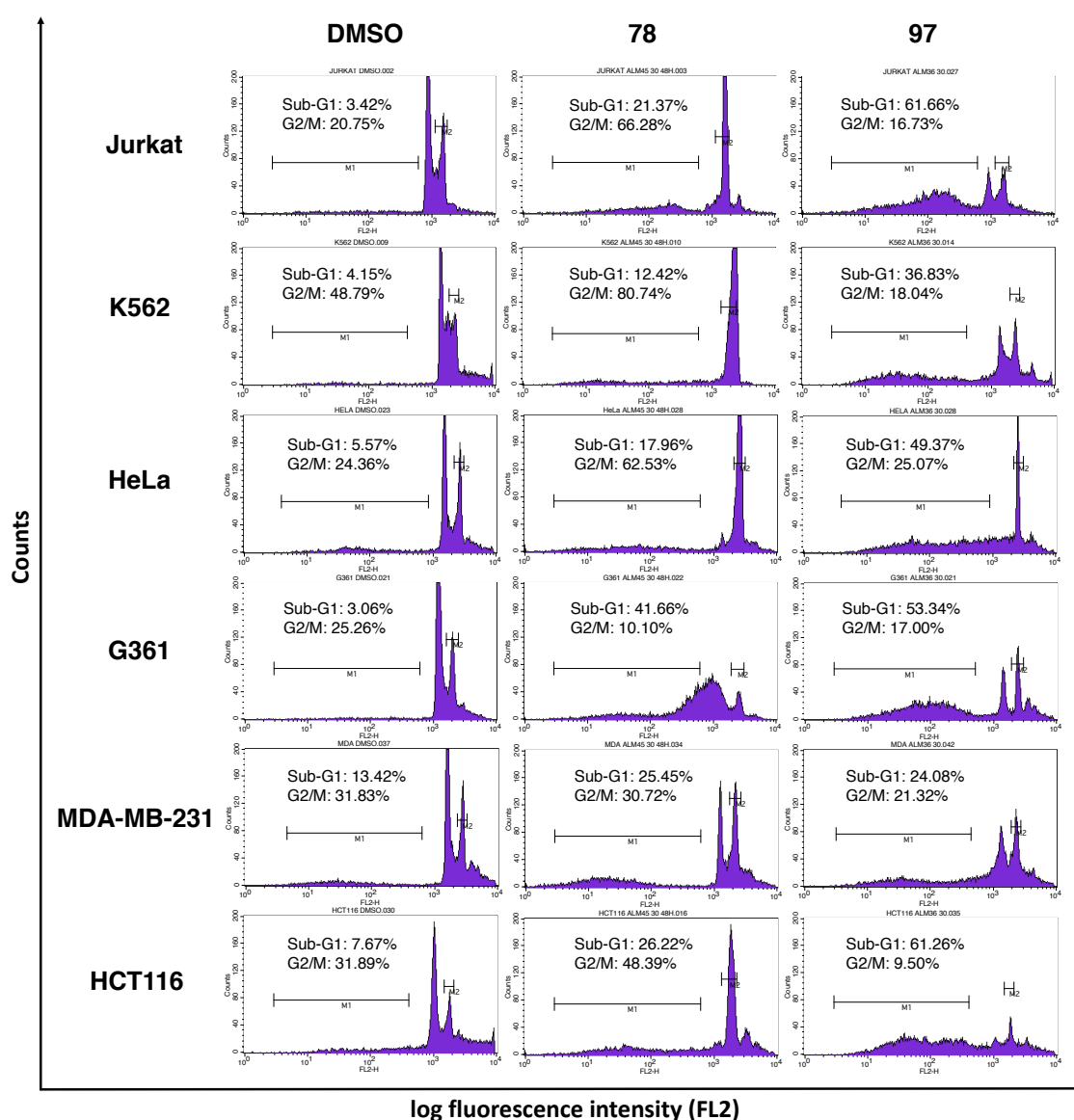
**Table 6** (continued)

### 4.3. Design, synthesis and biological evaluation of chemical library 3

Subfamily	Scaffold	Compd.	Jurkat	K562	HeLa	G361	MDA	HCT
<b>3b</b>		<b>70</b>	-1	1	1	0	0	7
		<b>71</b>	2	0	3	0	-1	10
		<b>72</b>	7	1	1	3	0	4
		<b>73</b>	1	-1	0	1	-1	1
		<b>74</b>	1	0	1	1	4	-1
		<b>75</b>	0	0	1	0	-1	-3
		<b>76</b>	0	6	3	1	1	-1
<b>3c</b>		<b>77</b>	-1	5	-5	0	4	2
		<b>78</b>	18	8	12	39	12	18
		<b>79</b>	2	3	-11	0	1	2
		<b>80</b>	10	-3	0	-1	-5	-15
		<b>81</b>	4	-3	0	-2	-1	-14
		<b>82</b>	2	-2	1	-2	-3	-15
		<b>83</b>	4	-5	18	-1	-4	-9
<b>3d</b>		<b>84</b>	-3	0	5	0	1	4
		<b>85</b>	-4	1	29	0	1	-2
		<b>86</b>	-5	1	6	0	-2	-2
		<b>87</b>	-10	0	4	1	3	8
		<b>88</b>	-10	1	5	2	3	-4
		<b>89</b>	-10	0	4	3	5	1
		<b>90</b>	2	1	12	1	1	0
<b>3e</b>		<b>91</b>	4	-1	2	12	8	4
		<b>92</b>	44	6	23	10	9	14
		<b>93</b>	59	14	39	7	13	38
		<b>94</b>	31	0	8	3	5	4
		<b>95</b>	41	4	27	4	11	8
		<b>96</b>	-5	2	6	1	5	3
		<b>97</b>	56	33	28	48	15	50

From the two open-purine analog **3a** and **3b** sets, compounds from the sublibrary **3a** containing the 4,6-disubstituted-5-nitropyrimidine scaffold did not exhibit any relevant activity in none of the cells used. Just to note, **63** led to a 24% sub-G1 cell accumulation of G361 cells. This percentage was lower when G361 cells were incubated with compound **65**, which has the methoxy group at  $R^2$  at *para* position rather than in *ortho* as **64**. The second pyrimidine based sublibrary, **3b**, which contains the 4,6-disubstituted-5-aminopyrimidine scaffold, was completely inactive in all the lines tested.

Sublibrary **3c** represents the first one of this series containing the purine ring. Compound **78**, which has a hydrogen at C8, and a *m*-methoxy phenyl group as R<sup>2</sup>, belongs to this family and induced low-moderate sub-G1 cell accumulation in all the lines although this effect was significantly higher in G361, where there were a 39% of the total cell population following 48h incubation time at 30  $\mu$ M concentration. Interestingly, cell cycle analysis showed that **78** produced a strong G2/M arrest in all the cell lines tested (Figure 33).



**Figure 33 | Effect of compounds 78 and 97 on the cell cycle of Jurkat, K562, HeLa, G361, MDA-MB-231 and HCT116 cells.** Cells were treated for 48 h with **78** and **97** at 30  $\mu$ M or their equivalent amounts of DMSO used as vehicle. Cells gated on the sub-G1(M1) and G2/M (M2) region after staining with propidium iodide are indicated.

Continuing with the exploration of the purine scaffold, the whole sublibrary **3d** was tested. Notably, compound **85** which only differs from **78** on the C8 position (with a methyl group instead of a hydrogen), did not show any activity in any of the cell lines but the HeLa cells, where it retained a moderate sub-G1 cell accumulation (29%). However, the G2/M arrest effect was not shown in any of the lines tested. Apart from **85**, none of the compounds from this group led to a significant activity.

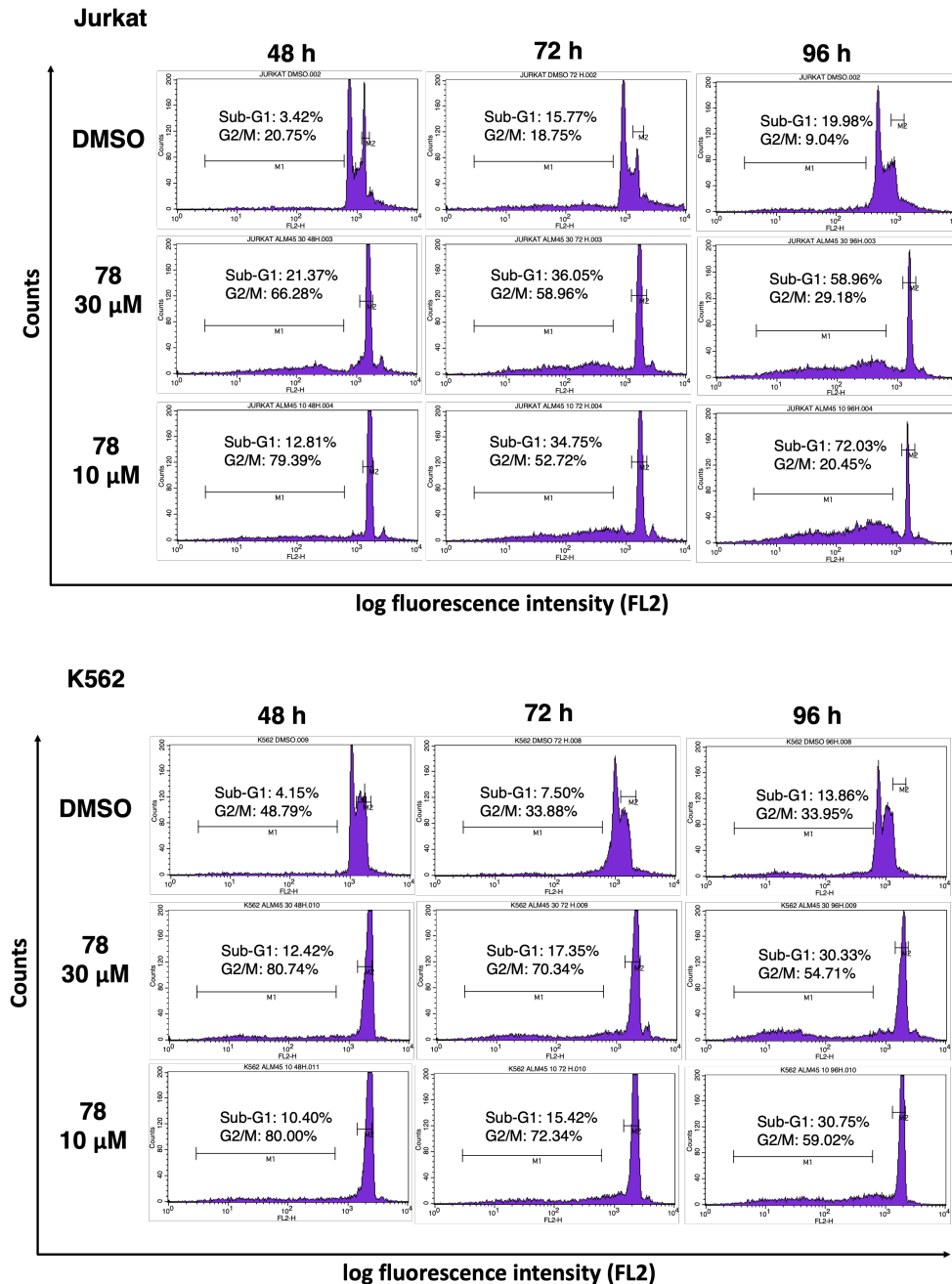
The last sublibrary of compounds belonging to chemical library 3 was **3e**, which contains analogs substituted at C8 position with a phenyl group. As it is shown in **Table 6**, this sub-set of compounds was the most active of the library. Apart from **91** and **96** which did not show any significant activity, the rest of the compounds from this series led to a moderate to high sub-G1 cell accumulation effect in the rest of the cell lines tested. Compounds **92** and **93** which only vary on the position of the methoxy group (in *meta* or *ortho*, respectively) at **R<sup>2</sup>**, exhibited the same cell line selectivity, being active against Jurkat, HeLa and HCT116 cells. However **93** showed higher accumulations of cells within the sub-G1 region (Jurkat 59%, HeLa 39%, HCT116 38%) than **92** (44%, 23% 14%, respectively). Compounds **94** and **95** were also active in Jurkat cells, whereas the latter exhibited a moderate effect in HeLa cells too. In contrast to the previous molecules, compound **97** displayed a wide range activity in all the lines tested even though this effect was considerably higher in Jurkat cells.

Lastly, the alkyne derivatives obtained for the five sub-libraries before the CuAAC reaction were also screened out in order to study their activities and compare them with the final compounds obtained with this reaction. Interestingly, all the alkynes were inactive in all the cell lines, suggesting that the large moieties at position 6 of the purine ring are essential for the activity.

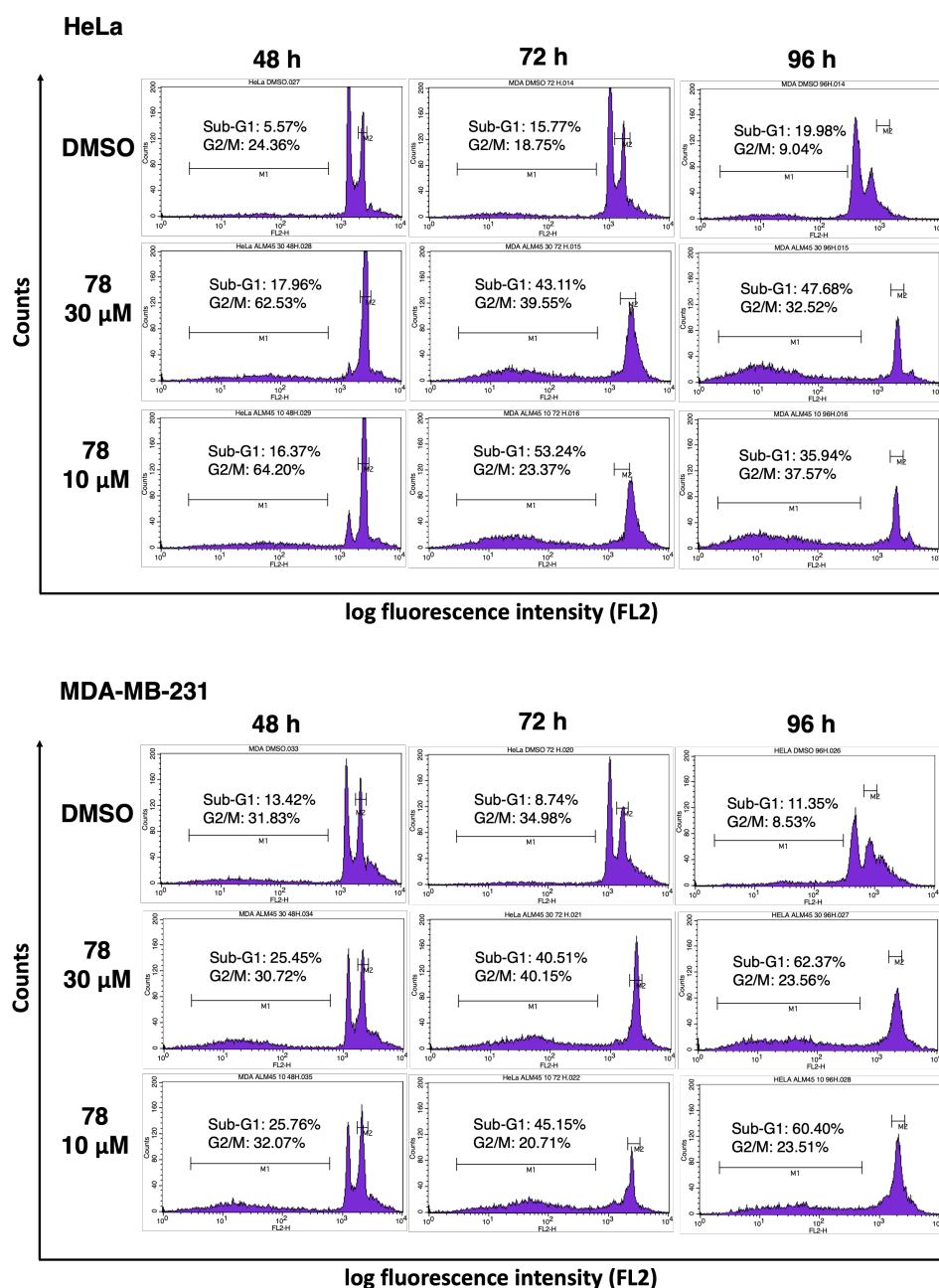
Due to the unexpected G2/M arrest effect of compound **78**, an additional experiment was designed to determine whether this activity was permanent or temporary. To do so, **78** was tested over the cell lines where it exhibited better activities (Jurkat, K562, HeLa, MDA-MB-231) at extended times (48, 72 and 96 h), at 30 and 10  $\mu$ M, using DMSO as negative control.

Compound **78** produced a strong G2/M arrest both at 30 and 10  $\mu$ M in all the cell lines used. This activity was very similar at both concentrations and gradually decreased

from 48 to 96 h (from 24 to 9% in Jurkat, 80 to 54 in K562, 62 to 32% in HeLa and 30 to 23% in MDA-MB-231) while the percentage of apoptotic cells increased (from 21 to 59%, 12 to 30%, 18 to 48% and 25 to 62%, respectively) (**Figure 34 and 35**).



**Figure 34 | Comparison of the effect of 78 on the cell cycle of Jurkat and K562 cells at 48, 72 and 96 h.** Cells were treated for 48, 72 or 96 h with 78 at 30 and 10 µM. DMSO (30 µM) was used as a negative control. Cells gated on the sub-G1(M1) and G2/M (M2) region after staining with propidium iodide are indicated.

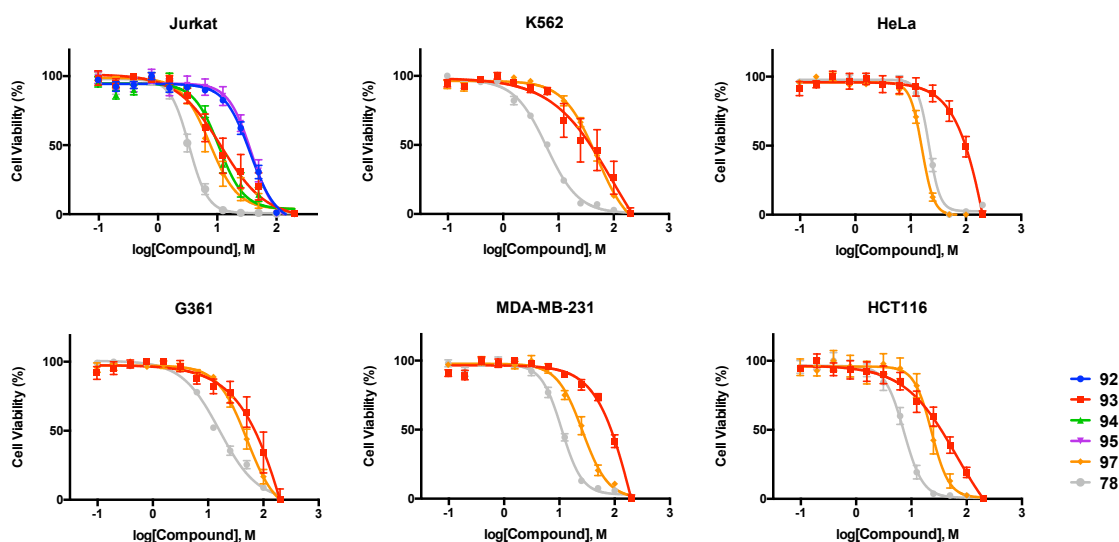


**Figure 35 | Comparison of the effect of 78 on the cell cycle of HeLa and MDA-MB-231 cells at 48, 72 and 96 h.** Cells were treated for 48, 72 or 96 h with 78 at 30 and 10  $\mu$ M. DMSO (30  $\mu$ M) was used as a negative control. Cells gated on the sub-G1(M1) and G2/M (M2) region after staining with propidium iodide are indicated.

#### 4.3.4. Cell proliferation studies

Once the third library was successfully analyzed for their impact on cell cycles, the compounds that showed a major impact were chosen for further cell viability assays.

In this way, compounds **78**, **92**, **93**, **94**, **95** and **97** were selected and their IC<sub>50</sub> values determined. Significant activities were observed in this phenotypic screening. Thus, IC<sub>50</sub> values were calculated for all the compounds in Jurkat cells and for **78**, **93** and **97** were also determined in the rest of cell lines (K562, HeLa, G361, MDA-MB-231 and HCT116).



Subfamily	<b>3e</b>					<b>3c</b>
R <sup>2</sup>	<b>92</b>	<b>94</b>	<b>95</b>	<b>93</b>	<b>97</b>	<b>78</b>
Cell/Compd.	<b>92</b>	<b>94</b>	<b>95</b>	<b>93</b>	<b>97</b>	<b>78</b>
Jurkat	36.21	37.61	10.64	11.65	<b>7.47</b>	<b>3.35</b>
K562						<b>6.07</b>
HeLa						21.47
G361						16.13
MDA-MB-231						11.02
HCT116						<b>7.35</b>

**Figure 36 | Dose-response curves and IC<sub>50</sub> values for compounds 78, 92, 93, 94, 95 and 97.** IC<sub>50</sub> values were determined by PrestoBlue™ cell viability assay after treating Jurkat, K562, HeLa, G361, MDA-MB-231 and HCT116 cells with compounds **92** – **97** and **78** for 5 days (dose range: 0.05 – 200 μM). Error bars ± SEM from n = 3. Values in the grey area were not calculated.

Cells were thus incubated in the presence of compounds for five days in concentrations ranging from 0.05 μM to 200 μM, and compared to **6d**. IC<sub>50</sub> values were

calculated using a 12-point half-log dose-response study and the results shown in **Figure 36**.

The data showed that all the selected drugs from this series exhibited a preferential activity over Jurkat cells than over the other cell lines, with two compounds, **97** and **78** showing potency values below 10  $\mu\text{M}$ . The most potent compound from this set was **78**, which showed the lowest  $\text{IC}_{50}$  value for Jurkat cells (3.35  $\mu\text{M}$ ) and also for the rest of cells except from HeLa. Hence, this compound exhibited a broad range of activity in all the lines tested, being also notable its effect in K562, HCT116 and MDA-MB-231 cells (with  $\text{IC}_{50}$  of 6.07  $\mu\text{M}$ , 7.35  $\mu\text{M}$  and 11.02  $\mu\text{M}$  respectively).

Compound **97**, unlike **78**, showed a more selective activity. This compound exhibited its primary activity in Jurkat cells with an  $\text{IC}_{50}$  of 7.47  $\mu\text{M}$  and an intermediate effect in HeLa cells (16.04  $\mu\text{M}$ ). Some activities were also appreciable in MDA-MB-231 and HCT116 but with  $\text{IC}_{50}$  values above 23  $\mu\text{M}$ .

Compound **93** was not as potent in Jurkat cells (11.65  $\mu\text{M}$ ) as the two previous compounds were. But despite of this, **93** exhibited a very high selective activity for this cell line, not being active in the other lines tested. **94** showed almost identical  $\text{IC}_{50}$  value to **93** in Jurkat cells. And finally, **92** and **95** exhibited higher but very close potency, 36.21  $\mu\text{M}$  and 37.61  $\mu\text{M}$ , respectively.

#### 4.3.5. Annexin-V analysis

To confirm the apoptotic activity of these compounds and at the same time compare their activity with **78**, which mainly produce a G2/M arrest, annexin-V flow cytometric analysis was carried out with **78**, and **97** as a representative of apoptotic compounds. Jurkat cells were treated with the mentioned compounds at 30  $\mu\text{M}$ , 10  $\mu\text{M}$ , 3  $\mu\text{M}$  and 1  $\mu\text{M}$ . Cells treated with DMSO (30  $\mu\text{M}$ ) and **6d** were used as negative and positive control, respectively (**Table 7** and **Figure 37**).

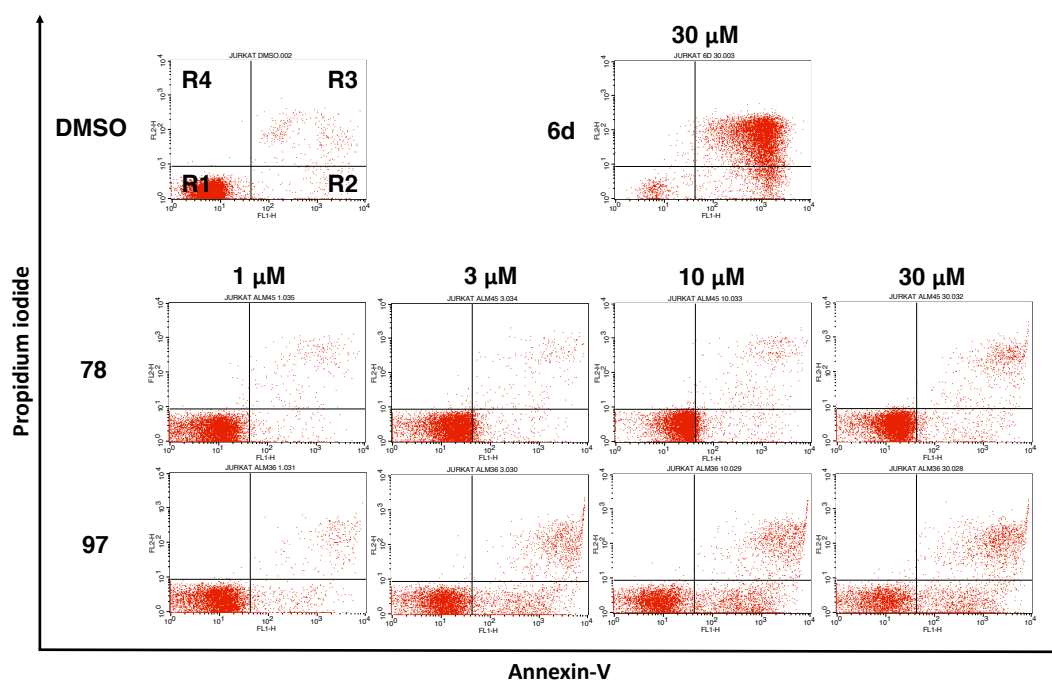
Jurkat cells treated with **78** presented an insignificant apoptotic cell population even at the highest concentration (30  $\mu\text{M}$ ). On the contrary, when Jurkat cells were treated with **97** a transition behavior from early to late apoptotic stages was detected. This effect



increased together with the compound concentration, and therefore confirming that this compound induce cell death by apoptosis in a dose-dependent manner.

**Table 7 | Summary of membrane phosphatidylserine expression after treatment of Jurkat cells with compounds 78 and 97.** The tables collect the percentage of cells within each region **R1** (viable cells), **R2** (early apoptotic cells), **R3** (late apoptotic cells) and **R4** (necrotic cells).

	78				97				DMSO
	1 $\mu$ M	3 $\mu$ M	10 $\mu$ M	30 $\mu$ M	1 $\mu$ M	3 $\mu$ M	10 $\mu$ M	30 $\mu$ M	30 $\mu$ M
<b>R1</b>	94	89	85	86	91	69	61	58	94
<b>R2</b>	3	7	10	6	6	20	25	15	3
<b>R3</b>	3	3	4	8	3	11	14	18	3
<b>R4</b>	0	0	1	0	0	0	0	0	0



**Figure 37 | Membrane phosphatidylserine expression after treatment of Jurkat cells with compounds 78 and 97.** Jurkat cells were treated for 48 h with the indicated doses and the percentages of apoptotic cells were measured by flow cytometry after double staining with propidium iodide and Annexin-V-FLUOS. Untreated cells (DMSO) and cells treated with **6d** were included as negative and positive controls.

#### 4.3.6. Physicochemical properties

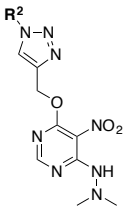
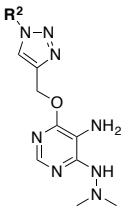
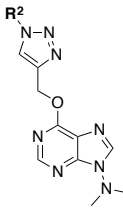
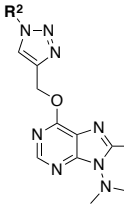
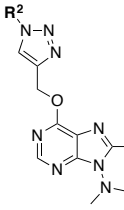
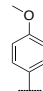
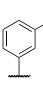
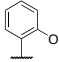
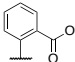
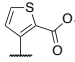
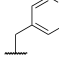
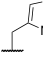
The compounds from this library displayed a broad range of cLog D values (calculated at pH 7.4) that went from -1.5 to 3.

### 4.3. Design, synthesis and biological evaluation of chemical library 3

The compounds from the sublibrary **3b** (Table 9) showed in overall the lowest cLog D values of the full library, most of them below -0.4 and therefore infringing the Lipinski's rule of five. This is due to the presence of a primary and secondary amino group attached to the pyrimidine ring, which strongly increase the basicity of the heterocyclic nitrogen atoms, increasing its pKa so that at pH 7.4 the N3 is mainly protonated. Consequently, this removes the druglikeness of these molecules, being consistent with none of these analogs were active in cells.

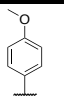
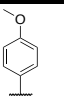
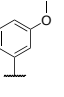
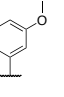
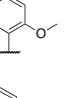
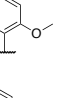
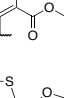
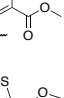
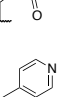
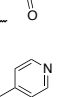
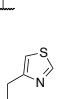
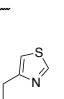


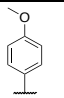
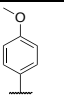
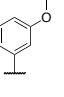
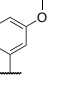
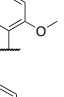
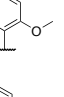
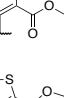
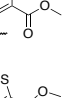
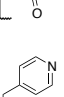
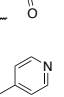
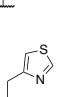
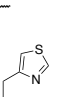


For the nitro-derivatives, the sublibrary **3a** (Table 8), due to the marked electron withdrawing effect of the nitro group, the N3 from the pyrimidine ring is far less basic than in the previous sub-set. As a result, this nitrogen is not protonated at pH 7.4 and therefore the cLog D values are much higher (1.26 – 2.54) than in the sublibrary **3a**.

**Table 8 | Molecular weight (MW) and cLog D values of compounds from the subfamily 3a.**

Subfamily 3a			
Compound	R <sup>2</sup>	MW	cLog D
			
<b>Subfamily 3a</b>	<b>Subfamily 3b</b>	<b>Subfamily 3c</b>	
			
<b>Subfamily 3d</b>	<b>Subfamily 3e</b>		
<b>63</b>		386.37	2.30
<b>64</b>		386.37	2.30
<b>65</b>		386.37	2.30
<b>66</b>		414.38	2.46
<b>67</b>		420.40	2.54
<b>68</b>		371.36	1.30
<b>69</b>		377.38	1.26

**Figure 38 | General structures of the compounds from the sublibraries 3a – 3e.**

**Table 9 | Molecular weight (MW) and cLog D values of compounds from the subfamily 3b, 3c, 3d and 3e. Values in red violate RO5.**

Subfamily 3b				Subfamily 3c			
Compound	R <sup>2</sup>	MW	cLog D	Compound	R <sup>2</sup>	MW	cLog D
70		356.39	-0.48	77		366.39	0.69
71		356.39	-0.48	78		366.39	0.69
72		356.39	-0.48	79		366.39	0.69
73		384.40	-0.32	80		394.40	0.85
74		390.42	-0.24	81		400.42	0.93
75		341.38	-1.48	82		351.37	-0.30
76		347.40	-1.52	83		357.40	-0.34
Subfamily 3d				Subfamily 3e			
Compound	R <sup>2</sup>	MW	cLog D	Compound	R <sup>2</sup>	MW	cLog D
84		380.41	0.82	91		442.48	2.72
85		380.41	0.82	92		442.48	2.72
86		380.41	0.82	93		442.48	2.72
87		408.42	0.98	94		470.49	2.88
88		414.44	1.06	95		476.52	2.96
89		365.40	-0.18	96		427.47	1.72
90		371.42	-0.22	97		433.49	1.68

### 4.3. Design, synthesis and biological evaluation of chemical library 3

In the case of the purine analogs the free amino groups are no longer presented. Consequently, the cLog D values are higher in the cycled analogs and they increase as the position C8 is substituted with larger groups, being lower for 8-H-substituted analogs (sublibrary **3c**) following by the methyl (**3d**) and the phenyl-substituted sublibrary (**3e**) (Tables 8, 9 and Figure 39). Therefore, the latter displayed the highest cLog D values of the entire library although they were not greater than 3.

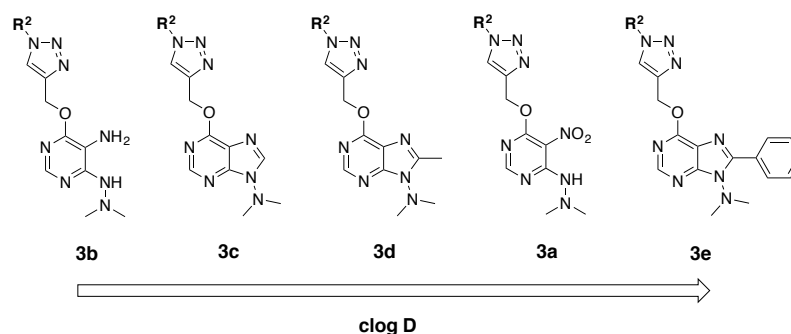


Figure 39 | General cLog D variation among the five subfamilies from the chemical library 3.

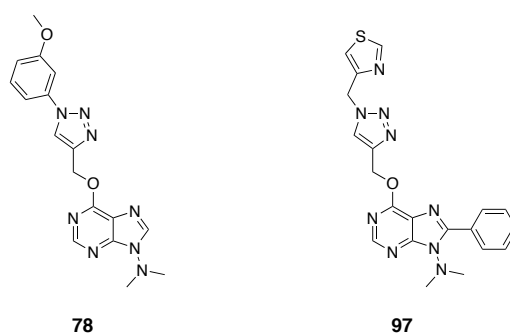
Regarding the substituents that modify the 1,2,3-triazole ring attached at the position C6, compounds that contain the ester moiety (**66 – 67**, **73 – 74**, **80 – 81**, **87 – 88**, **94 – 95**) exhibited very similar values among them, and in addition they conferred the highest cLog D values in each sublibrary.

Then with a difference about 0.2 came the three methoxy benzyl (anisole) isomers and finally the 4-methylpyridine and 4-methylthiazole residues. These last two gave to the final molecules a 1 cLog D unit decrease compared with the benzyl or thiophene ester moieties. Moreover, they provide very similar cLog D values because despite the nitrogen from the pyridine ring is much more basic ( $pK_a = 5.19$ ) than the nitrogen from the thiazole ( $pK_a = 2.18$ ), both groups at pH 7.4 are not protonated.

## 4.4. Optimization of compounds 78 and 97

### 4.4.1. Design of optimized 78- and 97-derived libraries

From the results of the library 3, two hits had been identified: **78**, a compound coming from the sub-library **3c**, with a strong but promiscuous G2-arrest activity; and **97**, a compound coming from the sub-library **3e**, slightly less potent but with a much more selective apoptotic effect.



**Figure 40** | Chemical structures of compounds **78** (G2/M arrest effect) and **97** (apoptotic activity).

Both compounds came from a library designed to explore the C8 and C6 positions of the purine ring, whereas the N9 position remained fixed with the *N,N*-dimethylamino group. Therefore, in order to explore the N9 position and at the same time try to optimize the potency and specificity of these compounds, two additional libraries were designed by the introduction of different groups at the N9 position of the **78** and **97** scaffolds (**Figure 40**). Thus, five different substituents were selected to replace the *N,N*-dimethylamino group. They can be divided in two groups:

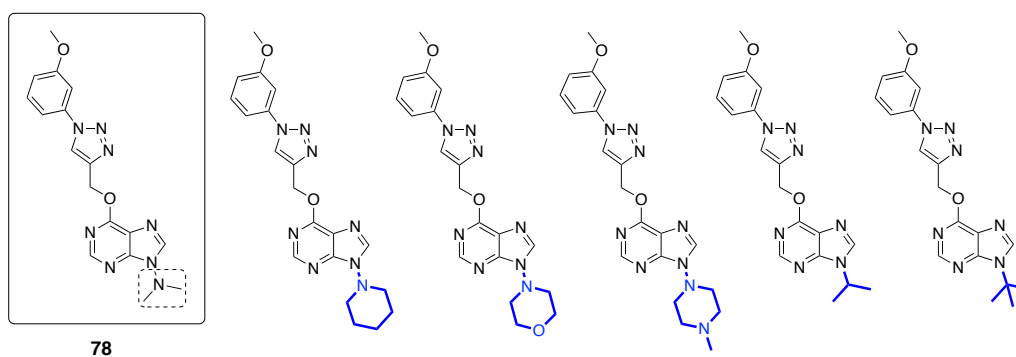
- **Derived from 1-azaheterocycloalkane-1-yl:** Piperidin-1-yl, morpholin-4-yl, 4-methylpiperazin-1-yl groups. These substituents, as in the case of both hit compounds, maintain a nitrogen-nitrogen bond at N9 position of the purine scaffold. However, they differ from the *N,N*-dimethylamino moiety on their size and polarity, and were selected to explore the nature of this position and at the same time provide other physicochemical properties to the new derivatives.
- **Derived from alkyl groups:** Isopropyl and *tert*-butyl groups. In contrast to the previous three substituents, these are alkyl groups, hence they do not contain the

nitrogen-nitrogen bond at N9. They were selected because they represent the classical substitution at this position, which is traditionally used to enhance the binding affinity.

The introduction of these groups was made using the same synthetic route employed for the generation of the library 3 and cycloheteroalkane hydrazines and *N*-alkylamines to modify N9 of the purine ring.

## 4.4.2. Optimization of lead compound 78

### 4.4.2.1. Synthesis of the 78-derived optimized library



**Figure 41 | Proposed compounds to explore the N9 position of 78.**

For the introduction of the six different groups, piperidin-1-yl, morpholin-4-yl, 4-methylpiperazin-1-yl, isopropyl and the *tert*-butyl group at the N9 position of the purine ring (**Figure 41**), commercially available 4,6-dichloro-5-nitropyrimidine (**45**) was initially substituted at C4 position via  $S_NAr$  with propargyl alcohol in THF, providing the alkyne **57** in good yield (67%). Then the chlorine atom from **57** was substituted with the appropriate cycloheteroalkane hydrazine or *N*-alkylamine to give rise to the 4,6-disubstituted-5-nitropyrimidine intermediates (**107 – 111**) in good to excellent yields (46 – 90%). Then the nitro group was reduced with iron and ammonium chloride in a refluxing mixture of water and ethanol to afford the 4,6-disubstituted-5-aminopyrimidine (**112 – 116**) in good yields (31 – 76%). These compounds were then treated with trimethyl orthoformate and a catalytic amount of methanesulfonic acid to give rise to 6-propargyloxypurines **117 – 121** in good to excellent yields (49 – 94%). In the last step, these intermediates underwent a CuAAC reaction with 3-methoxyphenyl azide to provide the final molecules **122 – 126** in good to excellent yields (53 – 82%) (**Figure 42**).

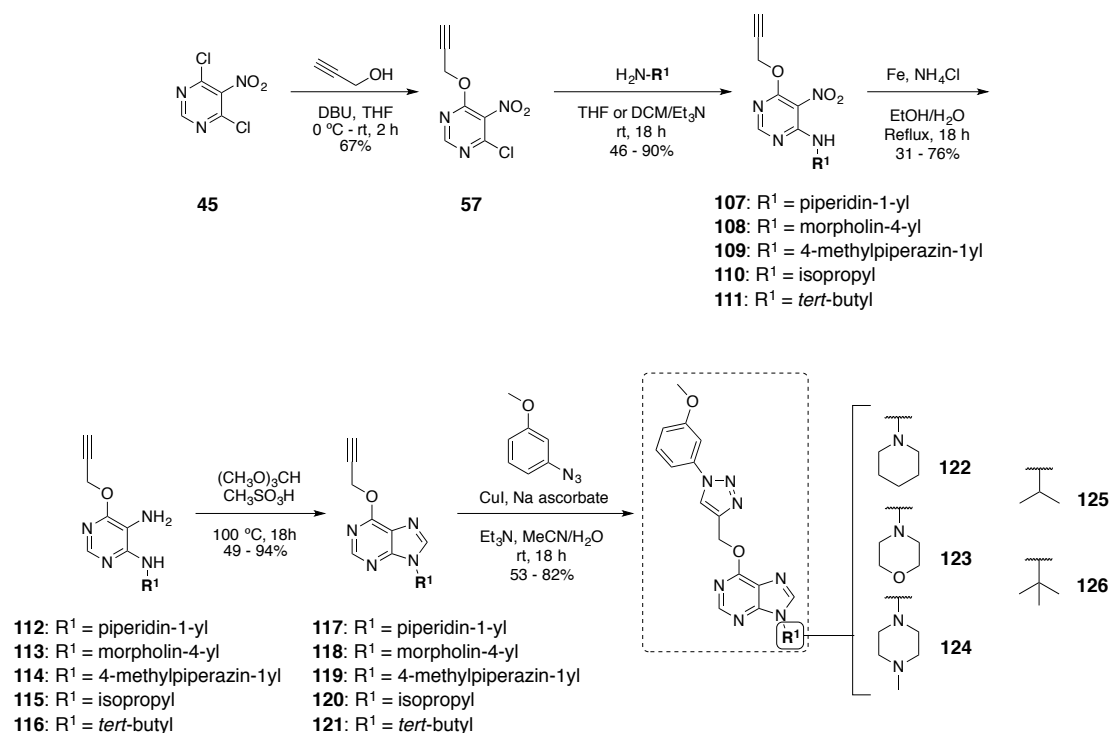


Figure 42 | Synthetic route for the preparation of compounds 122 – 126.

#### 4.4.2.2. Cell cycle analyses

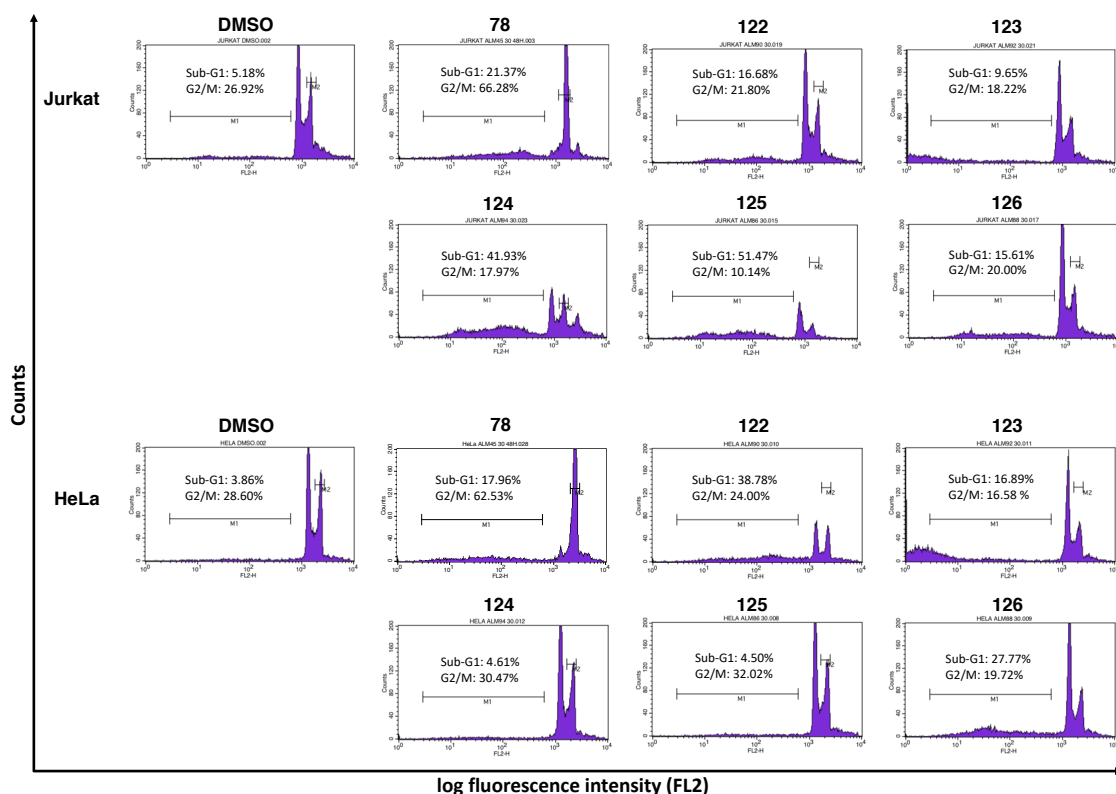
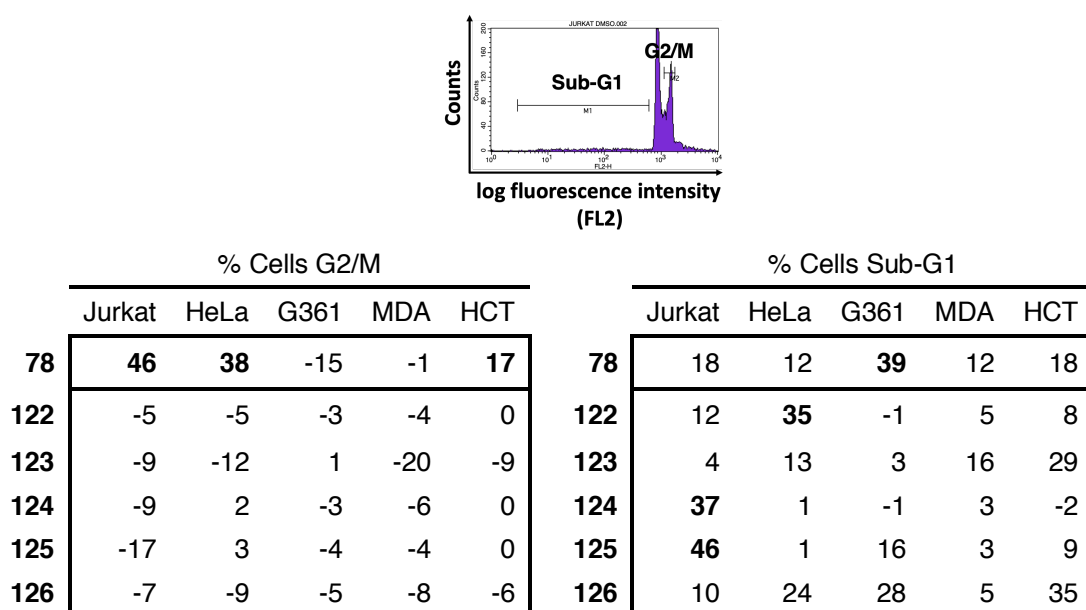
Once the five proposed analogs were synthesized they were tested at a single dose (30  $\mu\text{M}$ ) for 48 h in the same human cancer cell line panel used for the previous libraries and their activities were detected by analyzing alterations in the cell cycle.

With the aim of determining if the chemical modifications included in these new analogs had enhanced the cell arrest properties of the lead compound **78**, the cell cycle analyses were initially performed analyzing the percentage of accumulated cells in the G2-phase. The results were compared with **78** and presented in **Table 10** and **Figure 43**.

With this activity taken away from this compound set, a further analysis of the sub-G1 region was carried out to evaluate whether the modifications made in the lead compound had switched the G2/M arrest for an apoptotic activity (sub-G1 cell accumulation).

#### 4.4. Optimization of compounds 78 and 97

**Table 10 | Summary of the effect in the sub-G1 and G2/M region of compounds 122 – 126 compared with 78.** The data represent percentage of cell population within the G2/M (M2) region and sub-G1(M1) region, after subtracting values from negative controls (DMSO) in each cell line.



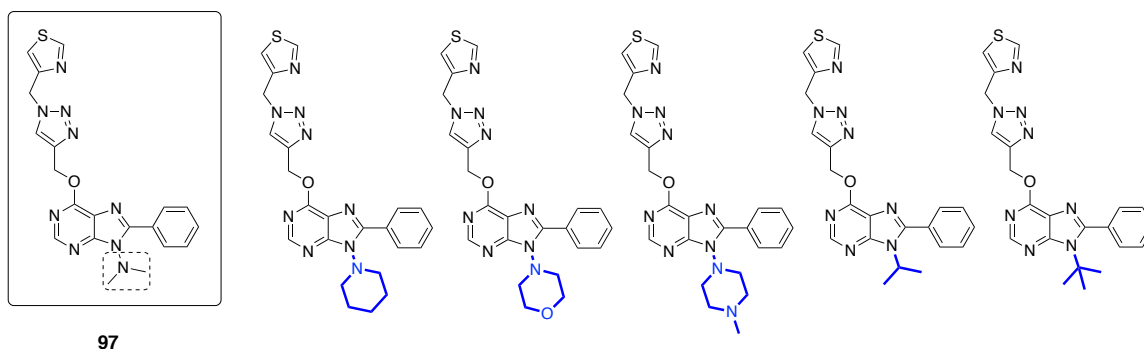
**Figure 43 | Representative experiment where is shown the effect of compounds 78, 122 – 126 over Jurkat and HeLa cells.** Cells were incubated during 48 h with the indicated compounds at 30  $\mu$ M. Then were stained with propidium iodide and analyzed by flow cytometry.



Some of the compounds tested showed an increase in the sub-G1 cell population up to 46% for **125** or 37% in the case of compound **124**, both in Jurkat cells. Other substantial activities were also displayed by **126** in HCT116 and **122** in HeLa with a 35% in both cases. However, none of these derivatives exhibited greater activities than the compounds from the subfamily **3c**.

#### 4.4.3. Optimization of lead compound **97**

For the synthesis of this five-member library (**Figure 44**) was employed the same synthetic methodology previously explained for the generation of the optimized **78** compounds.



**Figure 44** | Proposed compounds to explore the N9 position of **97**.

##### 4.4.3.1. Synthesis of the **97**-derived optimized library

The formation of the intermediate pyrimidines **107** – **111** was achieved following a sequential substitution of both chlorine atoms at position 4 and 6 of the pyrimidine ring by using propargyl alcohol (67% yield) and the appropriate cycloheteroalkane hydrazine or *N*-alkylamine (46 – 90% yield).

The subsequent nitro reduction with iron and ammonium chloride in a mixture of ethanol and water followed by a cyclization with trimethyl orthobenzoate afforded the 6-propargyloxypurines **126** – **130** in good yields. The final compounds **131** – **135** were obtained from **126** – **130** by a CuAAC reaction with 4-(azidomethyl)thiazole in good to excellent yields (61 – 86%) (**Figure 45**).

#### 4.4. Optimization of compounds 78 and 97

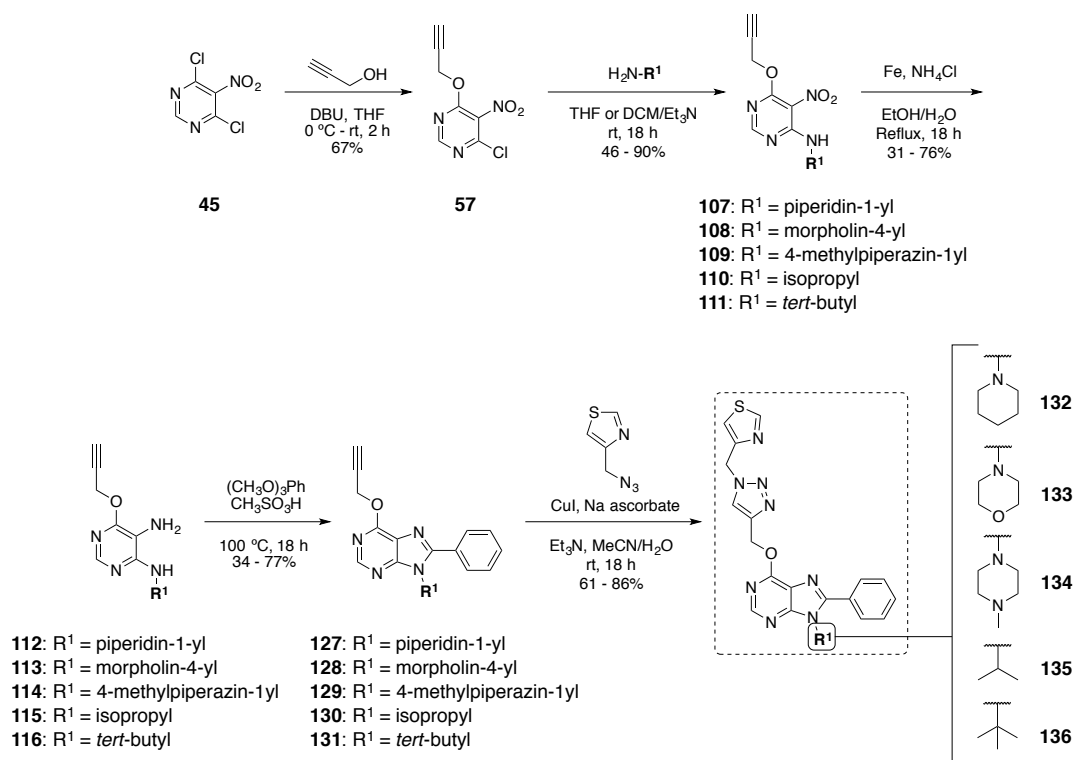


Figure 45 | Synthetic route for the preparation of compounds 132 – 136

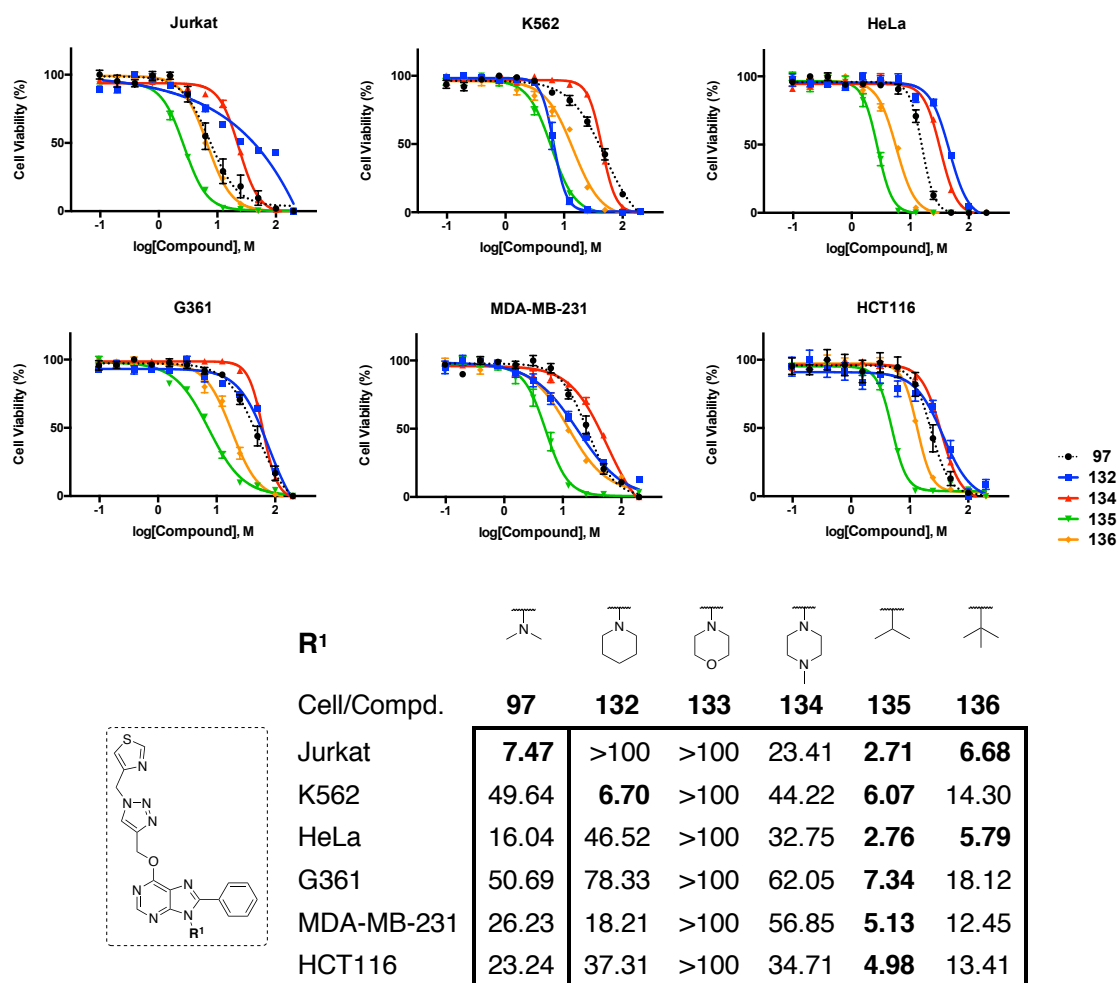
#### 4.4.3.2. Cell viability studies

Cell viability studies were conducted with compounds **132** – **136** upon Jurkat, K562, HeLa, G361, MDA-MB-231 and HCT116 cell lines and the results were plotted in **Figure 46**. It is important to highlight the activities of the compounds **132**, **133** and **134**, which contain the nitrogen-nitrogen bond at N9 from the compounds **135** and **136** that contain a nitrogen-carbon bond instead. The last two compounds contain the isopropyl and *tert*-butyl group respectively at the N9 position of the purine ring, and unlike **97**, they showed high but promiscuous activities in all the cell lines tested.

Notably, compound **135** exhibited greater activities than **97**, showing IC<sub>50</sub> values of 2.71 μM and 2.76 μM in Jurkat and HeLa cells, respectively. Similarly, **136** presented the same activity profile though it was less potent.

In contrast to the two previous molecules, compound **132**, which contains a piperidin-1-yl group at N9 displayed an outstanding switch on the cell selectivity from the lead compound **97**. The activity of the latter over Jurkat cells was totally removed and

in a similar way over HeLa cells, whereas **132** showed high selectivity and potency over K562 cells, with an  $IC_{50}$  of 6.7  $\mu$ M.



**Figure 46 | Dose-response curves and calculated  $IC_{50}$  values for compounds **97** and **132** – **136**.**  $IC_{50}$  values were determined by PrestoBlue™ cell viability assay after treating Jurkat, K562, HeLa, G361, MDA-MB-231 and HCT116 cells with compounds **97**, **132** – **136** for 5 days (dose range: 0.1 – 200  $\mu$ M). Error bars  $\pm$  SEM from  $n = 3$ . Dose-response curves for **133** are not shown.

On the other hand, the introduction of a morpholin-4-yl and 4-methylpiperazin-1-yl group at N9 position led to a non-active compound in the first case (**133**) and a promiscuous but not potent compound in the second (**134**).

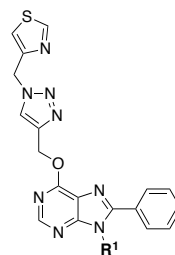
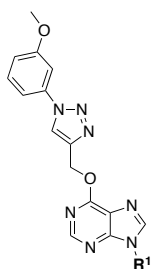
#### 4.4.4. Physicochemical properties

The replacement of the *N,N*-dimethylamino group from **78** and **97** with five different moieties consequently modified the properties of these molecules (**Table 11**). However,

#### 4.4. Optimization of compounds 78 and 97

all the compounds showed cLog D values that fitted within the appropriate drug-like range.

**Table 11 | Molecular weight (MW) and cLog D values of compounds from the optimization of 78 and 97.**



Compound	R <sup>1</sup>	MW	cLog D
<b>78</b>		366.39	0.69
<b>122</b>		406.45	1.54
<b>123</b>		408.42	0.48
<b>124</b>		421.47	-0.05
<b>125</b>		365.40	2.49
<b>126</b>		379.42	2.77

Compound	R <sup>1</sup>	MW	cLog D
<b>97</b>		433.49	1.68
<b>132</b>		473.56	2.53
<b>133</b>		475.53	1.46
<b>134</b>		488.57	0.79
<b>135</b>		432.51	3.48
<b>136</b>		446.53	3.76

The large lipophilicity of the *tert*-butyl group meant the increase of the cLog D value in 2 units and similarly but slightly lower occurred with the isopropyl group. On the other hand, regarding the substituent derived from the *N,N*-dialkylhydrazines, only the piperidin-1-yl group gave an increase in the cLog D (0.85 units) compared to the *N,N*-dimethylaminated compounds. This could be explained with the three additional cycloalkyl carbons and the bigger size of the substituent.

Finally, the introduction of the morpholin-4-yl group changed the polarity of the substituent, but it slightly decreased the cLog D (0.21 units). However, when at this position was attached the 4-methylpiperazin-1-yl moiety the cLog D dropped 0.74 units.

This reduction is produced because the tertiary nitrogen at the position 4 of the piperazine is highly basic (pKa around 8), so at pH 7.4 these species are mostly protonated.



## **5. Discussion**

---





The era of classical chemotherapy for cancer treatment is giving way to the use of much more selective and less harmful therapies known as target therapies. In this novel therapeutic field, protein kinases play a key role in the development of cancer disease since deregulation of these proteins is linked to the development of cancer and others diseases.<sup>65-74</sup> For this reason, in recent years, great resources are being allocated for the development of selective inhibitors of these proteins.

Most of the kinase inhibitors used in the clinic are small molecules and usually share similar chemical structures. Among them, the purine scaffold and its derivatives are one of the most commonly used and from which potent drugs and inhibitors have emerged.<sup>227</sup>

Our group developed a new family of 18 purines substituted at position C6 by an ether moiety, using a novel synthetic route.<sup>209</sup> The active compounds of this library exhibited a potent and selective pro-apoptotic activity over Jurkat cells, being the hit compound **6a** a selective DAPK1 inhibitor.<sup>210</sup>

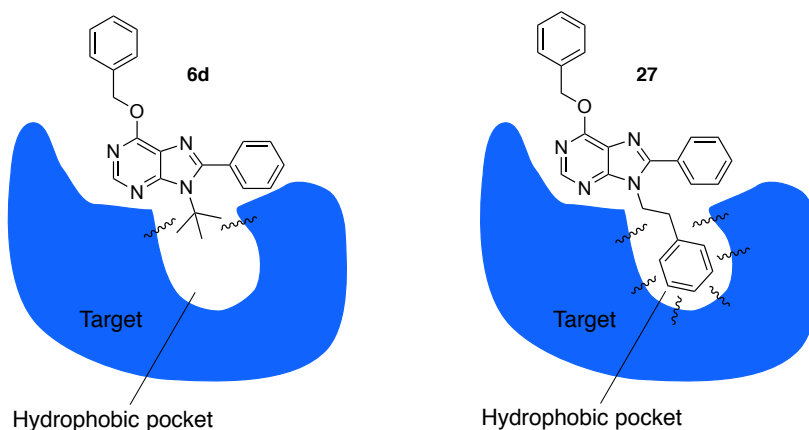
In this thesis, we have analyzed the biological anticancer activity of the 6-alkoxypurine scaffold by generating different libraries of substituted analogs at positions C2, C6, C8 and N9, with the aim of improving the pro-apoptotic activities of the lead compound **6d** over Jurkat cells, generate derivatives with better physicochemical properties and explore the 6-alkoxypurine core. All of this guided by a phenotypic approach, using a panel of 6 cancer cell lines that includes hematopoietic (Jurkat and K562) and non-hematopoietic (HeLa, G361, MDA-MB-231 and HCT116) cells.

As a result, 64 final compounds derived from 6-alkoxypurine were synthesized in 5 different libraries (including 2 optimized libraries). Initially, in order to improve the activity of **6d** an array of 14 compounds (library 1) was generated through the above-mentioned synthetic methodology. This allowed the introduction of alkyl groups and aromatic substituents at positions C6, C8 and N9 of the purine ring, as well as the introduction of an amino group at C2 and the isolation of Schiff bases for sterically hindered compounds. However, the introduction of hindered hydrophobic substituents at N9 was the only successful way to enhance the phenotypic activity of these compounds in Jurkat cell line.

The presence of an amino group at C2 has been reported to act as a stabilizer in some kinase inhibitors by the formation of an additional hydrogen bond with the target.<sup>259</sup>

However, the introduction of this amino group to the **6d** structure led to inactive compounds, suggesting that this amino group rather than acting as stabilizer seems to block the access to the binding site or blocking the bond formation with the target. Similarly occurs with the inactive Schiff base intermediates, although these results were much more predictable as the imine functionality creates a deep structure alteration on the compounds since the purine ring is no longer conserved. However, despite these Schiff base intermediates were not active, the fact that they were isolated exclusively for those compounds that have bulky substituents at C8 reinforces the mechanistic proposal made by the group in which the imine formation was highlighted as a key intermediate step for the generation of final compounds when the reaction goes through the use of hindered *N,N*-dimethylamides (**Route B**).<sup>209</sup>

On the other hand, compounds **27** and **28**, which contain a phenethyl group at N9 instead of the *tert*-butyl group presented in **6d**, showed a substantial 2-fold potency improvement. This could suggest that despite both moieties are able to interact with a hydrophobic pocket of the target, the phenethyl group, due to its two-carbon alkyl chain, could extend the phenyl group to a hydrophobic pocket further away from the catalytic pocket of a kinase/target, establishing stronger interactions with it than the smaller *tert*-butyl group (**Figure 47**).



**Figure 47 | Biological hypothesis of the interaction of the *tert*-butyl and phenethyl groups with the target.** Curved lines represent hydrophobic interactions.

In addition, the hypothesis that these inhibitors interact with a hydrophobic pocket of the target is also reinforced when the activities of **27** and **28** are compared. Despite of being very close analogs, they differ on the presence of a *para*-substituted bromine atom at the substituents at C6 and C8. This atoms make **28** more lipophilic and consequently

lead to a potency improvement, from an  $IC_{50}$  of 9.99  $\mu$ M (**27**) to 7.29  $\mu$ M (**28**). Moreover, **27** and **28** not just showed a great pro-apoptotic activity towards Jurkat cells as **6d** when comparing with K562 cell line but also they did not have any effect on the four adherent cell lines tested. This demonstrate the great selectivity of this pharmacophore unit against acute T cell leukemia. However, the introduction of larger substituents, such as the phenethyl group, at N9 had also an undesirable effect on the solubility of the derivatives, which exhibited cLog D values above 6 and consequently on their practical application *in vitro* and *in vivo*.

To solve the solubility issues of these compounds, chemical library 2 was developed by the simply but groundbreaking introduction of *N,N*-dialkylamino or 1-azacycloalkane-1-yl groups at N9. The additional nitrogen atom presented on these new purine scaffolds generated analogs such as **51** and **52**, with very similar structural size to **6d** but with cLog D values (1.06 – 3.98) within the druglikeness range. However, despite this substantial physicochemical improvement, none of these analogs retained the activity in the cell tested. This fact could be explained because, although the size of *N,N*-dialkylamino or 1-azacycloalkane-1-yl groups is very similar to the isopropyl (**6a**) or *tert*-butyl (**6d**) groups, the presence of the additional nitrogen atom at this position confers the molecule the ability to establish polar interactions with the target, such as hydrogen or ionic bonds, which in this case seems to disturb the biological interaction of these analogs.

From a synthetic point of view, the *N,N*-dialkylamino and 1-azacycloalkane-1-yl groups were initially introduced by a coupling reaction of a chloropyrimidine with the corresponding hydrazines. After cyclization of the yielded diaminopyrimidines, 6-chloropurines were then substituted via nucleophilic aromatic substitution ( $S_NAr$ ) with benzyl alcohol under strong basic conditions. However, the latter step did not work with 8-phenyl-substituted compounds and the starting 6-chloropurines were recovered. Although  $S_NAr$  reactions on 6-chloropurines with different alcohols is a common method to introduce variability at the C6 position, these reactions are typically carried out on 8-methyl or 8-H-substituted purines.<sup>239,260</sup> Therefore, the inability to generate the designed 8-phenyl substituted compounds, suggest the implication of this phenyl group. This moiety could difficult the chlorine displacement as a consequence of its steric hindrance, and since the purine scaffold is not particularly activated, the reaction did not take place. However, the complete inhibition of the  $S_NAr$  will need to be investigated in the future.

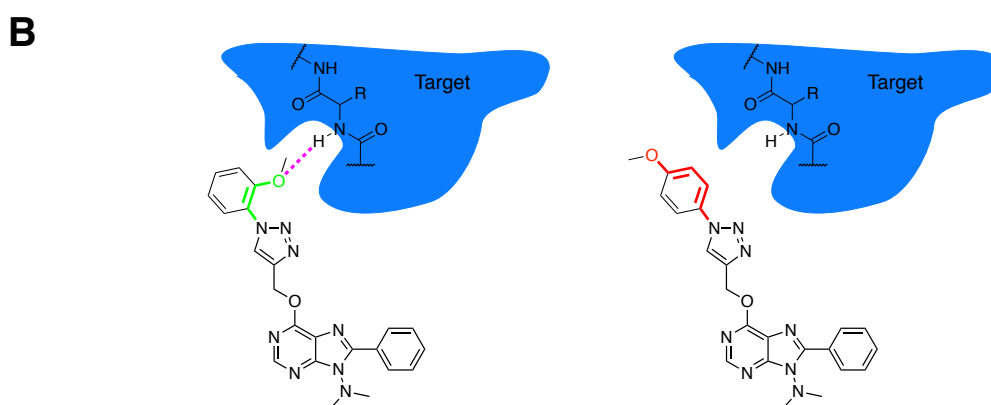
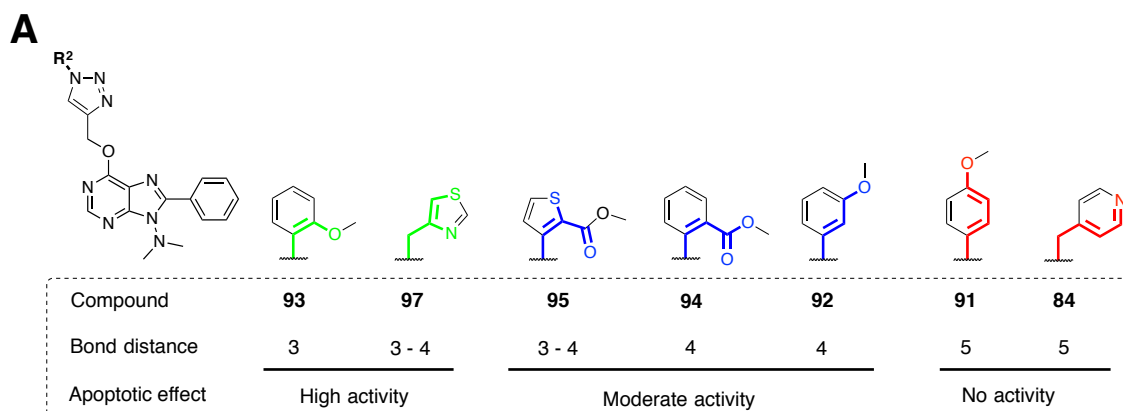
To prepare the 8-phenyl-substituted analogs, the synthetic route was redesigned and the substituents at C6 and N9 were introduced by two consecutive S<sub>N</sub>Ar reactions over the 4,5-dichloro-5-nitropyrimidine core, following by the nitro reduction and ring closure steps. This synthesis offers many benefits when compared to the synthetic route used to obtain chemical library 1. Firstly, due to the activated positions where the displacements take place, the reactions are carried out faster, under milder conditions and consequently made it compatible with more functional groups. Secondly, it does allow to introduce more structure diversity as substituents at C8 and C6 can be different, making this new synthetic procedure very versatile and useful for the generation of purine libraries and derivatives.

The remarkable druglikeness improvement of the compounds from chemical library 2 compared to **6a**, **6d**, **27** and **28**, together with the wide exploration possibilities offered by this new synthetic route, led us to design a series of 35 compounds (chemical library 3) derived from the 6-alkoxy-9-dimethylaminopurine scaffold and its open analogs by the smart implementation of a CuAAC diversification strategy at C6 position.

From this library, only compounds that contain the conserved purine ring and were substituted at 8-position with a phenyl group (sublibrary **3e**) showed significant pro-apoptotic activities, which is consistent with the structure of the previous pro-apoptotic compounds (**6a**, **6d**, **27** and **28**). In addition, the presence of the substituted-1,2,3-triazole group is a key structural feature for the activity, as their corresponding alkyne precursor **62** did not show any activity on cells. This fact also correlates with the biological inactivity of compound **51**, which contains an electronically similar group, the benzyloxy moiety at C6 instead the propargyloxy from **62**. All this indicates that C8-phenyl-substituted compounds that bear the *N,N*-dimethylamino group at N9 need the presence of 2-(1-arylsubstituted-1,2,3-triazol-4-yl)methoxy at C6 to exhibit pro-apoptotic activities.

However, within the substituents attached to the triazole ring, not all led to active compounds. Thus the *para*-anisole (**91**) and the 4-methylpyridine (**84**) were not active. Remarkably, these two groups were the only ones that presented their functionalities attached at the furthest positions from the triazole core (at 5-bond distance). Contrary to this, active compounds contained the functional groups from the triazole substituents attached at the nearest positions, *ortho*-position for the methoxy group (**93**) and

equivalent bond distance for the nitrogen of the thiazole ring (3-bond distance, **97**). Finally, compounds that showed moderate apoptotic activities presented their functional groups at intermediate distances, 4-bond distance (**95**, **94**, **92**) (**Figure 48A**).



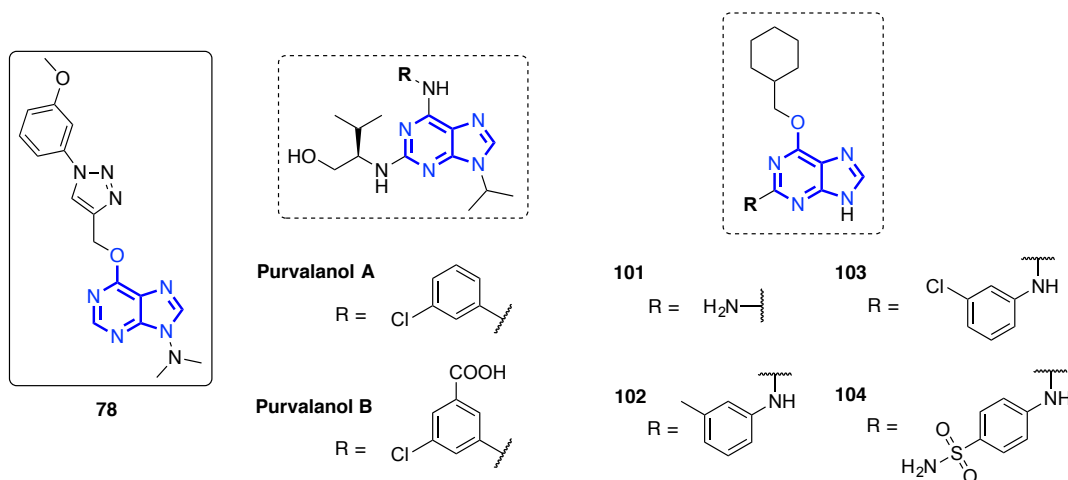
**Figure 48 | Relationship between the triazole functionalization and the in vitro activity of the molecules.** (A) Correlation between biological activity and the distance between the triazole ring and the nearest heteroatom from the substituent at N1. (B) Biological hypothesis of this correlation.

The relation between the location of the functional groups attached to the triazole ring and the compound activity may suggest that these functionalities are involved in the interaction of these molecules with the biological target. This could be due to an hydrogen bond formation that only can be established when the heteroatoms of these groups are located at the appropriate distance from the hydrogen bond donor of the target (**Figure 48B**).

On the other hand, compound **78** was the only active non-8-phenylsubstituted purine analog from chemical library 3. However, instead of exhibit pro-apoptotic activities, **78** induced a robust G2/M-arrest effect in Jurkat, K562 and HeLa cells. This result was very interesting as no other compounds from the library exhibited this activity, not even their

very close 8-methy or 8-phenyl-substituted analogs (**85**, **92**) and neither their *para* or *ortho*-anisole isomers (**77**, **79**).

A reasonable explanation to this unexpected activity could be that the C8-H-substituted purine scaffold contained in **78** is a template presented in many cyclin-dependent kinase (CDK) inhibitors (**Purvalanol A**, **Purvalanol B**),<sup>261</sup> some of them containing the oxygen atom attached to C6 (**101**, **102**, **103**, **104**)<sup>262,263</sup> (**Figure 49**).

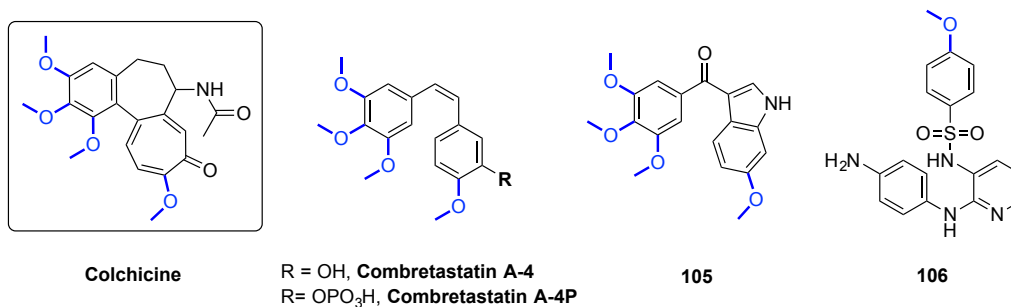


**Figure 49** | Chemical structures of representative C8-H-substituted CDK1 inhibitors.

These inhibitors have been widely studied for targeted anticancer therapy because their target proteins are critical regulatory enzymes that drive all cell cycle transitions.<sup>264</sup> Specifically, CDK1 activity has been documented to be critical for initiation and transition through mitosis.<sup>265</sup> Hence, CDK1 inhibition has been reported to arrest human cells at the G2/M border of the cell cycle and extended inhibition of this protein (above 24 h) ultimately leads to apoptosis induction in tumor cells.<sup>266–268</sup> Therefore, the structural similarity of some CDK1 inhibitors with **78**, together with the observed G2/M arrest effect suggest that this compound may act as a CDK1 inhibitor.

In addition, although CDK1 inhibition for up to 24 h is well tolerated, it has been reported that longer exposure induces apoptosis in cancer cells.<sup>267</sup> This effect was confirmed when **78** was incubated at extended times (48, 72 and 96 h) on Jurkat, K562, HeLa and MDA-MB-231 cells, where the initial G2/M cell population gradually decreased and the apoptotic population increased.

However, other plausible explanation for the antimetabolic effect of **78** would be that this compound acts as a microtubule-targeting agent. Microtubules play an important role in several cellular processes, particularly in the formation of the mitotic spindle during the process of mitosis. Hence, compounds that target these structures either by inhibiting or promoting the tubulin polymerization are molecules with desirable biological effects for cancer therapy.<sup>269,270</sup> Examples of compounds with these activities used clinically to treat cancer are vinca alkaloids, colchicine, taxanes and derivatives.

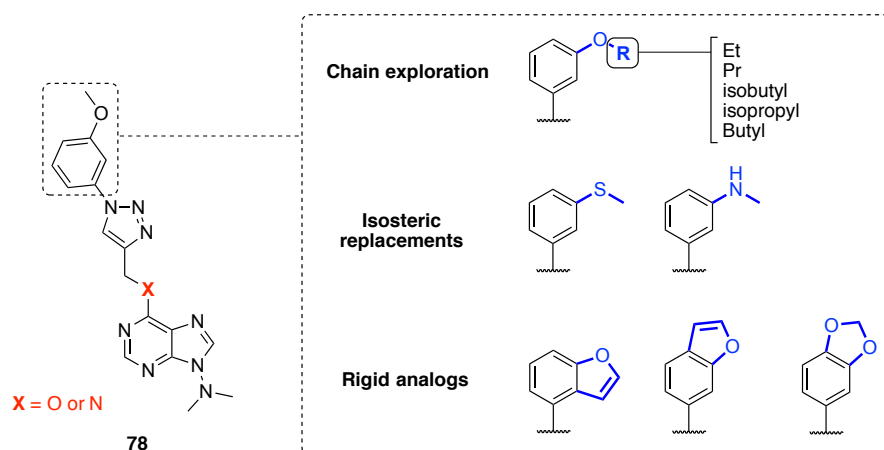


**Figure 50 | Chemical structures of representative microtubule-destabilizing colchicine analogs.**

Although the structures of these families are very diverse, it is known that the presence of methoxy groups attached to benzene rings are critical for the activity, especially for compounds that bind to the colchicine binding site.<sup>271,272</sup> Therefore, many colchicine analogs like **Combretastatin A-4**, **Combretastatin A-4P**, **105** and **106** (**Figure 50**), designed as microtubule-destabilizing agents, have been developed by the simplification of the colchicine scaffold trying to generate analogs with improved potency and solubility.<sup>273–275</sup> This way, due to the potent G2/M arrest and the presence of the methoxy phenyl group, both characteristic features of colchicine analogs, make us to consider that compound **78** may interact with the tubulin assembly in a similar way colchicine analogs do.

The optimization process of compound **78** by the introduction of different 1-azaheterocycloalkane-1-yl and alkyl groups at the N9 position did not improve the G2/M arrest effect, indeed none of the modifications led to derivatives with this activity. This result together with the efforts made on chemical library 3, where the attachment of groups at C8 or the substituent modifications carried out on the triazole ring gave rise to inactive compounds, highlighted the significance of each substituent in **78** to maintain the G2/M arrest activity.

Therefore, future optimizations process should focus on the study of positions that have not been explored yet. This could be done by the replacement of the ether functionality through which substituent at the C6 are attached to the purine ring. Thus, the introduction of a secondary amino group, which is widely present in many purine-based drugs, instead of the ether groups should be explored (**Figure 51**).



**Figure 51 | Suggested structural changes to explore the biological implication of the methoxy group and the ether moiety.**

Other interesting study would be a comprehensive evaluation of the role of the *meta*-methoxy group attached to the phenyl ring that substituted the 1,2,3-triazole core from the C6 moiety, which could be carried out following different strategies:

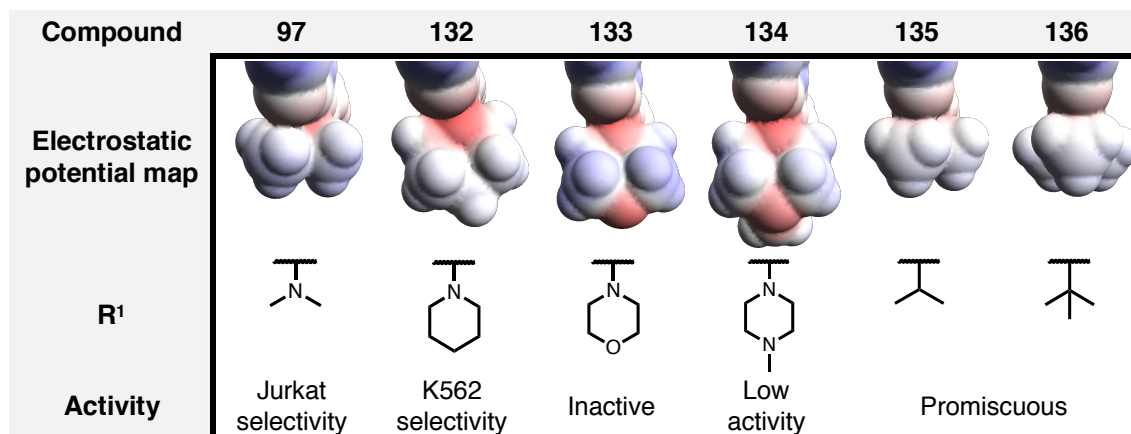
- Building analogs with larger alkyloxy substituents such as ethoxy, propoxy, isobutoxy, isopropoxy, and n-butoxy.
- Generating derivatives by the isosteric replacement of the methoxy group by the methylthio or methylamino groups.
- Constructing rigid oxygen-contained cycled analogs, such as benzofurane and 1,3-benzodioxole.

In addition, in order to test the two hypotheses that have been proposed to explain the biological activity of this compound, target deconvolution strategy can be initiated by enzymatic assays performed with the isolated CDK1 protein to determine its IC<sub>50</sub> value, as well as biochemical or cellular assays to determine if this compound interferes with microtubule assembly.<sup>276</sup>



The optimization process carried out on compound **97** led to compounds that showed very interesting properties, and remarkably that the modifications at N9 changed the cell selectivity of the new compounds compared with **97**. Thus, the selective effect of **97** for Jurkat cells ( $IC_{50}$  of 7.47  $\mu$ M) completely switched to K562 cells for its derivative **132** ( $IC_{50}$  of 6.7  $\mu$ M), led to an inactive compound (**133**) and gave rise to various promiscuous compounds (**134**, **135**, **136**). This effect could be explained by the different electronic distribution on each substituent at N9, that as a consequence lead to molecules that exhibit different biological behaviors.

Thus, the isopropyl and *tert*-butyl groups are lipophilic substituents that allows **135** and **136** to interact indiscriminately with hydrophobic regions of target. This fact correlates with their potent but very promiscuous activities in all the cell lines tested. However, although the introduction of the *N,N*-dimethylamino group led to a very structural-related analog, (**97**), the less electron density of their methyl groups makes this substituent less lipophilic. This, together with the presence of the additional nitrogen atom, prevent **97** to easily form hydrophobic interactions, as a consequence this compound only exhibited activity on Jurkat cells (**Figure 52**).



**Figure 52** | Graphical representation of the electrostatic potential map of the groups attached at the purine N9 position in compounds **97** and **132** – **136**. Red, blue and white colors indicates negative, positive and neutral charged regions, respectively.

The structural expansion of the *N,N*-dimethylamino group led to **132**. In this case, the piperidine group is highly lipophilic and shows very similar electrostatic potential map compared to the isopropyl or *tert*-butyl groups (**Figure 52**). However, the nitrogen atom, which can establish polar interactions and the size difference made this compound distinguished from the alkylated substituted compounds **97**, **135** and **136**. Probably due

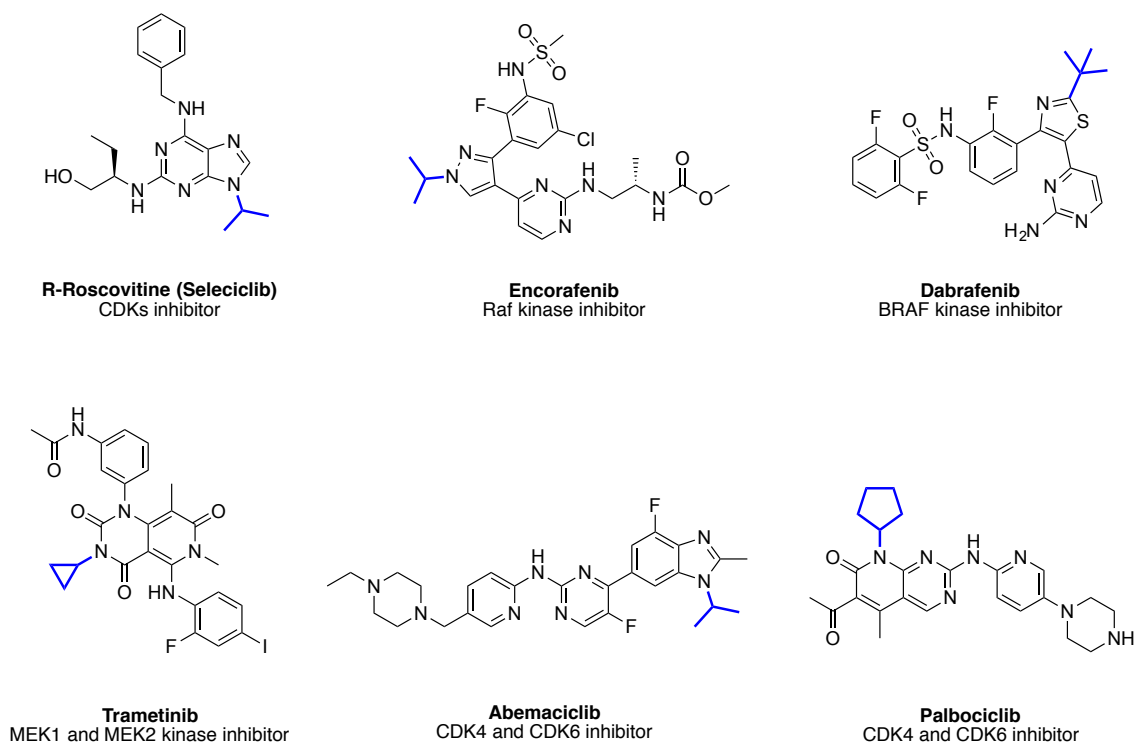
to this two features, **132** was not able to interact with its targets on Jurkat, such as **97**, but it did better on K562.

The introduction of an oxygen atom to obtain the morpholine derivative **133** led to an inactive compound. Interestingly, in this case the moiety exhibits the most different electronic distribution, as the oxygen atom polarizes this substituent and therefore changes the lipophilic character of the groups presented at this position. Similarly occurs with **134**, although the methyl mitigates the polarization and consequently this compound exhibited some activity.

To the previous electronic distribution explanation must be added the hydrogen bonding ability that the *N,N*-dimethylamino and 1-azacycloalkane-1-yl derivatives have. The nitrogen atom attached to N9 can act as an hydrogen bond acceptor and establish polar interactions with the target. This could make these compounds interact more specifically with some targets rather than others.

Either way, the results of this study indicated that the simply but pioneering introduction of a nitrogen atom into the alkylated moieties at the purine 9-position have an strong effect on the selectivity profile of these compounds. At this point, this work should progress towards the identification of the biological target for the selective compounds **97** and **132**, to later *in silico* or by co-crystallization with the target confirm the proposed hypothesis. That being the case, this findings will have a number of important implications for future practice to refine the activities of other small molecule inhibitors.

Thus, the replacement of isopropyl and *tert*-butyl groups for *N,N*-dimethylamine or 1-azaheterocycloalkane-1-yl groups could be extended to recognized purine-based kinase inhibitors like Roscovitine (experimental drug), SKLB1206 or VS5584 (both in clinical trials) and also to many FDA approved kinase inhibitors that contain these groups, such as Encorafenib (Braftovi<sup>®</sup>, Arrat Biopharma) o Dabrafenib (Tafinlar<sup>®</sup>, GSK) or Ceritinib (Zykyadia<sup>®</sup>, Novartis). Moreover, this could be extended to their close bioisosters cyclopropyl group (Lenvatinib, Trametinib) or cyclopentyl group (Ruxolitinib, Palbociclib) (**Figure 53**).



**Figure 53 | Chemical structures of representative FDA approved small molecule protein kinase inhibitors containing isopropyl, *tert*-butyl, cyclopropyl or cyclopentyl groups.**



## **6. Conclusions**

---



The 6-alkoxypurine core has demonstrated to be a versatile scaffold for the generation of biologically active compounds against different cancer cell lines. In addition, the presented synthetic methodologies have allowed the straightforward generation of a great variety of these analogs.

1. A library of 64 compounds based on the 6-alkoxypurine scaffold and substituted at positions C2, C6, C8 or N9 has been synthesized by using four different synthetic routes.
2. The introduction of hindered hydrophobic substituents at the N9 position of the **6d** scaffold enhanced the selective pro-apoptotic effect over Jurkat cells observed for compounds **27** and **28**, which showed a 2-fold potency improvement.
3. We reported for the first time purine-based analogs containing *N,N*-dimethylamine or 1-azacycloalkan-1-yl groups at N9 position, giving rise to compounds that exhibit significant improvements in their physicochemical properties compared to classical alkylated compounds.
4. The new synthetic route designed by the introduction of a CuAAC reaction generated a great structural variety of compounds with two different phenotypic activities: apoptosis induction and G2/M arrest.
5. The optimization process of the pro-apoptotic compound **97** showed that the moiety attached at N9 modulates the selectivity of the compound against different cell lines. Hence, the novel introduction of a nitrogen-nitrogen bond at N9 allowed the generation of some compounds which showed cell-restricted effects, whereas removal of this structural feature leads to analogues with potent but broad tissue specificity.





## **7. References**

---



- (1) Hajdu, S. I.; Vadmal, M.; Tang, P. A Note from History: Landmarks in History of Cancer, Part 7. *Cancer* **2015**, *121* (15), 2480–2513. <https://doi.org/10.1002/cncr.29365>.
- (2) Breasted, J. H. *The Edwin Smith Surgical Papyrus*; 1930; Vol. 3. <https://doi.org/10.1126/science.26.678.918>.
- (3) David, A. R.; Zimmerman, M. R. Cancer: An Old Disease, a New Disease or Something in Between? *Nat. Rev. Cancer* **2010**, *10* (10), 728–733. <https://doi.org/10.1038/nrc2914>.
- (4) Papavramidou, N.; Papavramidis, T.; Demetriou, T. Ancient Greek and Greco–Roman Methods in Modern Surgical Treatment of Cancer. *Ann. Surg. Oncol.* **2010**, *17* (3), 665–667. <https://doi.org/10.1245/s10434-009-0886-6>.
- (5) World Health Organization. Cancer <https://www.who.int/news-room/fact-sheets/detail/cancer> (accessed May 27, 2019).
- (6) Steward, B.W.; Wild, C. P. *World Cancer Report*; 2014.
- (7) World Health Organisation. *Latest Global Cancer Data*; 2018.
- (8) International Agency for Research on Cancer. Global Cancer Observatory <https://gco.iarc.fr/> (accessed May 27, 2019).
- (9) Bray, F.; Ferlay, J.; Soerjomataram, I.; Siegel, R. L.; Torre, L. A.; Jemal, A. Global Cancer Statistics 2018: GLOBOCAN Estimates of Incidence and Mortality Worldwide for 36 Cancers in 185 Countries. *CA. Cancer J. Clin.* **2018**, *68* (6), 394–424. <https://doi.org/10.3322/caac.21492>.
- (10) Wilson, B. E.; Jacob, S.; Yap, M. L.; Ferlay, J.; Bray, F.; Barton, M. B. Estimates of Global Chemotherapy Demands and Corresponding Physician Workforce Requirements for 2018 and 2040: A Population-Based Study. *Lancet Oncol.* **2019**, *2045* (19), 1–11. [https://doi.org/10.1016/S1470-2045\(19\)30163-9](https://doi.org/10.1016/S1470-2045(19)30163-9).
- (11) Miller, K. D.; Siegel, R. L.; Lin, C. C.; Mariotto, A. B.; Kramer, J. L.; Rowland, J. H.; Stein, K. D.; Alteri, R.; Jemal, A. Cancer Treatment and Survivorship Statistics, 2016. *CA. Cancer J. Clin.* **2016**, *66* (4), 271–289. <https://doi.org/10.3322/caac.21349>.
- (12) Sullivan, R.; Alatise, O. I.; Anderson, B. O.; Audisio, R.; Autier, P.; Aggarwal, A.; Balch, C.; Brennan, M. F.; Dare, A.; D’Cruz, A.; et al. Global Cancer Surgery: Delivering Safe, Affordable, and Timely Cancer Surgery. *The Lancet Oncology*. 2015, pp 1193–1224. [https://doi.org/10.1016/S1470-2045\(15\)00223-5](https://doi.org/10.1016/S1470-2045(15)00223-5).
- (13) Benjamin, D. J. The Efficacy of Surgical Treatment of Cancer - 20 Years Later. *Med. Hypotheses* **2014**, *82* (4), 412–420. <https://doi.org/10.1016/j.mehy.2014.01.004>.
- (14) Wyld, L.; Audisio, R. A.; Poston, G. J. The Evolution of Cancer Surgery and Future Perspectives. *Nat. Rev. Clin. Oncol.* **2015**, *12* (2), 115–124. <https://doi.org/10.1038/nrclinonc.2014.191>.
- (15) Surgery for Cancer - National Cancer Institute <https://www.cancer.gov/about-cancer/treatment/types/surgery> (accessed May 28, 2019).
- (16) Yap, M. L.; Zubizarreta, E.; Bray, F.; Ferlay, J.; Barton, M. Global Access to Radiotherapy Services: Have We Made Progress During the Past Decade? *J. Glob. Oncol.* **2016**, *2* (4), 207–215. <https://doi.org/10.1200/jgo.2015.001545>.
- (17) Deborah E. Citrin, M. D. Recent Developments in Radiotherapy. *N Engl J Med.* 2017, pp 1065–1075. <https://doi.org/10.1056/NEJMra1608986>.
- (18) Radiation Therapy for Cancer - National Cancer Institute <https://www.cancer.gov/about-cancer/treatment/types/radiation-therapy> (accessed May 28, 2019).
- (19) M.R., H.; M., B.; A.K., S.; R.J., K.; J.D., B.; J.J., G. Use of Radioactive Iodine for Thyroid Cancer. *JAMA - J. Am. Med. Assoc.* **2011**, *306* (7), 721–728.

## 7. References

---

- (20) Colvin, O. M. Alkylating Agents. *Encycl. Cancer* **2002**, No. 1994, 35–42. <https://doi.org/10.1016/B0-12-227555-1/00001-0>.
- (21) Scholar, E. *Antimetabolites*; 2008. <https://doi.org/10.1016/B978-008055232-3.61036-0>.
- (22) Longley, D. B.; Harkin, D. P.; Johnston, P. G. 5-Fluorouracil: Mechanisms of Action and Clinical Strategies. *Nat. Rev. Cancer* **2003**, 3 (5), 330–338. <https://doi.org/10.1038/nrc1074>.
- (23) Bachur, N. R. Anthracyclines. *Encyclopedia of Cancer, Second Edition*; 2002; Vol. 1, pp 57–61.
- (24) Szulawska, A.; Czyz, M. Molecular Mechanisms of Anthracyclines Action. *Postep. Hig Med Dosw.* **2006**, 60, 78–100.
- (25) Mckinnon, P. J. Topoisomerases and the Regulation of Neural Function. *Nat. Rev. Neurosci.* **2016**, 17 (11), 673–679. <https://doi.org/10.1038/nrn.2016.101>.
- (26) Chen, T.; Sun, Y.; Ji, P.; Kopetz, S.; Zhang, W. Topoisomerase IIa in Chromosome Instability and Personalized Cancer Therapy. *Oncogene* **2015**, 34 (31), 4019–4031. <https://doi.org/10.1038/onc.2014.332>.
- (27) Martino, E.; Casamassima, G.; Castiglione, S.; Cellupica, E.; Pantalone, S.; Papagni, F.; Rui, M.; Siciliano, A. M.; Collina, S. Vinca Alkaloids and Analogues as Anti-Cancer Agents: Looking Back, Peering Ahead. *Bioorganic Med. Chem. Lett.* **2018**, 28 (17), 2816–2826. <https://doi.org/10.1016/j.bmcl.2018.06.044>.
- (28) Cook, M.; Johnson, N. Pre-Surgical Chemotherapy for Breast Cancer May Be Associated with Improved Outcomes. *Am. J. Surg.* **2018**, 215 (5), 931–934. <https://doi.org/10.1016/j.amjsurg.2018.03.020>.
- (29) Ta, L.; Ba, W.; Heus, P.; He, K.; Lawrie, T. A.; Winter-roach, B. A.; Heus, P.; Kitchener, H. C. Adjuvant (Post-Surgery) Chemotherapy for Early Stageepithelial Ovarian Cancer. *Cochrane Database Syst. Rev.* **2016**, No. 12. <https://doi.org/10.1002/14651858.CD004706.pub5>. Copyright.
- (30) Wong, R. K.; Malthaner, R. Combined Chemotherapy and Radiotherapy (without Surgery) Compared with Radiotherapy Alone in Localized Carcinoma of the Esophagus. *Cochrane Database Syst. Rev.* **2010**, No. 1. <https://doi.org/10.1002/14651858.cd002092.pub3>.
- (31) Joo, W. D.; Visintin, I.; Mor, G. Targeted Cancer Therapy - Are the Days of Systemic Chemotherapy Numbered? *Maturitas*. Elsevier Ireland Ltd 2013, pp 308–314. <https://doi.org/10.1016/j.maturitas.2013.09.008>.
- (32) Rodon Ahnert, J.; Gray, N.; Mok, T.; Gainor, J. What It Takes to Improve a First-Generation Inhibitor to a Second- or Third-Generation Small Molecule. *Am. Soc. Clin. Oncol. Educ. B.* **2019**, No. 39, 196–205. [https://doi.org/10.1200/EDBK\\_242209](https://doi.org/10.1200/EDBK_242209).
- (33) Baudino, T. A. Targeted Cancer Therapy: The Next Generation of Cancer Treatment. *Curr. Drug Discov. Technol.* **2015**, 12 (1), 3–20.
- (34) Aggarwal, S. Targeted Cancer Therapies. *Nat. Rev. Drug Discov.* **2010**, 9 (6), 427–428. <https://doi.org/10.1038/nrd3186>.
- (35) Hochhaus, A.; Larson, R. A.; Guilhot, F.; Radich, J. P.; Branford, S.; Hughes, T. P.; Baccarani, M.; Deininger, M. W.; Cervantes, F.; Fujihara, S.; et al. Long-Term Outcomes of Imatinib Treatment for Chronic Myeloid Leukemia. *N. Engl. J. Med.* **2017**, 376 (10), 917–927. <https://doi.org/10.1056/NEJMoal609324>.
- (36) Arbour, K. C.; Riely, G. J. Diagnosis and Treatment of Anaplastic Lymphoma Kinase-Positive Non-Small Cell Lung Cancer. *Hematology/Oncology Clinics of North America*. Elsevier Inc 2017, pp 101–111. <https://doi.org/10.1016/j.hoc.2016.08.012>.
- (37) Ritchie, M.; Tchistiakova, L.; Scott, N. Implications of Receptor-Mediated Endocytosis and Intracellular Trafficking Dynamics in the Development of Antibody Drug Conjugates. *MAbs* **2013**, 5 (1), 13–21. <https://doi.org/10.4161/mabs.22854>.

- (38) Golay, J.; Introna, M. Mechanism of Action of Therapeutic Monoclonal Antibodies: Promises and Pitfalls of in Vitro and in Vivo Assays. *Arch. Biochem. Biophys.* **2012**, *526* (2), 146–153. <https://doi.org/10.1016/j.abb.2012.02.011>.
- (39) Ferrara, N.; Hillan, K. J.; Gerber, H. P.; Novotny, W. Discovery and Development of Bevacizumab, an Anti-VEGF Antibody for Treating Cancer. *Nature Reviews Drug Discovery.* 2004, pp 391–400. <https://doi.org/10.1038/nrd1381>.
- (40) Chiavenna, S. M.; Jaworski, J. P.; Vendrell, A. State of the Art in Anti-Cancer MAbs. *J. Biomed. Sci.* **2017**, *24* (1), 1–12. <https://doi.org/10.1186/s12929-016-0311-y>.
- (41) Joanne Graham, M. M. and P. K. Cetuximab. *Nat. Rev. Drug Discov.* **2004**, *3*, 549–550. <https://doi.org/10.1038/nrd1445>.
- (42) Hanahan, D.; Weinberg, R. A. Hallmarks of Cancer: The next Generation. *Cell* **2011**, *144* (5), 646–674. <https://doi.org/10.1016/j.cell.2011.02.013>.
- (43) Cruz, E.; Kayser, V. Monoclonal Antibody Therapy of Solid Tumors: Clinical Limitations and Novel Strategies to Enhance Treatment Efficacy. *Biol. Targets Ther.* **2019**, *Volume 13*, 33–51. <https://doi.org/10.2147/btt.s166310>.
- (44) Kamath, S. D.; Kumthekar, P. U. Immune Checkpoint Inhibitors for the Treatment of Central Nervous System (CNS) Metastatic Disease. *Front. Oncol.* **2018**, *8* (September), 1–7. <https://doi.org/10.3389/fonc.2018.00414>.
- (45) Riley, R. S.; June, C. H.; Langer, R.; Mitchell, M. J. Delivery Technologies for Cancer Immunotherapy. *Nat. Rev. Drug Discov.* **2019**, *18* (3), 175–196. <https://doi.org/10.1038/s41573-018-0006-z>.
- (46) Darwin, P.; Toor, S. M.; Sasidharan Nair, V.; Elkord, E. Immune Checkpoint Inhibitors: Recent Progress and Potential Biomarkers. *Experimental and Molecular Medicine.* Springer US 2018, pp 1–11. <https://doi.org/10.1038/s12276-018-0191-1>.
- (47) Mayor, P.; Starbuck, K.; Zsiros, E. Adoptive Cell Transfer Using Autologous Tumor Infiltrating Lymphocytes in Gynecologic Malignancies. *Gynecol. Oncol.* **2018**, *150* (2), 361–369. <https://doi.org/10.1016/j.ygyno.2018.05.024>.
- (48) Fan, J.; Shang, D.; Han, B.; Song, J.; Chen, H.; Yang, J.-M. Adoptive Cell Transfer: Is It a Promising Immunotherapy for Colorectal Cancer? *Theranostics* **2018**, *8* (20), 5784–5800. <https://doi.org/10.7150/thno.29035>.
- (49) Zheng, P. P.; Kros, J. M.; Li, J. Approved CAR T Cell Therapies: Ice Bucket Challenges on Glaring Safety Risks and Long-Term Impacts. *Drug Discovery Today.* Elsevier Ltd 2018, pp 1175–1182. <https://doi.org/10.1016/j.drudis.2018.02.012>.
- (50) G.Q., P.; S.A., R. Adoptive Cell Transfer for Patients with Metastatic Melanoma: The Potential and Promise of Cancer Immunotherapy. *Cancer Control* **2013**, *20* (4), 289–297.
- (51) Margolin, K.; Lazarus, M.; Kaufman, H. L. Cytokines in the Treatment of Cancer. *Cancer Immunother. Paradig. Pract. Promise* **2013**, *9781461447* (1), 173–210. [https://doi.org/10.1007/978-1-4614-4732-0\\_7](https://doi.org/10.1007/978-1-4614-4732-0_7).
- (52) Gontero, P.; Bohle, A.; Malmstrom, P. U.; O'Donnell, M. A.; Oderda, M.; Sylvester, R.; Witjes, F. The Role of Bacillus Calmette-Guérin in the Treatment of Non-Muscle-Invasive Bladder Cancer. *Eur. Urol.* **2010**, *57* (3), 410–429. <https://doi.org/10.1016/j.eururo.2009.11.023>.
- (53) Fuge, O.; Vasdev, N.; Allchorne, P.; Green, J. S. Immunotherapy for Bladder Cancer. *Research and Reports in Urology.* 2015, pp 65–79. <https://doi.org/10.2147/RRU.S63447>.
- (54) Oun, R.; Moussa, Y. E.; Wheate, N. J. The Side Effects of Platinum-Based Chemotherapy Drugs: A Review for Chemists. *Dalt. Trans.* **2018**, *47* (19), 6645–6653. <https://doi.org/10.1039/c8dt00838h>.

## 7. References

---

- (55) Sun, C. C.; Bodurka, D. C.; Weaver, C. B.; Rasu, R.; Wolf, J. K.; Bevers, M. W.; Smith, J. A.; Wharton, J. T.; Rubenstein, E. B. Rankings and Symptom Assessments of Side Effects from Chemotherapy: Insights from Experienced Patients with Ovarian Cancer. *Support. Care Cancer* **2005**, *13* (4), 219–227. <https://doi.org/10.1007/s00520-004-0710-6>.
- (56) Love, R. R.; Leventhal, H.; Easterling, D. V.; Nerenz, D. R. Side Effects and Emotional Distress during Cancer Chemotherapy. *Cancer* **1989**, *63* (3), 604–612. [https://doi.org/10.1002/1097-0142\(19890201\)63:3<604::AID-CNCR2820630334>3.0.CO;2-2](https://doi.org/10.1002/1097-0142(19890201)63:3<604::AID-CNCR2820630334>3.0.CO;2-2).
- (57) Monsuez, J. J.; Charniot, J. C.; Vignat, N.; Artigou, J. Y. Cardiac Side-Effects of Cancer Chemotherapy. *Int. J. Cardiol.* **2010**, *144* (1), 3–15. <https://doi.org/10.1016/j.ijcard.2010.03.003>.
- (58) Charles Sawyers. Targeted Cancer Therapy. *Nature* **2004**, *432*, 294–297.
- (59) Ward, R. A.; Goldberg, F. *Kinase Drug Discovery*; Royal Society of Chemistry, 2018. <https://doi.org/10.1021/jm800475y>.
- (60) Roskoski, R. Properties of FDA-Approved Small Molecule Protein Kinase Inhibitors. *Pharmacol. Res.* **2019**, *144* (March), 19–50. <https://doi.org/10.1016/j.phrs.2019.03.006>.
- (61) Ficarro, S. B.; Mcclelland, M. L.; Stukenberg, P. T.; Burke, D. J.; Ross, M. M.; Shabanowitz, J.; Hunt, D. F.; White, F. M. Phosphoproteome Analysis by Mass Spectrometry and Its Application To. *Nat. Biotechnol.* **2002**, *20*, 301–305.
- (62) Cohen, P. The Regulation of Protein Function by Multisite Phosphorylation – a 25 Year Update. *Trends Biochem Sci* **2000**, *25* (12), 596–601. [https://doi.org/10.1016/S0968-0004\(00\)01712-6](https://doi.org/10.1016/S0968-0004(00)01712-6).
- (63) Varshavsky, A. Regulated Protein Degradation. *Trends Biochem. Sci.* **2005**, *30* (6), 283–286. <https://doi.org/10.1016/j.tibs.2005.04.005>.
- (64) Thomas, S. M.; Brugge, J. S. Cellular Functions Regulated By Src Family Kinases. *Annu. Rev. Cell Dev. Biol.* **1997**, *13* (1), 513–609. <https://doi.org/10.1146/annurev.cellbio.13.1.513>.
- (65) Yang, G.; Chang, B.; Yang, F.; Guo, X.; Cai, K. Q.; Xiao, X.; Wang, H.; Sen, S.; Hung, M. C.; Mills, G. B.; et al. Aurora Kinase A Promotes Ovarian Tumorigenesis through Dysregulation of the Cell Cycle and Suppression of BRCA2. *Clin. Cancer Res.* **2010**, *16* (12), 3171–3181. <https://doi.org/10.1158/1078-0432.CCR-09-3171>.
- (66) Welsh, S. J.; Churchman, M. L.; Togni, M.; Mullighan, C. G.; Hagman, J. Deregulation of Kinase Signaling and Lymphoid Development in EBF1-PDGFRB ALL Leukemogenesis. *Leukemia* **2018**, *32* (1), 38–48. <https://doi.org/10.1038/leu.2017.166>.
- (67) Wen, Z.; Jin, K.; Shen, Y.; Yang, Z.; Li, Y.; Wu, B.; Tian, L.; Shoor, S.; Roche, N. E.; Goronzy, J. J.; et al. N-Myristoyltransferase Deficiency Impairs Activation of Kinase AMPK and Promotes Synovial Tissue Inflammation. *Nat. Immunol.* **2019**, *20* (3), 313–325. <https://doi.org/10.1038/s41590-018-0296-7>.
- (68) Novarino, G.; El-Fishawy, P.; Kayserili, H.; Meguid, N. A.; Scott, E. M.; Schroth, J.; Silhavy, J. L.; Kara, M.; Khalil, R. O.; Ben-Omran, T.; et al. Mutations in BCKD-Kinase Lead to a Potentially Treatable Form of Autism with Epilepsy. *Science* (80-. ). **2012**, *338* (6105), 394–397. <https://doi.org/10.1126/science.1224631>.
- (69) Sogi, K. M.; Lien, K. A.; Johnson, J. R.; Krogan, N. J.; Stanley, S. A. The Tyrosine Kinase Inhibitor Gefitinib Restricts Mycobacterium Tuberculosis Growth through Increased Lysosomal Biogenesis and Modulation of Cytokine Signaling. *ACS Infect. Dis.* **2017**, *3* (8), 564–574. <https://doi.org/10.1021/acsinfectdis.7b00046>.
- (70) Shimokawa, H.; Sunamura, S.; Satoh, K. RhoA/Rho-Kinase in the Cardiovascular System. *Circ. Res.* **2016**, *118* (2), 352–366. <https://doi.org/10.1161/CIRCRESAHA.115.306532>.
- (71) J. Henriksen, E. Dysregulation of Glycogen Synthase Kinase-3 in Skeletal Muscle and the Etiology of Insulin Resistance and Type 2 Diabetes. *Curr. Diabetes Rev.* **2010**, *6* (5), 285–293.

- <https://doi.org/10.2174/157339910793360888>.
- (72) Iqbal, K.; Liu, F.; Gong, C. X. Tau and Neurodegenerative Disease: The Story so Far. *Nat. Rev. Neurol.* **2016**, *12* (1), 15–27. <https://doi.org/10.1038/nrneurol.2015.225>.
- (73) Levitzki, A. Protein Kinase Inhibitors as a Therapeutic Modality. *Acc. Chem. Res.* **2003**, *36* (6), 462–469. <https://doi.org/10.1021/ar0201207>.
- (74) Ochoa, D.; Bradley, D.; Beltrao, P. Evolution, Dynamics and Dysregulation of Kinase Signalling. *Curr. Opin. Struct. Biol.* **2018**, *48*, 133–140. <https://doi.org/10.1016/j.sbi.2017.12.008>.
- (75) Wu, P.; Nielsen, T. E.; Clausen, M. H. Small-Molecule Kinase Inhibitors: An Analysis of FDA-Approved Drugs. *Drug Discov. Today* **2016**, *21* (1), 5–10. <https://doi.org/10.1016/j.drudis.2015.07.008>.
- (76) Hidaka, H.; Inagaki, M.; Kawamoto, S.; Sasaki, Y. Isoquinolinesulfonamides, Novel and Potent Inhibitors of Cyclic Nucleotide Dependent Protein Kinase and Protein Kinase C. *Biochemistry* **1984**, *23* (21), 5036–5041. <https://doi.org/10.1021/bi00316a032>.
- (77) Capdeville, R.; Buchdunger, E.; Zimmermann, J.; Matter, A. Glivec (ST1571, Imatinib), a Rationally Developed, Targeted Anticancer Drug. *Nat. Rev. Drug Discov.* **2002**, *1* (7), 493–502. <https://doi.org/10.1038/nrd839>.
- (78) Robert Jr., R. US Food and Drug Administration approved small molecule protein kinase inhibitors <http://www.brimr.org/PKI/PKIs.htm> (accessed May 29, 2019).
- (79) André, F.; Ciruelos, E.; Rubovszky, G.; Campone, M.; Loibl, S.; Rugo, H. S.; Iwata, H.; Conte, P.; Mayer, I. A.; Kaufman, B.; et al. Alpelisib for PIK3CA -Mutated, Hormone Receptor–Positive Advanced Breast Cancer. *N. Engl. J. Med.* **2019**, *380* (20), 1929–1940. <https://doi.org/10.1056/nejmoa1813904>.
- (80) Ando, Y.; Iwasa, S.; Takahashi, S.; Saka, H.; Kakizume, T.; Natsume, K.; Suenaga, N.; Quadt, C.; Yamada, Y. Phase I Study of Alpelisib (BYL719), an  $\alpha$ -Specific PI3K Inhibitor, in Japanese Patients with Advanced Solid Tumors. *Cancer Sci.* **2019**, *110* (3), 1021–1031. <https://doi.org/10.1111/cas.13923>.
- (81) Hanrs, S. K.; Hunter, T. The Eukaryotic Protein Kinase Superfamily: ( Catalytic ) Domam Structure and Classification of The. *FASEB J.* **1988**.
- (82) Xing, L.; Klug-Mcleod, J.; Rai, B.; Lunney, E. A. Kinase Hinge Binding Scaffolds and Their Hydrogen Bond Patterns. *Bioorganic Med. Chem.* **2015**, *23* (19), 6520–6527. <https://doi.org/10.1016/j.bmc.2015.08.006>.
- (83) Johnson, L. N.; Lowe, E. D.; Noble, M. E.; Owen, D. J. The Eleventh Datta Lecture. The Structural Basis for Substrate Recognition and Control by Protein Kinases. *FEBS Lett.* **1998**, *430* (1–2), 1–11.
- (84) Manning, G.; Whyte, D. B.; Martinez, R.; Hunter, T.; Sudarsanam, S. The Protein Kinase Complement of the Human Genome. *Science* (80-. ). **2002**, *298* (December).
- (85) Mortenson, P. N.; Berdini, V.; O'Reilly, M. Fragment-Based Approaches to the Discovery of Kinase Inhibitors. *Methods Enzymol.* **2014**, *548* (C), 69–92. <https://doi.org/10.1016/B978-0-12-397918-6.00003-3>.
- (86) Wu, P.; Nielsen, T. E.; Clausen, M. H. FDA-Approved Small-Molecule Kinase Inhibitors. *Trends Pharmacol. Sci.* **2015**. <https://doi.org/10.1016/j.tips.2015.04.005>.
- (87) Rabiller, M.; Getlik, M.; Klüter, S.; Richters, A.; Tückmantel, S.; Simard, J. R.; Rauh, D. Proteus in the World of Proteins: Conformational Changes in Protein Kinases. *Arch. Pharm. (Weinheim)*. **2010**, *343* (4), 193–206. <https://doi.org/10.1002/ardp.201000028>.
- (88) Fang, Z.; Grütter, C.; Rauh, D. Strategies for the Selective Regulation of Kinases with Allosteric Modulators: Exploiting Exclusive Structural Features. *ACS Chem. Biol.* **2013**, *8* (1), 58–70.

## 7. References

---

- <https://doi.org/10.1021/cb300663j>.
- (89) Modi, V.; Dunbrack, R. L. Defining a New Nomenclature for the Structures of Active and Inactive Kinases. *Proc. Natl. Acad. Sci.* **2019**, *116* (14), 6818–6827. <https://doi.org/10.1073/pnas.1814279116>.
- (90) Palmieri, L.; Rastelli, G. Ac Helix Displacement As a General Approach for Allosteric Modulation of Protein Kinases. *Drug Discov. Today* **2013**, *18* (7–8), 407–414. <https://doi.org/10.1016/j.drudis.2012.11.009>.
- (91) Zhang, J.; Yang, P. L.; Gray, N. S. Targeting Cancer with Small Molecule Kinase Inhibitors. *Nat. Rev. Cancer* **2009**, *9* (1), 28–39. <https://doi.org/10.1038/nrc2559>.
- (92) Van Linden, O. P. J.; Kooistra, A. J.; Leurs, R.; De Esch, I. J. P.; De Graaf, C. KLIFS: A Knowledge-Based Structural Database to Navigate Kinase-Ligand Interaction Space. *J. Med. Chem.* **2014**, *57* (2), 249–277. <https://doi.org/10.1021/jm400378w>.
- (93) Wu, P.; Clausen, M. H.; Nielsen, T. E. Allosteric Small-Molecule Kinase Inhibitors. *Pharmacol. Ther.* **2015**, *156*, 59–68. <https://doi.org/10.1016/j.pharmthera.2015.10.002>.
- (94) Gavrin, L. K.; Saiah, E. Approaches to Discover Non-ATP Site Kinase Inhibitors. *Medchemcomm* **2013**, *4* (1), 41–51. <https://doi.org/10.1039/c2md20180a>.
- (95) Li, R.; Stafford, J. A. Kinase Inhibitor Drugs. *Kinase Inhib. Drugs* **2009**, *3*, 1–510. <https://doi.org/10.1002/9780470524961>.
- (96) Traxler, P.; Furet, P. Strategies toward the Design of Novel and Selective Protein Tyrosine Kinase Inhibitors. *Pharmacol. Ther.* **1999**, *82* (2–3), 195–206. [https://doi.org/10.1016/S0163-7258\(98\)00044-8](https://doi.org/10.1016/S0163-7258(98)00044-8).
- (97) Zhao, Z.; Wu, H.; Wang, L.; Liu, Y.; Knapp, S.; Liu, Q.; Gray, N. S. Exploration of Type II Binding Mode: A Privileged Approach for Kinase Inhibitor Focused Drug Discovery? *ACS Chem. Biol.* **2014**, *9* (6), 1230–1241. <https://doi.org/10.1021/cb500129t>.
- (98) Fabbro, D.; Cowan-Jacob, S. W.; Moebitz, H. Ten Things You Should Know about Protein Kinases: IUPHAR Review 14. *Br. J. Pharmacol.* **2015**, *172* (11), 2675–2700. <https://doi.org/10.1111/bph.13096>.
- (99) Vanderpool, D.; Johnson, T. O.; Ping, C.; Bergqvist, S.; Alton, G.; Phonephaly, S.; Rui, E.; Luo, C.; Deng, Y. L.; Grant, S.; et al. Characterization of the CHK1 Allosteric Inhibitor Binding Site. *Biochemistry* **2009**, *48* (41), 9823–9830. <https://doi.org/10.1021/bi900258v>.
- (100) Cox, K. J.; Shomin, C. D.; Ghosh, I. Tinkering Outside the Kinase ATP Box: Allosteric (Type IV) and Bivalent (Type V) Inhibitors of Protein Kinases. *Future Med. Chem.* **2011**, *3* (1), 29–43. <https://doi.org/10.4155/fmc.10.272>.
- (101) Lamba, V.; Ghosh, I. New Directions in Targeting Protein Kinases: Focusing Upon True Allosteric and Bivalent Inhibitors. *Curr. Pharm. Des.* **2012**, *18* (20), 2936–2945. <https://doi.org/10.2174/138161212800672813>.
- (102) Gower, C. M.; Chang, M. E. K.; Maly, D. J. Bivalent Inhibitors of Protein Kinases. *Crit. Rev. Biochem. Mol. Biol.* **2014**, *49* (2), 102–115. <https://doi.org/10.3109/10409238.2013.875513>.
- (103) Zhao, Z.; Bourne, P. E. Progress with Covalent Small-Molecule Kinase Inhibitors. *Drug Discov. Today* **2018**, *23* (3), 727–735. <https://doi.org/10.1016/j.drudis.2018.01.035>.
- (104) Liu, Q.; Sabnis, Y.; Zhao, Z.; Zhang, T.; Buhrlage, S. J.; Jones, L. H.; Gray, N. S. Developing Irreversible Inhibitors of the Protein Kinase Cysteine. *Chem. Biol.* **2013**, *20* (2), 146–159. <https://doi.org/10.1016/j.chembiol.2012.12.006>.
- (105) Barf, T.; Kaptein, A. Irreversible Protein Kinase Inhibitors: Balancing the Benefits and Risks. *J. Med. Chem.* **2012**, *55* (14), 6243–6262. <https://doi.org/10.1021/jm3003203>.



- (106) Miller, R. M.; Paavilainen, V. O.; Krishnan, S.; Serafimova, I. M.; Taunton, J. Electrophilic Fragment-Based Design of Reversible Covalent Kinase Inhibitors. *J. Am. Chem. Soc.* **2013**, *135* (14), 5298–5301. <https://doi.org/10.1021/ja401221b>.
- (107) Serafimova, I. M.; Pufall, M. A.; Krishnan, S.; Duda, K.; Cohen, M. S.; Maglathlin, R. L.; McFarland, J. M.; Miller, R. M.; Frödin, M.; Taunton, J. Reversible Targeting of Noncatalytic Cysteines with Chemically Tuned Electrophiles. *Nat. Chem. Biol.* **2012**, *8* (5), 471–476. <https://doi.org/10.1038/nchembio.925>.
- (108) Bradshaw, J. M.; McFarland, J. M.; Paavilainen, V. O.; Bisconte, A.; Tam, D.; Phan, V. T.; Romanov, S.; Finkle, D.; Shu, J.; Patel, V.; et al. Prolonged and Tunable Residence Time Using Reversible Covalent Kinase Inhibitors. *Nat. Chem. Biol.* **2015**, *11* (7), 525–531. <https://doi.org/10.1038/nchembio.1817>.
- (109) Hughes, J. P.; Rees, S. S.; Kalindjian, S. B.; Philpott, K. L. Principles of Early Drug Discovery. *Br. J. Pharmacol.* **2011**, *162* (6), 1239–1249. <https://doi.org/10.1111/j.1476-5381.2010.01127.x>.
- (110) Murray, C. W.; Rees, D. C. The Rise of Fragment-Based Drug Discovery. *Nat. Chem.* **2009**, *1* (3), 187–192. <https://doi.org/10.1038/nchem.217>.
- (111) Terstappen, G. C.; Schlüpen, C.; Raggiaschi, R.; Gaviraghi, G. Target Deconvolution Strategies in Drug Discovery. *Nat. Rev. Drug Discov.* **2007**, *6* (11), 891–903. <https://doi.org/10.1038/nrd2410>.
- (112) MacArron, R.; Banks, M. N.; Bojanic, D.; Burns, D. J.; Cirovic, D. A.; Garyantes, T.; Green, D. V. S.; Hertzberg, R. P.; Janzen, W. P.; Paslay, J. W.; et al. Impact of High-Throughput Screening in Biomedical Research. *Nat. Rev. Drug Discov.* **2011**, *10* (3), 188–195. <https://doi.org/10.1038/nrd3368>.
- (113) Pereira, D. A.; Williams, J. A. Origin and Evolution of High Throughput Screening. *Br. J. Pharmacol.* **2007**, *152* (1), 53–61. <https://doi.org/10.1038/sj.bjp.0707373>.
- (114) Broach, J. R.; Thorner, J. High-Throughput Screening for Drug Discovery. *Nature* **1996**, *384* (6604 SUPPL.), 14–16. <https://doi.org/10.1038/384014a0>.
- (115) Li, B.; Liu, Y.; Uno, T.; Gray, N. Creating Chemical Diversity to Target Protein Kinases. *Comb. Chem. High Throughput Screen.* **2012**, *7* (5), 453–472. <https://doi.org/10.2174/1386207043328580>.
- (116) Huggins, D. J.; Venkitaraman, A. R.; Spring, D. R. Rational Methods for the Selection of Diverse Screening Compounds. *ACS Chem. Biol.* **2011**, *6* (3), 208–217. <https://doi.org/10.1021/cb100420r>.
- (117) Inglese, J.; Johnson, R. L.; Simeonov, A.; Xia, M.; Zheng, W.; Austin, C. P.; Auld, D. S. High-Throughput Screening Assays for the Identification of Chemical Probes. *Nat. Chem. Biol.* **2007**, *3* (8), 466–479. <https://doi.org/10.1038/nchembio.2007.17>.
- (118) Von Ahsen, O.; Bömer, U. High-Throughput Screening for Kinase Inhibitors. *ChemBioChem* **2005**, *6* (3), 481–490. <https://doi.org/10.1002/cbic.200400211>.
- (119) Wildey, M. J.; Haunso, A.; Tudor, M.; Webb, M.; Connick, J. H. *High-Throughput Screening*, Second Edi.; Elsevier Ltd, 2017; Vol. 50. <https://doi.org/10.1016/bs.armc.2017.08.004>.
- (120) Ferguson, F. M.; Gray, N. S. Kinase Inhibitors: The Road Ahead. *Nat. Rev. Drug Discov.* **2018**, *17* (5), 353–376. <https://doi.org/10.1038/nrd.2018.21>.
- (121) Lipinski, C. A.; Lombardo, F.; Dominy, B. W.; Feeney, P. J. Experimental and Computational Approaches to Estimate Solubility and Permeability in Drug Discovery and Development Settings. *Adv. Drug Deliv. Rev.* **2012**, *64* (SUPPL.), 4–17. <https://doi.org/10.1016/j.addr.2012.09.019>.
- (122) Lipinski, C. A. Lead- and Drug-like Compounds: The Rule-of-Five Revolution. *Drug Discov. Today Technol.* **2004**, *1* (4), 337–341. <https://doi.org/10.1016/j.ddtec.2004.11.007>.
- (123) Congreve, M.; Carr, R.; Murray, C.; Jhoti, H. A ‘Rule of Three’ for Fragment-Based Lead Discovery? *Drug Discov. Today* **2003**, *8* (19), 876–877. <https://doi.org/10.1016/S1359->

## 7. References

---

- 6446(03)02831-9.
- (124) Owens, J.; Lipinski, C. A. Chris Lipinski Discusses Life and Chemistry after the Rule of Five. *Drug Discov. Today* **2003**, *8* (1), 12–16. [https://doi.org/10.1016/S1359-6446\(02\)02556-4](https://doi.org/10.1016/S1359-6446(02)02556-4).
- (125) Bleicher, K. H.; Böhm, H.-J.; Müller, K.; Alanine, A. I. Hit and Lead Generation: Beyond High-Throughput Screening. *Nat. Rev. Drug Discov.* **2003**, *2* (5), 369–378. <https://doi.org/10.1038/nrd1086>.
- (126) Hefti, F. F. Requirements for a Lead Compound to Become a Clinical Candidate. *BMC Neurosci.* **2008**, *9* (SUPPL. 3), 1–7. <https://doi.org/10.1186/1471-2202-9-S3-S7>.
- (127) Druker, B. J. Perspectives on the Development of a Molecularly Targeted Agent. *Cancer Cell* **2002**, *1* (1), 31–36. [https://doi.org/10.1016/S1535-6108\(02\)00025-9](https://doi.org/10.1016/S1535-6108(02)00025-9).
- (128) How Imatinib Transformed Leukemia Treatment - National Cancer Institute <https://www.cancer.gov/research/progress/discovery/gleevec> (accessed Jun 10, 2019).
- (129) Roskoski, R. STI-571: An Anticancer Protein-Tyrosine Kinase Inhibitor. *Biochem. Biophys. Res. Commun.* **2003**, *309* (4), 709–717. <https://doi.org/10.1016/j.bbrc.2003.08.055>.
- (130) Bomhard, E. M.; Herbold, B. A. *Genotoxic Activities of Aniline and Its Metabolites and Their Relationship to the Carcinogenicity of Aniline in the Spleen of Rats*; 2005; Vol. 35. <https://doi.org/10.1080/10408440500442384>.
- (131) Kugler-Steigmeier, M. E.; Friederich, U.; Graf, U.; Lutz, W. K.; Maier, P.; Schlatter, C. Genotoxicity of Aniline Derivatives in Various Short-Term Tests. *Mutat. Res. - Fundam. Mol. Mech. Mutagen.* **1989**, *211* (2), 279–289. [https://doi.org/10.1016/0027-5107\(89\)90011-0](https://doi.org/10.1016/0027-5107(89)90011-0).
- (132) Gill, A. New Lead Generation Strategies for Protein Kinase Inhibitors - Fragment Based Screening Approaches. *Mini-Reviews Med. Chem.* **2005**, *4* (3), 301–311. <https://doi.org/10.2174/1389557043487385>.
- (133) Hajduk, P. J.; Greer, J. A Decade of Fragment-Based Drug Design: Strategic Advances and Lessons Learned. *Nat. Rev. Drug Discov.* **2007**, *6* (3), 211–219. <https://doi.org/10.1038/nrd2220>.
- (134) Fattori, D. Molecular Recognition: The Fragment Approach in Lead Generation. *Drug Discov. Today* **2004**, *9* (5), 229–238. [https://doi.org/10.1016/S1359-6446\(03\)03007-1](https://doi.org/10.1016/S1359-6446(03)03007-1).
- (135) Bamborough, P.; Brown, M. J.; Christopher, J. A.; Chung, C. W.; Mellor, G. W. Selectivity of Kinase Inhibitor Fragments. *J. Med. Chem.* **2011**, *54* (14), 5131–5143. <https://doi.org/10.1021/jm200349b>.
- (136) Beswick, P.; Naylor, A. The Role of Medicinal Chemistry in the Drug Discovery Process. *Drug Discov. Dev. Technol. Transit.* **2012**, 119–134. <https://doi.org/10.1016/B978-0-7020-4299-7.00009-3>.
- (137) Tsai, J.; Lee, J. T.; Wang, W.; Zhang, J.; Cho, H.; Mamo, S.; Bremer, R.; Gillette, S.; Kong, J.; Haass, N. K.; et al. Discovery of a Selective Inhibitor of Oncogenic B-Raf Kinase with Potent Antimelanoma Activity. *Proc. Natl. Acad. Sci.* **2008**, *105* (8), 3041–3046. <https://doi.org/10.1073/pnas.0711741105>.
- (138) Kim, A.; Cohen, M. S. The Discovery of Vemurafenib for the Treatment of BRAF-Mutated Metastatic Melanoma. *Expert Opin. Drug Discov.* **2016**, *11* (9), 907–916. <https://doi.org/10.1080/17460441.2016.1201057>.
- (139) Kirkin, V.; Joos, S.; Zörnig, M. The Role of Bcl-2 Family Members in Tumorigenesis. *Biochim. Biophys. Acta - Mol. Cell Res.* **2004**, *1644* (2–3), 229–249. <https://doi.org/10.1016/j.bbamcr.2003.08.009>.
- (140) Letai, A.; Sorcinelli, M. D.; Beard, C.; Korsmeyer, S. J. Antiapoptotic BCL-2 Is Required for Maintenance of a Model Leukemia. *Cancer Cell* **2004**, *6* (3), 241–249. <https://doi.org/10.1016/j.ccr.2004.07.011>.

- (141) Davies, T. G.; Marko, H. *Fragment-Based Drug Discovery and X-Ray Crystallography*; 2012; Vol. 317. [https://doi.org/10.1016/0302-4598\(80\)87026-7](https://doi.org/10.1016/0302-4598(80)87026-7).
- (142) Oltersdorf, T.; Elmore, S. W.; Shoemaker, A. R.; Armstrong, R. C.; Augeri, D. J.; Belli, B. A.; Bruncko, M.; Deckwerth, T. L.; Dinges, J.; Hajduk, P. J.; et al. An Inhibitor of Bcl-2 Family Proteins Induces Regression of Solid Tumours. *Nature* **2005**, *435* (7042), 677–681. <https://doi.org/10.1038/nature03579>.
- (143) Davids, M. S.; Letai, A. ABT-199: Taking Dead Aim at BCL-2. *Cancer Cell* **2013**, *23* (2), 139–141. <https://doi.org/10.1016/j.ccr.2013.01.018>.
- (144) Souers, A. J.; Levenson, J. D.; Boghaert, E. R.; Ackler, S. L.; Catron, N. D.; Chen, J.; Dayton, B. D.; Ding, H.; Enschede, S. H.; Fairbrother, W. J.; et al. ABT-199, a Potent and Selective BCL-2 Inhibitor, Achieves Antitumor Activity While Sparing Platelets. *Nat. Med.* **2013**, *19* (2), 202–208. <https://doi.org/10.1038/nm.3048>.
- (145) Moffat, J. G.; Vincent, F.; Lee, J. A.; Eder, J.; Prunotto, M. Opportunities and Challenges in Phenotypic Drug Discovery: An Industry Perspective. *Nat. Rev. Drug Discov.* **2017**, *16* (8), 531–543. <https://doi.org/10.1038/nrd.2017.111>.
- (146) Kotz, J. Phenotypic Screening, Take Two. *Sci. Exch.* **2012**, *5* (15), 380–380. <https://doi.org/10.1038/scibx.2012.380>.
- (147) Sams-Dodd, F. Target-Based Drug Discovery: Is Something Wrong? Define Rational Drug Discovery Programs. *Drug Discov. Today* **2005**, *10* (2), 139–147.
- (148) Swinney, D. C.; Anthony, J. How Were New Medicines Discovered? *Nat. Rev. Drug Discov.* **2011**, *10* (7), 507–519. <https://doi.org/10.1038/nrd3480>.
- (149) Eder, J.; Sedrani, R.; Wiesmann, C. The Discovery of First-in-Class Drugs: Origins and Evolution. *Nat. Rev. Drug Discov.* **2014**, *13* (8), 577–587. <https://doi.org/10.1038/nrd4336>.
- (150) Moffat, J. G.; Rudolph, J.; Bailey, D. Phenotypic Screening in Cancer Drug Discovery—Past, Present and Future. *Nat. Rev. Drug Discov.* **2014**, *13* (8), 588–602. <https://doi.org/10.1038/nrd4366>.
- (151) Swinney, D. C. Phenotypic vs. Target-Based Drug Discovery for First-in-Class Medicines. *Clin. Pharmacol. Ther.* **2013**, *93* (4), 299–301. <https://doi.org/10.1038/clpt.2012.236>.
- (152) Warchal, S. J.; Unciti-Broceta, A.; Carragher, N. O. Next-Generation Phenotypic Screening. *Future Med. Chem.* **2016**, *8* (11), 1331–1347. <https://doi.org/10.4155/fmc-2016-0025>.
- (153) Szabo, M.; Akusjärvi, S. S.; Saxena, A.; Liu, J.; Chandrasekar, G.; Kitambi, S. S. Cell and Small Animal Models for Phenotypic Drug Discovery. *Drug Des. Devel. Ther.* **2017**, *11*, 1957–1967. <https://doi.org/10.2147/DDDT.S129447>.
- (154) Kubota, K.; Funabashi, M.; Ogura, Y. Target Deconvolution from Phenotype-Based Drug Discovery by Using Chemical Proteomics Approaches. *Biochim. Biophys. Acta - Proteins Proteomics* **2019**, *1867* (1), 22–27. <https://doi.org/10.1016/j.bbapap.2018.08.002>.
- (155) Guidance for industry content and format of investigational new drug applications (INDs) for phase 1 studies of drugs, including well-characterized, therapeutic, biotechnology-derived products. FDA <https://www.fda.gov/regulatory-information/search-fda-guidance-documents/content-and-format-investigational-new-drug-applications-inds-phase-1-studies-drugs-including-well> (accessed Jun 15, 2019).
- (156) Gregori-Puigjane, E.; Setola, V.; Hert, J.; Crews, B. A.; Irwin, J. J.; Lounkine, E.; Marnett, L.; Roth, B. L.; Shoichet, B. K. Identifying Mechanism-of-Action Targets for Drugs and Probes. *Proc. Natl. Acad. Sci.* **2012**, *109* (28), 11178–11183. <https://doi.org/10.1073/pnas.1204524109>.
- (157) Liu, Y.; Bishop, A.; Witucki, L.; Kraybill, B.; Shimizu, E.; Tsien, J.; Ubersax, J.; Blethrow, J.; Morgan, D. O.; Shokat, K. M. Structural Basis for Selective Inhibition of Src Family Kinases by PP1. *Chem. Biol.* **1999**, *6* (9), 671–678. [https://doi.org/10.1016/S1074-5521\(99\)80118-5](https://doi.org/10.1016/S1074-5521(99)80118-5).

## 7. References

---

- (158) Fraser, C.; Dawson, J. C.; Dowling, R.; Houston, D. R.; Weiss, J. T.; Munro, A. F.; Muir, M.; Harrington, L.; Webster, S. P.; Frame, M. C.; et al. Rapid Discovery and Structure-Activity Relationships of Pyrazolopyrimidines That Potently Suppress Breast Cancer Cell Growth via SRC Kinase Inhibition with Exceptional Selectivity over ABL Kinase. *J. Med. Chem.* **2016**, *59* (10), 4697–4710. <https://doi.org/10.1021/acs.jmedchem.6b00065>.
- (159) Fraser, C.; Carragher, N. O.; Unciti-Broceta, A. ECF309: A Potent, Selective and Cell-Permeable MTOR Inhibitor. *Medchemcomm* **2016**, *7* (3), 471–477. <https://doi.org/10.1039/c5md00493d>.
- (160) Fuchs, Y.; Steller, H. Programmed Cell Death in Animal Development and Disease. *Cell* **2011**, *147* (4), 742–758. <https://doi.org/10.1016/j.cell.2011.10.033>.
- (161) Galluzzi, L.; Vitale, I.; Aaronson, S. A.; Abrams, J. M.; Adam, D.; Agostinis, P.; Alnemri, E. S.; Altucci, L.; Amelio, I.; Andrews, D. W.; et al. Molecular Mechanisms of Cell Death: Recommendations of the Nomenclature Committee on Cell Death 2018. *Cell Death Differ.* **2018**, *25* (3), 486–541. <https://doi.org/10.1038/s41418-017-0012-4>.
- (162) Ouyang, L.; Shi, Z.; Zhao, S.; Wang, F. T.; Zhou, T. T.; Liu, B.; Bao, J. K. Programmed Cell Death Pathways in Cancer: A Review of Apoptosis, Autophagy and Programmed Necrosis. *Cell Prolif.* **2012**, *45* (6), 487–498. <https://doi.org/10.1111/j.1365-2184.2012.00845.x>.
- (163) Dikic, I.; Elazar, Z. Mechanism and Medical Implications of Mammalian Autophagy. *Nat. Rev. Mol. Cell Biol.* **2018**, *19* (6), 349–364. <https://doi.org/10.1038/s41580-018-0003-4>.
- (164) Yu, L.; Chen, Y.; Tooze, S. A. Autophagy Pathway: Cellular and Molecular Mechanisms. *Autophagy* **2018**, *14* (2), 207–215. <https://doi.org/10.1080/15548627.2017.1378838>.
- (165) Rubinsztein, D. C.; Shpilka, T.; Elazar, Z. Mechanisms of Autophagosome Biogenesis. *Curr. Biol.* **2012**, *22* (1), R29–R34. <https://doi.org/10.1016/j.cub.2011.11.034>.
- (166) Hansen, M.; Rubinsztein, D. C.; Walker, D. W. Autophagy as a Promoter of Longevity: Insights from Model Organisms. *Nat. Rev. Mol. Cell Biol.* **2018**, *19* (9), 579–593. <https://doi.org/10.1038/s41580-018-0033-y>.
- (167) Conrad, M.; Angeli, J. P. F.; Vandenabeele, P.; Stockwell, B. R. Regulated Necrosis: Disease Relevance and Therapeutic Opportunities. *Nat. Rev. Drug Discov.* **2016**, *15* (5), 348–366. <https://doi.org/10.1038/nrd.2015.6>.
- (168) Paoli, P.; Giannoni, E.; Chiarugi, P. Anoikis Molecular Pathways and Its Role in Cancer Progression. *Biochim. Biophys. Acta - Mol. Cell Res.* **2013**, *1833* (12), 3481–3498. <https://doi.org/10.1016/j.bbamcr.2013.06.026>.
- (169) Friedmann Angeli, J. P.; Krysko, D. V.; Conrad, M. Ferroptosis at the Crossroads of Cancer-Acquired Drug Resistance and Immune Evasion. *Nat. Rev. Cancer* **2019**, *19* (7), 405–414. <https://doi.org/10.1038/s41568-019-0149-1>.
- (170) Bergsbaken, T.; Fink, S. L.; Cookson, B. T. Pyroptosis: Host Cell Death and Inflammation. *Nat. Rev. Microbiol.* **2009**, *7* (2), 99–109. <https://doi.org/10.1038/nrmicro2070>.
- (171) Elmore, S. Apoptosis: A Review of Programmed Cell Death. *Toxicol. Pathol.* **2007**, *35* (4), 495–516. <https://doi.org/10.1080/01926230701320337>.
- (172) Taylor, R. C.; Cullen, S. P.; Martin, S. J. Apoptosis: Controlled Demolition at the Cellular Level. *Nat. Rev. Mol. Cell Biol.* **2008**, *9* (3), 231–241. <https://doi.org/10.1038/nrm2312>.
- (173) Lopez, J.; Tait, S. W. G. Mitochondrial Apoptosis: Killing Cancer Using the Enemy Within. *Br. J. Cancer* **2015**, *112* (6), 957–962. <https://doi.org/10.1038/bjc.2015.85>.
- (174) Ichim, G.; Tait, S. W. G. A Fate Worse than Death: Apoptosis as an Oncogenic Process. *Nat. Rev. Cancer* **2016**, *16* (8), 539–548. <https://doi.org/10.1038/nrc.2016.58>.
- (175) Pfeiffer, C. M.; Singh, A. T. K. Apoptosis: A Target for Anticancer Therapy. *Int. J. Mol. Sci.* **2018**, *19* (2). <https://doi.org/10.3390/ijms19020448>.

- (176) Hanahan, D.; Weinberg, R. The Hallmarks of Cancer. *Cell* **2000**, *100*, 57–70.
- (177) Wong, R. S. Y. Apoptosis in Cancer: From Pathogenesis to Treatment. *J. Exp. Clin. Cancer Res.* **2011**, *30* (1). <https://doi.org/10.1186/1756-9966-30-87>.
- (178) Kale, J.; Osterlund, E. J.; Andrews, D. W. BCL-2 Family Proteins: Changing Partners in the Dance towards Death. *Cell Death Differ.* **2018**, *25* (1), 65–80. <https://doi.org/10.1038/cdd.2017.186>.
- (179) Hata, A. N.; Engelman, J. A.; Faber, A. C. The BCL2 Family: Key Mediators of the Apoptotic Response to Targeted Anticancer Therapeutics. *Cancer Discov.* **2015**, *5* (5), 475–487. <https://doi.org/10.1158/2159-8290.CD-15-0011>.
- (180) Campbell, K. J.; Tait, S. W. G. Targeting BCL-2 Regulated Apoptosis in Cancer. *Open Biol.* **2018**, *8* (5), 1–11. <https://doi.org/10.1098/rsob.180002>.
- (181) Sanchez-Vega, F.; Mina, M.; Armenia, J.; Chatila, W. K.; Luna, A.; La, K. C.; Dimitriadou, S.; Liu, D. L.; Kantheti, H. S.; Saghafinia, S.; et al. Oncogenic Signaling Pathways in The Cancer Genome Atlas. *Cell* **2018**, *173* (2), 321–337.e10. <https://doi.org/10.1016/j.cell.2018.03.035>.
- (182) Bykov, V. J. N.; Eriksson, S. E.; Bianchi, J.; Wiman, K. G. Targeting Mutant P53 for Efficient Cancer Therapy. *Nat. Rev. Cancer* **2018**, *18* (2), 89–102. <https://doi.org/10.1038/nrc.2017.109>.
- (183) Aubrey, B. J.; Kelly, G. L.; Janic, A.; Herold, M. J.; Strasser, A. How Does P53 Induce Apoptosis and How Does This Relate to P53-Mediated Tumour Suppression? *Cell Death Differ.* **2018**, *25* (1), 104–113. <https://doi.org/10.1038/cdd.2017.169>.
- (184) Silke, J.; Meier, P. Inhibitor of apoptosis (IAP) Proteins—Modulators of Cell Death and Inflammation. *Cold Spring Harb. Perspect. Biol.* **2013**, *5* (2), 1–20. <https://doi.org/10.1101/cshperspect.a008730>.
- (185) Gyrd-Hansen, M.; Meier, P. IAPs: From Caspase Inhibitors to Modulators of NF- $\kappa$ B, Inflammation and Cancer. *Nat. Rev. Cancer* **2010**, *10* (8), 561–574. <https://doi.org/10.1038/nrc2889>.
- (186) Kocab, A. J.; Duckett, C. S. Inhibitor of Apoptosis Proteins as Intracellular Signaling Intermediates. *FEBS J.* **2016**, *283* (2), 221–231. <https://doi.org/10.1111/febs.13554>.
- (187) Leonard, B. C.; Johnson, D. E. Signaling by Cell Surface Death Receptors: Alterations in Head and Neck Cancer. *Adv. Biol. Regul.* **2018**, *67* (October), 170–178. <https://doi.org/10.1016/j.jbior.2017.10.006>.
- (188) Antoon, J. W.; Lai, R.; Struckhoff, A. P.; Nitschke, A. M.; Elliott, S.; Martin, E. C.; Rhodes, L. V.; Yoon, N. S.; Salvo, V. A.; Shan, B.; et al. Altered Death Receptor Signaling Promotes Epithelial-to-Mesenchymal Transition and Acquired Chemoresistance. *Sci. Rep.* **2012**, *2*, 1–11. <https://doi.org/10.1038/srep00539>.
- (189) McIlwain, D. R.; Berger, T.; Mak, T. W.; Baehrecke, E. H.; Green, D. R.; Kornbluth, S.; Salvesen, G. S. Additional Perspectives on Cell Survival and Cell Death. *Cold Spring Harb Perspect Biol* **2013**, *5*, 8656–8657. <https://doi.org/10.1101/cshperspect.a008656>.
- (190) Brumatti, G.; Salmanidis, M.; Ekert, P. G. Crossing Paths: Interactions between the Cell Death Machinery and Growth Factor Survival Signals. *Cell. Mol. Life Sci.* **2010**, *67* (10), 1619–1630. <https://doi.org/10.1007/s00018-010-0288-8>.
- (191) Chang, F.; Steelman, L. S.; Lee, J. T.; Shelton, J. G.; Navolanic, P. M.; Blalock, W. L.; Franklin, R. A.; McCubrey, J. A. Signal Transduction Mediated by the Ras/Raf/MEK/ERK Pathway from Cytokine Receptors to Transcription Factors: Potential Targeting for Therapeutic Intervention. *Leukemia* **2003**, *17* (7), 1263–1293. <https://doi.org/10.1038/sj.leu.2402945>.
- (192) Mor, A.; Philips, M. R. Compartmentalized Ras/Mapk Signaling. *Annu. Rev. Immunol.* **2006**, *24* (1), 771–800. <https://doi.org/10.1146/annurev.immunol.24.021605.090723>.
- (193) Hemmings, B. A.; Restuccia, D. F. PI3K-PKB / Akt Pathway. *Cold Spring Harb. Perspect. Biol.* **2012**, *4* (9), 1–4. <https://doi.org/10.1101/cshperspect.a011189>.

## 7. References

---

- (194) Mayer, I. A.; Arteaga, C. L. The PI3K/AKT Pathway as a Target for Cancer Treatment. *Annu. Rev. Med.* **2015**, *67* (1), 11–28. <https://doi.org/10.1146/annurev-med-062913-051343>.
- (195) Hermida, M. A.; Dinesh Kumar, J.; Leslie, N. R. GSK3 and Its Interactions with the PI3K/AKT/MTOR Signalling Network. *Adv. Biol. Regul.* **2017**, *65*, 5–15. <https://doi.org/10.1016/j.jbior.2017.06.003>.
- (196) Sen, B.; Johnson, F. M. Regulation of Src Family Kinases in Human Cancers. *J. Signal Transduct.* **2011**, *2011*, 1–14. <https://doi.org/10.1155/2011/865819>.
- (197) Kim, N.; Chen, D.; Zhou, X. Z.; Lee, T. H. Death-Associated Protein Kinase 1 Phosphorylation in Neuronal Cell Death and Neurodegenerative Disease. *Int. J. Mol. Sci.* **2019**, *20* (13), 3131. <https://doi.org/10.3390/ijms20133131>.
- (198) Elbadawy, M.; Usui, T.; Yamawaki, H.; Sasaki, K. Novel Functions of Death-Associated Protein Kinases through Mitogen-Activated Protein Kinase-Related Signals. *Int. J. Mol. Sci.* **2018**, *19* (10). <https://doi.org/10.3390/ijms19103031>.
- (199) O’Shea, J. J.; Schwartz, D. M.; Villarino, A. V.; Gadina, M.; McInnes, I. B.; Laurence, A. The JAK-STAT Pathway: Impact on Human Disease and Therapeutic Intervention. *Annu. Rev. Med.* **2015**, *66* (1), 311–328. <https://doi.org/10.1146/annurev-med-051113-024537>.
- (200) Zwang, Y.; Jonas, O.; Chen, C.; Rinne, M. L.; Doench, J. G.; Piccioni, F.; Tan, L.; Huang, H. T.; Wang, J.; Ham, Y. J.; et al. Synergistic Interactions with PI3K Inhibition That Induce Apoptosis. *Elife* **2017**, *6*, 1–18. <https://doi.org/10.7554/eLife.24523>.
- (201) Shen, B.; Mao, W.; Ahn, J. C.; Chung, P. S.; He, P. Mechanism of HN-3 Cell Apoptosis Induced by Carboplatin: Combination of Mitochondrial Pathway Associated with Ca<sup>2+</sup> and the Nucleus Pathways. *Mol. Med. Rep.* **2018**, *18* (6), 4978–4986. <https://doi.org/10.3892/mmr.2018.9507>.
- (202) Pilco-Ferreto, N.; Calaf, G. M. Influence of Doxorubicin on Apoptosis and Oxidative Stress in Breast Cancer Cell Lines. *Int. J. Oncol.* **2016**, *49* (2), 753–762. <https://doi.org/10.3892/ijo.2016.3558>.
- (203) Rosemeyer, H. The Chemodiversity of Purine as a Constituent of Natural Products. *Chem. Biodivers.* **2004**, *1* (3), 361–401. <https://doi.org/10.1002/cbdv.200490033>.
- (204) Welsch, M. E.; Snyder, S. A.; Stockwell, B. R. Privileged Scaffolds for Library Design and Drug Discovery. *Curr. Opin. Chem. Biol.* **2010**, *14* (3), 347–361. <https://doi.org/10.1016/j.cbpa.2010.02.018>.
- (205) Legraverend, M.; Grierson, D. S. The Purines: Potent and Versatile Small Molecule Inhibitors and Modulators of Key Biological Targets. *Bioorganic Med. Chem.* **2006**, *14* (12), 3987–4006. <https://doi.org/10.1016/j.bmc.2005.12.060>.
- (206) Norman, T. C.; Gray, N. S.; Koh, J. T.; Schultz, P. G. A Structure-Based Library Approach to Kinase Inhibitors. *J. Am. Chem. Soc.* **1996**, *118* (31), 7430–7431. <https://doi.org/10.1021/ja9614934>.
- (207) Fosu-Mensah, N. A.; Jiang, W.; Brancale, A.; Cai, J.; Westwell, A. D. The Discovery of Purine-Based Agents Targeting Triple-Negative Breast Cancer and the AB-Crystallin/VEGF Protein–Protein Interaction. *Med. Chem. Res.* **2019**, *28* (2), 182–202. <https://doi.org/10.1007/s00044-018-2275-9>.
- (208) Baraldi, P. G.; Broceta, A. U.; Infantas, M. J. P. D. Las; Mochun, J. J. D.; Espinosa, A.; Romagnoli, R. An Efficient One-Pot Synthesis of 6-Alkoxy-8,9-Dialkylpurines via Reaction of 5-Amino-4-Chloro-6-Alkylaminopyrimidines with N,N-Dimethylalkaneamides and Alkoxide Ions. *Tetrahedron* **2002**, *58* (38), 7607–7611. [https://doi.org/10.1016/S0040-4020\(02\)00867-0](https://doi.org/10.1016/S0040-4020(02)00867-0).
- (209) Pineda De Las Infantas Y Villatoro, M. J.; Unciti-Broceta, J. D.; Contreras-Montoya, R.; Garcia-Salcedo, J. A.; Gallo Mezo, M. A.; Unciti-Broceta, A.; Diaz-Mochon, J. J. Amide-Controlled, One-Pot Synthesis of Tri-Substituted Purines Generates Structural Diversity and Analogues with

- Trypanocidal Activity. *Sci. Rep.* **2015**, *5*, 2–10. <https://doi.org/10.1038/srep09139>.
- (210) Pineda de las Infantas, M. J.; Torres-Rusillo, S.; Unciti-Broceta, J. D.; Fernandez-Rubio, P.; Luque-Gonzalez, M. A.; Gallo, M. a.; Unciti-Broceta, A.; Molina, I. J.; Diaz-Mochon, J. J. Synthesis of 6,8,9 Poly-Substituted Purine Analogue Libraries as pro-Apoptotic Inducers of Human Leukemic Lymphocytes and DAPK-1 Inhibitors. *Org. Biomol. Chem.* **2015**, *13* (18), 5224–5234. <https://doi.org/10.1039/C5OB00230C>.
- (211) Singh, P.; Ravanan, P.; Talwar, P. Death Associated Protein Kinase 1 (DAPK1): A Regulator of Apoptosis and Autophagy. *Front. Mol. Neurosci.* **2016**, *9* (June), 1–11. <https://doi.org/10.3389/fnmol.2016.00046>.
- (212) Simon, B.; Huart, A. S.; Temmerman, K.; Vahokoski, J.; Mertens, H. D. T.; Komadina, D.; Hoffmann, J. E.; Yumerefendi, H.; Svergun, D. I.; Kursula, P.; et al. Death-Associated Protein Kinase Activity Is Regulated by Coupled Calcium/Calmodulin Binding to Two Distinct Sites. *Structure* **2016**, *24* (6), 851–861. <https://doi.org/10.1016/j.str.2016.03.020>.
- (213) Torres-Rusillo, S. Inducción de Apoptosis En Células TumORAles Mediante Inhibidores Selectivos de DAPK1, University of Granada, 2014.
- (214) Bissantz, C.; Kuhn, B.; Stahl, M. Corrections to A Medicinal Chemist's Guide to Molecular Interactions. *J. Med. Chem.* **2010**, *53* (16), 6241–6241. <https://doi.org/10.1021/jm100950p>.
- (215) Chen, D.; Oezguen, N.; Urvil, P.; Ferguson, C.; Dann, S. M.; Savidge, T. C. Regulation of Protein-Ligand Binding Affinity by Hydrogen Bond Pairing. *Sci. Adv.* **2016**, *2* (3), e1501240. <https://doi.org/10.1126/sciadv.1501240>.
- (216) Swain, M. Chemicalize.Org. *J. Chem. Inf. Model.* **2012**, *52* (2), 613–615. <https://doi.org/10.1021/ci300046g>.
- (217) Miao, B.; Degterev, A. *Methods to Analyze Cellular Necroptosis*; 2009; Vol. 559. [https://doi.org/10.1007/978-1-60327-017-5\\_6](https://doi.org/10.1007/978-1-60327-017-5_6).
- (218) Lorente-Macías, Á.; Benítez-Quesada, M.; Molina, I. J.; Unciti-Broceta, A.; Díaz-Mochón, J. J.; Pineda de las Infantas Villatoro, M. J. 1H and 13C Assignments of 6-, 8-, 9- Substituted Purines. *Magnetic Resonance in Chemistry*. 2018, pp 852–859. <https://doi.org/10.1002/mrc.4743>.
- (219) Koopman, G.; Reutelingsperger, C. P.; Kuijten, G. A.; Keehnen, R. M.; Pals, S. T.; van Oers, M. H. Annexin V for Flow Cytometric Detection of Phosphatidylserine Expression on B Cells Undergoing Apoptosis. *Blood* **1994**, *84* (5), 1415–1420.
- (220) Jeannin, P.; Bonnefoy, J.-Y.; Lecoanet-Henchoz, S.; Caron, G.; Moine, V.; Aubry, J.-P.; Blaecke, A.; Herbault, N. Annexin V Used for Measuring Apoptosis in the Early Events of Cellular Cytotoxicity. *Cytometry* **2002**, *37* (3), 197–204. [https://doi.org/10.1002/\(sici\)1097-0320\(19991101\)37:3<197::aid-cyto6>3.0.co;2-l](https://doi.org/10.1002/(sici)1097-0320(19991101)37:3<197::aid-cyto6>3.0.co;2-l).
- (221) Liu, X.; Testa, B.; Fahr, A. Lipophilicity and Its Relationship with Passive Drug Permeation. *Pharm. Res.* **2011**, *28* (5), 962–977. <https://doi.org/10.1007/s11095-010-0303-7>.
- (222) Zhong, M.; Robins, M. J. Regiospecific N9 Alkylation of 6-(Heteroaryl)Purines: Shielding of N7 by a Proximal Heteroaryl C-H. *J. Org. Chem.* **2006**, *71* (23), 8901–8906. <https://doi.org/10.1021/jo061759h>.
- (223) Gray, N. S.; Kwon, S.; Schultz, P. G. Combinatorial Synthesis of 2,9-Substituted Purines. *Tetrahedron Lett.* **1997**, *38* (7), 1161–1164. [https://doi.org/10.1016/S0040-4039\(97\)00014-2](https://doi.org/10.1016/S0040-4039(97)00014-2).
- (224) Gucký, T.; Řezníčková, E.; Radošová Muchová, T.; Jorda, R.; Klejová, Z.; Malínková, V.; Berka, K.; Bazgier, V.; Ajani, H.; Lepšík, M.; et al. Discovery of N2-(4-Amino-Cyclohexyl)-9-Cyclopentyl- N6-(4-Morpholin-4-Ylmethyl-Phenyl)- 9H-Purine-2,6-Diamine as a Potent FLT3 Kinase Inhibitor for Acute Myeloid Leukemia with FLT3 Mutations. *J. Med. Chem.* **2018**, *61* (9), 3855–3869. <https://doi.org/10.1021/acs.jmedchem.7b01529>.

## 7. References

---

- (225) Coxon, C. R.; Anscombe, E.; Harnor, S. J.; Martin, M. P.; Carbain, B.; Golding, B. T.; Hardcastle, I. R.; Harlow, L. K.; Korolchuk, S.; Matheson, C. J.; et al. Cyclin-Dependent Kinase (CDK) Inhibitors: Structure – Activity Relationships and Insights into the CDK - 2 Selectivity of 6 - Substituted 2 - Arylamino-purines. *J. Med. Chem.* **2017**. <https://doi.org/10.1021/acs.jmedchem.6b01254>.
- (226) Gray, N. S.; Wodicka, L.; Thunnissen, A. M. W. H.; Norman, T. C.; Kwon, S.; Espinoza, F. H.; Morgan, D. O.; Barnes, G.; LeClerc, S.; Meijer, L.; et al. Exploiting Chemical Libraries, Structure, and Genomics in the Search for Kinase Inhibitors. *Science (80- )*. **1998**, *281* (5376), 533–538. <https://doi.org/10.1126/science.281.5376.533>.
- (227) Meijer, L.; Raymond, E. Roscovitine and Other Purines as Kinase Inhibitors. From Starfish Oocytes to Clinical Trials. *Acc. Chem. Res.* **2003**, *36* (6), 417–425. <https://doi.org/10.1021/ar0201198>.
- (228) Schulze-Gahmen, U.; Brandsen, J.; Jones, H. D.; Morgan, D. O.; Meijer, L.; Vesely, J.; Kim, S. - H. Multiple Modes of Ligand Recognition: Crystal Structures of Cyclin-dependent Protein Kinase 2 in Complex with ATP and Two Inhibitors, Olomoucine and Isopentenyladenine. *Proteins Struct. Funct. Bioinforma.* **1995**, *22* (4), 378–391. <https://doi.org/10.1002/prot.340220408>.
- (229) Benson, C.; White, J.; De Bono, J.; O'Donnell, A.; Raynaud, F.; Cruickshank, C.; McGrath, H.; Walton, M.; Workman, P.; Kaye, S.; et al. A Phase I Trial of the Selective Oral Cyclin-Dependent Kinase Inhibitor Seliciclib (CYC202; R-Roscovitine), Administered Twice Daily for 7 Days Every 21 Days. *Br. J. Cancer* **2007**, *96* (1), 29–37. <https://doi.org/10.1038/sj.bjc.6603509>.
- (230) Pan, Y.; Xu, Y.; Feng, S.; Luo, S.; Zheng, R.; Yang, J.; Wang, L.; Zhong, L.; Yang, H.-Y.; Wang, B.-L.; et al. SKLB1206, a Novel Orally Available Multikinase Inhibitor Targeting EGFR Activating and T790M Mutants, ErbB2, ErbB4, and VEGFR2, Displays Potent Antitumor Activity Both In Vitro and In Vivo. *Mol. Cancer Ther.* **2012**, *11* (4), 952–962. <https://doi.org/10.1158/1535-7163.mct-11-0679>.
- (231) Hart, S.; Novotny-Diermayr, V.; Goh, K. C.; Williams, M.; Tan, Y. C.; Ong, L. C.; Cheong, A.; Ng, B. K.; Amalini, C.; Madan, B.; et al. VS-5584, a Novel and Highly Selective PI3K/MTOR Kinase Inhibitor for the Treatment of Cancer. *Mol. Cancer Ther.* **2013**, *12* (2), 151–161. <https://doi.org/10.1158/1535-7163.mct-12-0466>.
- (232) Rheault, T. R.; Stellwagen, J. C.; Adjabeng, G. M.; Hornberger, K. R.; Petrov, K. G.; Waterson, A. G.; Dickerson, S. H.; Mook, R. A.; Laquerre, S. G.; King, A. J.; et al. Discovery of Dabrafenib: A Selective Inhibitor of Raf Kinases with Antitumor Activity against B-Raf-Driven Tumors. *ACS Med. Chem. Lett.* **2013**, *4* (3), 358–362. <https://doi.org/10.1021/ml4000063>.
- (233) Regan, J.; Capolino, A.; Cirillo, P. F.; Gilmore, T.; Graham, A. G.; Hickey, E.; Kroe, R. R.; Madwed, J.; Moriak, M.; Nelson, R.; et al. Structure-Activity Relationships of the P38 $\alpha$  MAP Kinase Inhibitor 1-(5-Tert-Butyl-2-p-Tolyl-2H-Pyrazol-3-Yl)-3-[4-(2-Morpholin-4-Yl-Ethoxy) Naphthalen-1-Yl]Urea (BIRB 796). *J. Med. Chem.* **2003**, *46* (22), 4676–4686. <https://doi.org/10.1021/jm030121k>.
- (234) Wang, Y.; Shakespeare, W. C.; Huang, W. S.; Sundaramoorthi, R.; Lentini, S.; Das, S.; Liu, S.; Banda, G.; Wen, D.; Zhu, X.; et al. Novel N9-Arenethenyl Purines as Potent Dual Src/Abl Tyrosine Kinase Inhibitors. *Bioorganic Med. Chem. Lett.* **2008**, *18* (17), 4907–4912. <https://doi.org/10.1016/j.bmcl.2008.06.042>.
- (235) Surry, D. S.; Buchwald, S. L. Dialkylbiaryl Phosphines in Pd-Catalyzed Amination: A User's Guide. *Chem. Sci.* **2011**, *2* (1), 27–50. <https://doi.org/10.1039/c0sc00331j>.
- (236) Henderson, J. L.; Buchwald, S. L. Efficient Pd-Catalyzed Amination Reactions for Heterocycle Functionalization. *Org. Lett.* **2010**, *12* (20), 4442–4445. <https://doi.org/10.1021/ol101929v>.
- (237) Cacchi, S.; Fabrizi, G.; Goggiamani, A.; Sgalla, S. Palladium-Catalyzed N-Arylation of N,N-Dialkylhydrazines with Aryl Chlorides. *Adv. Synth. Catal.* **2007**, *349* (3), 453–458. <https://doi.org/10.1002/adsc.200600299>.



- (238) Aguado, L. Microwave-Assisted Synthesis of 9-Arylpurines. **2009**, 210–212.
- (239) Canela, M.-D.; Liekens, S.; Camarasa, M.-J.; Priego, E. M.; Pérez-Pérez, M.-J. Synthesis and Antiproliferative Activity of 6-Phenylaminopurines. *Eur. J. Med. Chem.* **2014**, *87*, 421–428. <https://doi.org/10.1016/j.ejmech.2014.09.093>.
- (240) Aguado, L.; Thibaut, H. J.; Priego, E. M.; Jimeno, M. L.; Camarasa, M. J.; Neyts, J.; Pérez-Pérez, M. J. 9-Arylpurines as a Novel Class of Enterovirus Inhibitors. *J. Med. Chem.* **2010**, *53* (1), 316–324. <https://doi.org/10.1021/jm901240p>.
- (241) C.J. Waalboer, D.; P.J.T. Rutjes, F. Synthesis and Biological Activity of Novel. *ITB J. Sci.* **2011**, *43* (6), 95–112. <https://doi.org/10.5614/itbj.sci.2011.43.2.3>.
- (242) Chen, H.; Nilsen, C. N.; Choudhury, A.; Sorgi, K. L. A Safe and Convenient Synthesis of 4-Benzyloxy-3-Chloroaniline. *Arkivoc* **2008**, *2008* (14), 1–6. <https://doi.org/10.3998/ark.5550190.0009.e01>.
- (243) Volpini, R.; Dal Ben, D.; Lambertucci, C.; Marucci, G.; Mishra, R. C.; Ramadori, A. T.; Klotz, K. N.; Trincavelli, M. L.; Martini, C.; Cristalli, G. Adenosine A2A Receptor Antagonists: New 8-Substituted 9-Ethyladenines as Tools for in Vivo Rat Models of Parkinson's Disease. *ChemMedChem* **2009**, *4* (6), 1010–1017. <https://doi.org/10.1002/cmdc.200800434>.
- (244) Hein, J. E.; Fokin, V. V. Copper-Catalyzed Azide-Alkyne Cycloaddition (CuAAC) and beyond: New Reactivity of Copper(i) Acetylides. *Chem. Soc. Rev.* **2010**, *39* (4), 1302–1315. <https://doi.org/10.1039/b904091a>.
- (245) Hou, W.; Luo, Z.; Zhang, G.; Cao, D.; Li, D.; Ruan, H.; Helen, B.; Su, L.; Xu, H. European Journal of Medicinal Chemistry Click Chemistry-Based Synthesis and Anticancer Activity Evaluation of Novel C-14 1, 2, 3-Triazole Dehydroabiatic Acid Hybrids. **2017**, *138*, 1042–1052. <https://doi.org/10.1016/j.ejmech.2017.07.049>.
- (246) Kolb, H. C.; Finn, M. G.; Sharpless, K. B. Click Chemistry : Diverse Chemical Function from a Few Good Reactions.
- (247) Finn, M. G.; Fokin, V. V. Click Chemistry: Function Follows Form. *Chem. Soc. Rev.* **2010**, *39* (4), 1231. <https://doi.org/10.1039/c003740k>.
- (248) Wu, P.; Feldman, A. K.; Nugent, A. K.; Hawker, C. J.; Scheel, A.; Voit, B.; Pyun, J.; Fréchet, J. M. J.; Sharpless, K. B.; Fokin, V. V. Efficiency and Fidelity in a Click-Chemistry Route to Triazole Dendrimers by the Copper(I)-Catalyzed Ligation of Azides and Alkynes. *Angew. Chemie - Int. Ed.* **2004**, *43* (30), 3928–3932. <https://doi.org/10.1002/anie.200454078>.
- (249) Horne, W. S.; Yadav, M. K.; Stout, C. D.; Ghadiri, M. R. Heterocyclic Peptide Backbone Modifications in an  $\alpha$ -Helical Coiled Coil. *J. Am. Chem. Soc.* **2004**, *126* (47), 15366–15367. <https://doi.org/10.1021/ja0450408>.
- (250) Muller, M. Anthraquinones as Pharamacological Tools and Drugs - Incorrect Reference. *Med. Res. Rev.* **2016**, *36* (4), 705–748. <https://doi.org/10.1002/med>.
- (251) Dheer, D.; Singh, V.; Shankar, R. Medicinal Attributes of 1,2,3-Triazoles: Current Developments. *Bioorg. Chem.* **2017**, *71*, 30–54. <https://doi.org/10.1016/j.bioorg.2017.01.010>.
- (252) Le Corre, L.; Girard, A. L.; Aubertin, J.; Radvanyi, F.; Benoist-Lasselin, C.; Jonquoy, A.; Mugniery, E.; Legeai-Mallet, L.; Busca, P.; Le Merrer, Y. Synthesis and Biological Evaluation of a Triazole-Based Library of Pyrido[2,3-d]Pyrimidines as FGFR3 Tyrosine Kinase Inhibitors. *Org. Biomol. Chem.* **2010**, *8* (9), 2164–2173. <https://doi.org/10.1039/b923882d>.
- (253) Kumar, A.; Ahmad, I.; Chhikara, B. S.; Tiwari, R.; Mandal, D.; Parang, K. Synthesis of 3-Phenylpyrazolopyrimidine-1,2,3-Triazole Conjugates and Evaluation of Their Src Kinase Inhibitory and Anticancer Activities. *Bioorganic Med. Chem. Lett.* **2011**, *21* (5), 1342–1346. <https://doi.org/10.1016/j.bmcl.2011.01.047>.

## 7. References

---

- (254) Klein, M.; Dinér, P.; Dorin-Semblat, D.; Doerig, C.; Grötli, M. Synthesis of 3-(1,2,3-Triazol-1-Yl)- and 3-(1,2,3-Triazol-4-Yl)-Substituted Pyrazolo[3,4-d]Pyrimidin-4-Amines via Click Chemistry: Potential Inhibitors of the Plasmodium Falciparum PfPK7 Protein Kinase. *Org. Biomol. Chem.* **2009**, *7* (17), 3421–3429. <https://doi.org/10.1039/b906482f>.
- (255) Kalesh, K. A.; Liu, K.; Yao, S. Q. Rapid Synthesis of Abelson Tyrosine Kinase Inhibitors Using Click Chemistry. *Org. Biomol. Chem.* **2009**, *7* (24), 5129–5136. <https://doi.org/10.1039/b913333j>.
- (256) Orlandi, M.; Brenna, D.; Harms, R.; Jost, S.; Benaglia, M. Recent Developments in the Reduction of Aromatic and Aliphatic Nitro Compounds to Amines. *Org. Process Res. Dev.* **2018**, *22* (4), 430–445. <https://doi.org/10.1021/acs.oprd.6b00205>.
- (257) Romagnoli, R.; Baraldi, P. G.; Prencipe, F.; Oliva, P.; Baraldi, S.; Salvador, M. K.; Lopez-Cara, L. C.; Bortolozzi, R.; Mattiuzzo, E.; Basso, G.; et al. Design, Synthesis and Biological Evaluation of 3-Substituted-2-Oxindole Hybrid Derivatives as Novel Anticancer Agents. *Eur. J. Med. Chem.* **2017**, *134*, 258–270. <https://doi.org/10.1016/j.ejmech.2017.03.089>.
- (258) Myers, S. H.; Temps, C.; Houston, D. R.; Brunton, V. G.; Unciti-Broceta, A. Development of Potent Inhibitors of Receptor Tyrosine Kinases by Ligand-Based Drug Design and Target-Biased Phenotypic Screening. *J. Med. Chem.* **2018**, *61* (5), 2104–2110. <https://doi.org/10.1021/acs.jmedchem.7b01605>.
- (259) Park, H.; Jeong, Y.; Hong, S. Structure-Based de Novo Design and Biochemical Evaluation of Novel BRAF Kinase Inhibitors. *Bioorganic Med. Chem. Lett.* **2012**, *22* (2), 1027–1030. <https://doi.org/10.1016/j.bmcl.2011.11.124>.
- (260) Huang, L. K.; Cherng, Y. C.; Cheng, Y. R.; Jang, J. P.; Chao, Y. L.; Cherng, Y. J. An Efficient Synthesis of Substituted Cytosines and Purines under Focused Microwave Irradiation. *Tetrahedron* **2007**, *63* (24), 5323–5327. <https://doi.org/10.1016/j.tet.2007.02.124>.
- (261) Wang, Q.; Su, L.; Liu, N.; Zhang, L.; Xu, W.; Fang, H. Cyclin Dependent Kinase 1 Inhibitors: A Review of Recent Progress. *Curr. Med. Chem.* **2011**, *18* (13), 2025–2043. <https://doi.org/10.2174/092986711795590110>.
- (262) Davies, T. G.; Bentley, J.; Arris, C. E.; Boyle, F. T.; Curtin, N. J.; Endicott, J. A.; Gibson, A. E.; Golding, B. T.; Griffin, R. J.; Hardcastle, I. R.; et al. Structure-Based Design of a Potent Purine-Based Cyclin-Dependent Kinase Inhibitor. *Nat. Struct. Biol.* **2002**, *9* (10), 745–749. <https://doi.org/10.1038/nsb842>.
- (263) Arris, C. E.; Boyle, F. T.; Calvert, A. H.; Curtin, N. J.; Endicott, J. A.; Garman, E. F.; Gibson, A. E.; Golding, B. T.; Grant, S.; Griffin, R. J.; et al. Identification of Novel Purine and Pyrimidine Cyclin-Dependent Kinase Inhibitors with Distinct Molecular Interactions and Tumor Cell Growth Inhibition Profiles. *J. Med. Chem.* **2000**, *43* (15), 2797–2804. <https://doi.org/10.1021/jm990628o>.
- (264) Hohegger, H.; Takeda, S.; Hunt, T. Cyclin-Dependent Kinases and Cell-Cycle Transitions: Does One Fit All? *Nat. Rev. Mol. Cell Biol.* **2008**, *9* (11), 910–916. <https://doi.org/10.1038/nrm2510>.
- (265) Asghar, U.; Witkiewicz, A. K.; Turner, N. C.; Knudsen, E. S. The History and Future of Targeting Cyclin-Dependent Kinases in Cancer Therapy. *Nat. Rev. Drug Discov.* **2015**, *14* (2), 130–146. <https://doi.org/10.1038/nrd4504>.
- (266) Heuvel, S. Van Den; Harlow, E. Distinct Roles for CDKs in Cell Cycle Control. *Science (80-. )*. **1993**.
- (267) Vassilev, L. T.; Tovar, C.; Chen, S.; Knezevic, D.; Zhao, X.; Sun, H.; Heimbrook, D. C.; Chen, L. Selective Small-Molecule Inhibitor Reveals Critical Mitotic Functions of Human CDK1. *Proc. Natl. Acad. Sci.* **2006**, *103* (28), 10660–10665. <https://doi.org/10.1073/pnas.0600447103>.
- (268) Terrano, D. T.; Upreti, M.; Chambers, T. C. Cyclin-Dependent Kinase 1-Mediated Bcl-XL/Bcl-2 Phosphorylation Acts as a Functional Link Coupling Mitotic Arrest and Apoptosis. *Mol. Cell. Biol.* **2010**, *30* (3), 640–656. <https://doi.org/10.1128/mcb.00882-09>.

- (269) Liu, Y.-M.; Chen, H.-L.; Lee, H.-Y.; Liou, J.-P. Tubulin Inhibitors: A Patent Review. *Expert Opin. Ther. Pat.* **2014**, *24* (1), 69–88. <https://doi.org/10.1517/13543776.2014.859247>.
- (270) Lu, Y.; Chen, J.; Xiao, M.; Li, W.; Miller, D. D. An Overview of Tubulin Inhibitors That Interact with the Colchicine Binding Site. *Pharm. Res.* **2012**, *29* (11), 2943–2971. <https://doi.org/10.1007/s11095-012-0828-z>.
- (271) Andreu, J. M.; Perez-Ramirez, B.; Gorbunoff, M. J.; Ayala, D.; Timasheff, S. N. Role of the Colchicine Ring A and Its Methoxy Groups in the Binding to Tubulin and Microtubule Inhibition. *Biochemistry* **1998**, *37* (23), 8356–8368. <https://doi.org/10.1021/bi9728553>.
- (272) Hadjeri, M.; Peiller, E. L.; Beney, C.; Deka, N.; Lawson, M. A.; Dumontet, C.; Boumendjel, A. Antimitotic Activity of 5-Hydroxy-7-Methoxy-2-Phenyl-4-Quinolones. *J. Med. Chem.* **2004**, *47* (20), 4964–4970. <https://doi.org/10.1021/jm049876x>.
- (273) Romagnoli, R.; Baraldi, P. G.; Salvador, M. K.; Prencipe, F.; Lopez-Cara, C.; Schiaffino Ortega, S.; Brancale, A.; Hamel, E.; Castagliuolo, I.; Mitola, S.; et al. Design, Synthesis, in Vitro, and in Vivo Anticancer and Antiangiogenic Activity of Novel 3-Arylamino-benzofuran Derivatives Targeting the Colchicine Site on Tubulin. *J. Med. Chem.* **2015**, *58* (7), 3209–3222. <https://doi.org/10.1021/acs.jmedchem.5b00155>.
- (274) Sangjun, S.; de Jong, E.; Nijmeijer, S.; Mutarapat, T.; Ruchirawat, S.; van den Berg, M.; van Duursen, M. B. M. Induction of Cell Cycle Arrest in Human MCF-7 Breast Cancer Cells by Cis-Stilbene Derivatives Related to VIOXX ®. *Toxicol. Lett.* **2009**, *186* (2), 115–122. <https://doi.org/10.1016/j.toxlet.2009.01.017>.
- (275) Bueno, O.; Estévez Gallego, J.; Martins, S.; Prota, A. E.; Gago, F.; Gómez-Sanjuan, A.; Camarasa, M. J.; Barasoain, I.; Steinmetz, M. O.; Díaz, J. F.; et al. High-Affinity Ligands of the Colchicine Domain in Tubulin Based on a Structure-Guided Design. *Sci. Rep.* **2018**, *8* (1), 1–17. <https://doi.org/10.1038/s41598-018-22382-x>.
- (276) Sum, C. S.; Nickischer, D.; Lei, M.; Weston, A.; Zhang, L.; Schweizer, L. Establishing a High-Content Analysis Method for Tubulin Polymerization to Evaluate Both the Stabilizing and Destabilizing Activities of Compounds. *Curr. Chem. Genomics Transl. Med.* **2014**, *8* (1), 16–26. <https://doi.org/10.2174/2213988501408010016>.

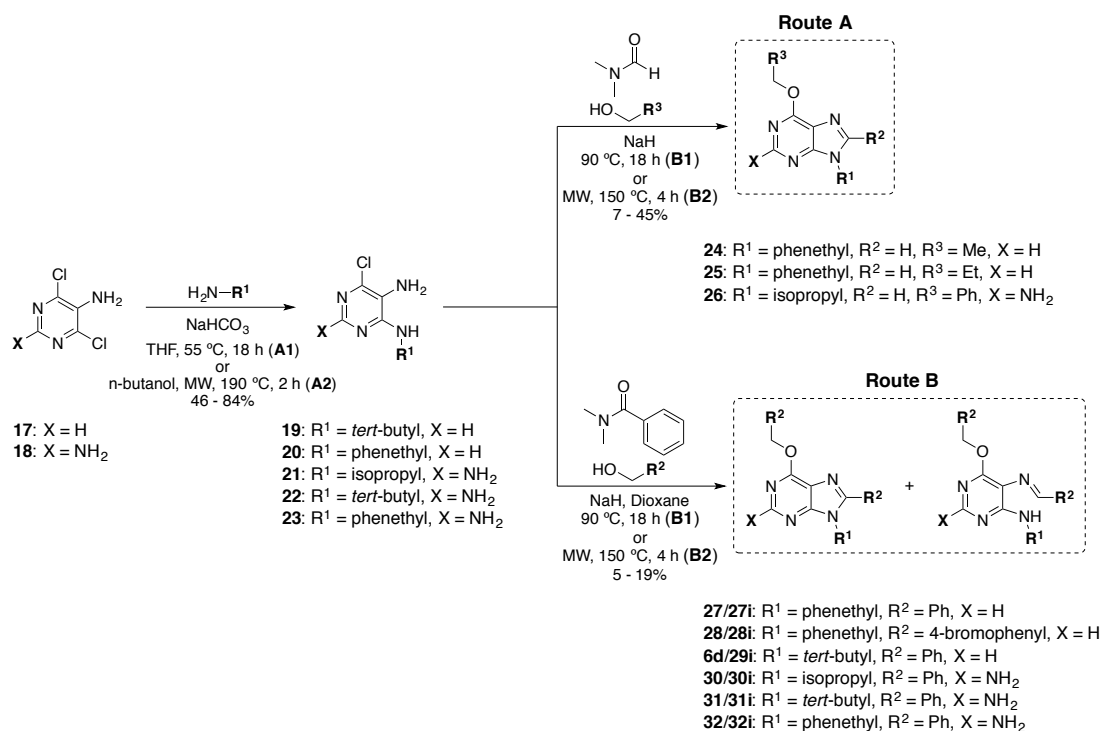


# Appendix

---

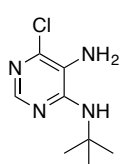


## A. General synthesis for the compounds from chemical library 1

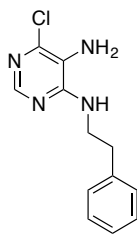


- **General procedure A1:**

To a stirred 0.48 M solution of 5-amino-4,6-dichloropyrimidine (**17**) (1 equiv.) in dry THF was added  $\text{NaHCO}_3$  (2 equiv.). The mixture was then heated to  $55\text{ }^\circ\text{C}$  and at this temperature a 1.6 M solution of the appropriate amine (2 equiv.) in THF was added dropwise. The mixture was heated at reflux for 18 h and then cooled to room temperature. The mixture was diluted with dichloromethane, filtered, the solvent removed under reduced pressure and the crude material was purified by silica gel column chromatography.



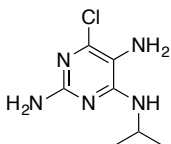
**(19) 5-amino-4-(tert-butylamino)-6-chloropyrimidine.** The crude product was purified via silica gel column chromatography (Ethyl acetate/Hexane 25%) to provide the title compound as a white solid (851.2 mg, 4.233 mmol, 46% yield).  $^1\text{H-NMR}$  (400 MHz,  $\text{CDCl}_3$ ):  $\delta$  8.05 (1H, s, CH), 4.82 (2H, bs,  $\text{NH}_2$ ), 1.92 (1H, bs, NH), 1.46 (9H, s, 3 x  $\text{CH}_3$ ).  $^{13}\text{C-NMR}$  (101 MHz,  $\text{CDCl}_3$ ):  $\delta$  158.11 (C), 152.49 (CH), 135.25 (C), 101.82 (C), 51.47 (C), 29.86 (3 x  $\text{CH}_3$ ). **HRMS** (ES + ve),  $\text{C}_8\text{H}_{14}\text{N}_4\text{Cl}$  ( $\text{M} + \text{H}$ ) $^+$ : Calculated 201.0907. Obtained 201.0893.



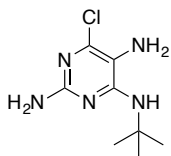
**(20) 5-amino-6-chloro-4-(phenethylamino)pyrimidine.** The crude product was purified via silica gel column chromatography (Ethyl acetate/Hexane 33%) to provide the title compound as a yellow solid (1.13 g, 4.533 mmol, 50% yield). **<sup>1</sup>H-NMR** (400 MHz, CDCl<sub>3</sub>): δ 8.13 (1H, s, CH), 7.37 (2H, t, *J* = 7.2 Hz, 2 x CH), 7.34 – 7.24 (3H, m, 3 x CH), 5.19 (1H, bs, NH), 3.88 – 3.78 (2H, m, CH<sub>2</sub>), 3.25 (2H, bs, NH<sub>2</sub>), 3.01 (2H, t, *J* = 7.0 Hz, CH<sub>2</sub>). **<sup>13</sup>C-NMR** (101 MHz, CDCl<sub>3</sub>): δ 155.09 (C), 149.60 (CH), 142.57 (C), 138.95 (C), 128.91 (2 x CH), 128.80 (2 x CH), 126.72 (CH), 122.04 (C), 42.78 (CH<sub>2</sub>), 35.54 (CH<sub>2</sub>). **HRMS** (ES + ve), C<sub>12</sub>H<sub>14</sub>N<sub>4</sub>Cl (M + H)<sup>+</sup>: Calculated 249.0907. Obtained 249.0902.

• **General procedure A2:**

A microwave vial was charged with a 0.4 M solution of 4,6-dichloropyrimidine-2,5-diamine (**18**) (1 equiv.) in n-butanol, NaHCO<sub>3</sub> (2.5 equiv.) and the appropriate amine (5 equiv.). Then the mixture was heated at 190 °C for 2 h using microwave radiation. The mixture was diluted with dichloromethane, filtered, the solvent removed under reduced pressure and the crude material was purified by silica gel column chromatography.

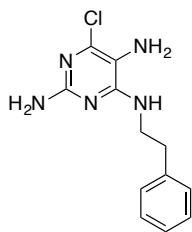


**(21) 2,5-diamino-6-chloro-4-(isopropylamino)pyrimidine.** The crude product was purified via silica gel column chromatography (Ethyl acetate/Hexane 66%) to provide the title compound as an off-white solid (189.7 mg, 0.978 mmol, 58% yield). **<sup>1</sup>H-NMR** (400 MHz, CDCl<sub>3</sub>): δ 5.39 (1H, s, CH), 4.79 (2H, bs, NH<sub>2</sub>), 4.28 – 4.07 (1H, m, CH), 2.66 (2H, bs, NH<sub>2</sub>), 1.23 (6H, d, *J* = 6.5 Hz, 2 x CH<sub>3</sub>). **<sup>13</sup>C-NMR** (126 MHz, CDCl<sub>3</sub>): δ 158.45 (C), 157.37 (C), 146.61 (C), 111.73 (C), 42.92 (CH), 22.96 (2 x CH<sub>3</sub>). **HRMS** (ES + ve), C<sub>7</sub>H<sub>13</sub>N<sub>5</sub>Cl (M + H)<sup>+</sup>: Calculated 202.0859. Obtained 202.0849.



**(22) 2,5-diamino-4-(tert-butylamino)-6-chloropyrimidine.** The crude product was purified via silica gel column chromatography (Ethyl acetate/Hexane 20-33%) to provide the title compound as a dark green solid (187 mg, 0.865 mmol, 47 yield%). **<sup>1</sup>H-NMR** (400 MHz, CDCl<sub>3</sub>): δ 5.37 (1H, bs, NH), 4.67 (2H, bs, NH<sub>2</sub>), 2.73 (2H, bs, NH<sub>2</sub>), 1.41 (9H, s, 3 x CH<sub>3</sub>). **<sup>13</sup>C-NMR** (126 MHz, CDCl<sub>3</sub>): δ 158.91 (C), 157.27 (C), 147.53 (C), 111.80 (C), 51.98 (C), 28.97 (3 x CH<sub>3</sub>). **HRMS** (ES + ve), C<sub>8</sub>H<sub>15</sub>N<sub>5</sub>Cl (M + H)<sup>+</sup>: Calculated 216.1016. Obtained 216.1009.

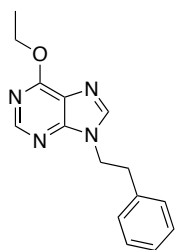




**(23) 2,5-diamino-6-chloro-4-(phenethylamino)pyrimidine.** The crude product was purified via silica gel column chromatography (Ethyl acetate/Hexane 33%) to provide the title compound as a yellow solid (406.8 mg, 1.54 mmol, 84% yield). **<sup>1</sup>H-NMR** (400 MHz, CDCl<sub>3</sub>): δ 7.32 (2H, t, *J* = 7.4 Hz, 2 x CH), 7.28 – 7.14 (3H, m, 3 x CH), 5.42 (1H, bs, NH), 4.65 (2H, bs, NH<sub>2</sub>), 3.66 (2H, q, *J* = 6.7 Hz, CH<sub>2</sub>), 2.90 (2H, t, *J* = 6.7 Hz, CH<sub>2</sub>), 2.65 (2H, bs, NH<sub>2</sub>). **<sup>13</sup>C-NMR** (101 MHz, CDCl<sub>3</sub>): δ 159.21 (C), 157.91 (C), 148.36 (C), 139.20 (C), 128.91 (2 x CH), 128.76 (2 x CH), 126.63 (CH), 111.75 (C), 42.37 (CH<sub>2</sub>), 35.76 (CH<sub>2</sub>). **HRMS** (ES + ve), C<sub>12</sub>H<sub>15</sub>N<sub>5</sub>Cl (M + H)<sup>+</sup>: Calculated 264.1016. Obtained 264.1022.

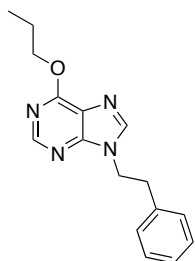
- **General procedure B1:**

A suspension of NaH (60%) in mineral oil (10 equiv.) was dissolved in a mixture cooled at 0 °C constituted both from the appropriate alcohol (10 equiv.) and amide (10 equiv.). When *N,N*-dimethylbenzamide (DMB) was used as the amide source dioxane was employed as a solvent. The solution was stirred at room temperature for 30 min and then at 90 °C for the same time. At 90 °C, the corresponding diaminopyrimidine (**19**, **20**) (1 equiv.) dissolved in the appropriate amide (50 equiv.) was added dropwise and the mixture heated for 18 h. The reaction mixture was quenched to pH 7 with saturated aqueous NH<sub>4</sub>Cl, extracted with dichloromethane and washed with saturated brine. The combined organic extracts were dried over anhydrous Na<sub>2</sub>SO<sub>4</sub>, filtered and the solvent was removed under reduced pressure. The residue was purified by silica gel column chromatography.

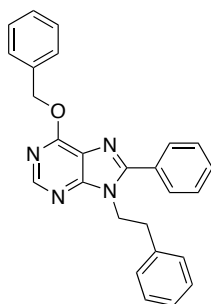


**(24) 6-ethoxy-9-phenethyl-9H-purine.** The crude product was purified via silica gel column chromatography (Ethyl acetate/Hexane 33-100%) to provide the title compound as a yellow solid (50.4 mg, 0.187 mmol, 45% yield). **<sup>1</sup>H-NMR** (400 MHz, CDCl<sub>3</sub>): δ 8.60 (1H, s, CH), 7.58 (1H, s, CH), 7.37 – 7.24 (3H, m, 3 x CH), 7.13 – 7.07 (2H, m, 2 x CH), 4.72 (2H, q, *J* = 7.1 Hz, OCH<sub>2</sub>), 4.54 (2H, t, *J* = 7.0 Hz, CH<sub>2</sub>), 3.24 (2H, t, *J* = 7.0 Hz, CH<sub>2</sub>), 1.57 (3H, t, *J* = 7.1 Hz, CH<sub>3</sub>). **<sup>13</sup>C-NMR** (101 MHz, CDCl<sub>3</sub>): δ 160.95 (C), 152.16 (CH), 152.05 (C), 142.15 (CH), 137.34 (C), 128.95 (2 x CH), 128.77 (2 x CH), 127.17

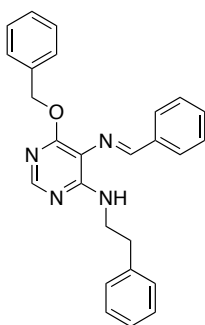
(CH), 121.57 (C), 63.21 (CH<sub>2</sub>), 45.73 (CH<sub>2</sub>), 36.25 (CH<sub>2</sub>), 14.61 (CH<sub>3</sub>). **HRMS** (ES + ve), C<sub>15</sub>H<sub>17</sub>N<sub>4</sub>O (M + H)<sup>+</sup>: Calculated 269.1402. Obtained 269.1402.



**(25) 9-phenethyl-6-propoxy-9H-purine.** The crude product was purified via silica gel column chromatography (Ethyl acetate/Hexane 50-66%) to provide the title compound as a brown solid (24.9 mg, 0.088 mmol, 19% yield). **<sup>1</sup>H-NMR** (400 MHz, CDCl<sub>3</sub>): δ 8.54 (1H, s, CH), 7.54 (1H, s, CH), 7.31 – 7.18 (3H, m, 3 x CH), 7.08 – 7.01 (2H, m, 2 x CH), 4.56 (2H, t, *J* = 7.0 Hz, OCH<sub>2</sub>), 4.48 (2H, t, *J* = 7.0 Hz, CH<sub>2</sub>), 3.18 (2H, t, *J* = 7.0 Hz, CH<sub>2</sub>), 2.00 – 1.86 (2H, m, CH<sub>2</sub>), 1.08 (3H, t, *J* = 7.5 Hz, CH<sub>3</sub>). **<sup>13</sup>C-NMR** (101 MHz, CDCl<sub>3</sub>): δ 161.18 (C), 152.23 (CH), 152.08 (C), 142.18 (CH), 137.36 (C), 129.02 (2 x CH), 128.84 (2 x CH), 127.26 (CH), 121.51 (C), 69.01 (CH<sub>2</sub>), 45.83 (CH<sub>2</sub>), 36.32 (CH<sub>2</sub>), 22.36 (CH<sub>2</sub>), 10.57 (CH<sub>3</sub>). **HRMS** (ES + ve), C<sub>16</sub>H<sub>19</sub>N<sub>4</sub>O (M + H)<sup>+</sup>: Calculated 283.1559. Obtained 283.1559.

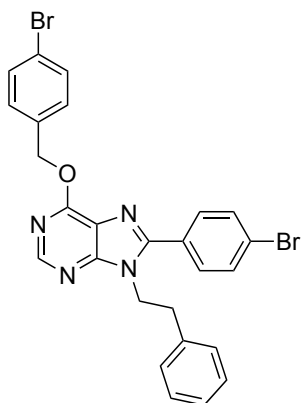


**(27) 6-(benzyloxy)-9-phenethyl-8-phenyl-9H-purine.** The crude product was purified via silica gel column chromatography (Ethyl acetate/Hexane 25%) to provide the title compound as a white solid (7.6 mg, 0.019 mmol, 5% yield). **<sup>1</sup>H-NMR** (400 MHz, CDCl<sub>3</sub>): δ 8.58 (1H, s, CH), 7.60 – 7.53 (2H, m, 2 x CH), 7.52 – 7.41 (3H, m, 3 x CH), 7.39 – 7.24 (5H, m, 5 x CH), 7.21 – 7.13 (3H, m, 3 x CH), 6.96 – 6.87 (2H, m, 2 x CH), 5.71 (2H, s, OCH<sub>2</sub>), 4.56 (2H, t, *J* = 7.4 Hz, CH<sub>2</sub>), 3.10 (2H, t, *J* = 7.4 Hz, CH<sub>2</sub>). **<sup>13</sup>C-NMR** (126 MHz, CDCl<sub>3</sub>): δ 161.23 (C), 158.80 (C), 154.40 (CH), 139.32 (C), 137.42 (C), 136.96 (C), 131.17 (CH), 129.89 (C), 129.12 (2 x CH), 128.81 (2 x CH), 128.78 (2 x CH), 128.66 (2 x CH), 128.34 (2 x CH), 128.13 (CH), 127.85 (2 x CH), 126.59 (CH), 111.10 (C), 68.25 (CH<sub>2</sub>), 42.36 (CH<sub>2</sub>), 36.18 (CH<sub>2</sub>). **HRMS** (ES + ve), C<sub>26</sub>H<sub>23</sub>N<sub>4</sub>O (M + H)<sup>+</sup>: Calculated 407.1872. Obtained 407.1848.



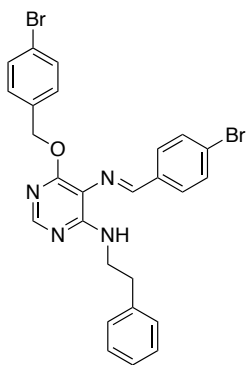
**(27i) 5-(benzylideneamino)-6-(benzyloxy)-4-(phenethylamino)pyrimidine.** The crude product was purified via silica gel column chromatography (Ethyl acetate/Hexane 20%) to provide the title compound as a brown solid (30.1 mg, 0.074 mmol, 19% yield). **<sup>1</sup>H-NMR** (500 MHz, CDCl<sub>3</sub>): δ 9.17 (1H, s, CH), 8.19 (1H, s, CH), 7.68 – 7.61 (2H, m, 2 x CH), 7.47 – 7.40 (7H, m, 7 x CH), 7.40 – 7.35 (3H, m, 3 x CH), 7.34 – 7.27 (3H, m, 3 x CH), 6.30 (1H, bs, NH), 5.51 (2H, s, OCH<sub>2</sub>),

3.83 (2H, q,  $J = 6.5$  Hz, CH<sub>2</sub>), 2.97 (2H, t,  $J = 6.8$  Hz, CH<sub>2</sub>). **<sup>13</sup>C-NMR** (126 MHz, CDCl<sub>3</sub>):  $\delta$  161.22 (CH), 158.79 (C), 154.40 (CH), 139.32 (C), 137.42 (C), 136.95 (C), 131.17 (CH), 129.89 (C), 129.12 (2 x CH), 128.81 (2 x CH), 128.77 (2 x CH), 128.66 (2 x CH), 128.34 (2 x CH), 128.12 (CH), 127.84 (2 x CH), 126.58 (CH), 111.09 (C), 68.25 (CH<sub>2</sub>), 42.37 (CH<sub>2</sub>), 36.18 (CH<sub>2</sub>). **HRMS** (ES + ve), C<sub>26</sub>H<sub>25</sub>N<sub>4</sub>O (M + H)<sup>+</sup>: Calculated 409.2028. Obtained 409.2039.



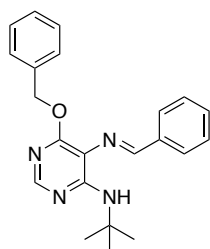
**(28) 6-(4-bromobenzyloxy)-8-(4-bromophenyl)-9-phenethyl-9H-purine.** The crude product was purified via silica gel column chromatography (Ethyl acetate/Hexane 25%) to provide the title compound as an orange solid (15.1 mg, 0.027 mmol, 7% yield). **<sup>1</sup>H-NMR** (500 MHz, CDCl<sub>3</sub>):  $\delta$  8.56 (1H, s, CH), 7.58 – 7.54 (1H, m, CH), 7.53 – 7.41 (7H, m, 7 x CH), 7.31 – 7.27 (2H, m, 2 x CH), 7.20 – 7.14 (2H, m, 2 x CH), 6.97 – 6.89 (1H, m, 1 x CH), 5.02 (2H, s, OCH<sub>2</sub>), 4.56 (2H, t,  $J$

= 6.8 Hz, 2 x CH), 3.10 (2H, t,  $J = 6.8$  Hz, 2 x CH). **<sup>13</sup>C-NMR** (126 MHz, CDCl<sub>3</sub>):  $\delta$  159.93 (C), 158.10 (C), 151.48 (CH), 137.12 (C), 136.01 (C), 135.37 (C), 133.68 (C), 131.72 (2 x CH), 130.19 (C), 130.14 (2 x CH), 129.48 (C), 129.20 (2 x CH), 129.02 (2 x CH), 128.66 (2 x CH), 126.89 (CH), 121.86 (C), 114.93 (2 x CH), 69.28 (CH<sub>2</sub>), 45.52 (CH<sub>2</sub>), 35.58 (CH<sub>2</sub>). **HRMS** (ES + ve), C<sub>26</sub>H<sub>21</sub>N<sub>4</sub>OBr<sub>2</sub> (M + H)<sup>+</sup>: Calculated 563.0082. Obtained 563.0092.



**(28i) 6-(4-bromobenzyloxy)-5-[(4-bromobenzylidene)amino]-4-(phenethylamino)pyrimidine.** The crude product was purified via silica gel column chromatography (Ethyl acetate/Hexane 25%) to provide the title compound as an orange solid (9.7 mg, 0.017 mmol, 4% yield). **<sup>1</sup>H-NMR** (400 MHz, CDCl<sub>3</sub>):  $\delta$  9.11 (1H, s, CH), 9.06 (1H, s, CH), 8.17 (1H, s, CH), 7.69 – 7.62 (1H, m, CH), 7.58 – 7.41 (5H, m, 5 x CH), 7.38 – 7.27 (6H,

m, 6 x CH), 5.45 (2H, s, OCH<sub>2</sub>), 3.83 (2H, q,  $J = 6.5$  Hz, CH<sub>2</sub>), 2.96 (2H, t,  $J = 6.5$  Hz, CH<sub>2</sub>). **<sup>13</sup>C-NMR** (126 MHz, CDCl<sub>3</sub>):  $\delta$  159.66 (C), 158.66 (CH), 154.57 (CH), 139.21 (C), 137.24 (C), 136.21 (C), 135.90 (C), 132.09 (2 x CH), 131.81 (2 x CH), 129.90 (C), 129.61 (2 x CH), 129.12 (2 x CH), 128.84 (2 x CH), 128.38 (2 x CH), 126.66 (CH), 122.18 (C), 110.83 (C), 67.50 (CH<sub>2</sub>), 42.29 (CH<sub>2</sub>), 36.09 (CH<sub>2</sub>). **HRMS** (ES + ve), C<sub>26</sub>H<sub>23</sub>N<sub>4</sub>OBr<sub>2</sub> (M + H)<sup>+</sup>: Calculated 565.0239. Obtained 565.0245.



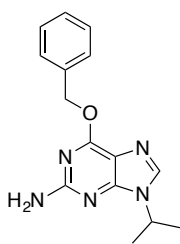
**(29i) 5-(benzylideneamino)-6-(benzyloxy)-4-(tert-butylamino)pyrimidine.**

The crude product was purified via silica gel column chromatography (Ethyl acetate/Hexane 10-33%) to provide the title compound as a yellow solid (15.6 mg, 0.043 mmol, 6% yield).

**<sup>1</sup>H-NMR** (300 MHz, CDCl<sub>3</sub>): δ 9.17 (1H, s, CH), 8.15 (1H, s, CH), 7.81 – 7.71 (2H, m, 2 x CH), 7.49 – 7.33 (8H, m, 8 x CH), 6.28 (1H, bs, NH), 5.50 (2H, s, OCH<sub>2</sub>), 1.54 (9H, s, 3 x CH<sub>3</sub>). **HRMS** (ES + ve), C<sub>22</sub>H<sub>25</sub>N<sub>4</sub>O (M + H)<sup>+</sup>: Calculated 361.2028. Obtained 361.2041.

• **General procedure B2:**

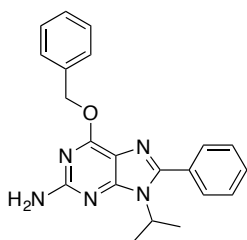
A microwave vial was charged with a suspension of NaH (60%) in mineral oil (10 equiv.), *N,N*-dimethylformamide (DMF) (40 equiv.) and the appropriate alcohol (10 equiv.). Then the corresponding triaminopyrimidine (**21** – **23**) (1 equiv.) dissolved in DMF (80 equiv.) was added dropwise and the mixture heated at 150 °C for 4 h using microwave radiation. When DMB was used as the amide source dioxane was employed as a solvent. The reaction mixture was quenched to pH 7 with saturated aqueous NH<sub>4</sub>Cl, extracted with dichloromethane and washed with saturated brine. The combined organic extracts were dried over anhydrous Na<sub>2</sub>SO<sub>4</sub>, filtered and the solvent was removed under reduced pressure. The residue was purified by silica gel column chromatography.



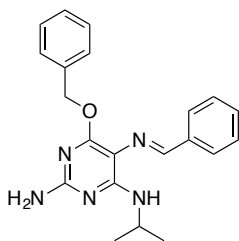
**(26) 2-amino-6-(benzyloxy)-9-isopropyl-9H-purine.**

The crude product was purified via silica gel column chromatography (Ethyl acetate/Hexane 50-100%) to provide the title compound as a red solid (8.5 mg, 0.03 mmol, 7% yield). **<sup>1</sup>H-NMR** (500 MHz, CDCl<sub>3</sub>): δ 7.68 (1H, s, CH), 7.53 – 7.47 (2H, m, 2 x CH), 7.37 – 7.27 (3H, m, 3 x CH), 5.56

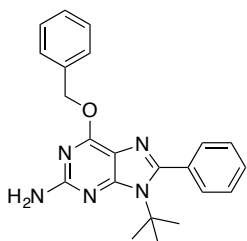
(2H, s, OCH<sub>2</sub>), 4.84 (2H, bs, NH<sub>2</sub>), 4.73 – 4.63 (1H, m, CH), 1.54 (6H, d, *J* = 6.8 Hz, 2 x CH<sub>3</sub>). **<sup>13</sup>C-NMR** (126 MHz, CDCl<sub>3</sub>): δ 161.14 (C), 159.00 (C), 153.78 (C), 137.08 (CH), 136.71 (C), 128.49 (2 x CH), 128.38 (2 x CH), 128.06 (CH), 116.10, 68.10 (CH<sub>2</sub>), 46.66 (CH), 22.75 (2 x CH<sub>3</sub>). **HRMS** (ES + ve), C<sub>15</sub>H<sub>18</sub>N<sub>5</sub>O (M + H)<sup>+</sup>: Calculated 284.1511. Obtained 284.1510.



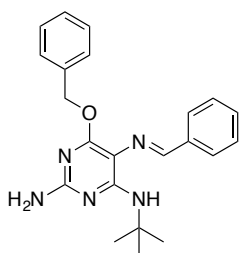
**(30) 2-amino-6-(benzyloxy)-9-isopropyl-8-phenyl-9H-purine.** The crude product was purified via silica gel column chromatography (Ethyl acetate/Hexane 33%) to provide the title compound as a brown solid (11 mg, 0.031 mmol, 6% yield). **<sup>1</sup>H-NMR** (400 MHz, CDCl<sub>3</sub>): δ 7.64 – 7.56 (2H, m, 2 x CH), 7.58 – 7.42 (5H, m, 5 x CH), 7.39 – 7.31 (3H, m, 3 x CH), 5.58 (2H, s, OCH<sub>2</sub>), 4.84 (2H, bs, NH<sub>2</sub>), 4.68 – 4.55 (1H, m, CH), 1.64 (6H, d, *J* = 6.8 Hz, 2 x CH<sub>3</sub>). **<sup>13</sup>C-NMR** (126 MHz, CDCl<sub>3</sub>): δ 160.95 (C), 158.20 (C), 150.34 (C), 136.81 (C), 131.74 (C), 129.74 (CH), 129.61 (2 x CH), 128.68 (2 x CH), 128.61 (2 x CH), 128.45 (2 x CH), 128.05 (CH), 127.13 (C), 116.15 (C), 68.02 (CH<sub>2</sub>), 49.31 (CH), 21.16 (2 x CH<sub>3</sub>). **HRMS** (ES + ve), C<sub>21</sub>H<sub>22</sub>N<sub>5</sub>O (M + H)<sup>+</sup>: Calculated 360.1824. Obtained 360.1820.



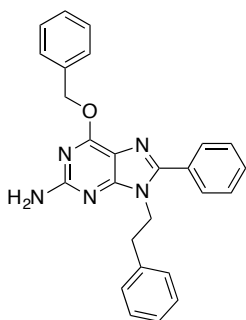
**(30i) 2-amino-5-(benzylideneamino)-6-(benzyloxy)-4-(isopropylamino)pyrimidine.** The crude product was purified via silica gel column chromatography (Ethyl acetate/Hexane 33%) to provide the title compound as a yellow solid (29.9 mg, 0.083 mmol, 16% yield). **<sup>1</sup>H-NMR** (400 MHz, CDCl<sub>3</sub>): δ 9.10 (1H, s, CH), 7.73 – 7.65 (1H, m, CH), 7.47 – 7.27 (9H, m, 9 x CH), 6.22 (1H, bs, NH), 5.43 (2H, s, OCH<sub>2</sub>), 4.84 (2H, bs, NH<sub>2</sub>), 4.32 – 4.19 (1H, m, CH), 1.27 (6H, d, *J* = 6.5 Hz, 2 x CH<sub>3</sub>). **<sup>13</sup>C-NMR** (126 MHz, CDCl<sub>3</sub>): δ 160.51 (C), 155.24 (CH), 141.04 (C), 138.48 (C), 137.29 (C), 134.60 (C), 129.94 (CH), 128.68 (2 x CH), 128.58 (CH), 127.96 (CH), 127.82 (CH), 127.76 (CH), 127.55 (CH), 127.11 (2 x CH), 103.59 (C), 67.78 (CH<sub>2</sub>), 42.56 (CH), 23.38 (2 x CH<sub>3</sub>). **HRMS** (ES + ve), C<sub>21</sub>H<sub>24</sub>N<sub>5</sub>O (M + H)<sup>+</sup>: Calculated 362.1981. Obtained 362.1978.



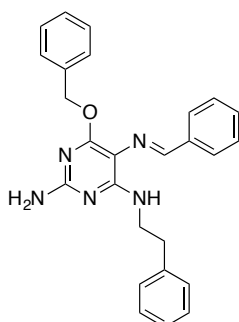
**(31) 2-amino-6-(benzyloxy)-9-(tert-butyl)-8-phenyl-9H-purine.** The crude product was purified via silica gel column chromatography (Ethyl acetate/Hexane 20%) to provide the title compound as a brown solid (10.7 mg, 0.029 mmol, 7% yield). **<sup>1</sup>H-NMR** (400 MHz, CDCl<sub>3</sub>): δ 7.58 – 7.25 (10H, m, 10 x CH), 5.54 (2H, s, OCH<sub>2</sub>), 4.79 (2H, bs, NH<sub>2</sub>), 1.58 (9H, s, 3 x CH<sub>3</sub>). **<sup>13</sup>C-NMR** (101 MHz, CDCl<sub>3</sub>): δ 161.04 (C), 157.69 (C), 150.44 (C), 136.76 (C), 135.52 (C), 130.20 (2 x CH), 129.22 (CH), 128.73 (2 x CH), 128.42 (2 x CH), 128.04 (CH), 127.88 (2 x CH), 127.14 (C), 115.92 (C), 68.00 (CH<sub>2</sub>), 60.10 (C), 30.88 (3 x CH<sub>3</sub>). **HRMS** (ES + ve), C<sub>22</sub>H<sub>24</sub>N<sub>5</sub>O (M + H)<sup>+</sup>: Calculated 374.1981. Obtained 374.1965.



**(31i) 2-amino-5-(benzylideneamino)-6-(benzyloxy)-4-(tert-butylamino)pyrimidine.** The crude product was purified via silica gel column chromatography (Ethyl acetate/Hexane 20%) to provide the title compound as a yellow solid (7.3 mg, 0.019 mmol, 5% yield). **<sup>1</sup>H-NMR** (500 MHz, CDCl<sub>3</sub>): δ 9.11 (1H, s, CH), 7.72 – 7.66 (2H, m, 2 x CH), 7.48 – 7.30 (8H, m, 8 x CH), 6.50 (1H, bs, NH), 5.45 (2H, s, OCH<sub>2</sub>), 4.69 (2H, bs, NH<sub>2</sub>), 1.53 (9H, s, 3 x CH<sub>3</sub>). **<sup>13</sup>C-NMR** (126 MHz, CDCl<sub>3</sub>): δ 161.77 (C), 160.22 (C), 159.22 (C), 154.67 (CH), 138.60 (C), 137.49 (C), 129.79 (CH), 128.66 (2 x CH), 128.54 (2 x CH), 127.86 (CH), 127.77 (2 x CH), 127.45 (2 x CH), 103.94 (C), 67.49 (CH<sub>2</sub>), 51.41 (C), 29.47 (3 x CH<sub>3</sub>). **HRMS** (ES + ve), C<sub>22</sub>H<sub>26</sub>N<sub>5</sub>O (M + H)<sup>+</sup>: Calculated 376.2137. Obtained 376.2152.



**(32) 2-amino-6-(benzyloxy)-9-phenethyl-8-phenyl-9H-purine.** The crude product was purified via silica gel column chromatography (Ethyl acetate/Hexane 25%) to provide the title compound as an orange solid (13.3 mg, 0.03 mmol, 9% yield). **<sup>1</sup>H-NMR** (400 MHz, CDCl<sub>3</sub>): δ 7.51 – 7.47 (3H, m, 3 x CH), 7.41 (2H, d, *J* = 7.2 Hz, 2 x CH), 7.38 – 7.32 (4H, m, 4 x CH), 7.31 – 7.27 (2H, m, 2 x CH), 7.20 – 7.17 (2H, m, *J* = 5.1, 2.0 Hz, 2 x CH), 6.97 – 6.93 (2H, m, 2 x CH), 5.58 (2H, s, OCH<sub>2</sub>), 4.70 (2H, bs, NH<sub>2</sub>), 4.36 (2H, t, *J* = 7.6 Hz, CH<sub>2</sub>), 3.04 (2H, t, *J* = 7.6 Hz, CH<sub>2</sub>). **<sup>13</sup>C-NMR** (101 MHz, CDCl<sub>3</sub>): δ 160.68 (C), 158.73 (C), 156.00 (C), 137.88 (C), 136.94 (C), 130.41 (C), 129.57 (CH), 129.16 (2 x CH), 128.87 (2 x CH), 128.70 (2 x CH), 128.66 (CH), 128.62 (2 x CH), 128.54 (2 x CH), 128.44 (2 x CH), 127.68 (CH), 126.81 (C), 115.22 (C), 68.00 (CH<sub>2</sub>), 46.27 (CH<sub>2</sub>), 45.23 (CH<sub>2</sub>). **HRMS** (ES + ve), C<sub>26</sub>H<sub>23</sub>N<sub>5</sub>ONa (M + Na)<sup>+</sup>: Calculated 444.1800. Obtained 444.1814.



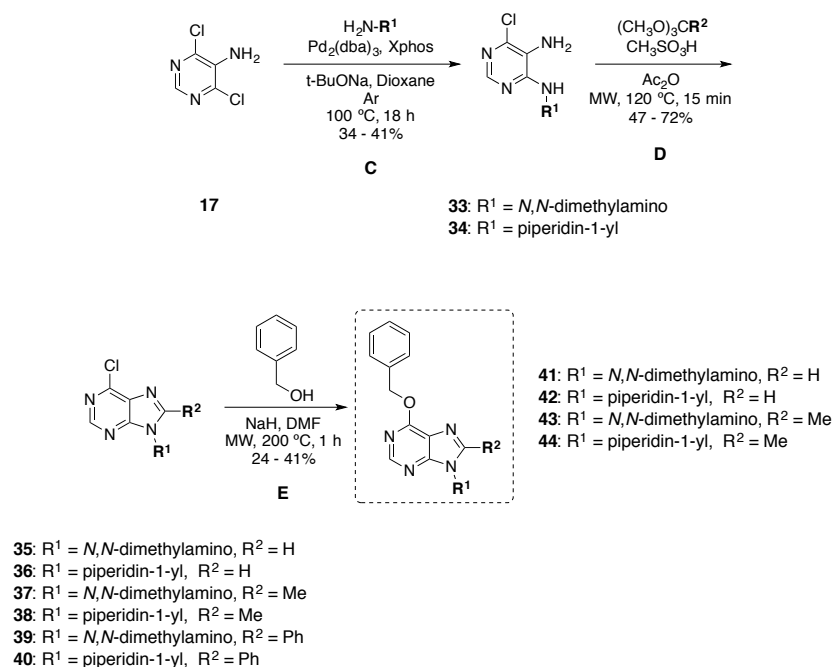
**(32i) 2-amino-5-(benzylideneamino)-6-(benzyloxy)-4-(phenethylamino)pyrimidine.** The crude product was purified via silica gel column chromatography (Ethyl acetate/Hexane 25%) to provide the title compound as a yellow solid (21.1 mg, 0.05 mmol, 14% yield). **<sup>1</sup>H-NMR** (400 MHz, CDCl<sub>3</sub>): δ 9.08 (1H, s, CH), 7.62 – 7.54 (2H, m, 2 x CH), 7.45 – 7.25 (12H, m, 12 x CH), 7.21 – 7.13 (1H, m, CH), 6.47 (1H, bs, NH), 5.44 (2H, s, OCH<sub>2</sub>), 5.20 (2H, bs, NH<sub>2</sub>), 3.75 (2H, q, *J* = 6.7 Hz, CH<sub>2</sub>), 2.92 (2H, t, *J* = 6.7 Hz, CH<sub>2</sub>). **<sup>13</sup>C-NMR** (101 MHz, CDCl<sub>3</sub>): δ 160.62 (C), 158.99 (C), 153.98 (CH), 140.13 (C), 139.73 (C), 138.73

---

(C), 137.56 (C), 129.65 (CH), 129.11 (2 x CH), 128.75 (2 x CH), 128.57 (2 x CH), 127.85 (2 x CH), 127.70 (2 x CH), 127.50 (2 x CH), 127.18 (CH), 126.43 (CH), 103.47 (C), 67.58 (CH<sub>2</sub>), 45.85 (CH<sub>2</sub>), 42.27 (CH<sub>2</sub>). **HRMS** (ES + ve), C<sub>26</sub>H<sub>26</sub>N<sub>5</sub>O (M + H)<sup>+</sup>: Calculated 424.2137. Obtained 424.2140.

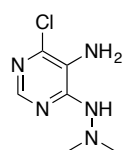
## B. General synthesis for the compounds from chemical library 2

## Chemical library 2a.



## • General procedure C:

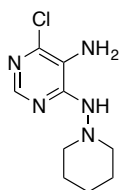
In a round bottom flask, tris(dibenzylideneacetone)dipalladium(0) ( $\text{Pd}_2(\text{dba})_3$ ) (279.2 mg, 0.3 mmol, 0.025 equiv.) and 2-dicyclohexylphosphino-2',4',6'-triisopropylbiphenyl (Xphos) (290.7 mg, 0.61 mmol, 0.05 equiv.) were stirred in dioxane (15 mL) at room temperature under argon for 30 min. Then 5-amino-4,6-dichloropyrimidine (**17**) (2 g, 12.2 mmol, 1 equiv.), t-BuONa (1.6 g, 17.07 mmol, 1.4 equiv.), dioxane (15 mL) and *N,N*-dimethylhydrazine or 1-aminopiperidine (24.4 mmol, 2 equiv.) were added. The reaction was allowed to stir at  $100\text{ }^\circ\text{C}$  for 18 h and then cooled to room temperature and filtered through a pad of Celite. The Celite pad was washed with ethyl acetate (50 mL) and the filtrate was concentrated under reduced pressure. The residue was purified by silica gel column chromatography.



**(33) 5-amino-6-chloro-4-(2,2-dimethylhydrazinyl)pyrimidine.** The crude product was purified via silica gel column chromatography (Ethyl acetate/Hexane 66-100%) to provide the title compound as a white solid (937.5 mg, 4.985 mmol, 41% yield).  $^1\text{H-NMR}$  (400 MHz,  $\text{CDCl}_3$ ):  $\delta$  7.90 (1H, s, CH), 5.62 (1H, bs, NH), 5.07 (2H, bs,  $\text{NH}_2$ ), 2.61 (6H, s, 2 x  $\text{CH}_2$ ).  $^{13}\text{C-NMR}$  (101 MHz,



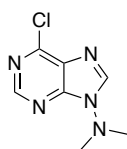
CDCl<sub>3</sub>):  $\delta$  151.12 (C), 146.43 (CH), 142.97 (C), 125.27 (C), 48.82 (2 x CH<sub>3</sub>). **HRMS** (ES + ve), C<sub>6</sub>H<sub>11</sub>N<sub>5</sub>Cl (M + H)<sup>+</sup>: Calculated 188.0703. Obtained 188.0716.



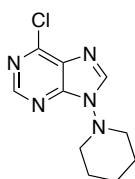
**(34) 5-amino-6-chloro-4-[(piperidin-1-yl)amino]pyrimidine.** The crude product was purified via silica gel column chromatography (Ethyl acetate/Hexane 50-66%) to provide the title compound as an orange solid (937.7 mg, 4.111 mmol, 34% yield). **<sup>1</sup>H-NMR** (500 MHz, CDCl<sub>3</sub>):  $\delta$  7.88 (1H, s, CH), 5.77 (1H, bs, NH), 5.21 (2H, bs, NH<sub>2</sub>), 2.77 (4H, t, 2 x CH<sub>2</sub>), 1.73 – 1.65 (4H, m, 2 x CH<sub>2</sub>), 1.47 – 1.43 (2H, m, CH<sub>2</sub>). **<sup>13</sup>C-NMR** (126 MHz, CDCl<sub>3</sub>):  $\delta$  151.08 (C), 146.31 (CH), 142.86 (C), 125.28 (C), 58.45 (2 x CH<sub>2</sub>), 25.70 (2 x CH<sub>2</sub>), 23.13 (CH<sub>2</sub>). **HRMS** (ES + ve), C<sub>9</sub>H<sub>15</sub>N<sub>5</sub>Cl (M + H)<sup>+</sup>: Calculated 228.1016. Obtained 228.1035.

• **General procedure D:**

A microwave vial was charged with a 0.2 M solution of the corresponding diaminopyrimidine (**33**, **34**) (1 equiv.) in acetic anhydride, the appropriate orthoester (1.5 equiv.) and methanesulfonic acid (0.2 equiv.). The mixture was heated at 120 °C for 15 min using microwave radiation. The reaction mixture was diluted with dichloromethane and the crude mixture was washed with saturated NaHCO<sub>3</sub> solution and saturated brine. The organic phase was dried over anhydrous Na<sub>2</sub>SO<sub>4</sub>, filtered and the solvent was removed under reduced pressure. The crude material was purified by silica gel column chromatography.

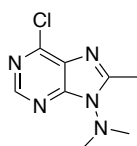


**(35) 6-chloro-9-(dimethylamino)-9H-purine.** The crude product was purified via silica gel column chromatography (Ethyl acetate/Hexane 20-25%) to provide the title compound as a white solid (30.2 mg, 0.152 mmol, 53% yield). **<sup>1</sup>H-NMR** (400 MHz, CDCl<sub>3</sub>):  $\delta$  8.72 (1H, s, CH), 8.18 (1H, s, CH), 3.17 (6H, s, 2 x CH<sub>3</sub>). **<sup>13</sup>C-NMR** (101 MHz, CDCl<sub>3</sub>):  $\delta$  151.79 (C), 151.49 (CH), 150.78 (C), 145.25 (CH), 130.71 (C), 46.95 (2 x CH<sub>3</sub>). **HRMS** (ES + ve), C<sub>7</sub>H<sub>9</sub>N<sub>5</sub>Cl (M + H)<sup>+</sup>: Calculated 198.0546. Obtained 198.0547.

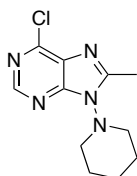


**(36) 6-chloro-9-(piperidin-1-yl)-9H-purine.** The crude product was purified via silica gel column chromatography (Ethyl acetate/Hexane 20-50%) to provide the title compound as an off-white solid (124.9 mg, 0.525 mmol, 59% yield). **<sup>1</sup>H-NMR** (400 MHz, CDCl<sub>3</sub>):  $\delta$  8.71 (1H, s, CH), 8.20

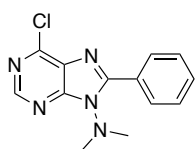
(1H, s, CH), 3.48 (4H, t,  $J = 5.2$  Hz, 2 x CH<sub>2</sub>), 1.87 – 1.77 (4H, m, 2 x CH<sub>2</sub>), 1.66 – 1.55 (2H, m, CH<sub>2</sub>). <sup>13</sup>C-NMR (101 MHz, CDCl<sub>3</sub>): δ 151.74 (C), 151.40 (CH), 150.96 (C), 145.46 (CH), 130.68 (C), 55.99 (2 x CH<sub>2</sub>), 26.17 (2 x CH<sub>2</sub>), 23.09 (CH<sub>2</sub>). **HRMS** (ES + ve), C<sub>10</sub>H<sub>13</sub>N<sub>5</sub>Cl (M + H)<sup>+</sup>: Calculated 238.0859. Obtained 238.0842.



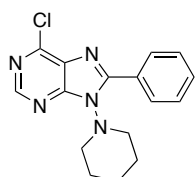
**(37) 6-chloro-8-methyl-9-(dimethylamino)-9H-purine.** The crude product was purified via silica gel column chromatography (Ethyl acetate/Hexane 20-33%) to provide the title compound as a white solid (80 mg, 0.377 mmol, 47% yield). <sup>1</sup>H-NMR (400 MHz, CDCl<sub>3</sub>): δ 8.62 (1H, s, CH), 3.15 (6H, s, 2 x CH<sub>3</sub>), 2.64 (3H, s, CH<sub>3</sub>). <sup>13</sup>C-NMR (101 MHz, CDCl<sub>3</sub>): δ 156.27 (C), 151.92 (C), 150.41 (CH), 149.60 (C), 129.47 (C), 45.76 (2 x CH<sub>3</sub>), 13.86 (CH<sub>3</sub>). **HRMS** (ES + ve), C<sub>8</sub>H<sub>11</sub>N<sub>5</sub>Cl (M + H)<sup>+</sup>: Calculated 212.0703. Obtained 212.0720.



**(38) 6-chloro-8-methyl-9-(piperidin-1-yl)-9H-purine.** The crude product was purified via silica gel column chromatography (Ethyl acetate/Hexane 20%) to provide the title compound as a white solid (65.9 mg, 0.261 mmol, 72% yield). <sup>1</sup>H-NMR (400 MHz, CDCl<sub>3</sub>): δ 8.60 (1H, s, CH), 3.89 (2H, t,  $J = 11.2$  Hz, CH<sub>2</sub>), 3.06 (2H, t,  $J = 11.2$  Hz, CH<sub>2</sub>), 2.62 (3H, s, CH<sub>3</sub>), 1.91 – 1.66 (6H, m, 3 x CH<sub>2</sub>). <sup>13</sup>C-NMR (126 MHz, CDCl<sub>3</sub>): δ 156.41 (C), 152.16 (C), 150.26 (CH), 149.53 (C), 129.34 (C), 54.51 (2 x CH<sub>2</sub>), 26.37 (2 x CH<sub>2</sub>), 23.10 (CH<sub>2</sub>), 13.85 (CH<sub>3</sub>). **HRMS** (ES + ve), C<sub>11</sub>H<sub>15</sub>N<sub>5</sub>Cl (M + H)<sup>+</sup>: Calculated 252.1016. Obtained 252.0995.



**(39) 6-chloro-9-(dimethylamino)-8-phenyl-9H-purine.** The crude product was purified via silica gel column chromatography (Ethyl acetate/Hexane 10%) to provide the title compound as a white solid (164.2 mg, 0.599 mmol, 54% yield). <sup>1</sup>H-NMR (400 MHz, CDCl<sub>3</sub>): δ 8.69 (1H, s, CH), 8.30 – 8.22 (2H, m, 2 x CH), 7.59 – 7.46 (3H, m, 3 x CH), 3.25 (6H, s, 2 x CH<sub>3</sub>). <sup>13</sup>C-NMR (101 MHz, CDCl<sub>3</sub>): δ 154.18 (C), 152.85 (C), 150.67 (CH), 150.59 (C), 131.34 (CH), 130.00 (C), 129.85 (2 x CH), 128.58 (2 x CH), 128.33 (C), 45.53 (2 x CH<sub>3</sub>). **HRMS** (ES + ve), C<sub>13</sub>H<sub>13</sub>N<sub>5</sub>Cl (M + H)<sup>+</sup>: Calculated 274.0859. Obtained 274.0841.

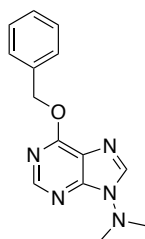


**(40) 6-chloro-8-phenyl-9-(piperidin-1-yl)-9H-purine.** The crude product was purified via silica gel column chromatography (Ethyl acetate/Hexane 15%) to provide the title compound as a white solid

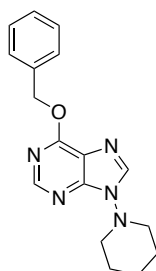
(201.5 mg, 0.641 mmol, 48% yield). **<sup>1</sup>H-NMR** (400 MHz, CDCl<sub>3</sub>): δ 8.68 (1H, s, CH), 8.33 – 8.26 (2H, m, 2 x CH), 7.59 – 7.47 (3H, m, 3 x CH), 4.07 (2H, t, *J* = 11.3 Hz, CH<sub>2</sub>), 3.21 (2H, t, *J* = 11.3 Hz, CH<sub>2</sub>), 1.97 – 1.62 (6H, m, 3 x CH<sub>2</sub>). **<sup>13</sup>C-NMR** (101 MHz, CDCl<sub>3</sub>): δ 154.21 (C), 153.15 (C), 150.58 (CH), 150.49 (C), 131.28 (CH), 129.97 (2 x CH), 129.93 (C), 128.49 (2 x CH), 128.43 (C), 54.28 (2 x CH<sub>2</sub>), 26.31 (2 x CH<sub>2</sub>), 23.14 (CH<sub>2</sub>). **HRMS** (ES + ve), C<sub>16</sub>H<sub>17</sub>N<sub>5</sub>Cl (M + H)<sup>+</sup>: Calculated 314.1172. Obtained 314.1158.

• **General procedure E:**

A microwave vial was charged with a suspension of NaH (60%) in mineral oil (5 equiv.), and a 1.4 M solution of the appropriate alcohol (5 equiv.) in DMF. The mixture was stirred for 30 min. Then a 0.28 M solution of the corresponding 6-chloropurine (**35** – **40**) (1 equiv.) in DMF was added dropwise and the mixture heated at 200 °C for 1 h using microwave radiation. The reaction mixture was diluted with dichloromethane, quenched to pH 7 with saturated aqueous NH<sub>4</sub>Cl, extracted with dichloromethane and washed with saturated brine. The combined organic extracts were dried over anhydrous Na<sub>2</sub>SO<sub>4</sub>, filtered and the solvent was evaporated. The residue was purified by silica gel column chromatography.

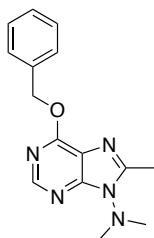


**(41) 6-(benzyloxy)-9-(dimethylamino)-9H-purine.** The crude product was purified via silica gel column chromatography (Ethyl acetate/Hexane 50%) to provide the title compound as an off-white oil (9.5 mg, 0.035 mmol, 26% yield). **<sup>1</sup>H-NMR** (400 MHz, CDCl<sub>3</sub>): δ 8.00 (1H, s, CH), 7.87 (1H, s, CH), 7.40 – 7.27 (5H, m, 5 x CH), 5.26 (2H, s, OCH<sub>2</sub>), 3.09 (6H, s, 2 x CH<sub>3</sub>). **<sup>13</sup>C-NMR** (101 MHz, CDCl<sub>3</sub>): δ 156.74 (C), 152.23 (C), 146.50 (CH), 139.13 (CH), 136.16 (C), 129.18 (2 x CH), 128.49 (CH), 128.37 (2 x CH), 123.55 (C), 49.27 (CH<sub>2</sub>), 47.43 (2 x CH<sub>3</sub>). **HRMS** (ES + ve), C<sub>14</sub>H<sub>16</sub>N<sub>5</sub>O (M + H)<sup>+</sup>: Calculated 270.1355. Obtained 270.1375.

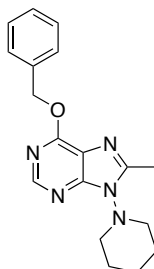


**(42) 6-(benzyloxy)-9-(piperidin-1-yl)-9H-purine.** The crude product was purified via silica gel column chromatography (Ethyl acetate/Hexane 33-90%) to provide the title compound as a white oil (17.9 mg, 0.058 mmol, 24% yield). **<sup>1</sup>H-NMR** (400 MHz, CDCl<sub>3</sub>): δ 7.98 (1H, s, CH), 7.87 (1H, s, CH), 7.39 – 7.24 (5H, m, 5 x CH), 5.24 (2H, s, OCH<sub>2</sub>),

3.36 (4H, t,  $J = 5.2$  Hz, 2 x CH<sub>2</sub>), 1.83 – 1.73 (4H, m, 2 x CH<sub>2</sub>), 1.60 – 1.50 (2H, m, CH<sub>2</sub>). <sup>13</sup>C-NMR (101 MHz, CDCl<sub>3</sub>): δ 156.75 (C), 146.81 (C), 146.31 (CH), 139.35 (CH), 136.15 (C), 129.12 (2 x CH), 128.42 (CH), 128.32 (2 x CH), 123.46 (C), 56.50 (2 x CH<sub>2</sub>), 49.22 (CH<sub>2</sub>), 26.16 (2 x CH<sub>2</sub>), 23.18 (CH<sub>2</sub>). HRMS (ES + ve), C<sub>17</sub>H<sub>20</sub>N<sub>5</sub>O (M + H)<sup>+</sup>: Calculated 310.1668. Obtained 310.1680.

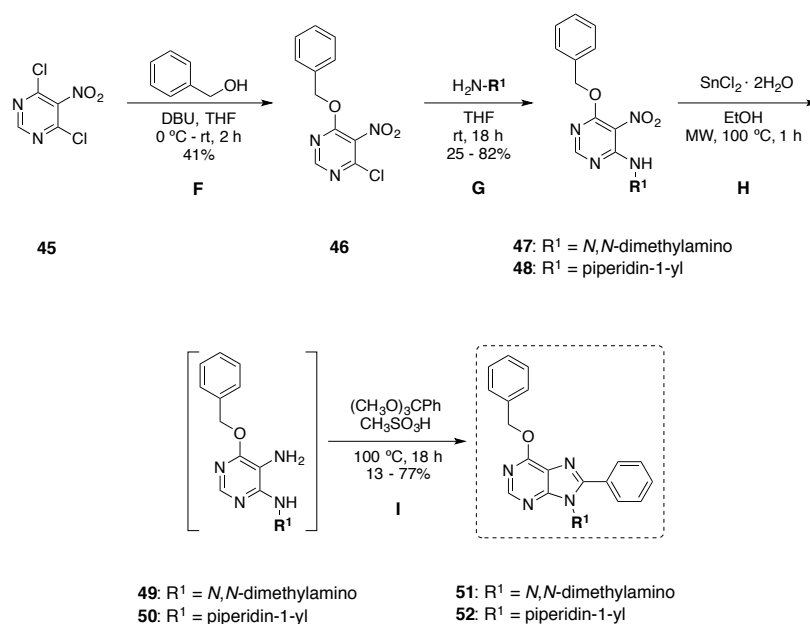


**(43) 6-(benzyloxy)-8-methyl-9-(dimethylamino)-9H-purine.** The crude product was purified via silica gel column chromatography (Ethyl acetate/Hexane 75-100%) to provide the title compound as a white solid (31.6 mg, 0.111 mmol, 41% yield). <sup>1</sup>H-NMR (400 MHz, CDCl<sub>3</sub>): δ 7.89 (1H, s, CH), 7.37 – 7.25 (5H, m, 5 x CH), 5.24 (2H, s, OCH<sub>2</sub>), 3.06 (6H, s, 2 x CH<sub>3</sub>), 2.48 (3H, s, CH<sub>3</sub>). <sup>13</sup>C-NMR (101 MHz, CDCl<sub>3</sub>): δ 156.42 (C), 149.69 (C), 147.64 (C), 145.13 (CH), 136.36 (C), 129.07 (2 x CH), 128.32 (CH), 128.30 (2 x CH), 122.10 (C), 49.00 (CH<sub>2</sub>), 46.05 (2 x CH<sub>3</sub>), 13.30 (CH<sub>3</sub>). HRMS (ES + ve), C<sub>15</sub>H<sub>18</sub>N<sub>5</sub>O (M + H)<sup>+</sup>: Calculated 284.1511. Obtained 284.1504.



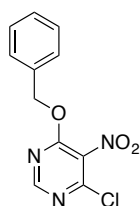
**(44) 6-(benzyloxy)-8-methyl-9-(piperidin-1-yl)-9H-purine.** The crude product was purified via silica gel column chromatography (Ethyl acetate/Hexane 33-100%) to provide the title compound as a white oil (21.6 mg, 0.067 mmol, 33% yield). <sup>1</sup>H-NMR (400 MHz, CDCl<sub>3</sub>): δ 7.88 (1H, s, CH), 7.37 – 7.24 (5H, m, 5 x CH), 5.23 (2H, s, OCH<sub>2</sub>), 3.72 (2H, t,  $J = 5.2$  Hz, CH<sub>2</sub>), 3.07 (2H, t,  $J = 5.2$  Hz, CH<sub>2</sub>), 2.48 (3H, s, CH<sub>3</sub>), 1.86 – 1.62 (6H, m, 3 x CH<sub>2</sub>). <sup>13</sup>C-NMR (101 MHz, CDCl<sub>3</sub>): δ 156.43 (C), 149.88 (C), 147.81 (C), 144.95 (CH), 136.36 (C), 129.07 (2 x CH), 128.33 (2 x CH), 128.31 (CH), 121.94 (C), 54.86 (2 x CH<sub>2</sub>), 48.99 (CH<sub>2</sub>), 26.44 (2 x CH<sub>2</sub>), 23.24 (CH<sub>2</sub>), 13.28 (CH<sub>3</sub>). HRMS (ES + ve), C<sub>18</sub>H<sub>22</sub>N<sub>5</sub>O (M + H)<sup>+</sup>: Calculated 324.1824. Obtained 324.1844.

## Chemical library 2b.



- **General procedure F:**

1,8-Diazabicyclo[5.4.0]undec-7-ene (2.06 mL, 13.65 mmol, 1.5 equiv.) was added to the solution of benzyl alcohol (9.1 mmol, 1 equiv.) in dry THF (10 mL) at 23 °C, and the mixture was stirred for 30 min. The solution was added, dropwise over 45 min, into a solution of 4,6-dichloronitropyrimidine (**45**) (1.76 g, 9.1 mmol, 1 equiv.) in dry THF (30 mL) at 0 °C via a dropping funnel maintaining the internal temperature at 0 °C. The mixture was allowed to warm to room temperature over 1 h. The solvent was removed under reduced pressure and the resulting residue was partitioned between dichloromethane (150 mL) and water (150 mL). The layers were separated and the organic phase was washed with saturated brine (2 x 50 mL), dried over anhydrous Na<sub>2</sub>SO<sub>4</sub> and filtered. The solvent was removed under reduced pressure and the crude material was purified by silica gel column chromatography.

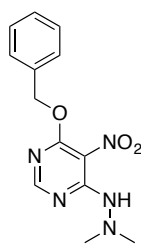


**(46) 4-(benzyloxy)-6-chloro-5-nitropyrimidine.** The crude product was purified via silica gel column chromatography (Ethyl acetate/Hexane 15-25%) to provide the title compound as a white solid (784.6 mg, 2.953 mmol, 41% yield). <sup>1</sup>H-NMR (500 MHz, CDCl<sub>3</sub>): δ 8.64 (1H, s, CH), 7.44 – 7.32 (5H, m, 5 x CH), 5.59 (2H, s, OCH<sub>2</sub>). <sup>13</sup>C-NMR (126 MHz, CDCl<sub>3</sub>): δ 161.26 (C),

157.55 (CH), 151.84 (C), 134.17 (C), 132.90 (C), 129.08 (CH), 128.92 (2 x CH), 128.37 (2 x CH), 71.00 (CH<sub>2</sub>).

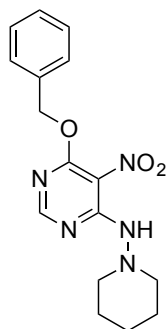
• **General procedure G:**

To a 0.2 M solution of **46** (1 equiv.) in dry THF was added dropwise *N,N*-dimethylhydrazine or 1-aminopiperidine (2 equiv.) with the temperature being maintained at 23 °C and the mixture was allowed to stir for 18 h at room temperature. The solvent from the crude was evaporated under reduced pressure and the residue was partitioned between dichloromethane and water. The layers were separated and the organic phase was washed with saturated brine, dried over anhydrous Na<sub>2</sub>SO<sub>4</sub> and filtered. The solvent was removed under reduced pressure and the crude material was purified by silica gel column chromatography.



**(47) 6-(benzyloxy)-5-nitro-4-(2,2-dimethylhydrazinyl)pyrimidine.**

The crude product was purified via silica gel column chromatography (Ethyl acetate/Hexane 30-50%) to provide the title compound as a yellow solid (58.1 mg, 0.2 mmol, 53% yield). **<sup>1</sup>H-NMR** (500 MHz, CDCl<sub>3</sub>): δ 8.65 (1H, s, NH), 8.36 (1H, s, CH), 7.50 – 7.45 (2H, m, 2 x CH), 7.41 – 7.34 (2H, m, 2 x CH), 7.36 – 7.29 (1H, m, CH), 5.57 (2H, s, OCH<sub>2</sub>), 2.69 (6H, s, 2 x CH<sub>3</sub>). **<sup>13</sup>C-NMR** (126 MHz, CDCl<sub>3</sub>): δ 162.20 (C), 159.46 (CH), 143.67 (C), 135.60 (C), 128.71 (2 x CH), 128.40 (CH), 127.89 (2 x CH), 103.19 (C), 69.66 (CH<sub>2</sub>), 48.03 (2 x CH<sub>3</sub>). **HRMS** (ES + ve), C<sub>13</sub>H<sub>16</sub>N<sub>5</sub>O<sub>3</sub> (M + H)<sup>+</sup>: Calculated 290.1253. Obtained 290.1249.



**(48) 6-(benzyloxy)-5-nitro-4-[(piperidin-1-yl)amino]-pyrimidine.**

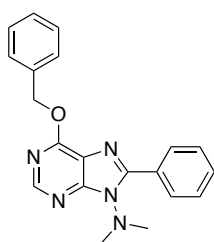
The crude product was purified via silica gel column chromatography (Ethyl acetate/Hexane 25-50%) to provide the title compound as a yellow solid (48 mg, 0.145 mmol, 25% yield). **<sup>1</sup>H-NMR** (500 MHz, CDCl<sub>3</sub>): δ 8.31 (1H, s, CH), 7.45 – 7.43 (2H, m, 2 x CH), 7.41 – 7.35 (2H, m, 2 x CH), 7.35 – 7.29 (1H, m, CH), 5.54 (2H, s, OCH<sub>2</sub>), 2.96 – 2.70 (4H, m, 2 x CH<sub>2</sub>), 1.87 – 1.60 (6H, m, 3 x CH<sub>2</sub>). **<sup>13</sup>C-NMR** (126 MHz, CDCl<sub>3</sub>): δ 163.63 (C), 158.99 (CH), 151.08 (C), 135.68 (C), 128.70 (2 x CH), 128.36 (CH), 127.81 (2 x CH), 103.91 (C), 69.44 (CH<sub>2</sub>), 57.43 (2 x CH<sub>2</sub>), 25.16 (2 x CH<sub>2</sub>), 23.23 (CH<sub>2</sub>). **HRMS** (ES + ve), C<sub>16</sub>H<sub>20</sub>N<sub>5</sub>O<sub>3</sub> (M + H)<sup>+</sup>: Calculated 330.1566. Obtained 330.1541.

- **General procedure H:**

A microwave vial was charged with a 0.32 M solution of the corresponding nitropyrimidine (**47**, **48**) (1 equiv.) in ethanol and tin (II) chloride dihydrate (5 equiv.). The reaction was heated at 100 °C for 1 h using microwave radiation. The mixture was then quenched to pH 7 with saturated aqueous NaHCO<sub>3</sub>, extracted with ethyl acetate and washed with saturated brine. The combined organic extracts were dried over anhydrous Na<sub>2</sub>SO<sub>4</sub>, filtered and the solvent was removed under reduced pressure. The crude material was directly used for the next step without further purification.

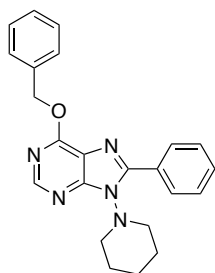
- **General procedure I:**

A microwave vial was charged with the corresponding diaminopyrimidine (**49**, **50**) (1 equiv.) the orthoester (3 equiv.) and methanesulfonic acid (0.2 equiv.). The reaction vial was sealed and placed in a pre-heated oil bath at 100 °C. The reaction was allowed to stir for 18 h and then cooled to room temperature. The reaction mixture was diluted with dichloromethane and the crude mixture was washed with saturated aqueous NaHCO<sub>3</sub> and saturated brine. The organic phase was dried over anhydrous Na<sub>2</sub>SO<sub>4</sub>, filtered and the solvent was removed under reduced pressure. The crude material was purified by silica gel column chromatography.



**(51) 6-(benzyloxy)-9-(dimethylamino)-8-phenyl-9H-purine.**

The crude product was purified via silica gel column chromatography (Ethyl acetate/Hexane 20%) to provide the title compound as a white solid (16.2 mg, 0.047 mmol, 28% yield). **<sup>1</sup>H-NMR** (500 MHz, CDCl<sub>3</sub>): δ 8.50 (1H, s, CH), 8.25 – 8.18 (2H, m, 2 x CH), 7.59 – 7.53 (2H, m, 2 x CH), 7.52 – 7.43 (3H, m, 3 x CH), 7.39 – 7.34 (2H, m, 2 x CH), 7.34 – 7.28 (1H, m, CH), 5.71 (2H, s, OCH<sub>2</sub>), 3.23 (6H, s, 2 x CH<sub>3</sub>). **<sup>13</sup>C-NMR** (126 MHz, CDCl<sub>3</sub>): δ 160.45 (C), 153.26 (C), 151.06 (C), 150.77 (CH), 136.51 (C), 130.44 (CH), 129.56 (2 x CH), 129.19 (C), 128.68 (2 x CH), 128.55 (2 x CH), 128.37 (2 x CH), 128.25 (CH), 120.10 (C), 68.41 (CH<sub>2</sub>), 45.56 (2 x CH<sub>3</sub>). **HRMS** (ES + ve), C<sub>20</sub>H<sub>20</sub>N<sub>5</sub>O (M + H)<sup>+</sup>: Calculated 346.1668. Obtained 346.1636.

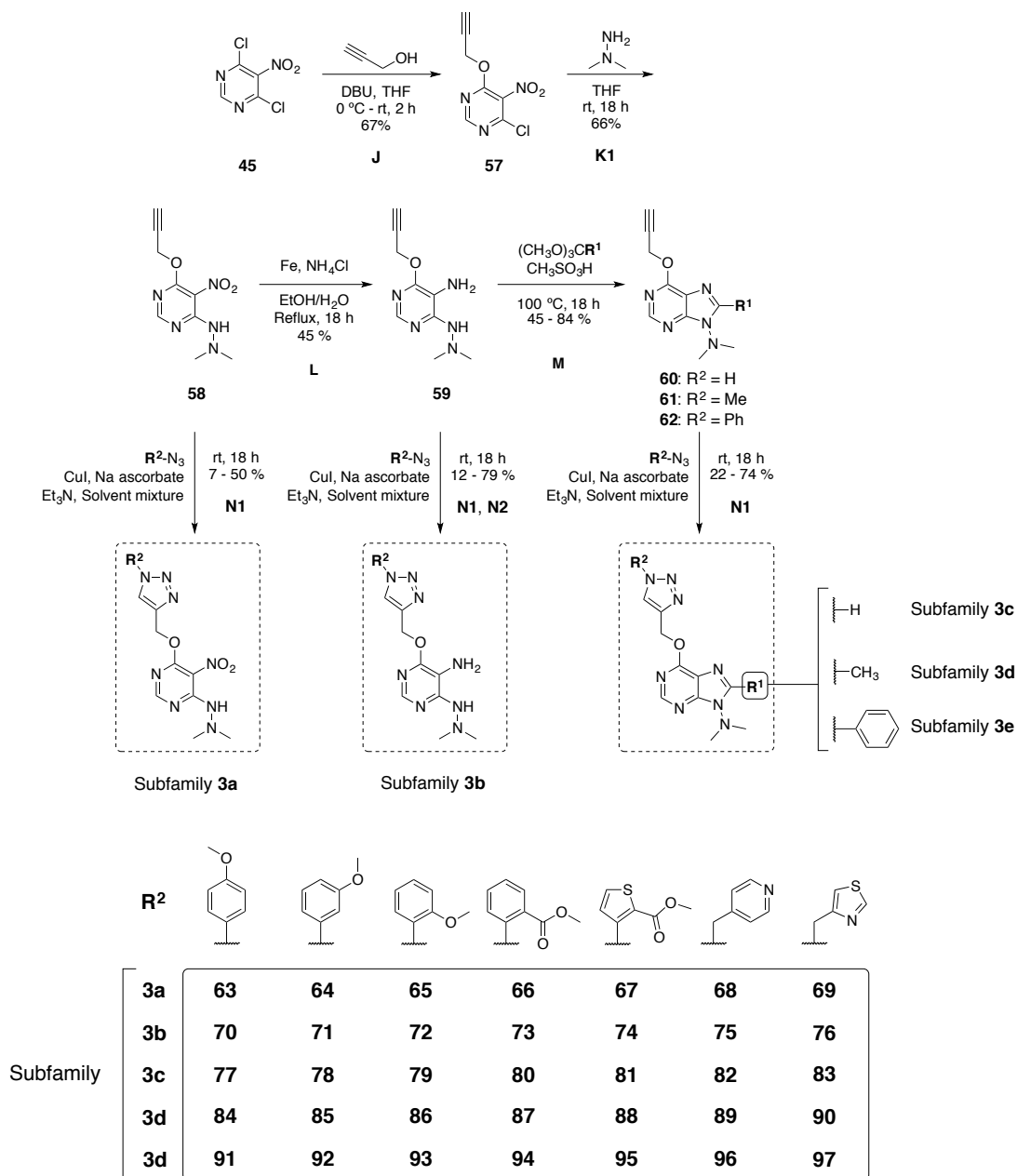


**(52) 6-(benzyloxy)-8-phenyl-9-(piperidin-1-yl)-9H-purine.**

The crude product was purified via silica gel column chromatography (Ethyl acetate/Hexane 25%) to provide the title compound as a white solid (6.4 mg, 0.016 mmol, 17% yield). **<sup>1</sup>H-NMR** (500 MHz, CDCl<sub>3</sub>): δ 8.49 (1H, s, CH), 8.29 – 8.22 (2H, m, 2 x CH), 7.59 – 7.53 (2H, m, 2 x CH), 7.50 – 7.43 (3H, m, 3 x CH), 7.39 – 7.33 (2H, m, 2 x CH), 7.33 – 7.28 (1H, m, CH), 5.71 (2H, s, OCH<sub>2</sub>), 4.06 (2H, t, *J* = 11.2 Hz, CH<sub>2</sub>), 3.19 (2H, t, *J* = 11.2 Hz, CH<sub>2</sub>), 1.86 – 1.68 (6H, m, 3 x CH<sub>2</sub>). **<sup>13</sup>C-NMR** (126 MHz, CDCl<sub>3</sub>): δ 160.46 (C), 153.58 (C), 151.05 (C), 150.66 (CH), 136.55 (C), 130.35 (CH), 129.66 (2 x CH), 129.26 (C), 128.69 (2 x CH), 128.55 (2 x CH), 128.25 (2 x CH), 128.23 (CH), 120.02 (C), 68.38 (CH<sub>2</sub>), 54.27 (2 x CH<sub>2</sub>), 26.36 (2 x CH<sub>2</sub>), 23.20 (CH<sub>2</sub>). **HRMS** (ES + ve), C<sub>23</sub>H<sub>24</sub>N<sub>5</sub>O (M + H)<sup>+</sup>: Calculated 386.1981. Obtained 386.1960.



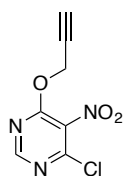
### C. General synthesis for the compounds from chemical library 3:



#### • General procedure J:

1,8-Diazabicyclo[5.4.0]undec-7-ene (1.5 equiv.) was added to a 0.9 M solution of propargyl alcohol (1 equiv.) in dry THF and the mixture was stirred at 23 °C for 30 min. The prepared solution was added, dropwise over 45 min, into a 0.3 M solution of 4,6-dichloronitropyrimidine (**45**) (1 equiv.) in dry THF at 0 °C via a dropping funnel maintaining the internal temperature at 0 °C. The mixture was allowed to warm to room temperature over 1 h. The solvent was removed under reduced pressure and the resulting

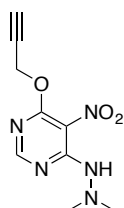
residue was partitioned between dichloromethane and water. The layers were separated and the organic phase was washed with saturated brine, dried over anhydrous Na<sub>2</sub>SO<sub>4</sub> and filtered. The solvent was removed under reduced pressure and the crude material was purified by silica gel column chromatography.



**(57) 4-chloro-5-nitro-6-(prop-2-yn-1-yloxy)pyrimidine.** The crude product was purified via silica gel column chromatography (Ethyl acetate/Hexane 20%) to provide the title compound as a white solid (1.30 g, 6.087 mmol, 67% yield). **<sup>1</sup>H-NMR** (500 MHz, CDCl<sub>3</sub>): δ 8.68 (1H, s, CH), 5.15 (2H, d, *J* = 2.4 Hz, OCH<sub>2</sub>), 2.58 (1H, t, *J* = 2.4 Hz, CH). **<sup>13</sup>C-NMR** (126 MHz, CDCl<sub>3</sub>): δ 160.39 (C), 157.48 (CH), 152.21 (C), 132.70 (C), 77.11 (C), 76.06 (CH), 56.72 (CH<sub>2</sub>).

- **General procedure K1:**

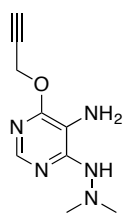
To a 0.2 M solution of **57** (1 equiv.) in dry THF was added dropwise *N,N*-dimethylhydrazine (2 equiv.) with the temperature being maintained at 23 °C and the mixture was allowed to stir for 18 h at room temperature. The solvent from the crude was evaporated under reduced pressure and the residue was partitioned between dichloromethane and water. The layers were separated and the organic phase was washed with saturated brine, dried over anhydrous Na<sub>2</sub>SO<sub>4</sub> and filtered. The solvent was removed under reduced pressure and the crude material was purified by silica gel column chromatography.



**(58) 4-(2,2-dimethylhydrazinyl)-5-nitro-6-(prop-2-yn-1-yloxy)pyrimidine.** The crude product was purified via silica gel column chromatography (Ethyl acetate/Hexane 18-66%) to provide the title compound as a yellow solid (1.04 g, 4.368 mmol, 66% yield). **<sup>1</sup>H-NMR** (500 MHz, CDCl<sub>3</sub>): δ 8.72 (1H, bs, NH), 8.38 (1H, s, CH), 5.12 (2H, d, *J* = 2.4 Hz, OCH<sub>2</sub>), 2.70 (6H, s, 2 x CH<sub>3</sub>), 2.53 (1H, t, *J* = 2.4 Hz, CH). **<sup>13</sup>C-NMR** (126 MHz, CDCl<sub>3</sub>): δ 162.85 (C), 159.36 (CH), 156.10 (C), 129.89 (C), 77.49 (C), 75.86 (CH), 55.53 (CH<sub>2</sub>), 48.00 (2 x CH<sub>3</sub>). **HRMS** (ES + ve), C<sub>9</sub>H<sub>12</sub>N<sub>5</sub>O<sub>3</sub> (M + H)<sup>+</sup>: Calculated 238.0940. Obtained 238.0953.

- **General procedure L:**

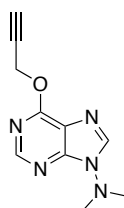
To a 0.19 M solution of **58** (1 equiv.) in a mixture of ethanol and water (4:1 v/v) was added iron powder (5 equiv.) and NH<sub>4</sub>Cl (5 equiv.). The mixture was refluxed for 18 h, cooled to room temperature and filtered through a pad of Celite. The filtrate was diluted with water and extracted with dichloromethane. The combined organic layers were washed with water and saturated brine, dried over anhydrous Na<sub>2</sub>SO<sub>4</sub> and concentrated under reduced pressure. The crude residue was purified by silica gel column chromatography.



**(59) 5-amino-4-(2,2-dimethylhydrazinyl)-6-(prop-2-yn-1-yloxy)pyrimidine.** The crude product was purified via silica gel column chromatography (Ethyl acetate/Hexane 50-66%) to provide the title compound as a light yellow solid (357.9 mg, 1.72 mmol, 45% yield). **<sup>1</sup>H-NMR** (500 MHz, DMSO-*d*<sub>6</sub>): δ 7.69 (1H, s, CH), 7.09 (1H, bs, NH), 4.96 (2H, d, *J* = 2.4 Hz, OCH<sub>2</sub>), 4.70 (2H, bs, NH<sub>2</sub>), 3.47 (1H, t, *J* = 2.4 Hz, CH), 2.51 (6H, s, 2 x CH<sub>3</sub>). **<sup>13</sup>C-NMR** (126 MHz, DMSO-*d*<sub>6</sub>): δ 154.25 (C), 150.07 (C), 144.18 (CH), 112.93 (C), 79.81 (C), 77.15 (CH), 52.97 (CH<sub>2</sub>), 47.18 (2 x CH<sub>3</sub>). **HRMS** (ES + ve), C<sub>9</sub>H<sub>14</sub>N<sub>5</sub>O (M + H)<sup>+</sup>: Calculated 208.1198. Obtained 208.1187.

- **General procedure M:**

A microwave vial was charged with **59** (1 equiv.), the **orthoester** (3 equiv.) and methanesulfonic acid (0.2 equiv.). The reaction vial was sealed and placed in a pre-heated oil bath at 100 °C. The reaction was allowed to stir for 18 h and then cooled to room temperature. The reaction mixture was diluted with dichloromethane and the crude mixture was washed with saturated NaHCO<sub>3</sub> solution and saturated brine. The organic phase was dried over anhydrous Na<sub>2</sub>SO<sub>4</sub>, filtered and the solvent was removed under reduced pressure. The crude material was purified by silica gel column chromatography.

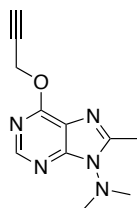


**(60) 9-(dimethylamino)-6-(prop-2-yn-1-yloxy)-9H-purine.** The crude product was purified via silica gel column chromatography (Ethyl acetate/Hexane 30-60%) to provide the title compound as a white solid (98.3 mg, 0.451 mmol, 84% yield). **<sup>1</sup>H-NMR** (500 MHz, CDCl<sub>3</sub>): δ 8.55 (1H, s, CH), 8.01 (1H, s, CH), 5.23 (2H, d, *J* = 2.4 Hz, OCH<sub>2</sub>), 3.16 (6H, s, 2 x CH<sub>3</sub>), 2.49 (1H, t, *J* = 2.4 Hz, CH). **<sup>13</sup>C-NMR** (126 MHz, CDCl<sub>3</sub>): δ 159.78 (C), 151.44 (CH), 151.37 (C),

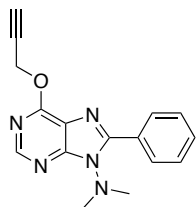
### C. General synthesis for the compounds from chemical library 3:

---

142.31 (CH), 120.70 (C), 78.23 (C), 75.25 (CH), 54.25 (CH<sub>2</sub>), 47.02 (2 x CH<sub>3</sub>). **HRMS** (ES + ve), C<sub>10</sub>H<sub>12</sub>N<sub>5</sub>O (M + H)<sup>+</sup>: Calculated 218.1042. Obtained 218.1048.



**(61) 8-methyl-9-(dimethylamino)-6-(prop-2-yn-1-yloxy)-9H-purine.** The crude product was purified via silica gel column chromatography (Ethyl acetate/Hexane 25:30%) to provide the title compound as a white solid (78.2 mg, 0.337 mmol, 51% yield). **<sup>1</sup>H-NMR** (500 MHz, CDCl<sub>3</sub>): δ 8.47 (1H, s, CH), 5.19 (2H, d, *J* = 2.4 Hz, OCH<sub>2</sub>), 3.14 (6H, s, 2 x CH<sub>3</sub>), 2.57 (3H, s, CH<sub>3</sub>), 2.47 (1H, t, *J* = 2.4 Hz, CH). **<sup>13</sup>C-NMR** (126 MHz, CDCl<sub>3</sub>): δ 158.59 (C), 152.86 (C), 152.50 (C), 150.20 (CH), 119.25 (C), 78.39 (C), 75.08 (CH), 54.00 (CH<sub>2</sub>), 45.78 (2 x CH<sub>3</sub>), 13.62 (CH<sub>3</sub>). **HRMS** (ES + ve), C<sub>11</sub>H<sub>14</sub>N<sub>5</sub>O (M + H)<sup>+</sup>: Calculated 232.1198. Obtained 232.1204.

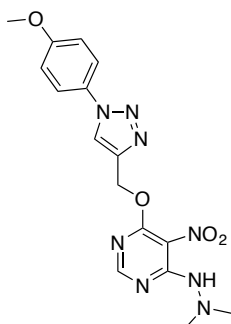


**(62) 9-(dimethylamino)-8-phenyl-6-(prop-2-yn-1-yloxy)-9H-purine.** The crude product was purified via silica gel column chromatography (Ethyl acetate/Hexane 15-18%) to provide the title compound as a white solid (141 mg, 0.479 mmol, 45% yield). **<sup>1</sup>H-NMR** (500 MHz, CDCl<sub>3</sub>): δ 8.54 (1H, s, CH), 8.28 – 8.19 (2H, m, 2 x CH), 7.52 – 7.44 (3H, m, 3 x CH), 5.25 (2H, d, *J* = 2.5 Hz, OCH<sub>2</sub>), 3.23 (6H, s, 2 x CH<sub>3</sub>), 2.49 (1H, t, *J* = 2.4 Hz, CH). **<sup>13</sup>C-NMR** (126 MHz, CDCl<sub>3</sub>): δ 159.28 (C), 153.42 (C), 151.32 (C), 150.60 (CH), 130.56 (CH), 129.52 (2 x CH), 129.05 (C), 128.38 (2 x CH), 119.99 (C), 78.39 (C), 75.15 (CH), 54.11 (CH<sub>2</sub>), 45.53 (2 x CH<sub>3</sub>). **HRMS** (ES + ve), C<sub>16</sub>H<sub>16</sub>N<sub>5</sub>O (M + H)<sup>+</sup>: Calculated 294.1355. Obtained 294.1338.

#### • General procedure N1:

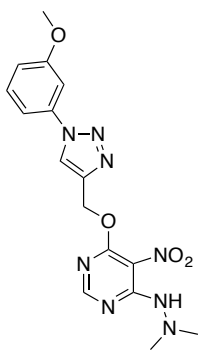
A 0.045 M solution of the corresponding alkyne (**58** – **62**) (1 equiv.) in a mixture of dioxane and water (9:1 v/v) was placed on an oven-dried microwave vial and the mixture was stirred until complete solubilization. Then the corresponding azide (0.5 M in methyl *tert*-butyl ether, MTBE, 1 equiv.), sodium ascorbate (0.1 equiv.), copper (I) iodide (0.25 equiv.) and triethylamine (0.4 equiv.) were added. The reaction vial was sealed, evacuated, backfilled with argon and the mixture allowed to stir at room temperature for 18 h. The mixture was partitioned between dichloromethane and water. The layers were separated and the organic phase was washed with saturated brine, dried over anhydrous

Na<sub>2</sub>SO<sub>4</sub> and filtered. The solvent was removed under reduced pressure and the crude material was purified by silica gel column chromatography.



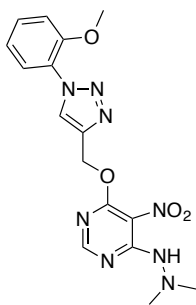
**(63) 6-([1-(4-methoxyphenyl)-1H-1,2,3-triazol-4-yl]methoxy}-4-(2,2-dimethylhydrazinyl)-5-nitropyrimidine.**

The crude product was purified via silica gel column chromatography (Ethyl acetate/Hexane 25-100%) to provide the title compound as a white solid (23.4 mg, 0.06 mmol, 29% yield). **<sup>1</sup>H-NMR** (400 MHz, CDCl<sub>3</sub>): δ 8.40 (1H, s, CH), 8.04 (1H, s, CH), 7.62 (2H, d, *J* = 9.0 Hz, 2 x CH), 7.01 (2H, d, *J* = 9.0 Hz, 2 x CH), 5.74 (2H, s, OCH<sub>2</sub>), 5.29 (1H, s, NH), 3.86 (3H, s, CH<sub>3</sub>), 2.69 (6H, s, 2 x CH<sub>3</sub>). **<sup>13</sup>C-NMR** (101 MHz, CDCl<sub>3</sub>): δ 165.26 (C), 160.10 (C), 159.47 (CH), 156.09 (C), 143.42 (C), 130.48 (C), 122.47 (2 x CH), 122.05 (CH), 119.26 (C), 114.93 (2 x CH), 61.80 (CH<sub>2</sub>), 55.78 (CH<sub>3</sub>), 47.99 (2 x CH<sub>3</sub>). **HRMS** (ES + ve), C<sub>16</sub>H<sub>19</sub>N<sub>8</sub>O<sub>4</sub> (M + H)<sup>+</sup>: Calculated 387.1529. Obtained 387.1518.



**(64) 6-([1-(3-methoxyphenyl)-1H-1,2,3-triazol-4-yl]methoxy}-4-(2,2-dimethylhydrazinyl)-5-nitropyrimidine.**

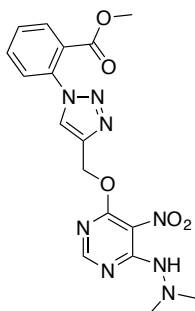
The crude product was purified via silica gel column chromatography (Ethyl acetate/Hexane 25-100%) to provide the title compound as a yellow solid (13.9 mg, 0.036 mmol, 42% yield). **<sup>1</sup>H-NMR** (400 MHz, CDCl<sub>3</sub>): δ 8.40 (1H, s, CH), 8.11 (1H, s, CH), 7.45 – 7.21 (3H, m, 3 x CH), 7.01 – 6.93 (1H, m, 1 x CH), 5.74 (2H, s, OCH<sub>2</sub>), 3.87 (3H, s, CH<sub>3</sub>), 2.69 (6H, s, 2 x CH<sub>3</sub>). **<sup>13</sup>C-NMR** (126 MHz, CDCl<sub>3</sub>): δ 171.26 (C), 163.34 (C), 160.74 (C), 159.45 (CH), 156.09 (C), 143.58 (C), 138.02 (C), 130.66 (CH), 121.98 (CH), 114.94 (CH), 112.66 (CH), 106.64 (CH), 61.70 (CH<sub>2</sub>), 55.78 (CH<sub>3</sub>), 47.98 (2 x CH<sub>3</sub>). **HRMS** (ES + ve), C<sub>16</sub>H<sub>19</sub>N<sub>8</sub>O<sub>4</sub> (M + H)<sup>+</sup>: Calculated 387.1529. Obtained 387.1491.



**(65) 6-([1-(2-methoxyphenyl)-1H-1,2,3-triazol-4-yl]methoxy}-4-(2,2-dimethylhydrazinyl)-5-nitropyrimidine.**

The crude product was purified via silica gel column chromatography (Ethyl acetate/Hexane 25-75%) to provide the title compound as a light brown oil (5.5 mg, 0.014 mmol, 7% yield). **<sup>1</sup>H-NMR** (400 MHz, CDCl<sub>3</sub>): δ 8.41 (1H, s, CH), 8.27 (1H, s, CH), 7.82 – 7.75 (1H, m, CH), 7.47 – 7.38 (1H, m, CH), 7.15 – 7.05 (2H, m, 2 x CH), 5.77 (2H, s, OCH<sub>2</sub>), 4.67 (1H, bs, NH), 3.90 (3H, s, CH<sub>3</sub>), 2.69 (6H, s, 2 x CH<sub>3</sub>). **<sup>13</sup>C-NMR** (126 MHz, CDCl<sub>3</sub>): δ 165.57 (C),

159.47 (CH), 157.42 (C), 156.14 (C), 151.27 (C), 142.22 (C), 130.38 (CH), 126.31 (C), 126.09 (CH), 125.65 (CH), 121.39 (CH), 112.41 (CH), 61.89 (CH<sub>2</sub>), 56.15 (CH<sub>3</sub>), 48.03 (2 x CH<sub>3</sub>). **HRMS** (ES + ve), C<sub>16</sub>H<sub>19</sub>N<sub>8</sub>O<sub>4</sub> (M + H)<sup>+</sup>: Calculated 387.1529. Obtained 387.1522.



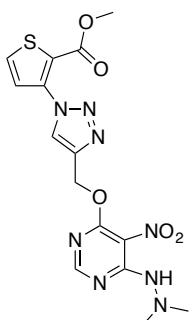
**(66) 6-({1-[2-(methoxycarbonyl)phenyl]-1H-1,2,3-triazol-4-yl}methoxy)-4-(2,2-dimethylhydrazinyl)-5-nitropyrimidine.** The

crude product was purified via silica gel column chromatography (Ethyl acetate/Hexane 25-85%) to provide the title compound as an orange oil (13.9 mg, 0.033 mmol, 15% yield). **<sup>1</sup>H-NMR** (400 MHz, CDCl<sub>3</sub>): δ

8.40 (1H, s, CH), 8.02 (1H, dd, *J* = 7.7, 1.7 Hz, CH), 7.99 (1H, s, CH),

7.68 (1H, td, *J* = 7.7, 1.7 Hz, CH), 7.61 (1H, td, *J* = 7.6, 1.4 Hz, CH), 7.51 (1H, dd, *J* = 7.8, 1.4 Hz, CH), 5.76 (2H, s, OCH<sub>2</sub>), 3.70 (3H, s, CH<sub>3</sub>), 3.14 (1H, s, NH), 2.69 (6H, s, 2 x CH<sub>3</sub>). **<sup>13</sup>C-NMR** (126 MHz, CDCl<sub>3</sub>): δ 171.27 (C), 165.60 (C), 163.43 (C), 159.39 (CH), 156.09 (C), 142.64 (C), 136.17 (C), 132.91 (CH), 131.48 (CH), 130.20 (CH), 127.63 (C), 127.05 (CH), 125.76 (CH), 61.76 (CH<sub>2</sub>), 52.77 (CH<sub>3</sub>), 47.99 (2 x CH<sub>3</sub>).

**HRMS** (ES + ve), C<sub>17</sub>H<sub>19</sub>N<sub>8</sub>O<sub>5</sub> (M + H)<sup>+</sup>: Calculated 415.1478. Obtained 415.1463.



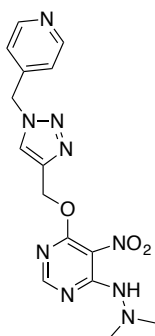
**(67) 6-({1-[2-(methoxycarbonyl)thiophen-3-yl]-1H-1,2,3-triazol-4-yl}methoxy)-4-(2,2-dimethylhydrazinyl)-5-nitropyrimidine.** The crude product was purified via silica gel column

chromatography (Ethyl acetate/Hexane 25-85%) to provide the title compound as a light yellow solid (13.4 mg, 0.032 mmol, 15% yield).

**<sup>1</sup>H-NMR** (500 MHz, CDCl<sub>3</sub>): δ 8.53 (1H, s, CH), 8.41 (1H, s, CH), 7.62

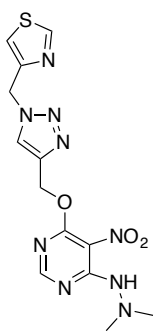
(1H, d, *J* = 5.4 Hz, CH), 7.51 (1H, d, *J* = 5.4 Hz, CH), 5.76 (2H, s, OCH<sub>2</sub>), 5.29 (1H, s, NH), 3.85 (3H, s, CH<sub>3</sub>), 2.69 (6H, s, 2 x CH<sub>3</sub>). **<sup>13</sup>C-NMR** (126 MHz, CDCl<sub>3</sub>): δ 163.30 (C), 160.73 (C), 159.40 (CH), 156.12 (C), 141.99 (C), 138.26 (C), 131.22 (CH), 126.94 (CH), 126.76 (CH), 122.43 (C), 110.12 (C), 61.57 (CH<sub>2</sub>), 52.77 (CH<sub>3</sub>), 48.00 (2 x CH<sub>3</sub>).

**HRMS** (ES + ve), C<sub>15</sub>H<sub>17</sub>N<sub>8</sub>O<sub>5</sub>S (M + H)<sup>+</sup>: Calculated 421.1043. Obtained 421.1025.



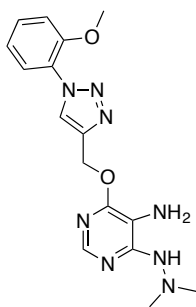
**(68) 4-(2,2-dimethylhydrazinyl)-5-nitro-6-([1-(pyridin-4-ylmethyl)-1H-1,2,3-triazol-4-yl]methoxy)pyrimidine.**

The crude product was purified via silica gel column chromatography (Methanol/Ethyl acetate 0-20%) to provide the title compound as a yellow oil (47 mg, 0.126 mmol, 50% yield). **<sup>1</sup>H-NMR** (500 MHz, CDCl<sub>3</sub>): δ 8.59 (2H, d, *J* = 6.0 Hz, 2 x CH), 8.34 (1H, s, CH), 7.71 (1H, s, CH), 7.10 (2H, d, *J* = 6.0 Hz, 2 x CH), 5.65 (2H, s, OCH<sub>2</sub>), 5.55 (2H, s, CH<sub>2</sub>), 2.66 (6H, s, 2 x CH<sub>3</sub>). **<sup>13</sup>C-NMR** (126 MHz, CDCl<sub>3</sub>): δ 163.20 (C), 159.26 (CH), 155.99 (C), 150.59 (2 x CH), 149.45 (C), 143.76 (C), 143.53 (C), 123.92 (CH), 122.20 (2 x CH), 61.65 (CH<sub>2</sub>), 52.85 (CH<sub>2</sub>), 47.90 (2 x CH<sub>3</sub>). **HRMS** (ES + ve), C<sub>15</sub>H<sub>18</sub>N<sub>9</sub>O<sub>3</sub> (M + H)<sup>+</sup>: Calculated 372.1533. Obtained 372.1513.



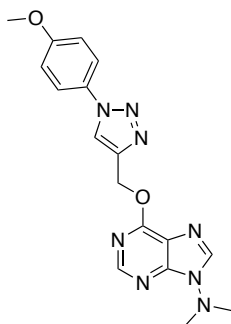
**(69) 4-(2,2-dimethylhydrazinyl)-5-nitro-6-([1-(thiazol-4-ylmethyl)-1H-1,2,3-triazol-4-yl]methoxy)pyrimidine.**

The crude product was purified via silica gel column chromatography (Methanol/Ethyl acetate 0-10%) to provide the title compound as a yellow oil (45.8 mg, 0.121 mmol, 48% yield). **<sup>1</sup>H-NMR** (500 MHz, CDCl<sub>3</sub>): δ 8.80 (1H, d, *J* = 2.0 Hz, CH), 8.35 (1H, s, CH), 7.87 (1H, s, CH), 7.31 (1H, d, *J* = 1.9 Hz, CH), 5.70 (2H, d, *J* = 0.7 Hz, CH<sub>2</sub>), 5.64 (2H, s, OCH<sub>2</sub>), 2.67 (6H, s, 2 x CH<sub>3</sub>). **<sup>13</sup>C-NMR** (126 MHz, CDCl<sub>3</sub>): δ 163.30 (C), 159.31 (CH), 156.08 (C), 154.20 (CH), 150.44 (C), 143.10 (C), 134.03 (C), 124.20 (CH), 118.04 (CH), 61.66 (CH<sub>2</sub>), 49.75 (CH<sub>2</sub>), 47.94 (2 x CH<sub>3</sub>). **HRMS** (ES + ve), C<sub>13</sub>H<sub>16</sub>N<sub>9</sub>O<sub>3</sub>S (M + H)<sup>+</sup>: Calculated 378.1097. Obtained 378.1075.

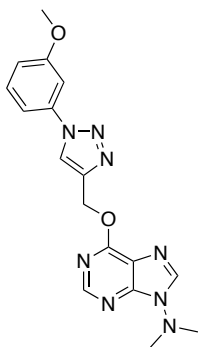


**(72) 5-amino-4-(2,2-dimethylhydrazinyl)-6-([1-(2-methoxyphenyl)-1H-1,2,3-triazol-4-yl]methoxy)pyrimidine.**

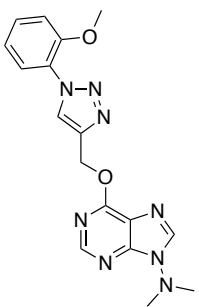
The crude product was purified via silica gel column chromatography (Methanol/Ethyl acetate 2%) to provide the title compound as a yellow oil (12.44 mg, 0.038 mmol, 15% yield). **<sup>1</sup>H-NMR** (400 MHz, CDCl<sub>3</sub>): δ 8.23 (1H, s, CH), 7.90 (1H, s, CH), 7.81 – 7.74 (1H, m, CH), 7.47 – 7.38 (1H, m, CH), 7.14 – 7.05 (2H, m, 2 x CH), 5.64 (2H, s, OCH<sub>2</sub>), 3.88 (3H, s, CH<sub>3</sub>), 2.59 (6H, s, 2 x CH<sub>3</sub>). **<sup>13</sup>C-NMR** (126 MHz, CDCl<sub>3</sub>): δ 155.90 (C), 155.01 (C), 151.22 (C), 146.97 (C), 142.60 (CH), 130.42 (CH), 126.46 (C), 126.37 (CH), 126.22 (C), 125.60 (CH), 121.38 (CH), 112.41 (CH), 60.17 (CH<sub>2</sub>), 56.17 (CH<sub>3</sub>), 48.35 (2 x CH<sub>3</sub>). **HRMS** (ES + ve), C<sub>16</sub>H<sub>21</sub>N<sub>8</sub>O<sub>2</sub> (M + H)<sup>+</sup>: Calculated 357.1787. Obtained 357.1803.



**(77) 6-([1-(4-methoxyphenyl)-1H-1,2,3-triazol-4-yl]methoxy)-9-(dimethylamino)-9H-purine.** The crude product was purified via silica gel column chromatography (Ethyl acetate/Hexane 25-100%) to provide the title compound as a white solid (20.5 mg, 0.056 mmol, 41% yield). **<sup>1</sup>H-NMR** (500 MHz, CDCl<sub>3</sub>): δ 8.56 (1H, s, CH), 8.08 (1H, s, CH), 7.99 (1H, s, CH), 7.60 (2H, d, *J* = 8.9 Hz, 2 x CH), 7.00 (2H, d, *J* = 8.9 Hz, 2 x CH), 5.85 (2H, s, OCH<sub>2</sub>), 3.85 (3H, s, CH<sub>3</sub>), 3.15 (6H, s, 2 x CH<sub>3</sub>). **<sup>13</sup>C-NMR** (126 MHz, CDCl<sub>3</sub>): δ 160.39 (C), 160.02 (C), 151.52 (CH), 151.30 (C), 143.89 (C), 142.12 (CH), 130.58 (C), 122.47 (2 x CH), 122.31 (CH), 120.68 (C), 114.90 (2 x CH), 60.39 (CH<sub>2</sub>), 55.75 (CH<sub>3</sub>), 47.02 (2 x CH<sub>3</sub>). **HRMS** (ES + ve), C<sub>17</sub>H<sub>19</sub>N<sub>8</sub>O<sub>2</sub> (M + H)<sup>+</sup>: Calculated 367.1631. Obtained 367.1605.

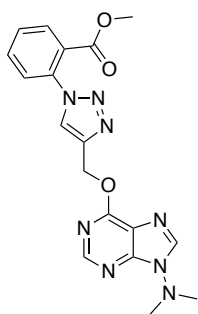


**(78) 6-([1-(3-methoxyphenyl)-1H-1,2,3-triazol-4-yl]methoxy)-9-(dimethylamino)-9H-purine.** The crude product was purified via silica gel column chromatography (Ethyl acetate/Hexane 25-100%) to provide the title compound as a white solid (29.9 mg, 0.081 mmol, 60% yield). **<sup>1</sup>H-NMR** (500 MHz, CDCl<sub>3</sub>): δ 8.56 (1H, s, CH), 8.16 (1H, s, CH), 7.99 (1H, s, CH), 7.42 – 7.21 (3H, m, 3 x CH), 6.99 – 6.92 (1H, m, CH), 5.86 (2H, s, OCH<sub>2</sub>), 3.86 (3H, s, CH<sub>3</sub>), 3.15 (6H, s, 2 x CH<sub>3</sub>). **<sup>13</sup>C-NMR** (126 MHz, CDCl<sub>3</sub>): δ 160.71 (C), 160.34 (C), 151.50 (CH), 151.31 (C), 144.07 (C), 142.14 (CH), 138.12 (C), 130.62 (CH), 122.19 (CH), 120.66 (C), 114.90 (CH), 112.66 (CH), 106.55 (CH), 60.32 (CH<sub>2</sub>), 55.76 (CH<sub>3</sub>), 47.01 (2 x CH<sub>3</sub>). **HRMS** (ES + ve), C<sub>17</sub>H<sub>19</sub>N<sub>8</sub>O<sub>2</sub> (M + H)<sup>+</sup>: Calculated 367.1631. Obtained 367.1620.

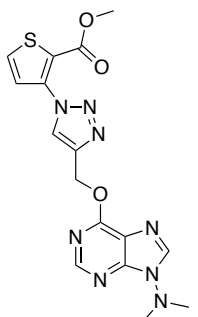


**(79) 6-([1-(2-methoxyphenyl)-1H-1,2,3-triazol-4-yl]methoxy)-9-(dimethylamino)-9H-purine.** The crude product was purified via silica gel column chromatography (Ethyl acetate/Hexane 25-100%) to provide the title compound as a yellow solid (35.7 mg, 0.097 mmol, 72% yield). **<sup>1</sup>H-NMR** (500 MHz, CDCl<sub>3</sub>): δ 8.56 (1H, s, CH), 8.27 (1H, s, CH), 7.98 (1H, s, CH), 7.73 (1H, dd, *J* = 7.9, 1.7 Hz, CH), 7.43 – 7.36 (1H, m, CH), 7.12 – 7.03 (2H, m, 2 x CH), 5.86 (2H, s, OCH<sub>2</sub>), 3.86 (3H, s, CH<sub>3</sub>), 3.14 (6H, s, 2 x CH<sub>3</sub>). **<sup>13</sup>C-NMR** (126 MHz, CDCl<sub>3</sub>): δ 160.47 (C), 151.49 (CH), 151.32 (C), 151.23 (C), 142.58 (C), 141.98 (CH), 130.29 (CH), 126.34 (C), 126.27 (CH), 125.71 (CH), 121.29 (CH), 120.65 (C), 112.33 (CH), 60.33 (CH<sub>2</sub>), 56.07 (CH<sub>3</sub>), 47.00 (2 x CH<sub>3</sub>). **HRMS** (ES + ve), C<sub>17</sub>H<sub>19</sub>N<sub>8</sub>O<sub>2</sub> (M + H)<sup>+</sup>: Calculated 367.1631. Obtained 367.1606.

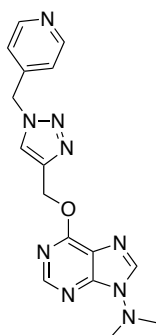




**(80) 6-({1-[2-(methoxycarbonyl)phenyl]-1H-1,2,3-triazol-4-yl}methoxy)-9-(dimethylamino)-9H-purine.** The crude product was purified via silica gel column chromatography (Ethyl acetate/Hexane 25-100%) to provide the title compound as a yellow solid (22.6 mg, 0.057 mmol, 41% yield). **<sup>1</sup>H-NMR** (500 MHz, CDCl<sub>3</sub>): δ 8.56 (1H, s, CH), 8.02 (1H, s, CH), 8.01 – 7.96 (2H, m, 2 x CH), 7.65 (1H, td, *J* = 7.7, 1.6 Hz, CH), 7.58 (1H, td, *J* = 7.6, 1.3 Hz, CH), 7.47 (1H, dd, *J* = 7.9, 1.3 Hz, CH), 5.88 (2H, s, OCH<sub>2</sub>), 3.66 (3H, s, CH<sub>3</sub>), 3.15 (6H, s, 2 x CH<sub>3</sub>). **<sup>13</sup>C-NMR** (126 MHz, CDCl<sub>3</sub>): δ 165.68 (C), 160.40 (C), 151.51 (CH), 151.29 (C), 143.20 (C), 142.09 (CH), 136.22 (C), 132.84 (CH), 131.39 (CH), 130.06 (CH), 127.66 (C), 126.90 (CH), 125.85 (CH), 120.66 (C), 60.30 (CH<sub>2</sub>), 52.69 (CH<sub>3</sub>), 47.01 (2 x CH<sub>3</sub>). **HRMS** (ES + ve), C<sub>18</sub>H<sub>19</sub>N<sub>8</sub>O<sub>3</sub> (M + H)<sup>+</sup>: Calculated 395.1580. Obtained 395.1610.

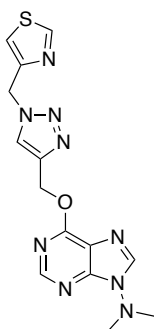


**(81) 6-({1-[2-(methoxycarbonyl)thiophen-3-yl]-1H-1,2,3-triazol-4-yl}methoxy)-9-(dimethylamino)-9H-purine.** The crude product was purified via silica gel column chromatography (Ethyl acetate/Hexane 25-100%) to provide the title compound as a light yellow solid (39.5 mg, 0.098 mmol, 71% yield). **<sup>1</sup>H-NMR** (500 MHz, CDCl<sub>3</sub>): δ 8.55 (1H, s, CH), 8.54 (1H, s, CH), 7.97 (1H, s, CH), 7.59 (1H, d, *J* = 5.4 Hz, CH), 7.47 (1H, d, *J* = 5.4 Hz, CH), 5.85 (2H, s, OCH<sub>2</sub>), 3.80 (3H, s, CH<sub>3</sub>), 3.13 (6H, s, 2 x CH<sub>3</sub>). **<sup>13</sup>C-NMR** (126 MHz, CDCl<sub>3</sub>): δ 160.67 (C), 160.35 (C), 151.47 (CH), 151.23 (C), 142.46 (C), 141.99 (CH), 138.34 (C), 131.14 (CH), 127.02 (CH), 126.73 (CH), 122.30 (C), 120.62 (C), 60.04 (CH<sub>2</sub>), 52.65 (CH<sub>3</sub>), 46.98 (2 x CH<sub>3</sub>). **HRMS** (ES + ve), C<sub>16</sub>H<sub>17</sub>N<sub>8</sub>O<sub>3</sub>S (M + H)<sup>+</sup>: Calculated 401.1144. Obtained 401.1111.

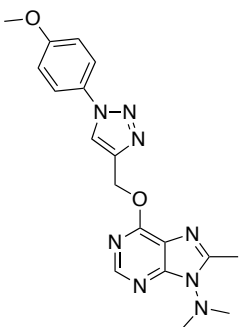


**(82) 9-(dimethylamino)-6-({1-[1-(pyridin-4-ylmethyl)-1H-1,2,3-triazol-4-yl]methoxy}-9H-purine.** The crude product was purified via silica gel column chromatography (Methanol/Ethyl acetate 0-20%) to provide the title compound as a white solid (26.1 mg, 0.074 mmol, 74% yield). **<sup>1</sup>H-NMR** (500 MHz, CDCl<sub>3</sub>): δ 8.60 (2H, d, *J* = 6.0 Hz, 2 x CH), 8.53 (1H, s, CH), 7.98 (1H, s, CH), 7.74 (1H, s, CH), 7.11 (2H, d, *J* = 6.0 Hz, 2 x CH), 5.78 (2H, s, OCH<sub>2</sub>), 5.54 (2H, s, CH<sub>2</sub>), 3.14 (6H, s, 2 x CH<sub>3</sub>). **<sup>13</sup>C-NMR** (126 MHz, CDCl<sub>3</sub>): δ 160.29 (C), 151.48 (CH), 151.29 (C), 150.72 (2 x CH), 144.31 (C), 143.49 (C), 142.16 (CH), 124.08 (CH), 122.29 (2 x CH), 120.59 (C), 60.30

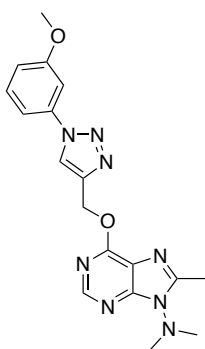
(CH<sub>2</sub>), 52.89 (CH<sub>2</sub>), 47.02 (2 x CH<sub>3</sub>). **HRMS** (ES + ve), C<sub>16</sub>H<sub>18</sub>N<sub>9</sub>O (M + H)<sup>+</sup>: Calculated 352.1634. Obtained 352.1623.



**(83) 9-(dimethylamino)-6-([1-(thiazol-4-ylmethyl)-1H-1,2,3-triazol-4-yl]methoxy)-9H-purine.** The crude product was purified via silica gel column chromatography (Methanol/Ethyl acetate 0-20%) to provide the title compound as a white solid (14.9 mg, 0.042 mmol, 42% yield). **<sup>1</sup>H-NMR** (500 MHz, CDCl<sub>3</sub>): δ 8.81 (1H, d, *J* = 2.0 Hz, CH), 8.54 (1H, s, CH), 7.97 (1H, s, CH), 7.91 (1H, s, CH), 7.31 (1H, d, *J* = 2.0 Hz, CH), 5.77 (2H, s, OCH<sub>2</sub>), 5.70 (2H, s, CH<sub>2</sub>), 3.15 (6H, s, 2 x CH<sub>3</sub>). **<sup>13</sup>C-NMR** (126 MHz, CDCl<sub>3</sub>): δ 160.40 (C), 154.15 (CH), 151.52 (CH), 151.27 (C), 150.60 (C), 143.69 (C), 142.05 (CH), 124.32 (CH), 120.63 (C), 118.07 (CH), 60.35 (CH<sub>2</sub>), 49.76 (CH<sub>2</sub>), 47.03 (2 x CH<sub>3</sub>). **HRMS** (ES + ve), C<sub>14</sub>H<sub>16</sub>N<sub>9</sub>OS (M + H)<sup>+</sup>: Calculated 358.1199. Obtained 358.1174.

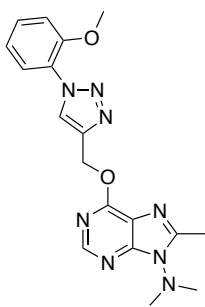


**(84) 6-([1-(4-methoxyphenyl)-1H-1,2,3-triazol-4-yl]methoxy)-8-methyl-9-(dimethylamino)-9H-purine.** The crude product was purified via silica gel column chromatography (Ethyl acetate/Hexane 25-100%) to provide the title compound as a white solid (11.2 mg, 0.029 mmol, 22% yield). **<sup>1</sup>H-NMR** (500 MHz, CDCl<sub>3</sub>): δ 8.49 (1H, s, CH), 8.07 (1H, s, CH), 7.60 (2H, d, *J* = 8.8 Hz, 2 x CH), 7.00 (2H, d, *J* = 8.8 Hz, 2 x CH), 5.83 (2H, s, OCH<sub>2</sub>), 3.85 (3H, s, CH<sub>3</sub>), 3.14 (6H, s, 2 x CH<sub>3</sub>), 2.55 (3H, s, CH<sub>3</sub>). **<sup>13</sup>C-NMR** (126 MHz, CDCl<sub>3</sub>): δ 160.00 (C), 159.22 (C), 152.68 (C), 152.45 (C), 150.29 (CH), 144.05 (C), 130.63 (C), 122.49 (2 x CH), 122.30 (CH), 119.23 (C), 114.90 (2 x CH), 60.18 (CH<sub>2</sub>), 55.75 (CH<sub>3</sub>), 45.78 (2 x CH<sub>3</sub>), 13.60 (CH<sub>3</sub>). **HRMS** (ES + ve), C<sub>18</sub>H<sub>21</sub>N<sub>8</sub>O<sub>2</sub> (M + H)<sup>+</sup>: Calculated 381.1787. Obtained 381.1763.

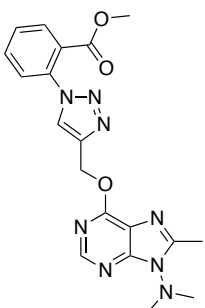


**(85) 6-([1-(3-methoxyphenyl)-1H-1,2,3-triazol-4-yl]methoxy)-8-methyl-9-(dimethylamino)-9H-purine.** The crude product was purified via silica gel column chromatography (Ethyl acetate/Hexane 25-100%) to provide the title compound as a yellow solid (34.5 mg, 0.09 mmol, 68% yield). **<sup>1</sup>H-NMR** (500 MHz, CDCl<sub>3</sub>): δ 8.48 (1H, s, CH), 8.14 (1H, s, CH), 7.41 – 7.19 (3H, m, 3 x CH), 6.98 – 6.92 (1H, m, CH), 5.82 (2H, s, OCH<sub>2</sub>), 3.86 (3H, s, CH<sub>3</sub>), 3.13 (6H, s, 2 x CH<sub>3</sub>),

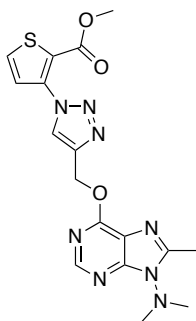
2.55 (3H, s, CH<sub>3</sub>). <sup>13</sup>C-NMR (126 MHz, CDCl<sub>3</sub>): δ 160.70 (C), 159.15 (C), 152.69 (C), 152.44 (C), 150.26 (CH), 144.22 (C), 138.14 (C), 130.61 (CH), 122.15 (CH), 119.19 (C), 114.88 (CH), 112.66 (CH), 106.51 (CH), 60.10 (CH<sub>2</sub>), 55.75 (CH<sub>3</sub>), 45.76 (2 x CH<sub>3</sub>), 13.58 (CH<sub>3</sub>). **HRMS** (ES + ve), C<sub>18</sub>H<sub>21</sub>N<sub>8</sub>O<sub>2</sub> (M + H)<sup>+</sup>: Calculated 381.1787. Obtained 381.1769.



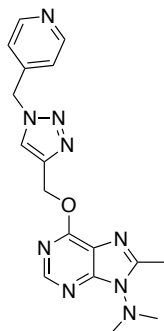
**(86) 6-([1-(2-methoxyphenyl)-1H-1,2,3-triazol-4-yl]methoxy)-8-methyl-9-(dimethylamino)-9H-purine.** The crude product was purified via silica gel column chromatography (Ethyl acetate/Hexane 25-100%) to provide the title compound as a yellow oil (31 mg, 0.081 mmol, 62% yield). <sup>1</sup>H-NMR (500 MHz, CDCl<sub>3</sub>): δ 8.48 (1H, s, CH), 8.25 (1H, s, CH), 7.72 (1H, dd, *J* = 7.9, 1.7 Hz, CH), 7.43 – 7.36 (1H, m, CH), 7.10 – 7.02 (2H, m, 2 x CH), 5.83 (2H, s, OCH<sub>2</sub>), 3.86 (3H, s, CH<sub>3</sub>), 3.13 (6H, s, 2 x CH<sub>3</sub>), 2.54 (3H, s, CH<sub>3</sub>). <sup>13</sup>C-NMR (126 MHz, CDCl<sub>3</sub>): δ 159.31 (C), 152.52 (C), 152.37 (C), 151.34 (C), 150.24 (CH), 142.73 (C), 130.25 (CH), 126.38 (C), 126.23 (CH), 125.73 (CH), 121.27 (CH), 119.20 (C), 112.31 (CH), 60.11 (CH<sub>2</sub>), 56.04 (CH<sub>3</sub>), 45.74 (2 x CH<sub>3</sub>), 13.55 (CH<sub>3</sub>). **HRMS** (ES + ve), C<sub>18</sub>H<sub>21</sub>N<sub>8</sub>O<sub>2</sub> (M + H)<sup>+</sup>: Calculated 381.1787. Obtained 381.1772.



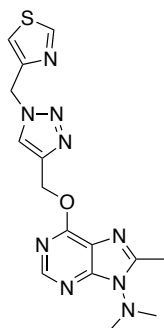
**(87) 6-([1-[2-(methoxycarbonyl)phenyl]-1H-1,2,3-triazol-4-yl]methoxy)-8-methyl-9-(dimethylamino)-9H-purine.** The crude product was purified via silica gel column chromatography (Ethyl acetate/Hexane 25-100%) to provide the title compound as an off-white solid (11.3 mg, 0.027 mmol, 30% yield). <sup>1</sup>H-NMR (500 MHz, CDCl<sub>3</sub>): δ 8.48 (1H, s, CH), 8.01 (1H, s, CH), 7.99 (1H, dd, *J* = 7.8, 1.6 Hz, CH), 7.66 (1H, td, *J* = 7.7, 1.6 Hz, CH), 7.58 (1H, td, *J* = 7.7, 1.3 Hz, CH), 7.47 (1H, dd, *J* = 7.9, 1.3 Hz, CH), 5.86 (2H, s, OCH<sub>2</sub>), 3.66 (3H, s, CH<sub>3</sub>), 3.14 (6H, s, 2 x CH<sub>3</sub>), 2.55 (3H, s, CH<sub>3</sub>). <sup>13</sup>C-NMR (126 MHz, CDCl<sub>3</sub>): δ 165.74 (C), 159.25 (C), 152.65 (C), 152.46 (C), 150.29 (CH), 143.40 (C), 136.26 (C), 132.83 (CH), 131.39 (CH), 130.03 (CH), 127.70 (C), 126.89 (CH), 125.77 (CH), 119.23 (C), 60.11 (CH<sub>2</sub>), 52.69 (CH<sub>3</sub>), 45.78 (2 x CH<sub>3</sub>), 13.60 (CH<sub>3</sub>). **HRMS** (ES + ve), C<sub>19</sub>H<sub>21</sub>N<sub>8</sub>O<sub>3</sub> (M + H)<sup>+</sup>: Calculated 409.1737. Obtained 409.1714.



**(88) 6-({1-[2-(methoxycarbonyl)thiophen-3-yl]-1H-1,2,3-triazol-4-yl}methoxy)-8-methyl-9-(dimethylamino)-9H-purine.** The crude product was purified via silica gel column chromatography (Ethyl acetate/Hexane 25-90%) to provide the title compound as a light yellow solid (28.6 mg, 0.069 mmol, 73% yield). **<sup>1</sup>H-NMR** (500 MHz, CDCl<sub>3</sub>): δ 8.52 (1H, s, CH), 8.48 (1H, s, CH), 7.60 (1H, d, *J* = 5.4 Hz, CH), 7.47 (1H, d, *J* = 5.4 Hz, CH), 5.83 (2H, s, OCH<sub>2</sub>), 3.80 (3H, s, CH<sub>3</sub>), 3.13 (6H, s, 2 x CH<sub>3</sub>), 2.54 (3H, s, CH<sub>3</sub>). **<sup>13</sup>C-NMR** (126 MHz, CDCl<sub>3</sub>): δ 160.70 (C), 159.23 (C), 152.56 (C), 152.41 (C), 150.27 (CH), 142.66 (C), 138.40 (C), 131.11 (CH), 126.99 (CH), 126.79 (CH), 122.37 (C), 119.21 (C), 59.85 (CH<sub>2</sub>), 52.66 (CH<sub>3</sub>), 45.75 (2 x CH<sub>3</sub>), 13.57 (CH<sub>3</sub>). **HRMS** (ES + ve), C<sub>17</sub>H<sub>19</sub>N<sub>8</sub>O<sub>3</sub>S (M + H)<sup>+</sup>: Calculated 415.1301. Obtained 415.1299.

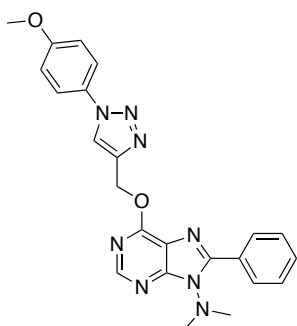


**(89) 8-methyl-9-(dimethylamino)-6-{{1-(pyridin-4-ylmethyl)-1H-1,2,3-triazol-4-yl}methoxy}-9H-purine.** The crude product was purified via silica gel column chromatography (Methanol/Ethyl acetate 0-20%) to provide the title compound as a white solid (23.1 mg, 0.063 mmol, 63% yield). **<sup>1</sup>H-NMR** (500 MHz, CDCl<sub>3</sub>): δ 8.59 (2H, d, *J* = 5.1 Hz, 2 x CH), 8.43 (1H, s, CH), 7.72 (1H, s, CH), 7.09 (2H, d, *J* = 5.1 Hz, 2 x CH), 5.74 (2H, s, OCH<sub>2</sub>), 5.52 (2H, s, CH<sub>2</sub>), 3.12 (6H, s, 2 x CH<sub>3</sub>), 2.53 (3H, s, CH<sub>3</sub>). **<sup>13</sup>C-NMR** (126 MHz, CDCl<sub>3</sub>): δ 159.08 (C), 152.70 (C), 152.41 (C), 150.68 (2 x CH), 150.21 (CH), 144.41 (C), 143.49 (C), 124.07 (CH), 122.30 (2 x CH), 119.10 (C), 60.05 (CH<sub>2</sub>), 52.83 (CH<sub>2</sub>), 45.74 (2 x CH<sub>3</sub>), 13.56 (CH<sub>3</sub>). **HRMS** (ES + ve), C<sub>17</sub>H<sub>20</sub>N<sub>9</sub>O (M + H)<sup>+</sup>: Calculated 366.1791. Obtained 366.1771.



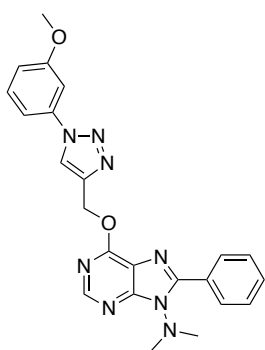
**(90) 8-methyl-9-(dimethylamino)-6-{{1-(thiazol-4-ylmethyl)-1H-1,2,3-triazol-4-yl}methoxy}-9H-purine.** The crude product was purified via silica gel column chromatography (Methanol/Ethyl acetate 0-10%) to provide the title compound as a yellow solid (27.5 mg, 0.074 mmol, 74% yield). **<sup>1</sup>H-NMR** (500 MHz, CDCl<sub>3</sub>): δ 8.80 (1H, d, *J* = 2.0 Hz, CH), 8.44 (1H, s, CH), 7.90 (1H, s, CH), 7.30 (1H, d, *J* = 2.0 Hz, CH), 5.72 (2H, s, OCH<sub>2</sub>), 5.69 (2H, s, CH<sub>2</sub>), 3.12 (6H, s, 2 x CH<sub>3</sub>), 2.53 (3H, s, CH<sub>3</sub>). **<sup>13</sup>C-NMR** (126 MHz, CDCl<sub>3</sub>): δ 159.13 (C), 154.23 (CH), 152.61 (C), 152.30 (C), 150.51 (C), 150.28 (CH), 143.72 (C), 124.34 (CH), 119.04 (C), 118.12 (CH), 60.07 (CH<sub>2</sub>), 49.69

(CH<sub>2</sub>), 45.74 (2 x CH<sub>3</sub>), 13.57 (CH<sub>3</sub>). **HRMS** (ES + ve), C<sub>15</sub>H<sub>18</sub>N<sub>9</sub>OS (M + H)<sup>+</sup>: Calculated 372.1355. Obtained 372.1373.



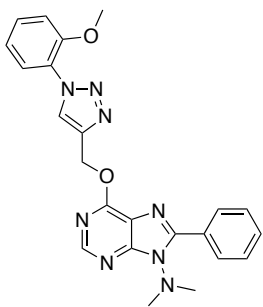
**(91)**      **6-([1-(4-methoxyphenyl)-1H-1,2,3-triazol-4-yl]methoxy)-9-(dimethylamino)-8-phenyl-9H-purine.** The crude product was purified via silica gel column chromatography (Ethyl acetate/Hexane 50%) to provide the title compound as a white solid (13.6 mg, 0.031 mmol, 43% yield). **<sup>1</sup>H-NMR** (500 MHz, CDCl<sub>3</sub>): δ 8.55 (1H, s, 1H), 8.25 –

8.17 (2H, m, 2 x CH), 8.10 (1H, s, CH), 7.61 (2H, d, *J* = 8.8 Hz, 2 x CH), 7.52 – 7.42 (3H, m, 3 x CH), 7.00 (2H, d, *J* = 8.8 Hz, 2 x CH), 5.90 (2H, s, OCH<sub>2</sub>), 3.85 (3H, s, CH<sub>3</sub>), 3.23 (6H, s, 2 x CH<sub>3</sub>). **<sup>13</sup>C-NMR** (126 MHz, CDCl<sub>3</sub>): δ 160.02 (C), 159.96 (C), 153.40 (C), 151.28 (C), 150.70 (CH), 144.03 (C), 130.63 (C), 130.53 (CH), 129.54 (2 x CH), 129.07 (C), 128.38 (2 x CH), 122.49 (2 x CH), 122.44 (CH), 120.02 (C), 114.90 (2 x CH), 60.28 (CH<sub>2</sub>), 55.76 (CH<sub>3</sub>), 45.56 (2 x CH<sub>3</sub>). **HRMS** (ES + ve), C<sub>23</sub>H<sub>23</sub>N<sub>8</sub>O<sub>2</sub> (M + H)<sup>+</sup>: Calculated 443.1944. Obtained 443.1907.

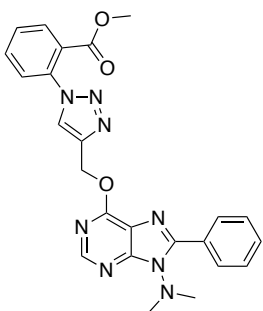


**(92)**      **6-([1-(3-methoxyphenyl)-1H-1,2,3-triazol-4-yl]methoxy)-9-(dimethylamino)-8-phenyl-9H-purine.** The crude product was purified via silica gel column chromatography (Ethyl acetate/Hexane 25-66%) to provide the title compound as a white solid (23.6 mg, 0.053 mmol, 63% yield). **<sup>1</sup>H-NMR** (500 MHz, CDCl<sub>3</sub>): δ 8.56 (1H, s, CH), 8.25 – 8.19 (2H, m, 2 x CH), 8.18 (1H, s, CH), 7.51 – 7.43 (3H, m, 3 x CH), 7.43 – 7.22 (3H,

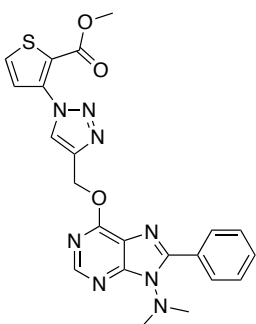
m, 3 x CH), 7.00 – 6.93 (1H, m, CH), 5.90 (2H, s, OCH<sub>2</sub>), 3.87 (3H, s, CH<sub>3</sub>), 3.24 (6H, s, 2 x CH<sub>3</sub>). **<sup>13</sup>C-NMR** (126 MHz, CDCl<sub>3</sub>): δ 160.73 (C), 159.92 (C), 153.41 (C), 151.32 (C), 150.70 (CH), 144.23 (C), 138.17 (C), 130.64 (CH), 130.54 (CH), 129.54 (2 x CH), 129.05 (C), 128.39 (2 x CH), 122.32 (CH), 120.01 (C), 114.91 (CH), 112.70 (CH), 106.58 (CH), 60.23 (CH<sub>2</sub>), 55.78 (CH<sub>3</sub>), 45.56 (2 x CH<sub>3</sub>). **HRMS** (ES + ve), C<sub>23</sub>H<sub>23</sub>N<sub>8</sub>O<sub>2</sub> (M + H)<sup>+</sup>: Calculated 443.1944. Obtained 443.1902.



**(93) 6-({1-[2-(methoxyphenyl)-1H-1,2,3-triazol-4-yl]methoxy}-9-(dimethylamino)-8-phenyl-9H-purine.** The crude product was purified via silica gel column chromatography (Ethyl acetate/Hexane 25-66%) to provide the title compound as a white solid (18.5 mg, 0.042 mmol, 48% yield). **<sup>1</sup>H-NMR** (500 MHz, CDCl<sub>3</sub>): δ 8.55 (1H, s, CH), 8.29 (1H, s, CH), 8.25 – 8.17 (2H, m, 2 x CH), 7.75 (1H, dd, *J* = 7.9, 1.7 Hz, CH), 7.50 – 7.43 (3H, m, 3 x CH), 7.43 – 7.38 (1H, m, CH), 7.12 – 7.04 (2H, m, 2 x CH), 5.91 (2H, s, OCH<sub>2</sub>), 3.87 (3H, s, CH<sub>3</sub>), 3.23 (6H, s, 2 x CH<sub>3</sub>). **<sup>13</sup>C-NMR** (126 MHz, CDCl<sub>3</sub>): δ 160.10 (C), 153.36 (C), 151.36 (C), 151.16 (C), 150.69 (CH), 142.76 (C), 130.48 (CH), 130.27 (CH), 129.53 (2 x CH), 129.11 (C), 128.36 (2 x CH), 126.43 (C), 126.40 (CH), 125.76 (CH), 121.33 (CH), 120.04 (C), 112.35 (CH), 60.27 (CH<sub>2</sub>), 56.08 (CH<sub>3</sub>), 45.54 (2 x CH<sub>3</sub>). **HRMS** (ES + ve), C<sub>23</sub>H<sub>23</sub>N<sub>8</sub>O<sub>2</sub> (M + H)<sup>+</sup>: Calculated 443.1944. Obtained 443.1907.

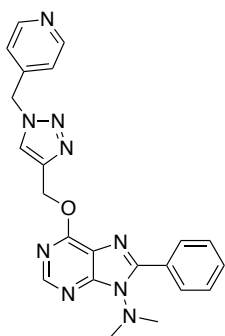


**(94) 6-({1-[2-(methoxycarbonyl)phenyl]-1H-1,2,3-triazol-4-yl}methoxy)-9-(dimethylamino)-8-phenyl-9H-purine.** The crude product was purified via silica gel column chromatography (Ethyl acetate/Hexane 33-60%) to provide the title compound as a white oil (17.7 mg, 0.037 mmol, 43% yield). **<sup>1</sup>H-NMR** (500 MHz, CDCl<sub>3</sub>): δ 8.54 (1H, s, CH), 8.25 – 8.17 (2H, m, 2 x CH), 8.04 (1H, s, CH), 7.99 (1H, dd, *J* = 7.8, 1.6 Hz, CH), 7.65 (1H, td, *J* = 7.7, 1.6 Hz, CH), 7.58 (1H, td, *J* = 7.6, 1.3 Hz, CH), 7.52 – 7.43 (4H, m, 4 x CH), 5.92 (2H, s, OCH<sub>2</sub>), 3.67 (3H, s, CH<sub>3</sub>), 3.23 (6H, s, 2 x CH<sub>3</sub>). **<sup>13</sup>C-NMR** (126 MHz, CDCl<sub>3</sub>): δ 165.74 (C), 159.96 (C), 153.38 (C), 151.23 (C), 150.69 (CH), 143.35 (C), 136.23 (C), 132.83 (CH), 131.38 (CH), 130.52 (CH), 130.03 (CH), 129.50 (2 x CH), 129.05 (C), 128.38 (2 x CH), 127.68 (C), 126.90 (CH), 125.93 (CH), 120.00 (C), 60.21 (CH<sub>2</sub>), 52.70 (CH<sub>3</sub>), 45.54 (2 x CH<sub>3</sub>). **HRMS** (ES + ve), C<sub>24</sub>H<sub>23</sub>N<sub>8</sub>O<sub>3</sub> (M + H)<sup>+</sup>: Calculated 471.1893. Obtained 471.1881.

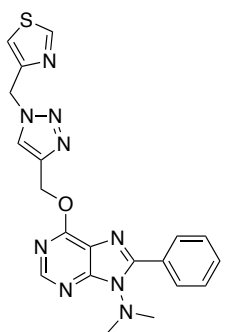


**(95) 6-({1-[2-(methoxycarbonyl)thiophen-3-yl]-1H-1,2,3-triazol-4-yl}methoxy)-9-(dimethylamino)-8-phenyl-9H-purine.** The crude product was purified via silica gel column chromatography (Ethyl acetate/Hexane 50%) to provide the title compound as a white solid (16.9 mg, 0.035 mmol, 51% yield). **<sup>1</sup>H-NMR** (500 MHz, CDCl<sub>3</sub>): δ 8.56 (1H, s, CH), 8.55 (1H, s, CH), 8.25 – 8.18 (2H, m, 2 x CH), 7.60 (1H, d, *J* = 5.4 Hz, CH), 7.49 (1H, d, *J* = 5.4 Hz, CH),

7.48 – 7.44 (3H, m, 3 x CH), 5.91 (2H, s, OCH<sub>2</sub>), 3.82 (3H, s, CH<sub>3</sub>), 3.23 (6H, s, 2 x CH<sub>3</sub>). <sup>13</sup>C-NMR (126 MHz, CDCl<sub>3</sub>): δ 160.74 (C), 159.99 (C), 153.37 (C), 151.16 (C), 150.70 (CH), 142.66 (C), 138.42 (C), 131.13 (CH), 130.48 (CH), 129.53 (2 x CH), 129.11 (C), 128.36 (2 x CH), 127.15 (CH), 126.82 (CH), 122.38 (C), 120.03 (C), 60.00 (CH<sub>2</sub>), 52.69 (CH<sub>3</sub>), 45.54 (2 x CH<sub>3</sub>). **HRMS** (ES + ve), C<sub>22</sub>H<sub>21</sub>N<sub>8</sub>O<sub>3</sub>S (M + H)<sup>+</sup>: Calculated 477.1457. Obtained 477.1432.



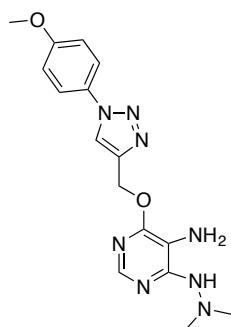
**(96) 9-(dimethylamino)-8-phenyl-6-{{1-(pyridin-4-ylmethyl)-1H-1,2,3-triazol-4-yl}methoxy}-9H-purine.** The crude product was purified via silica gel column chromatography (Methanol/Ethyl acetate 0-5%) to provide the title compound as a white solid (23.8 mg, 0.055 mmol, 65% yield). <sup>1</sup>H-NMR (500 MHz, CDCl<sub>3</sub>): δ 8.59 (2H, d, *J* = 6.0 Hz, 2 x CH), 8.51 (1H, s, CH), 8.21 – 8.14 (2H, m, 2 x CH), 7.76 (1H, s, CH), 7.51 – 7.41 (3H, m, 3 x CH), 7.11 (2H, d, *J* = 6.0 Hz, 2 x CH), 5.82 (2H, s, CH<sub>2</sub>), 5.54 (2H, s, CH<sub>2</sub>), 3.22 (6H, s, 2 x CH<sub>3</sub>). <sup>13</sup>C-NMR (126 MHz, CDCl<sub>3</sub>): δ 159.85 (C), 153.38 (C), 151.32 (C), 150.66 (2 x CH), 150.64 (CH), 144.40 (C), 143.57 (C), 130.57 (CH), 129.49 (2 x CH), 128.99 (C), 128.40 (2 x CH), 124.25 (CH), 122.32 (2 x CH), 119.92 (C), 60.18 (CH<sub>2</sub>), 52.86 (CH<sub>2</sub>), 45.55 (2 x CH<sub>3</sub>). **HRMS** (ES + ve), C<sub>22</sub>H<sub>22</sub>N<sub>9</sub>O (M + H)<sup>+</sup>: Calculated 428.1947. Obtained 428.1951.



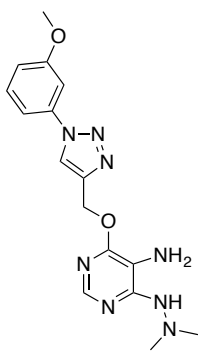
**(97) 9-(dimethylamino)-8-phenyl-6-{{1-(thiazol-4-ylmethyl)-1H-1,2,3-triazol-4-yl}methoxy}-9H-purine.** The crude product was purified via silica gel column chromatography (Methanol/Ethyl acetate 0-2.5%) to provide the title compound as a light yellow solid (25.9 mg, 0.06 mmol, 68% yield). <sup>1</sup>H-NMR (500 MHz, CDCl<sub>3</sub>): δ 8.79 (1H, d, *J* = 2.0 Hz, CH), 8.52 (1H, s, CH), 8.23 – 8.16 (2H, m, 2 x CH), 7.91 (1H, s, CH), 7.51 – 7.42 (3H, m, 3 x CH), 7.31 (1H, d, *J* = 2.0 Hz, CH), 5.80 (2H, s, OCH<sub>2</sub>), 5.70 (2H, s, CH<sub>2</sub>), 3.22 (6H, s, 2 x CH<sub>3</sub>). <sup>13</sup>C-NMR (126 MHz, CDCl<sub>3</sub>): δ 159.95 (C), 154.11 (CH), 153.33 (C), 151.17 (C), 150.67 (CH), 150.61 (C), 143.78 (C), 130.48 (CH), 129.50 (2 x CH), 129.06 (C), 128.35 (2 x CH), 124.42 (CH), 119.95 (C), 118.06 (CH), 60.22 (CH<sub>2</sub>), 49.72 (CH<sub>2</sub>), 45.53 (2 x CH<sub>3</sub>). **HRMS** (ES + ve), C<sub>20</sub>H<sub>20</sub>N<sub>9</sub>OS (M + H)<sup>+</sup>: Calculated 434.1512. Obtained 434.1515.

• **General procedure N2:**

- Procedure N1 was followed with the following changes:
- A mixture of acetonitrile/water (9:1 v/v) was used as a solvent.
- 0.2 equiv. were used of sodium ascorbate and 0.1 equiv. of copper (I) iodide.

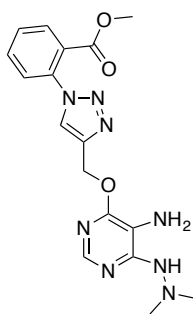


**(70) 5-amino-6-([1-(4-methoxyphenyl)-1H-1,2,3-triazol-4-yl]methoxy)-4-(2,2-dimethylhydrazinyl)-pyrimidine.** The crude product was purified via silica gel column chromatography (Ethyl acetate) to provide the title compound as a yellow oil (17.5 mg, 0.049 mmol, 12% yield). **<sup>1</sup>H-NMR** (500 MHz, CDCl<sub>3</sub>): δ 8.02 (1H, s, CH), 7.89 (1H, s, CH), 7.60 (2H, d, *J* = 8.5 Hz, 2 x CH), 7.00 (2H, d, *J* = 8.5 Hz, 2 x CH), 5.62 (2H, s, OCH<sub>2</sub>), 4.31 (2H, bs, NH<sub>2</sub>), 3.85 (3H, s, CH<sub>3</sub>), 2.57 (6H, s, 2 x CH<sub>3</sub>). **<sup>13</sup>C-NMR** (126 MHz, CDCl<sub>3</sub>): δ 160.03 (C), 156.80 (C), 149.54 (C), 144.97 (CH), 144.32 (C), 130.54 (C), 122.44 (CH), 122.42 (2 x CH), 114.90 (2 x CH), 114.18 (C), 59.50 (CH<sub>2</sub>), 55.76 (CH<sub>3</sub>), 48.58 (2 x CH<sub>3</sub>). **HRMS** (ES + ve), C<sub>16</sub>H<sub>21</sub>N<sub>8</sub>O<sub>2</sub> (M + H)<sup>+</sup>: Calculated 357.1787. Obtained 357.1753.

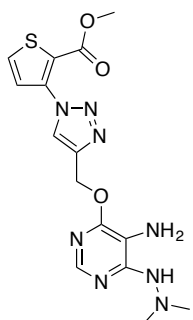


**(71) 5-amino-6-([1-(3-methoxyphenyl)-1H-1,2,3-triazol-4-yl]methoxy)-4-(2,2-dimethylhydrazinyl)-pyrimidine.** The crude product was purified via silica gel column chromatography (Ethyl acetate) to provide the title compound as a yellow solid (71.9 mg, 0.201 mmol, 79% yield). **<sup>1</sup>H-NMR** (500 MHz, CDCl<sub>3</sub>): δ 8.09 (1H, s, CH), 7.88 (1H, s, CH), 7.40 – 7.18 (3H, m, 3 x CH), 6.96 – 6.90 (1H, m, CH), 5.94 (1H, bs, NH), 5.61 (2H, s, OCH<sub>2</sub>), 4.99 (2H, bs, NH<sub>2</sub>), 3.84 (3H, s, CH<sub>3</sub>), 2.56 (6H, s, 2 x CH<sub>3</sub>). **<sup>13</sup>C-NMR** (126 MHz, CDCl<sub>3</sub>): δ 160.62 (C), 156.43 (C), 149.24 (C), 144.35 (CH), 144.23 (C), 137.96 (C), 130.58 (CH), 122.33 (CH), 114.73 (CH), 113.88 (C), 112.53 (CH), 106.53 (CH), 59.45 (CH<sub>2</sub>), 55.70 (CH<sub>3</sub>), 48.39 (2 x CH<sub>3</sub>). **HRMS** (ES + ve), C<sub>16</sub>H<sub>21</sub>N<sub>8</sub>O<sub>2</sub> (M + H)<sup>+</sup>: Calculated 357.1787. Obtained 357.1789.

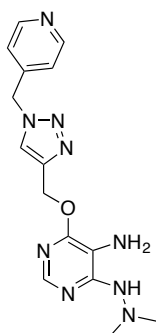




**(73) 5-amino-6-({1-[2-(methoxycarbonyl)phenyl]-1H-1,2,3-triazol-4-yl}methoxy)-4-(2,2-dimethylhydrazinyl)-pyrimidine.** The crude product was purified via silica gel column chromatography (Ethyl acetate) to provide the title compound as a yellow oil (27.6 mg, 0.072 mmol, 24% yield). **<sup>1</sup>H-NMR** (500 MHz, CDCl<sub>3</sub>): δ 7.99 (1H, dd, *J* = 7.8, 1.6 Hz, CH), 7.95 (1H, s, CH), 7.87 (1H, s, CH), 7.66 (1H, td, *J* = 7.7, 1.6 Hz, CH), 7.59 (1H, td, *J* = 7.6, 1.3 Hz, CH), 7.48 (1H, dd, *J* = 7.8, 1.3 Hz, CH), 5.65 (2H, s, OCH<sub>2</sub>), 5.59 (1H, bs, NH), 4.19 (2H, bs, NH<sub>2</sub>), 3.65 (3H, s, CH<sub>3</sub>), 2.57 (6H, s, 2 x CH<sub>3</sub>). **<sup>13</sup>C-NMR** (126 MHz, CDCl<sub>3</sub>): δ 165.64 (C), 156.78 (C), 149.51 (C), 144.95 (CH), 143.63 (C), 136.19 (C), 132.86 (CH), 131.40 (CH), 130.08 (CH), 127.57 (C), 126.95 (CH), 125.99 (CH), 114.19 (C), 59.49 (CH<sub>2</sub>), 52.64 (CH<sub>3</sub>), 48.56 (2 x CH<sub>3</sub>). **HRMS** (ES + ve), C<sub>17</sub>H<sub>21</sub>N<sub>8</sub>O<sub>3</sub> (M + H)<sup>+</sup>: Calculated 385.1737. Obtained 385.1703.



**(74) 5-amino-6-({1-[2-(methoxycarbonyl)thiophen-3-yl]-1H-1,2,3-triazol-4-yl}methoxy)-4-(2,2-dimethylhydrazinyl)-pyrimidine.** The crude product was purified via silica gel column chromatography (Ethyl acetate) to provide the title compound as a yellow oil (87.5 mg, 0.224 mmol, 59% yield). **<sup>1</sup>H-NMR** (500 MHz, CDCl<sub>3</sub>): δ 8.48 (1H, s, CH), 7.90 (1H, s, CH), 7.60 (1H, d, *J* = 5.2 Hz, CH), 7.49 (1H, d, *J* = 5.2 Hz, CH), 6.02 (1H, bs, NH), 5.63 (2H, s, OCH<sub>2</sub>), 4.59 (2H, bs, NH<sub>2</sub>), 3.80 (3H, s, CH<sub>3</sub>), 2.58 (6H, s, 2 x CH<sub>3</sub>). **<sup>13</sup>C-NMR** (126 MHz, CDCl<sub>3</sub>): δ 160.61 (C), 156.78 (C), 149.64 (C), 145.27 (CH), 142.95 (C), 138.26 (C), 131.13 (CH), 126.89 (CH), 126.63 (CH), 122.19 (C), 114.06 (C), 60.42 (CH<sub>2</sub>), 52.63 (CH<sub>3</sub>), 48.50 (2 x CH<sub>3</sub>). **HRMS** (ES + ve), C<sub>15</sub>H<sub>19</sub>N<sub>8</sub>O<sub>3</sub>S (M + H)<sup>+</sup>: Calculated 391.1301. Obtained 391.1283.

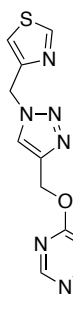


**(75) 5-amino-4-(2,2-dimethylhydrazinyl)-6-{{1-(pyridin-4-ylmethyl)-1H-1,2,3-triazol-4-yl}methoxy}pyrimidine.** The crude product was purified via silica gel column chromatography (Methanol/Ethyl acetate 10%) to provide the title compound as a yellow solid (57.4 mg, 0.168 mmol, 57% yield). **<sup>1</sup>H-NMR** (500 MHz, CDCl<sub>3</sub>): δ 8.57 (2H, d, *J* = 6.0 Hz, 2 x CH), 7.80 (1H, s, CH), 7.66 (1H, s, CH), 7.07 (2H, d, *J* = 6.0 Hz, 2 x CH), 5.53 (2H, s, OCH<sub>2</sub>), 5.52 (2H, s, CH<sub>2</sub>), 5.37 (1H, bs, NH), 4.36 (2H, bs, NH<sub>2</sub>), 2.53 (6H, s, 2 x CH<sub>3</sub>). **<sup>13</sup>C-NMR** (126 MHz, CDCl<sub>3</sub>): δ 156.80 (C), 150.59 (2 x CH), 149.90 (C), 145.47 (CH), 144.77 (C), 143.56 (C), 124.28

C. General synthesis for the compounds from chemical library 3:

---

(CH), 122.19 (2 x CH), 114.09 (C), 59.31 (CH<sub>2</sub>), 52.77 (CH<sub>2</sub>), 48.54 (2 x CH<sub>3</sub>). **HRMS** (ES + ve), C<sub>15</sub>H<sub>20</sub>N<sub>9</sub>O (M + H)<sup>+</sup>: Calculated 342.1791. Obtained 342.1787.



**(76) 5-amino-4-(2,2-dimethylhydrazinyl)-6-{{1-(thiazol-4-ylmethyl)-1*H*-1,2,3-triazol-4-yl}methoxy}pyrimidine.** The crude

product was purified via silica gel column chromatography (Methanol/Ethyl acetate 0-4%) to provide the title compound as a yellow

oil (83.8 mg, 0.241 mmol, 62% yield). **<sup>1</sup>H-NMR** (500 MHz, CDCl<sub>3</sub>): δ 8.78

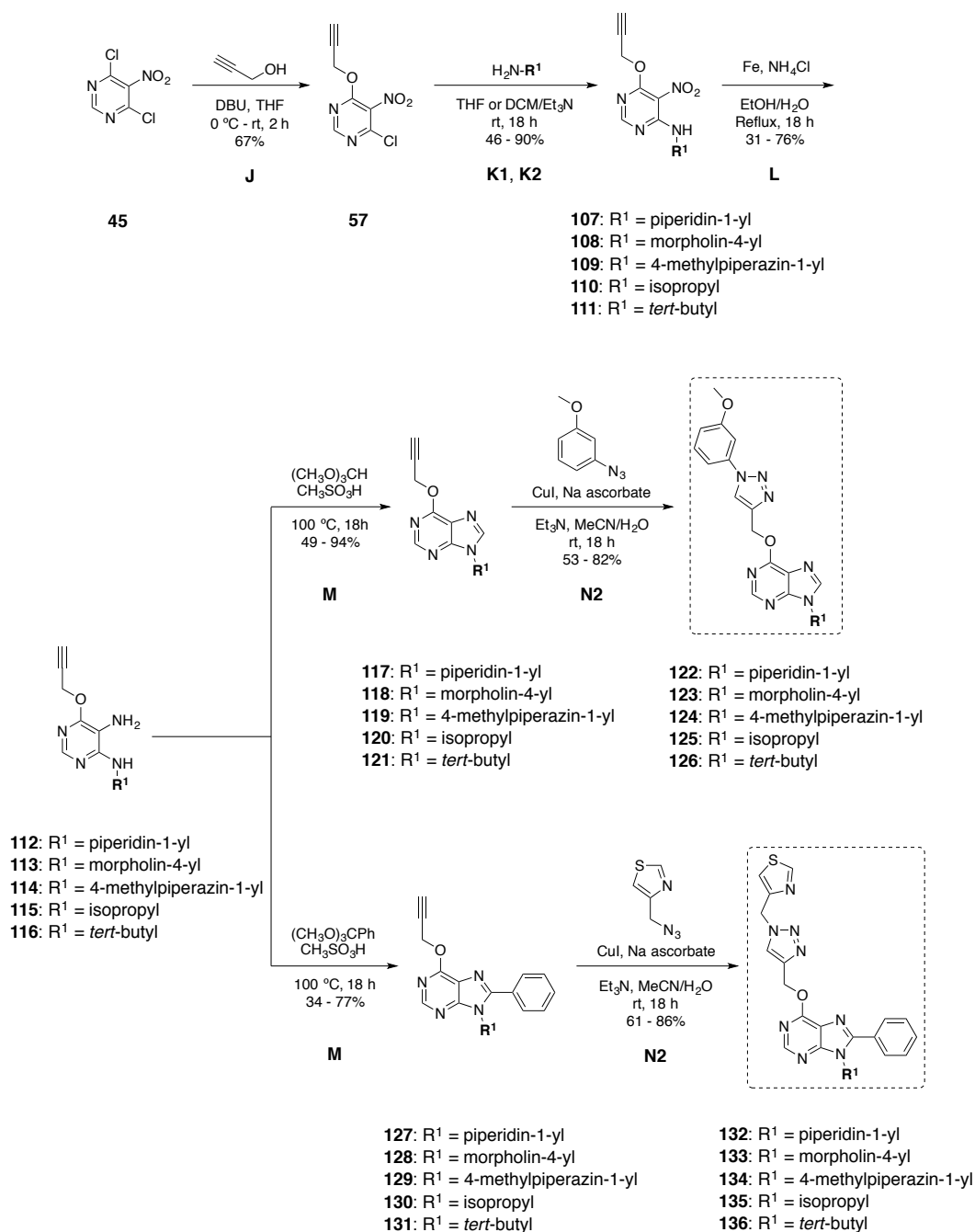
(1H, d, *J* = 2.0 Hz, CH), 7.82 (1H, s, CH), 7.81 (1H, s, CH), 7.29 (1H, d, *J*

= 2.0 Hz, CH), 5.67 (2H, s, OCH<sub>2</sub>), 5.62 (1H, bs, NH), 5.50 (2H, s, CH<sub>2</sub>), 4.76 (2H, bs, NH<sub>2</sub>), 2.52 (6H, s, 2 x CH<sub>3</sub>). **<sup>13</sup>C-NMR** (126 MHz, CDCl<sub>3</sub>): δ 156.79 (C), 154.16 (CH),

150.47 (C), 149.69 (C), 145.17 (CH), 144.09 (C), 124.33 (CH), 117.99 (CH), 114.01 (C), 59.43 (CH<sub>2</sub>), 49.62 (CH<sub>2</sub>), 48.45 (2 x CH<sub>3</sub>). **HRMS** (ES + ve), C<sub>13</sub>H<sub>18</sub>N<sub>9</sub>OS (M + H)<sup>+</sup>:

Calculated 348.1355. Obtained 348.1352.

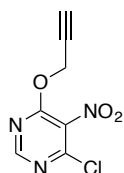
## D. General synthesis for the compounds from the optimization of compounds 78 and 97:



### • General procedure J:

1,8-Diazabicyclo[5.4.0]undec-7-ene (1.5 equiv.) was added to a 0.9 M solution of propargyl alcohol (1 equiv.) in dry THF and the mixture was stirred at 23 °C for 30 min. The prepared solution was added, dropwise over 45 min, into a 0.3 M solution of 4,6-dichloronitropyrimidine (**45**) (1 equiv.) in dry THF at 0 °C via a dropping funnel

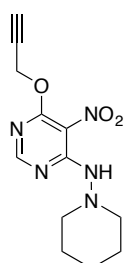
maintaining the internal temperature at 0 °C. The mixture was allowed to warm to room temperature over 1 h. The solvent was removed under reduced pressure and the resulting residue was partitioned between dichloromethane and water. The layers were separated and the organic phase was washed with saturated brine, dried over anhydrous Na<sub>2</sub>SO<sub>4</sub> and filtered. The solvent was removed under reduced pressure and the crude material was purified by silica gel column chromatography.



**(57) 4-chloro-5-nitro-6-(prop-2-yn-1-yloxy)pyrimidine.** The crude product was purified via silica gel column chromatography (Ethyl acetate/Hexane 20%) to provide the title compound as a white solid (1.30 g, 6.087 mmol, 67% yield). <sup>1</sup>H-NMR (500 MHz, CDCl<sub>3</sub>): δ 8.68 (1H, s, CH), 5.15 (2H, d, *J* = 2.4 Hz, OCH<sub>2</sub>), 2.58 (1H, t, *J* = 2.4 Hz, CH). <sup>13</sup>C-NMR (126 MHz, CDCl<sub>3</sub>): δ 160.39 (C), 157.48 (CH), 152.21 (C), 132.70 (C), 77.11 (C), 76.06 (CH), 56.72 (CH<sub>2</sub>).

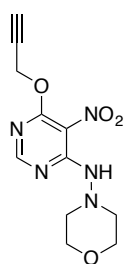
- **General procedure K1:**

To a 0.2 M solution of the compound **57** (1 equiv.) in dry THF was added dropwise the corresponding cycloalkane or cycloheteroalkane hydrazine (2 equiv.) with the temperature being maintained at 23 °C and the mixture was allowed to stir for 18 h at room temperature. The solvent from the crude was evaporated under reduced pressure and the residue was partitioned between dichloromethane and water. The layers were separated and the organic phase was washed with saturated brine, dried over anhydrous Na<sub>2</sub>SO<sub>4</sub> and filtered. The solvent was removed under reduced pressure and the crude material was purified by silica gel column chromatography.



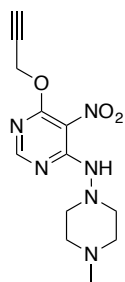
**(107) 5-nitro-4-[(piperidin-1-yl)amino]-6-(prop-2-yn-1-yloxy)pyrimidine.** The crude product was purified via silica gel column chromatography (Ethyl acetate/Hexane 15-75%) to provide the title compound as a white solid (912.9 mg, 3.282 mmol, 69% yield). <sup>1</sup>H-NMR (500 MHz, CDCl<sub>3</sub>): δ 8.90 (1H, bs, NH), 8.32 (1H, s, CH), 5.09 (2H, d, *J* = 2.5 Hz, OCH<sub>2</sub>), 2.88 (4H, t, 2 x CH<sub>2</sub>), 2.52 (1H, t, *J* = 2.4 Hz, CH), 1.86 – 1.63 (4H, m, 2 x CH<sub>2</sub>), 1.62 – 1.31 (2H, m, CH<sub>2</sub>). <sup>13</sup>C-NMR (126 MHz, CDCl<sub>3</sub>): δ 162.47 (C), 159.12 (CH), 155.34 (C), 115.97 (C), 77.49 (C), 75.82 (CH), 57.36 (2 x CH<sub>2</sub>), 55.34 (CH<sub>2</sub>), 25.11

(2 x CH<sub>2</sub>), 23.15 (CH<sub>2</sub>). **HRMS** (ES + ve), C<sub>12</sub>H<sub>16</sub>N<sub>5</sub>O<sub>3</sub> (M + H)<sup>+</sup>: Calculated 278.1253. Obtained 278.1251.



**(108) 4-[(morpholin-4-yl)amino]-5-nitro-6-(prop-2-yn-1-**

**yl)oxy)pyrimidine.** The crude product was purified via silica gel column chromatography (Ethyl acetate/Hexane 25-75%) to provide the title compound as an orange solid (1.49 g, 5.319 mmol, 56% yield). **<sup>1</sup>H-NMR** (400 MHz, CDCl<sub>3</sub>): δ 8.35 (1H, s, CH), 5.11 (2H, d, *J* = 2.4 Hz, OCH<sub>2</sub>), 3.82 (4H, t, 2 x CH<sub>2</sub>), 2.89 (4H, t, 2 x CH<sub>2</sub>), 2.53 (1H, t, *J* = 2.4 Hz, CH). **<sup>13</sup>C-NMR** (101 MHz, CDCl<sub>3</sub>): δ 159.66 (C), 154.37 (C), 144.18 (CH), 119.80 (C), 77.35 (C), 75.98 (CH), 66.29 (2 x CH<sub>2</sub>), 56.33 (2 x CH<sub>2</sub>), 55.53 (CH<sub>2</sub>). **HRMS** (ES + ve), C<sub>11</sub>H<sub>14</sub>N<sub>5</sub>O<sub>4</sub> (M + H)<sup>+</sup>: Calculated 280.1046. Obtained 280.1036.

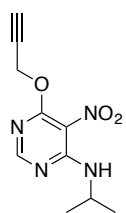


**(109) 4-[(4-methylpiperazin-1-yl)amino]-5-nitro-6-(prop-2-yn-1-**

**yl)oxy)pyrimidine.** The crude product was purified via silica gel column chromatography (Ethyl acetate/Hexane 25-100%) to provide the title compound as a yellow solid (1.27 g, 4.33 mmol, 46% yield). **<sup>1</sup>H-NMR** (400 MHz, CDCl<sub>3</sub>): δ 8.32 (1H, s, CH), 5.29 (1H, bs, NH), 5.09 (2H, d, *J* = 2.4 Hz, OCH<sub>2</sub>), 2.91 (4H, t, 2 x CH<sub>2</sub>), 2.61 (4H, t, 2 x CH<sub>2</sub>), 2.52 (1H, t, *J* = 2.4 Hz, CH), 2.32 (3H, s, CH<sub>3</sub>). **<sup>13</sup>C-NMR** (101 MHz, CDCl<sub>3</sub>): δ 158.23 (C), 155.45 (C), 145.26 (CH), 113.79 (C), 77.36 (C), 75.87 (CH), 55.69 (2 x CH<sub>2</sub>), 55.39 (CH<sub>2</sub>), 54.09 (2 x CH<sub>2</sub>), 45.75 (CH<sub>3</sub>). **HRMS** (ES + ve), C<sub>12</sub>H<sub>17</sub>N<sub>6</sub>O<sub>3</sub> (M + H)<sup>+</sup>: Calculated 293.1362. Obtained 293.1356.

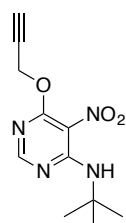
• **General procedure K2:**

To a 0.2 M solution of **57** (1 equiv.) in dichloromethane were added triethylamine (1.5 equiv.). Then the corresponding amine (isopropylamine or *tert*-butylamine) (1.5 equiv.) was added dropwise with the temperature being maintained at 23 °C and the mixture was allowed to stir for 18 h at room temperature. The solvent from the crude was evaporated under reduced pressure and the residue was partitioned between dichloromethane and water. The layers were separated and the organic phase was washed with saturated brine, dried over anhydrous Na<sub>2</sub>SO<sub>4</sub> and filtered. The solvent was removed under reduced pressure and the crude material was purified by silica gel column chromatography.



**(110) 4-(isopropylamino)-5-nitro-6-(prop-2-yn-1-yloxy)pyrimidine.**

The crude product was purified via silica gel column chromatography (Ethyl acetate/Hexane 10%) to provide the title compound as a yellow solid (1.04 g, 4.386 mmol, 87% yield). <sup>1</sup>H-NMR (400 MHz, CDCl<sub>3</sub>): δ 8.26 (1H, s, CH), 8.21 (1H, bs, NH), 5.11 (2H, d, *J* = 2.4 Hz, OCH<sub>2</sub>), 4.56 – 4.41 (1H, m, CH), 2.52 (1H, t, *J* = 2.5 Hz, CH), 1.29 (6H, d, *J* = 6.6 Hz, 2 x CH<sub>3</sub>). <sup>13</sup>C-NMR (126 MHz, CDCl<sub>3</sub>): δ 163.28 (C), 158.68 (CH), 156.40 (C), 115.70 (C), 77.70 (C), 75.67 (CH), 55.30 (CH<sub>2</sub>), 44.01 (CH), 22.74 (2 x CH<sub>3</sub>). HRMS (ES + ve), C<sub>10</sub>H<sub>13</sub>N<sub>4</sub>O<sub>3</sub> (M + H)<sup>+</sup>: Calculated 237.0988. Obtained 237.0995.

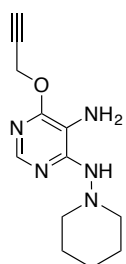


**(111) 4-(tert-butylamino)-5-nitro-6-(prop-2-yn-1-yloxy)pyrimidine.**

The crude product was purified via silica gel column chromatography (Ethyl acetate/Hexane 6%) to provide the title compound as a yellow oil (1.60 g, 6.372 mmol, 90% yield). <sup>1</sup>H-NMR (400 MHz, CDCl<sub>3</sub>): δ 8.36 (1H, bs, NH), 8.24 (1H, s, CH), 5.09 (2H, d, *J* = 2.4 Hz, OCH<sub>2</sub>), 2.51 (1H, t, *J* = 2.4 Hz, CH), 1.51 (9H, s, 3 x CH<sub>3</sub>). <sup>13</sup>C-NMR (126 MHz, CDCl<sub>3</sub>): δ 163.06 (C), 157.64 (CH), 156.76 (C), 116.11 (C), 77.74 (C), 75.58 (CH), 55.10 (CH<sub>2</sub>), 53.87 (C), 29.14 (3 x CH<sub>3</sub>). HRMS (ES + ve), C<sub>11</sub>H<sub>15</sub>N<sub>4</sub>O<sub>3</sub> (M + H)<sup>+</sup>: Calculated 251.1144. Obtained 251.1156.

• **General procedure L:**

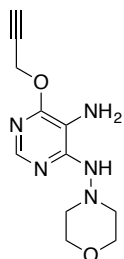
To a 0.19 M solution of the corresponding nitropyrimidine (**107 – 111**) (1 equiv.) in a mixture of ethanol and water (4:1 v/v) was added iron powder (5 equiv.) and NH<sub>4</sub>Cl (5 equiv.). The mixture was refluxed for 18 h, cooled to room temperature and filtered through a pad of Celite. The filtrate was diluted with water and extracted with dichloromethane. The combined organic layers were washed with water and saturated brine, dried over anhydrous Na<sub>2</sub>SO<sub>4</sub> and concentrated under reduced pressure. The crude residue was purified by silica gel column chromatography.



**(112) 5-amino-4-[(piperidin-1-yl)amino]-6-(prop-2-yn-1-yloxy)pyrimidine.**

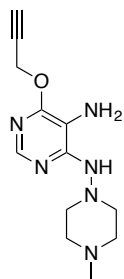
The crude product was purified via silica gel column chromatography (Ethyl acetate) to provide the title compound as a white solid (281.8 mg, 1.135 mmol, 36% yield). <sup>1</sup>H-NMR (500 MHz, CDCl<sub>3</sub>): δ 7.84 (1H, s, CH), 5.52 (1H, bs, NH), 5.01 (2H, d, *J* = 2.4 Hz, OCH<sub>2</sub>), 4.27 (2H, bs, NH<sub>2</sub>), 2.74 (4H, t, 2 x CH<sub>2</sub>), 2.48 (1H, t, *J* = 2.4 Hz, CH), 1.70 – 1.62 (4H, m, 2 x CH<sub>2</sub>),

1.46 – 1.38 (2H, m, CH<sub>2</sub>). <sup>13</sup>C-NMR (126 MHz, CDCl<sub>3</sub>): δ 156.24 (C), 149.78 (C), 145.31 (CH), 114.20 (C), 79.06 (C), 74.68 (CH), 58.22 (2 x CH<sub>2</sub>), 53.91 (CH<sub>2</sub>), 25.77 (2 x CH<sub>2</sub>), 23.32 (CH<sub>2</sub>). HRMS (ES + ve), C<sub>12</sub>H<sub>18</sub>N<sub>5</sub>O (M + H)<sup>+</sup>: Calculated 248.1511. Obtained 248.1521.



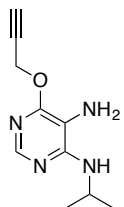
**(113) 5-amino-4-[(morpholin-4-yl)amino]-6-(prop-2-yn-1-yloxy)pyrimidine.**

The crude product was purified via silica gel column chromatography (Ethyl acetate/Hexane 50-75%) to provide the title compound as a light red solid (658 mg, 2.631 mmol, 50% yield). <sup>1</sup>H-NMR (400 MHz, CDCl<sub>3</sub>): δ 7.88 (1H, s, CH), 5.53 (1H, bs, NH), 5.03 (2H, d, *J* = 2.4 Hz, OCH<sub>2</sub>), 4.05 (2H, bs, NH<sub>2</sub>), 3.78 (4H, t, *J* = 4.7 Hz, 2 x CH<sub>2</sub>), 2.83 (4H, t, *J* = 4.7 Hz, 2 x CH<sub>2</sub>), 2.49 (1H, t, *J* = 2.5 Hz, CH). <sup>13</sup>C-NMR (101 MHz, CDCl<sub>3</sub>): δ 156.49 (C), 149.35 (C), 145.57 (CH), 114.29 (C), 78.92 (C), 74.82 (CH), 66.65 (2 x CH<sub>2</sub>), 57.25 (2 x CH<sub>2</sub>), 54.05 (CH<sub>2</sub>). HRMS (ES + ve), C<sub>11</sub>H<sub>16</sub>N<sub>5</sub>O<sub>2</sub> (M + H)<sup>+</sup>: Calculated 250.1304. Obtained 250.1302.



**(114) 5-amino-4-[(4-methylpiperazin-1-yl)amino]-6-(prop-2-yn-1-yloxy)pyrimidine.**

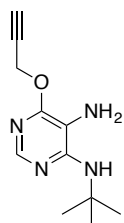
The crude product was purified via silica gel column chromatography (Methanol/Ethyl acetate 0-30%) to provide the title compound as an off-white solid (607.8 mg, 2.31 mmol, 53% yield). <sup>1</sup>H-NMR (400 MHz, CDCl<sub>3</sub>): δ 7.85 (1H, s, CH), 5.37 (1H, bs, NH), 5.01 (2H, d, *J* = 2.4 Hz, OCH<sub>2</sub>), 4.48 (2H, bs, NH<sub>2</sub>), 2.85 (4H, t, 2 x CH<sub>2</sub>), 2.56 (4H, t, 2 x CH<sub>2</sub>), 2.48 (1H, t, *J* = 2.4 Hz, CH), 2.31 (3H, s, CH<sub>3</sub>). <sup>13</sup>C-NMR (101 MHz, CDCl<sub>3</sub>): δ 156.43 (C), 149.74 (C), 145.73 (CH), 114.23 (C), 79.03 (C), 74.72 (CH), 56.51 (2 x CH<sub>2</sub>), 54.68 (CH<sub>2</sub>), 53.93 (2 x CH<sub>2</sub>), 45.72 (CH<sub>3</sub>). HRMS (ES + ve), C<sub>12</sub>H<sub>19</sub>N<sub>6</sub>O (M + H)<sup>+</sup>: Calculated 263.1620. Obtained 263.1625.



**(115) 5-amino-4-(isopropylamino)-6-(prop-2-yn-1-yloxy)pyrimidine.**

The crude product was purified via silica gel column chromatography (Ethyl acetate/Hexane 33%) to provide the title compound as a yellow solid (329.6 mg, 1.591 mmol, 76% yield). <sup>1</sup>H-NMR (400 MHz, CDCl<sub>3</sub>): δ 8.05 (1H, s, CH), 4.99 (2H, d, *J* = 2.4 Hz, OCH<sub>2</sub>), 4.54 (1H, bs, NH), 4.31 – 4.20 (1H, m, CH), 2.88 (2H, bs, NH<sub>2</sub>), 2.48 (1H, t, *J* = 2.4 Hz, CH), 1.23 (6H, d, *J* = 6.4 Hz, 2 x CH<sub>3</sub>). <sup>13</sup>C-NMR (126 MHz, CDCl<sub>3</sub>): δ 156.31 (C), 155.23 (C), 149.31 (CH), 108.69 (C), 79.18 (C), 74.68

(CH), 53.76 (CH<sub>2</sub>), 42.98 (CH), 23.35 (2 x CH<sub>3</sub>). **HRMS** (ES + ve), C<sub>10</sub>H<sub>15</sub>N<sub>4</sub>O (M + H)<sup>+</sup>: Calculated 207.1246. Obtained 207.1237.

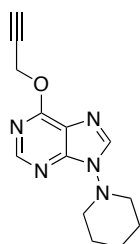


**(116) 5-amino-4-(tert-butylamino)-6-(prop-2-yn-1-yloxy)pyrimidine.**

The crude product was purified via silica gel column chromatography (Ethyl acetate/Hexane 20%) to provide the title compound as a blue oil (589.7 mg, 2.667 mmol, 31% yield). **<sup>1</sup>H-NMR** (400 MHz, CDCl<sub>3</sub>): δ 8.03 (1H, s, CH), 4.98 (2H, d, *J* = 2.4 Hz, OCH<sub>2</sub>), 4.59 (1H, bs, NH), 2.81 (2H, bs, NH<sub>2</sub>), 2.47 (1H, t, *J* = 2.4 Hz, CH), 1.48 (9H, s, 3 x CH<sub>3</sub>). **<sup>13</sup>C-NMR** (101 MHz, CDCl<sub>3</sub>): δ 156.35 (C), 156.09 (C), 149.01 (CH), 108.88 (C), 79.33 (C), 74.57 (CH), 53.62 (CH<sub>2</sub>), 51.96 (C), 29.49 (3 x CH<sub>3</sub>). **HRMS** (ES + ve), C<sub>11</sub>H<sub>17</sub>N<sub>4</sub>O (M + H)<sup>+</sup>: Calculated 221.1402. Obtained 221.1425.

• **General procedure M:**

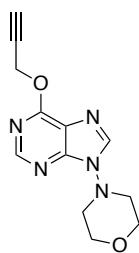
A microwave vial was charged with the corresponding diaminopyrimidine (**112** – **116**) (1 equiv.) the appropriate orthoester (3 equiv.) and methanesulfonic acid (0.2 equiv.). The reaction vial was sealed and placed in a pre-heated oil bath at 100 °C. The reaction was allowed to stir for 18 h and then cooled to room temperature. The reaction mixture was diluted with dichloromethane and the crude mixture was washed with saturated NaHCO<sub>3</sub> solution and saturated brine. The organic phase was dried over anhydrous Na<sub>2</sub>SO<sub>4</sub>, filtered and the solvent was removed under reduced pressure. The crude material was purified by silica gel column chromatography.



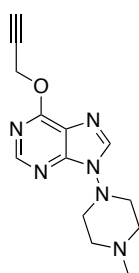
**(117) 9-(piperidin-1-yl)-6-(prop-2-yn-1-yloxy)-9H-purine.**

The crude product was purified via silica gel column chromatography (Ethyl acetate/Hexane 50%) to provide the title compound as a white solid (87.6 mg, 0.339 mmol, 61% yield). **<sup>1</sup>H-NMR** (500 MHz, CDCl<sub>3</sub>): δ 8.55 (1H, s, CH), 8.04 (1H, s, CH), 5.22 (2H, d, *J* = 2.4 Hz, OCH<sub>2</sub>), 3.46 (4H, t, *J* = 5.4 Hz, 2 x CH<sub>2</sub>), 2.49 (1H, t, *J* = 2.4 Hz, CH), 1.85 – 1.77 (4H, m, 2 x CH<sub>2</sub>), 1.64 – 1.56 (2H, m, CH<sub>2</sub>). **<sup>13</sup>C-NMR** (126 MHz, CDCl<sub>3</sub>): δ 159.76 (C), 151.52 (C), 151.37 (CH), 142.56 (CH), 120.60 (C), 78.24 (C), 75.24 (CH), 56.07 (2 x CH<sub>2</sub>), 54.24 (CH<sub>2</sub>), 26.20 (2 x CH<sub>2</sub>), 23.16 (CH<sub>2</sub>). **HRMS** (ES + ve), C<sub>13</sub>H<sub>16</sub>N<sub>5</sub>O (M + H)<sup>+</sup>: Calculated 258.1355. Obtained 258.1382.

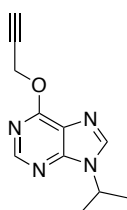




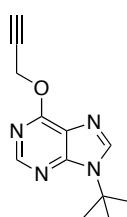
**(118) 9-(morpholin-4-yl)-6-(prop-2-yn-1-yloxy)-9H-purine.** The crude product was purified via silica gel column chromatography (Ethyl acetate) to provide the tittle compound as a white solid (155 mg, 0.596 mmol, 69% yield). **<sup>1</sup>H-NMR** (500 MHz, CDCl<sub>3</sub>): δ 8.56 (1H, s, CH), 8.06 (1H, s, CH), 5.23 (2H, d, *J* = 2.4 Hz, OCH<sub>2</sub>), 3.91 (4H, t, *J* = 4.7 Hz, 2 x CH<sub>2</sub>), 3.56 (4H, t, 2 x CH<sub>2</sub>), 2.50 (1H, t, *J* = 2.4 Hz, CH). **<sup>13</sup>C-NMR** (126 MHz, CDCl<sub>3</sub>): δ 159.81 (C), 151.65 (CH), 151.34 (C), 142.21 (CH), 120.54 (C), 78.13 (C), 75.33 (CH), 67.00 (2 x CH<sub>2</sub>), 55.03 (2 x CH<sub>2</sub>), 54.33 (CH<sub>2</sub>). **HRMS** (ES + ve), C<sub>12</sub>H<sub>14</sub>N<sub>5</sub>O<sub>2</sub> (M + H)<sup>+</sup>: Calculated 260.1147. Obtained 260.1139.



**(119) 9-(4-methylpiperazin-1-yl)-6-(prop-2-yn-1-yloxy)-9H-purine.** The crude product was purified via silica gel column chromatography (Methanol/Ethyl acetate 30%) to provide the tittle compound as an off-white solid (209.8 mg, 0.768 mmol, 94% yield). **<sup>1</sup>H-NMR** (500 MHz, CDCl<sub>3</sub>): δ 8.53 (1H, s, CH), 8.05 (1H, s, CH), 5.22 (2H, d, *J* = 2.4 Hz, OCH<sub>2</sub>), 3.52 (4H, t, 2 x CH<sub>2</sub>), 2.69 (4H, t, 2 x CH<sub>2</sub>), 2.49 (1H, t, *J* = 2.4 Hz, CH), 2.38 (3H, s, CH<sub>3</sub>). **<sup>13</sup>C-NMR** (126 MHz, CDCl<sub>3</sub>): δ 159.76 (C), 151.65 (CH), 151.41 (C), 141.93 (CH), 120.49 (C), 78.20 (C), 75.27 (CH), 54.94 (2 x CH<sub>2</sub>), 54.47 (2 x CH<sub>2</sub>), 54.26 (CH<sub>2</sub>), 45.81 (CH<sub>3</sub>). **HRMS** (ES + ve), C<sub>13</sub>H<sub>17</sub>N<sub>6</sub>O (M + H)<sup>+</sup>: Calculated 273.1464. Obtained 273.1463.



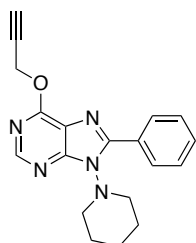
**(120) 9-isopropyl-6-(prop-2-yn-1-yloxy)-9H-purine.** The crude product was purified via silica gel column chromatography (Ethyl acetate/Hexane 75%) to provide the tittle compound as a light yellow solid (131.3 mg, 0.605 mmol, 49% yield). **<sup>1</sup>H-NMR** (500 MHz, CDCl<sub>3</sub>): δ 8.55 (1H, s, CH), 8.01 (1H, s, CH), 5.22 (2H, d, *J* = 2.4 Hz, OCH<sub>2</sub>), 4.93 – 4.83 (1H, m, CH), 2.48 (1H, t, *J* = 2.4 Hz, CH), 1.62 (6H, d, *J* = 6.9 Hz, 3 x CH<sub>2</sub>). **<sup>13</sup>C-NMR** (126 MHz, CDCl<sub>3</sub>): δ 159.54 (C), 152.22 (C), 151.60 (CH), 140.32 (CH), 121.88 (C), 78.30 (C), 75.16 (CH), 54.20 (CH<sub>2</sub>), 47.68 (CH), 22.72 (2 x CH<sub>3</sub>). **HRMS** (ES + ve), C<sub>11</sub>H<sub>13</sub>N<sub>4</sub>O (M + H)<sup>+</sup>: Calculated 217.1089. Obtained 217.1086.



**(121) 9-(tert-butyl)-6-(prop-2-yn-1-yloxy)-9H-purine.** The crude product was purified via silica gel column chromatography (Ethyl acetate/Hexane 25-50%) to provide the tittle compound as a light yellow oil (96.1 mg, 0.416 mmol, 61% yield). **<sup>1</sup>H-NMR** (400 MHz, CDCl<sub>3</sub>): δ 8.55 (1H,

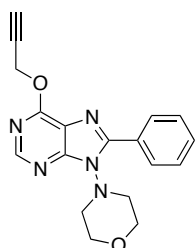
D. General synthesis for the compounds from the optimization of compounds 78 and 97:

s, CH), 8.04 (1H, s, CH), 5.22 (2H, d,  $J = 2.4$  Hz, OCH<sub>2</sub>), 2.48 (1H, t,  $J = 2.4$  Hz, CH), 1.81 (9H, s, 3 x CH<sub>3</sub>). <sup>13</sup>C-NMR (101 MHz, CDCl<sub>3</sub>): δ 159.65 (C), 152.80 (C), 150.83 (CH), 140.36 (CH), 122.87 (C), 78.40 (C), 75.11 (CH), 57.91 (C), 54.09 (CH<sub>2</sub>), 29.17 (3 x CH<sub>3</sub>). HRMS (ES + ve), C<sub>12</sub>H<sub>15</sub>N<sub>4</sub>O (M + H)<sup>+</sup>: Calculated 231.1246. Obtained 231.1237.



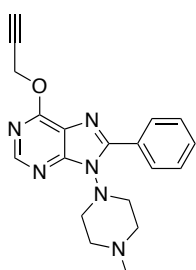
**(127) 8-phenyl-9-(piperidin-1-yl)-6-(prop-2-yn-1-yloxy)-9H-purine.** The crude product was purified via silica gel column chromatography (Ethyl acetate/Hexane 15-17%) to provide the title compound as a light yellow solid (174.8 mg, 0.532 mmol, 62% yield).

<sup>1</sup>H-NMR (500 MHz, CDCl<sub>3</sub>): δ 8.53 (1H, s, CH), 8.32 – 8.24 (2H, m, 2 x CH), 7.52 – 7.43 (3H, m, 3 x CH), 5.25 (2H, d,  $J = 2.4$  Hz, OCH<sub>2</sub>), 4.06 (2H, t,  $J = 10.3$  Hz, CH<sub>2</sub>), 3.20 (2H, t,  $J = 10.3$  Hz, CH<sub>2</sub>), 2.49 (1H, t,  $J = 2.4$  Hz, CH), 1.89 – 1.67 (6H, m, 3 x CH<sub>2</sub>). <sup>13</sup>C-NMR (126 MHz, CDCl<sub>3</sub>): δ 159.25 (C), 153.67 (C), 151.31 (C), 150.52 (CH), 130.52 (CH), 129.64 (2 x CH), 129.02 (C), 128.29 (2 x CH), 119.82 (C), 78.41 (C), 75.15 (CH), 54.26 (CH<sub>2</sub>), 54.10 (2 x CH<sub>2</sub>), 26.33 (2 x CH<sub>2</sub>), 23.16 (CH<sub>2</sub>). HRMS (ES + ve), C<sub>19</sub>H<sub>20</sub>N<sub>5</sub>O (M + H)<sup>+</sup>: Calculated 334.1668. Obtained 334.1646.



**(128) 9-(morpholin-4-yl)-8-phenyl-6-(prop-2-yn-1-yloxy)-9H-purine.** The crude product was purified via silica gel column chromatography (Ethyl acetate/Hexane 25-66%) to provide the title compound as a white solid (219.5 mg, 0.653 mmol, 55% yield).

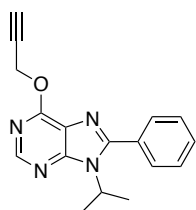
<sup>1</sup>H-NMR (400 MHz, CDCl<sub>3</sub>): δ 8.54 (1H, s, CH), 8.29 – 8.20 (2H, m, 2 x CH), 7.56 – 7.44 (3H, m, 3 x CH), 5.26 (2H, d,  $J = 2.4$  Hz, OCH<sub>2</sub>), 4.38 (2H, t, CH<sub>2</sub>), 3.06 (4H, t, 2 x CH<sub>2</sub>), 3.06 (2H, t, CH<sub>2</sub>), 2.50 (1H, t,  $J = 2.4$  Hz, CH). <sup>13</sup>C-NMR (101 MHz, CDCl<sub>3</sub>): δ 159.36 (C), 153.45 (C), 151.23 (C), 150.86 (CH), 130.72 (CH), 129.60 (2 x CH), 128.80 (C), 128.43 (2 x CH), 119.82 (C), 78.34 (C), 75.23 (CH), 67.17 (2 x CH<sub>2</sub>), 54.22 (CH<sub>2</sub>), 53.49 (2 x CH<sub>2</sub>). HRMS (ES + ve), C<sub>18</sub>H<sub>18</sub>N<sub>5</sub>O<sub>2</sub> (M + H)<sup>+</sup>: Calculated 336.1461. Obtained 336.1449.



**(129) 9-(4-methylpiperazin-1-yl)-8-phenyl-6-(prop-2-yn-1-yloxy)-9H-purine.** The crude product was purified via silica gel column chromatography (Methanol/Ethyl acetate 0-10%) to provide the title compound as an off-white solid (291.9 mg, 0.836 mmol, 77% yield).

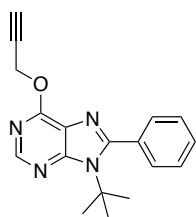
<sup>1</sup>H-NMR (400 MHz, CDCl<sub>3</sub>): δ 8.50 (1H, s, CH), 8.31 – 8.22 (2H, m, 2

x CH), 7.52 – 7.43 (3H, m, 3 x CH), 5.25 (2H, d,  $J = 2.4$  Hz, OCH<sub>2</sub>), 4.41 (2H, t, CH<sub>2</sub>), 3.08 (2H, t, CH<sub>2</sub>) 2.93 (4H, t, 2 x CH<sub>2</sub>), 2.48 (1H, t,  $J = 2.4$  Hz, CH), 2.39 (3H, s, CH<sub>3</sub>). <sup>13</sup>C-NMR (101 MHz, CDCl<sub>3</sub>): δ 159.28 (C), 153.66 (C), 151.17 (C), 150.74 (CH), 130.57 (CH), 129.58 (2 x CH), 128.98 (C), 128.35 (2 x CH), 119.88 (C), 78.42 (C), 75.14 (CH), 55.18 (2 x CH<sub>2</sub>), 54.12 (CH<sub>2</sub>), 52.61 (2 x CH<sub>2</sub>), 45.89 (CH<sub>3</sub>). **HRMS** (ES + ve), C<sub>19</sub>H<sub>21</sub>N<sub>6</sub>O (M + H)<sup>+</sup>: Calculated 349.1777. Obtained 349.1776.



**(130) 9-isopropyl-8-phenyl-6-(prop-2-yn-1-yloxy)-9H-purine.**

The crude product was purified via silica gel column chromatography (Ethyl acetate/Hexane 15-20%) to provide the title compound as a yellow solid (80.1 mg, 0.273 mmol, 34% yield). <sup>1</sup>H-NMR (400 MHz, CDCl<sub>3</sub>): δ 8.56 (1H, s, CH), 7.71 – 7.62 (2H, m, 2 x CH), 7.57 – 7.48 (3H, m, 3 x CH), 5.24 (2H, d,  $J = 2.5$  Hz, OCH<sub>2</sub>), 4.84 – 4.73 (1H, m, CH), 2.48 (1H, t,  $J = 2.4$  Hz, CH), 1.73 (6H, d,  $J = 6.8$  Hz, 2 x CH<sub>3</sub>). <sup>13</sup>C-NMR (101 MHz, CDCl<sub>3</sub>): δ 159.29 (C), 153.89 (C), 153.38 (C), 150.75 (CH), 130.40 (CH), 130.08 (C), 129.67 (2 x CH), 128.88 (2 x CH), 121.94 (C), 78.48 (C), 75.06 (CH), 54.03 (CH<sub>2</sub>), 50.04 (CH), 21.39 (2 x CH<sub>3</sub>). **HRMS** (ES + ve), C<sub>17</sub>H<sub>17</sub>N<sub>4</sub>O (M + H)<sup>+</sup>: Calculated 293.1402. Obtained 293.1388.



**(131) 9-(tert-butyl)-8-phenyl-6-(prop-2-yn-1-yloxy)-9H-purine.**

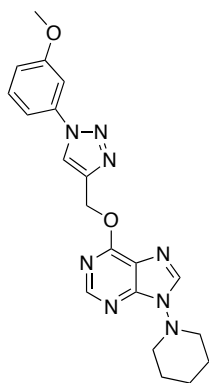
The crude product was purified via silica gel column chromatography (Ethyl acetate/Hexane 10%) to provide the title compound as a yellow oil (80.4 mg, 0.262 mmol, 46% yield). <sup>1</sup>H-NMR (400 MHz, CDCl<sub>3</sub>): δ 8.57 (1H, s, CH), 7.53 – 7.37 (5H, m, 5 x CH), 5.20 (2H, d,  $J = 2.4$  Hz, OCH<sub>2</sub>), 2.46 (1H, t,  $J = 2.5$  Hz, CH), 1.66 (9H, s, 3 x CH<sub>3</sub>). <sup>13</sup>C-NMR (101 MHz, CDCl<sub>3</sub>): δ 159.39 (C), 154.57 (C), 153.69 (C), 150.19 (CH), 134.75 (C), 129.93 (2 x CH), 129.67 (CH), 127.98 (2 x CH), 121.59 (C), 78.45 (C), 75.04 (CH), 61.05 (C), 53.99 (CH<sub>2</sub>), 31.02 (3 x CH<sub>3</sub>). **HRMS** (ES + ve), C<sub>18</sub>H<sub>19</sub>N<sub>4</sub>O (M + H)<sup>+</sup>: Calculated 307.1559. Obtained 307.1579.

• **General procedure N2:**

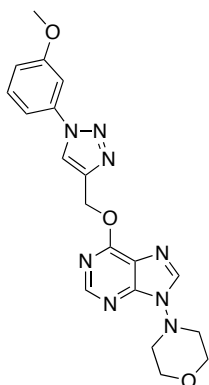
A 0.045 M solution of the corresponding alkyne (**117 – 121**, **127 – 131**) (1 equiv.) in a mixture of acetonitrile and water (9:1 v/v) was placed on an oven-dried microwave vial and the mixture was stirred until complete solubilization. Then the corresponding azide (0.5 M in methyl *tert*-butyl ether, MTBE, 1 equiv.), sodium ascorbate (0.2 equiv.), copper (I) iodide (0.1 equiv.) and triethylamine (0.4 equiv.) were added. The reaction vial was

D. General synthesis for the compounds from the optimization of compounds 78 and 97:

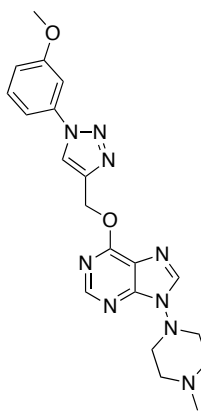
sealed, evacuated, backfilled with argon and the mixture allowed to stir at room temperature for 18 h. The mixture was partitioned between dichloromethane and water. The layers were separated and the organic phase was washed with saturated brine, dried over anhydrous Na<sub>2</sub>SO<sub>4</sub> and filtered. The solvent was removed under reduced pressure and the crude material was purified by silica gel column chromatography.



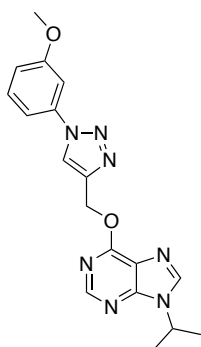
**(122)**      **6-([1-(3-methoxyphenyl)-1H-1,2,3-triazol-4-yl]methoxy)-9-(piperidin-1-yl)-9H-purine.** The crude product was purified via silica gel column chromatography (Ethyl acetate/Hexane 60%) to provide the title compound as a white solid (82.6 mg, 0.203 mmol, 82% yield). **<sup>1</sup>H-NMR** (500 MHz, CDCl<sub>3</sub>): δ 8.57 (1H, s, CH), 8.17 (1H, s, CH), 8.02 (1H, s, CH), 7.42 – 7.21 (3H, m, 3 x CH), 6.98 – 6.93 (1H, m, CH), 5.86 (2H, s, OCH<sub>2</sub>), 3.86 (3H, s, CH<sub>3</sub>), 3.46 (4H, t, *J* = 5.4 Hz, 2 x CH<sub>2</sub>), 1.85 – 1.77 (4H, m, 2 x CH<sub>2</sub>), 1.64 – 1.55 (2H, m, CH<sub>2</sub>). **<sup>13</sup>C-NMR** (126 MHz, CDCl<sub>3</sub>): δ 160.74 (C), 160.33 (C), 151.46 (CH), 151.40 (C), 144.12 (C), 142.39 (CH), 138.15 (C), 130.63 (CH), 122.17 (CH), 120.58 (C), 114.94 (CH), 112.68 (CH), 106.54 (CH), 60.35 (CH<sub>2</sub>), 56.07 (2 x CH<sub>2</sub>), 55.77 (CH<sub>3</sub>), 26.19 (2 x CH<sub>2</sub>), 23.15 (CH<sub>2</sub>). **HRMS** (ES + ve), C<sub>20</sub>H<sub>23</sub>N<sub>8</sub>O<sub>2</sub> (M + H)<sup>+</sup>: Calculated 407.1944. Obtained 407.1979.



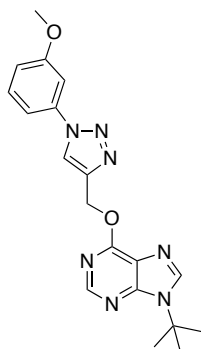
**(123)**      **6-([1-(3-methoxyphenyl)-1H-1,2,3-triazol-4-yl]methoxy)-9-(morpholin-4-yl)-9H-purine.** The crude product was purified via silica gel column chromatography (Ethyl acetate) to provide the title compound as a white solid (61.8 mg, 0.151 mmol, 53% yield). **<sup>1</sup>H-NMR** (500 MHz, CDCl<sub>3</sub>): δ 8.58 (1H, s, CH), 8.16 (1H, s, CH), 8.03 (1H, s, CH), 7.43 – 7.19 (3H, m, 3 x CH), 6.96 (1H, m, CH), 5.87 (2H, s, OCH<sub>2</sub>), 3.91 (4H, t, *J* = 4.7 Hz, 2 x CH<sub>2</sub>), 3.87 (3H, s, CH<sub>3</sub>), 3.57 (4H, t, 2 x CH<sub>2</sub>). **<sup>13</sup>C-NMR** (126 MHz, CDCl<sub>3</sub>): δ 160.75 (C), 160.43 (C), 151.71 (CH), 151.35 (C), 144.01 (C), 142.08 (CH), 138.13 (C), 130.65 (CH), 122.23 (CH), 120.65 (C), 114.94 (CH), 112.68 (CH), 106.59 (CH), 67.00 (2 x CH<sub>2</sub>), 60.38 (CH<sub>2</sub>), 55.79 (CH<sub>3</sub>), 55.03 (2 x CH<sub>2</sub>). **HRMS** (ES + ve), C<sub>19</sub>H<sub>21</sub>N<sub>8</sub>O<sub>3</sub> (M + H)<sup>+</sup>: Calculated 409.1737. Obtained 409.1741.



**(124)** **6-{{1-(3-methoxyphenyl)-1H-1,2,3-triazol-4-yl}methoxy}-9-(4-methylpiperazin-1-yl)-9H-purine.** The crude product was purified via silica gel column chromatography (Methanol/Ethyl acetate 30%) to provide the title compound as a white solid (75 mg, 0.178 mmol, 68% yield). **<sup>1</sup>H-NMR** (500 MHz, CDCl<sub>3</sub>): δ 8.56 (1H, s, CH), 8.16 (1H, s, CH), 8.04 (1H, s, CH), 7.42 – 7.19 (3H, m, 3 x CH), 6.98 – 6.93 (1H, m, CH), 5.86 (2H, s, OCH<sub>2</sub>), 3.87 (3H, s, CH<sub>3</sub>), 3.54 (4H, t, 2 x CH<sub>2</sub>), 2.68 (4H, t, 2 x CH<sub>2</sub>), 2.39 (3H, s, CH<sub>3</sub>). **<sup>13</sup>C-NMR** (126 MHz, CDCl<sub>3</sub>): δ 160.73 (C), 160.35 (C), 151.73 (CH), 151.40 (C), 144.08 (C), 141.80 (CH), 138.14 (C), 130.64 (CH), 122.21 (CH), 120.50 (C), 114.93 (CH), 112.68 (CH), 106.56 (CH), 60.34 (CH<sub>2</sub>), 55.78 (CH<sub>3</sub>), 54.93 (2 x CH<sub>2</sub>), 54.47 (2 x CH<sub>2</sub>), 45.80 (CH<sub>3</sub>). **HRMS** (ES + ve), C<sub>20</sub>H<sub>24</sub>N<sub>9</sub>O<sub>2</sub> (M + H)<sup>+</sup>: Calculated 422.2053. Obtained 422.2047.



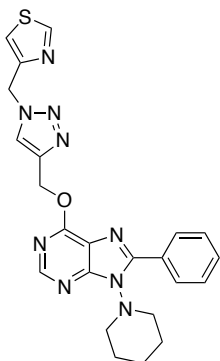
**(125)** **9-isopropyl-6-{{1-(3-methoxyphenyl)-1H-1,2,3-triazol-4-yl}methoxy}-9H-purine.** The crude product was purified via silica gel column chromatography (Ethyl acetate) to provide the title compound as a yellow oil (91.6 mg, 0.25 mmol, 75% yield). **<sup>1</sup>H-NMR** (500 MHz, CDCl<sub>3</sub>): δ 8.56 (1H, s, CH), 8.17 (1H, s, CH), 8.02 (1H, s, CH), 7.39 – 7.17 (3H, m, 3 x CH), 6.96 – 6.90 (1H, m, CH), 5.85 (2H, s, OCH<sub>2</sub>), 4.93 – 4.83 (1H, m, CH), 3.84 (3H, s, CH<sub>3</sub>), 1.60 (6H, d, *J* = 6.8 Hz, 2 x CH<sub>3</sub>). **<sup>13</sup>C-NMR** (126 MHz, CDCl<sub>3</sub>): δ 160.66 (C), 160.19 (C), 151.85 (C), 151.67 (CH), 144.15 (C), 140.18 (CH), 138.08 (C), 130.79 (C), 130.57 (CH), 122.14 (CH), 114.84 (CH), 112.61 (CH), 106.49 (CH), 60.26 (CH<sub>2</sub>), 55.72 (CH<sub>3</sub>), 47.70 (CH), 22.66 (2 x CH<sub>3</sub>). **HRMS** (ES + ve), C<sub>18</sub>H<sub>20</sub>N<sub>7</sub>O<sub>2</sub> (M + H)<sup>+</sup>: Calculated 366.1678. Obtained 366.1669.



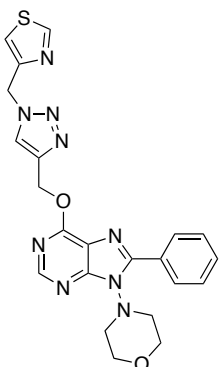
**(126)** **9-(tert-butyl)-6-{{1-(3-methoxyphenyl)-1H-1,2,3-triazol-4-yl}methoxy}-9H-purine.** The crude product was purified via silica gel column chromatography (Ethyl acetate/Hexane 10%) to provide the title compound as a yellow oil (77.2 mg, 0.203 mmol, 69% yield). **<sup>1</sup>H-NMR** (400 MHz, CDCl<sub>3</sub>): δ 8.55 (1H, s, CH), 8.17 (1H, s, CH), 8.07 (1H, s, CH), 7.40 – 7.17 (3H, m, 3 x CH), 6.96 – 6.89 (1H, m, CH), 5.85 (2H, s, OCH<sub>2</sub>), 3.84 (3H, s, CH<sub>3</sub>), 1.78 (9H, s, 3 x CH<sub>3</sub>). **<sup>13</sup>C-NMR** (101 MHz, CDCl<sub>3</sub>): δ 160.65 (C), 160.46 (C), 151.06 (C), 150.93 (CH), 144.22 (C),

D. General synthesis for the compounds from the optimization of compounds 78 and 97:

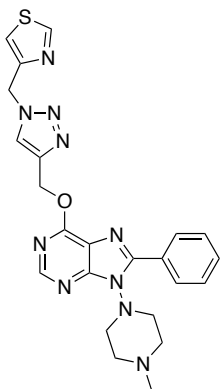
140.18 (C), 138.09 (CH), 130.55 (CH), 130.52 (C), 122.12 (CH), 114.82 (CH), 112.62 (CH), 106.49 (CH), 60.16 (CH<sub>2</sub>), 57.94 (C), 55.74 (CH<sub>3</sub>), 29.08 (3 x CH<sub>3</sub>). **HRMS** (ES + ve), C<sub>19</sub>H<sub>22</sub>N<sub>7</sub>O<sub>2</sub> (M + H)<sup>+</sup>: Calculated 380.1835. Obtained 380.1823.



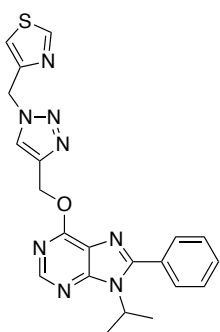
**(132) 8-phenyl-9-(piperidin-1-yl)-6-[[1-(thiazol-4-ylmethyl)-1H-1,2,3-triazol-4-yl]methoxy]-9H-purine.** The crude product was purified via silica gel column chromatography (Ethyl acetate) to provide the title compound as a light green solid (81.8 mg, 0.173 mmol, 82% yield). **<sup>1</sup>H-NMR** (500 MHz, CDCl<sub>3</sub>): δ 8.80 (1H, bs, CH), 8.52 (1H, s, CH), 8.26 – 8.21 (2H, m, 2 x CH), 7.95 (1H, s, CH), 7.51 – 7.42 (3H, m, 3 x CH), 7.32 (1H, bs, CH), 5.81 (2H, s, OCH<sub>2</sub>), 5.70 (2H, s, CH<sub>2</sub>), 4.05 (2H, t, CH<sub>2</sub>), 3.18 (2H, t, CH<sub>2</sub>), 1.90 – 1.64 (6H, m, 3 x CH<sub>2</sub>). **<sup>13</sup>C-NMR** (126 MHz, CDCl<sub>3</sub>): δ 159.90 (C), 154.13 (CH), 153.56 (C), 151.16 (C), 150.67 (CH), 150.63 (C), 143.84 (C), 130.53 (CH), 129.67 (2 x CH), 128.89 (C), 128.28 (2 x CH), 124.46 (CH), 119.62 (C), 118.08 (CH), 60.34 (CH<sub>2</sub>), 54.28 (2 x CH<sub>2</sub>), 49.75 (CH<sub>2</sub>), 26.32 (2 x CH<sub>2</sub>), 23.16 (CH<sub>2</sub>). **HRMS** (ES + ve), C<sub>23</sub>H<sub>24</sub>N<sub>9</sub>OS (M + H)<sup>+</sup>: Calculated 474.1825. Obtained 474.1845.



**(133) 9-(morpholin-4-yl)-8-phenyl-6-[[1-(thiazol-4-ylmethyl)-1H-1,2,3-triazol-4-yl]methoxy]-9H-purine.** The crude product was purified via silica gel column chromatography (Ethyl acetate/Hexane 25-100%) to provide the title compound as a white solid (74.1 mg, 0.156 mmol, 75% yield). **<sup>1</sup>H-NMR** (400 MHz, CDCl<sub>3</sub>): δ 8.80 (1H, bs, CH), 8.52 (1H, s, CH), 8.23 – 8.16 (2H, m, 2 x CH), 7.94 (1H, s, CH), 7.54 – 7.42 (3H, m, 3 x CH), 7.33 (1H, bs, CH), 5.81 (2H, s, OCH<sub>2</sub>), 5.70 (2H, s, CH<sub>2</sub>), 4.37 (2H, t, CH<sub>2</sub>), 3.88 (4H, t, 2 x CH<sub>2</sub>), 3.08 (2H, t, CH<sub>2</sub>). **<sup>13</sup>C-NMR** (101 MHz, CDCl<sub>3</sub>): δ 160.00 (C), 154.13 (CH), 153.34 (C), 151.06 (C), 150.95 (CH), 150.62 (C), 143.72 (C), 130.68 (CH), 129.59 (2 x CH), 128.73 (C), 128.41 (2 x CH), 124.47 (CH), 119.69 (C), 118.11 (CH), 67.15 (2 x CH<sub>2</sub>), 60.34 (CH<sub>2</sub>), 53.49 (2 x CH<sub>2</sub>), 49.74 (CH<sub>2</sub>). **HRMS** (ES + ve), C<sub>22</sub>H<sub>22</sub>N<sub>9</sub>O<sub>2</sub>S (M + H)<sup>+</sup>: Calculated 476.1617. Obtained 476.1608.



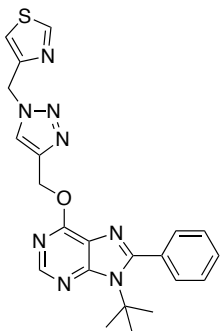
**(134) 9-(4-methylpiperazin-1-yl)-8-phenyl-6-([1-(thiazol-4-ylmethyl)-1H-1,2,3-triazol-4-yl]methoxy)-9H-purine.** The crude product was purified via silica gel column chromatography (Methanol/Ethyl acetate 10%) to provide the title compound as a white solid (61.7 mg, 0.126 mmol, 61% yield). **<sup>1</sup>H-NMR** (400 MHz, CDCl<sub>3</sub>): δ 8.78 (1H, d, *J* = 2.0 Hz, CH), 8.46 (1H, s, CH), 8.24 – 8.14 (2H, m, 2 x CH), 7.90 (1H, s, CH), 7.50 – 7.39 (3H, m, 3 x CH), 7.29 (1H, d, *J* = 2.0 Hz, CH), 5.78 (2H, s, OCH<sub>2</sub>), 5.68 (2H, s, CH<sub>2</sub>), 4.36 (2H, t, CH<sub>2</sub>), 3.09 (4H, t, 2 x CH<sub>2</sub>), (2H, t, CH<sub>2</sub>), 2.36 (3H, s, CH<sub>3</sub>). **<sup>13</sup>C-NMR** (101 MHz, CDCl<sub>3</sub>): δ 159.89 (C), 154.07 (CH), 153.52 (C), 150.95 (C), 150.72 (CH), 150.58 (C), 143.72 (C), 130.44 (CH), 129.51 (2 x CH), 128.92 (C), 128.27 (2 x CH), 124.44 (CH), 119.77 (C), 118.02 (CH), 60.16 (CH<sub>2</sub>), 55.14 (2 x CH<sub>2</sub>), 52.59 (2 x CH<sub>2</sub>), 49.68 (CH<sub>2</sub>), 45.88 (CH<sub>3</sub>). **HRMS** (ES + ve), C<sub>23</sub>H<sub>25</sub>N<sub>10</sub>OS (M + H)<sup>+</sup>: Calculated 489.1934. Obtained 489.1946.



**(135) 9-(isopropyl)-8-phenyl-6-([1-(thiazol-4-ylmethyl)-1H-1,2,3-triazol-4-yl]methoxy)-9H-purine.** The crude product was purified via silica gel column chromatography (Ethyl acetate) to provide the title compound as a white solid (78 mg, 0.18 mmol, 82% yield). **<sup>1</sup>H-NMR** (500 MHz, CDCl<sub>3</sub>): δ 8.79 (1H, d, *J* = 2.0 Hz, CH), 8.55 (1H, s, CH), 7.93 (1H, s, CH), 7.66 – 7.59 (2H, m, 2 x CH), 7.56 – 7.47 (3H, m, 3 x CH), 7.30 (1H, d, *J* = 2.0 Hz, CH), 5.79 (2H, s, OCH<sub>2</sub>), 5.69 (2H, d, *J* = 0.7 Hz, CH<sub>2</sub>), 4.76 (1H, m, CH), 1.72 (6H, d, *J* = 6.8 Hz, 2 x CH<sub>3</sub>). **<sup>13</sup>C-NMR** (126 MHz, CDCl<sub>3</sub>): δ 159.85 (C), 154.07 (CH), 153.66 (C), 153.08 (C), 150.90 (CH), 150.62 (C), 143.86 (C), 130.43 (CH), 129.84 (C), 129.65 (2 x CH), 128.86 (2 x CH), 124.34 (CH), 121.59 (C), 118.03 (CH), 60.28 (CH<sub>2</sub>), 50.05 (CH), 49.73 (CH<sub>2</sub>), 21.38 (2 x CH<sub>3</sub>). **HRMS** (ES + ve), C<sub>21</sub>H<sub>21</sub>N<sub>8</sub>OS (M + H)<sup>+</sup>: Calculated 433.1559. Obtained 433.1540.

D. General synthesis for the compounds from the optimization of compounds 78 and 97:

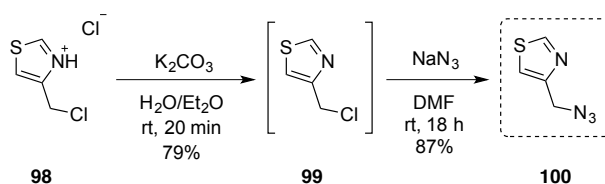
---



**(136) 9-(*tert*-butyl)-8-phenyl-6-{{1-(thiazol-4-ylmethyl)-1H-1,2,3-triazol-4-yl}methoxy}-9H-purine.** The crude product was purified via silica gel column chromatography (Ethyl acetate/Hexane 90%) to provide the title compound as a yellow oil (32.5 mg, 0.073 mmol, 86% yield). **<sup>1</sup>H-NMR** (500 MHz, CDCl<sub>3</sub>): δ 8.78 (1H, bs, CH), 8.57 (1H, s, CH), 7.94 (1H, s, CH), 7.49 – 7.37 (5H, m, 5 x CH), 7.30 (1H, bs, CH), 5.75 (2H, s, OCH<sub>2</sub>), 5.68 (2H, s, 2 x CH<sub>2</sub>), 1.65 (9H, s, 3 x CH<sub>3</sub>). **<sup>13</sup>C-NMR** (126 MHz, CDCl<sub>3</sub>): δ 159.87 (C), 154.27 (C), 154.08 (CH), 153.32 (C), 150.60 (C), 150.45 (CH), 143.79 (C), 129.92 (2 x CH), 129.81 (CH), 128.88 (C), 128.01 (2 x CH), 124.33 (CH), 120.99 (C), 118.07 (CH), 61.30 (C), 60.31 (CH<sub>2</sub>), 49.71 (CH<sub>2</sub>), 30.99 (3 x CH<sub>3</sub>). **HRMS** (ES + ve), C<sub>22</sub>H<sub>23</sub>N<sub>8</sub>OS (M + H)<sup>+</sup>: Calculated 447.1716. Obtained 447.1726.



### E. Synthesis of 4-(azidomethyl)thiazole (100)



To 4-(chloromethyl)thiazole hydrochloride (**98**) (500 mg, 2.94 mmol, 1 equiv.) was added 50% aqueous  $K_2CO_3$  (10 mL) and diethyl ether (4 mL). The mixture was stirred at room temperature for 20 min. The organic layer was separated, dried over  $Na_2SO_4$ , filtered and concentrated to dryness under reduced vacuum. The crude product was used without further purification to provide compound **99** as a light yellow solid (311.8 mg, 2.33 mmol, 79% yield).

The crude product of the above reaction (**99**) (311.8 mg, 2.33 mmol, 1 equiv.) was dissolved in anhydrous DMF (6 mL) and sodium azide (302.93 mg, 4.66 mmol, 2 equiv.) was added. The reaction was stirred for 18 h at room temperature and then quenched with saturated aqueous  $Na_2SO_4$ . The aqueous layer was extracted with ethyl acetate (3 x 50 mL), and the organic layer washed with water (3 x 50 mL) and saturated brine (3 x 20 mL). The organic layer was dried over  $Na_2SO_4$ , filtered, and the solvent was removed under reduced pressure. The crude product was used without further purification to provide the title compound (**100**) as a yellow oil (283.2 mg, 2.12 mmol, 87%) that was used as a 0.5 M solution in MTBE, and stored at  $-15\text{ }^\circ\text{C}$  in a topaz bottle.

**Raw analytical and spectral characterization data of the synthesized compounds is available at:**

